Technische Universität München
Lehrstuhl für Organische Chemie II

The Natural Product Acivicin as a Tool for ABPP and the Activity of Serine Hydrolases in Uterine Fibroids

Johannes Kreuzer

Vollständiger Abdruck der von der Fakultät für Chemie der Technischen Universität München zur Erlangung des akademischen Grades eines

Doktors der Naturwissenschaften

genehmigten Dissertation.

Vorsitzender: Univ-Prof. Dr. Michael Groll

Prüfer der Dissertation:

1. Univ-Prof. Dr. Stephan A. Sieber
2. Univ-Prof. Dr. Aymelt Itzen

Die Dissertation wurde am 10.03.2015 bei der Technischen Universität München eingereicht und durch die Fakultät für Chemie am 01.04.2015 angenommen.

Meiner Familie

Science never solves a problem without creating ten more.

George Bernard Shaw

Danksagung

Zuvorderst gilt mein Dank Prof. Dr. Stephan A.Sieber und Dr. Daniel Forler für die Betreuung, die Aufnahme an den Lehrstuhl für Organische Chemie 2 und die Abteilung Target Discovery-Global Technology der Bayer AG, die spannende Themenstellung, die vielen interessanten und hilfreichen Diskussionen, die technische Ausstattung und die Möglichkeit durch das Erlernen neuer Techniken meinen fachlichen Horizont in einer sehr tiefen Breite zu erweitern. Diese Unterstüztung hat entscheidend zum Erfolg dieser Arbeit beigetragen und meine Leidenschaft für wissenschaftliche Fragestellung enorm gefestigt.

Mein Dank gilt auch den Mitgliedern der Prüfungskommission für die Beurteilung und Prüfung der vorliegenden Dissertation.

Besonderer Dank gilt Mona Wolff, Katja Bäuml, Birgitt Wykhoff und Ute Goldberg für all die Hilfestellung bei bürokratischen und organisatorischen Fragen. Ohne euch wäre der Laboralltag undenkbar.Burghard Cordes danke ich für die Unterstützung und Einweisung bei der Messung von Massenspektren von niedermolekularen Verbindungen. Dank gilt auch Evelyn Bruckmaier für die Hilfe bei administrativen Angelegenheiten.

Prof. Dr. Rolf Breinbauer und Dr. Joanna Krysiak danke ich für die Möglichkeit zur Mitarbeit an der Charakterisierung von Pargyline abgeleiteten Sonden, die sehr erfolgreich war.

Für meine Zeit bei Bayer Schering möchte ich mich bei Dr. Volker Badock, Dr. Georg Beckmann, Dr. Michael Drosch, Dr. Hans-Dieter Pohlenz, Dr. Jörg Schneider und allen anderen nicht namentlich genannten Mitgliedern der Abteilung Target Discovery – Global Technology für die super Atmosphäre, die Hilfsbereitschaft und die tollen Gespräche. Dieser spannende Einblick in die industrielle Forschung wie die gesamte tolle Zeit in Berlin wird mir auf ewig im Gedächtnis bleiben.

Gleiches gilt natürlich für meine Kollegen seitens der TU München und Aviru. Allen voran den Mitlgliedern von Labor B dieser gesamten Zeit, Dr. Oliver Battenberg, Mathias Hackl, Franziska Mandl, Dr. Maximilian Pitscheider, Dr. Tanja Wirth und Weining Zhao (谢谢). Ein besonderer Dank gilt Dr. Nina Bach, für die Zeit und das Engagement beim reparieren, fehlersuchen, Instandhalten der Orbitrap und nano HPLC. Diese Zeit zählte zwar zu nervenaufreibendsten aber auch lehrreichsten Zeiten während meiner gesamten Doktorarbeit. Dr. Katrin Lorentz-Baath danke ich für Korrekturen dieser Arbeit und die Zeit und Hilfe beim Betreiben des Zellkulturlabors. Dr. Megan Wright, Philipp Kleiner und Wolfgang Heydenreuter danke ich für die Korrekturen an dieser Arbeit. Weiterer Dank gilt Dr. Thomas Böttcher, Maria Dahmen, Dr. Jürgen Eirich, Dr. Ronald Frohnapfel, Dr. Malte Gersch,

Maximilian Koch, Dr. Roman Kolb, Lena Kunold, Dr. Mathew Nodwell, Dr. Franziska Weinandy, Jan Vomacka, Christian Fetzer, Dr Georg Rudolph und allen anderen nicht namentlich genannten Mitgliedern des AK Siebers und AVIRU. Danke für die vielen heiteren Stunden, eure Hilfsbereitschaft, die anregenden Gespräche - einfach die gesamte Zeit.

Meinen Praktikanten Jochen Spiegel, Stephanie Robu, Martina Weineisen, Silvia Klotz, Marcus Wegmann, Malena Bestehorn und Marina Spona danke ich für die tolle Zusammenarbeit und ihr Engagement.

Dr. Daniel Betz, Dr. Reentje Harms, Dr. Sebastian Hock, Dr. Dominik Jantke und Laura Jantke, Sophie Jürgens, Dr. Mathias Köberl, Vesta Kohlmeier, Astrid Mahrla, Dr. Iulius Markovits und Monica Markovits, Christian Münchmeyer, Dr. Andreas Raba und Eva Raba, Dr. Stefan Reindl (Wurm), Korbinian Riener, Zhong Rui (Dr. Billy Ray, 谢谢), Dr. Lars-Arne Schaper, Dr. Johannes Schmid, Dr. Ingrid Span, Dr. Thomas Wagner, Michael Wilhelm, Dr Philip Zehetmaier, Dr. Susanna Zimmer und jeden den ich hier vergessen habe ein dickes Dankeschön für die Fußballabende, Fußballspielen, Grillabende, Feierabende, Pubquiz, Winter- und Sommerhütten, Überraschungspartys, Semesteressen, Kochabende und die vielen lustigen Stunden, die immer ein Lächeln auf mein Gesicht zauberten.

Zu guter Letzt gilt mein Dank meiner Familie, allen voran meinen Eltern Michael und Hannelore Kreuzer, die mich während des Studiums und der Promotion fortwährend unterstützt, motiviert und immer Rückhalt gegeben haben und natürlich meinen Brüdern Tobias, Daniel und Christian. Ohne Eure Unterstützung wäre das alles nie möglich gewesen. Vielen herzlichen Dank!

Introductory remark

Parts of this work have been published in international journals.

Table of Contents

1 General Introduction

1.1 Proteomics

In 1990 a project was launched to map the human genome and eleven years later in 2001 the first drafts of the human genome were published.[1, 2] This was a major milestone in science in general and one of the greatest achievements in the life science to date. But all milestones have in common that they are not the end of a mission but just the beginning of the next great steps. Today there are complete gene sequences available for many viruses, prokaryotes and eukaryotes and their number is still increasing. The mapping of the human genome enabled a deeper understanding of our biology in general but also of diseases, evolution, and mutations linked to cancer. With the blueprints, the genes, in hand the next level to investigate was the proteins. They represent the direct functional molecules and the machinery in living organisms. This was the birth of the field of proteomics, whose tasks are the identification and quantification of all proteins in the proteome, and furthermore the expression, interaction, localization, modification and function of these proteins in a cell. During the last two decades many developments in sample preparation, instrumentation and data analysis have steadily improved this discipline. Today proteomic analysis is dominated by a "bottom up" approach called "shotgun proteomics".[3-6] This approach generates peptides through proteolytic digestion that are separated by chromatography and analyzed by fragmentation and mass spectrometry. The peptide sequence is identified by comparing spectra with *in silico* generated spectra from a protein database and assigning these peptides to proteins. Common search algorithms for this process are SEQUEST, MASCOT and Andromeda.[7-10]

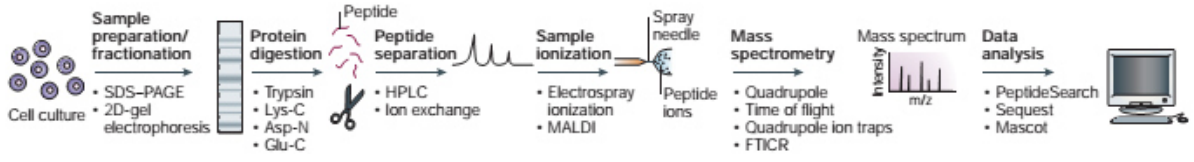

Figure 1. Typical proteomics workflow (reprinted by permission from Macmillan Publishers Ltd: Nature reviews. Molecular cell biology [11], copyright 2004).

The advantage of shotgun proteomics over "top down" proteomics (proteomics of intact proteins) lies in the superior fragmentation, ionization and separation of peptides compared to

proteins. Although the proteins are measured indirectly, shotgun proteomics can be adopted better to protein analysis and has become the workhorse of proteomics.

Recent advances in the human proteome identified 17,294 proteins of the 20,687 protein coding genes using human tissue samples, and 18,097 proteins using available data from cell lines, tissue samples and body fluids.[12-14] These advances not only benefit academic work but also the pharmaceutical industry during the drug discovery/target discovery process or clinical analytics. For clinical use, proteomics can be applied to identify biomarkers of certain diseases for earlier diagnosis, better treatment or for monitoring treatment progress. This makes proteomics an increasingly valuable tool for obtaining a deeper understanding of how life works.

1.2 Activity-Based Protein Profiling

The fast evolving field of proteomics has accelerated progress in the life sciences. Global protein analysis from complex proteomes has improved in terms of accuracy and measuring time. But abundance alone is not enough to understand protein functions in a cell. Many proteins are posttranslational activated and, though expressed in high abundance, can remain inactivated. Proteases are a well-known example of this type of protein. To study proteins based on their activity, organic chemistry is combined with biological methods in a technique called activity-based protein profiling.

The idea of using small molecules as probes for visualization dates back to the 1960s where radioactive labeled diisopropyl fluorophosphonate (a covalent serine hydrolase inhibitor) was used for cytochemical staining.[15, 16] Using an inhibitor enables labeling of only the active form of an enzyme, regardless of its abundance. In the 1990s this idea was further developed by attaching fluorescent reporters or biotin to inhibitors, that could then be visualized via western blot.[17-20] This eliminates the disadvantages of using radioactivity but alters the structure of the inhibitor and therefore could change the activity towards the protein. This was overcome by the introduction of an alkyne handle that can be modified bioorthogonally using the Huisgen-Sharpless-Meldal cycloaddition (click chemistry) after protein labeling.[21] Other bioorthogonal reactions such as the Staudinger ligation or tetrazine ligation have also been applied to ABPP, expanding the methods available for protein labeling, and even enabling multiple independent reactions in one sample.[22-24] The probe design is typically composed of three structural elements: the warhead or reactive group, that covalently reacts with the active site, a spacer/binding group, that separates the tag from the warhead and/or

increases selectivity of the probe, and the tag or ligation handle (figure 2). In the case of a noncovalent warhead, an additional photocrosslinker can be attached to the probes, that forms a reactive intermediate upon irradiation with UV light that reacts covalently with an electron rich residue nearby. Commonly used photocrosslinkers are benzophenones, arylazides and diazirines.[25-29]

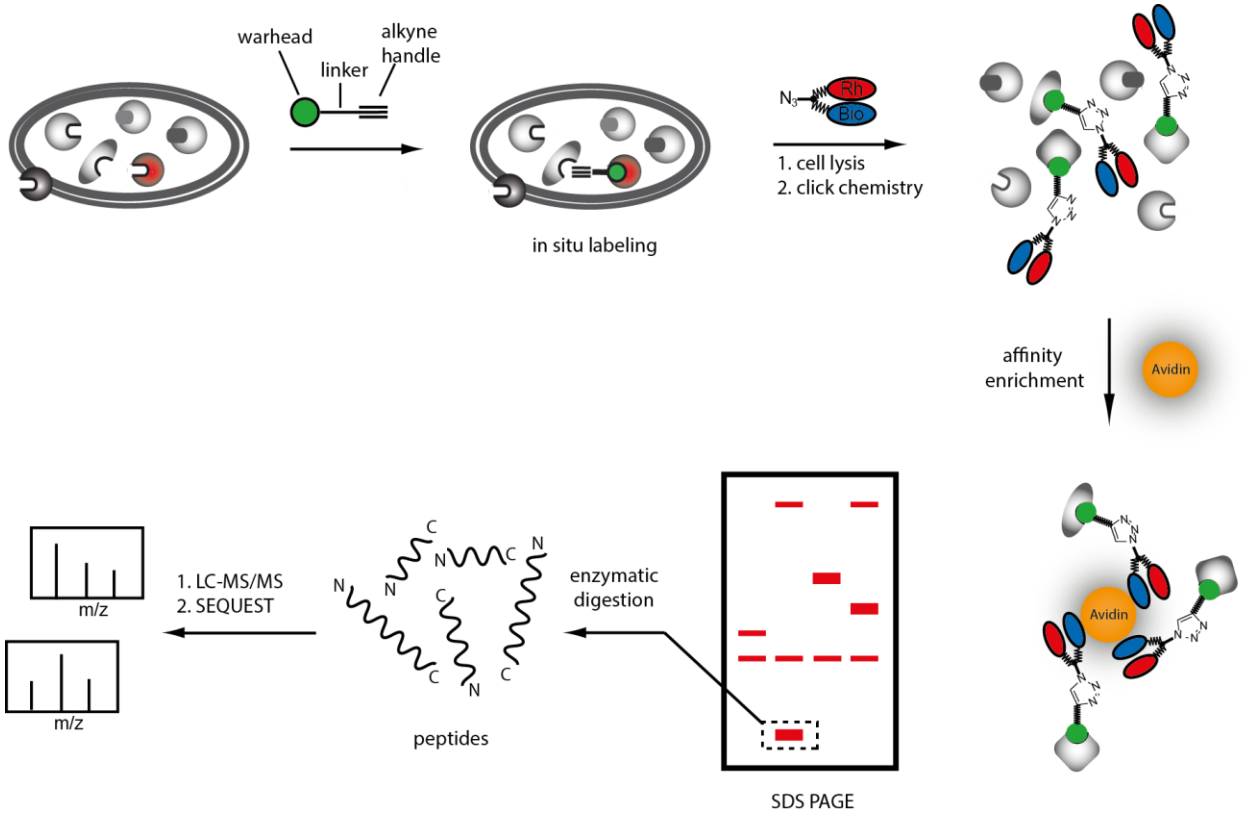

Figure 2. Activity-based protein profiling workflow with a natural product as a probe (figure taken from [30] - reproduced by permission of The Royal Society of Chemistry). (Rh stands for rhodamine and bio for biotin).

For analysis, a simple fluorescent readout on an SDS-PAGE gel or a western blot for a label such as biotin can be used. Far more important is the analysis using mass spectrometry, by incorporating ABPP into a "bottom up" proteomics workflow. ABPP is used to selectively label certain proteins with an affinity tag, e.g. biotin. By immobilizing the labeled proteins on a solid support (such as avidin-coated resin), the subsequent washing steps reduce the complexity of the protein sample and thereby enrich the labeled proteins for easier analysis.[31]

All these achievements have made it possible to study various classes of enzymes including serine hydrolases, cysteine proteases, metalloproteases, glucosidases, and many more, including enzymes which are pathogenesis associated.[26, 32-37] This technology enables analysis of a selected protein or proteins of interest in a all kinds of tissues, cells, plants, fungi

or bacteria. But ABPP is not only limited to study enzyme classes with probes based on inhibitors, it can also be used to study the interactions of drugs or natural products. This is done by converting the compound of interest into an activity-based probe (ABP) by attaching a ligation handle and if needed an additional photocrosslinker, as was done in studies on dasatinib, a Src/Abl kinase inhibitor, or for the antibiotic showdomycin.[38, 39]

So-called ‘competitive ABPP’ is also used to study new non-covalent inhibitors on known enzyme classes. In this case the inhibitor is incubated together with an ABP, e.g. fluorophosphonate for serine hydrolases, in the protein sample and fluorescence SDS-PAGE used as a readout. This procedure can be tuned for high throughput with the exchange of the SDS-PAGE readout for a fluorescence polarization-based readout of the unbound and bound ABP.[40] This technique is already applied widely. In summary, ABPP provides a powerful and reliable tool for investigation of enzymes, small molecules and their protein interactions and exploring new compounds.

2 Chemoproteomic Profiling of Acivicin

2.1 Special Introduction

2.1.1 Acivicin

Acivicin is a natural product that was isolated from the fermentation broth of *Streptomyces sviceus* during screens for new antimetabolite antibiotics.[41] Further screening of bioactivity revealed growth inhibition of L1210 cells (Mouse lymphocytic leukemia cell line), even using the impure broth. Purification and analysis revealed ((2*S*)-Amino((5*S*)-3-chloro-4,5-dihydro-1,2-oxazol-5-yl)ethanoic acid, later named acivicin, as the active compound.[42] Acivicin belongs to the class of non canonical amino acids and bears an electrophilic chlorodihydroisoxazole moiety that is unique among natural products. Acivicin showed inhibition of several glutamine dependent enzymes and is therefore considered a glutamine antimetabolite.[43]

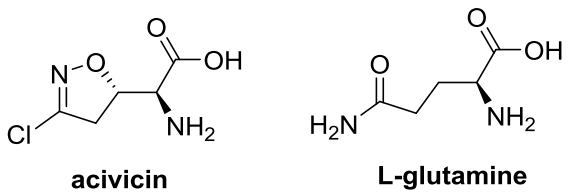

Figure 3. Acivicin and l-glutamine.

Target identification revealed a variety of enzymes including some, but not all, glutamine amidotransferases, CTP synthetase, anthranilate and glutamate synthetase, GMP synthetase, carbamoylphosphate synthetase II, FGAM synthetase and γ-glutamyltranspeptidase.[44-51] Several of these enzymes play important roles in purine and pyrimidine metabolism (see figure 4). Upon treatment with acivicin, intracellular uridine triphosphate concentrations increase while cytosine triphosphate and guanosine triphosphate levels decrease, with no significant change in adenosine triphosphate and inosine triphosphate levels.[46] These results confirm the effect of the inhibition on enzymes involved in the purine and pyrimidine metabolism. Further studies showing that exogenous administration of these nucleotides reverses the cytotoxic effect of acivicin and that blocking the nucleoside uptake by

dipyridamole restores the cytotoxic effect of acivicin, led to the conclusion that inhibition of purine and pyrimidine metabolism is the mode of action.[43, 52-55]

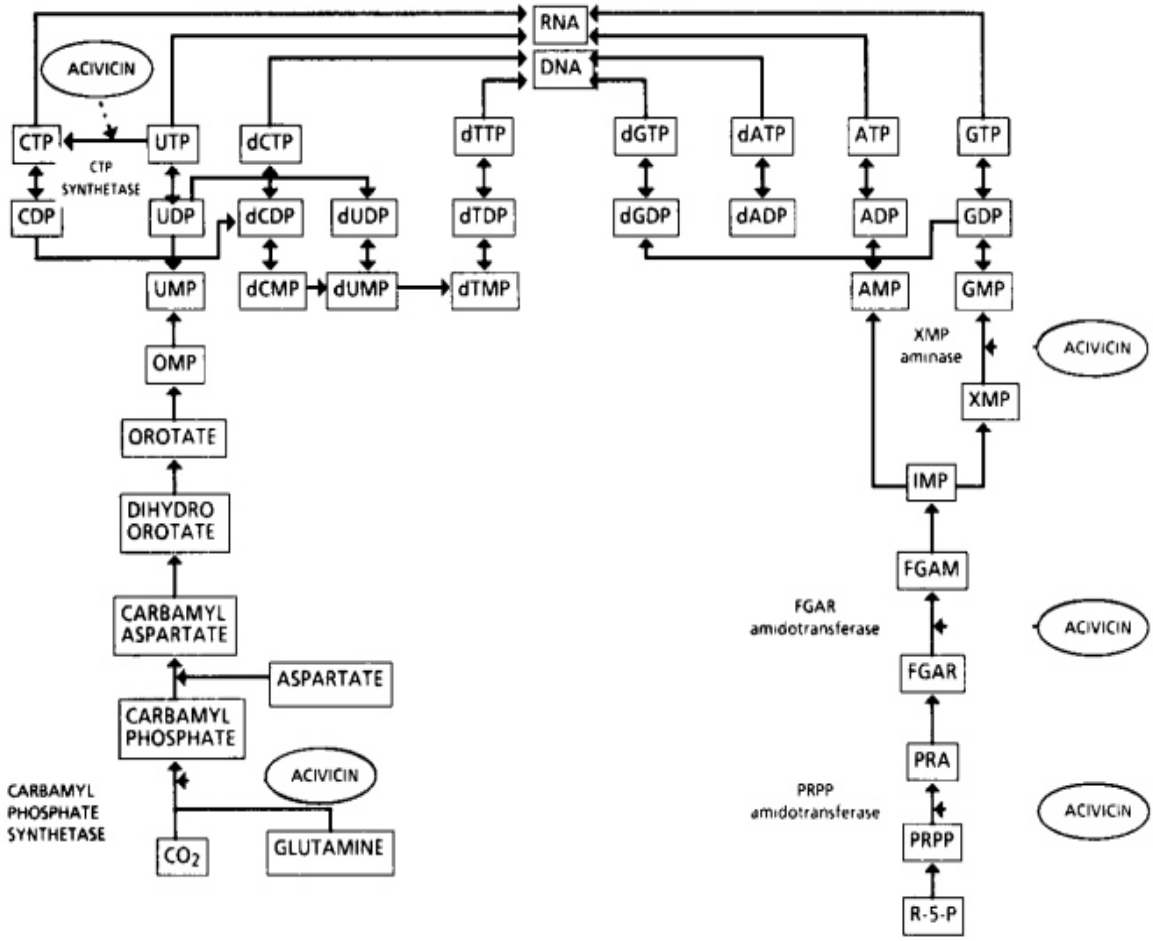

Figure 4. Biochemical pattern of enzyme inhibition by acivicin (reprinted from [43], with permission from Elsevier).

Aside from enzymes involved in purine and pyrimidine metabolism, acivicin showed inhibition of γ-glutamyltranspeptidase, an enzyme important for glutathione metabolism and in amino acid transport. Co-crystallization of ACV with bacterial γ-glutamyltranspeptidase (gGT) revealed the binding mode.[56-58] However, for the inhibition of bovine gGT an inhibition constant of 0.3 mM was observed and for full inactivation of the human enzyme, a concentration of 0.45 mM was necessary, both values that exceed clinically achievable levels and also above the clinically-relevant concentrations of acivicin (5-50 µM).[44, 59, 60] Moreover, no significant gGT dependent response could be obtained in a cellular apoptosis model.[61] This findings suggest that gGT inhibition is unlikely to be the mechanism behind the antitumor effect. However, acivicin is still advertised as a gGT inhibitor.

Acivicin was subject to several clinical trials during the 1980s and 1990s, which investigated its use for treatment of a variety of cancers including lung cancer, colorectal cancer, astrocytoma, hepatocellular carcinoma glioblastoma and breast cancer, where acivicin was used either alone for treatment or in combination with other chemotherapeutics like doxorubicin and cisplatin. However, none of these trials proceeded beyond phase 2 because of prominent negative side effects.[62-70] The side effects ranged from neurotoxic effects like lethargy, fatigue, disorientation, depression, headaches to severe neurotoxic effects like hallucinations, anxiety, paranoia or amnesia (at higher concentrations) and gastrointestinal side effects like nausea, vomiting, diarrhea and stomatitis.[43] This resulted in a decrease in research into this natural product.

However recent research into acivicin as a possible treatment of the African sleeping sickness caused by the parasite *Trypanosoma brucei* showed promising results and raised new interest in the compound. The inhibition of human CTP synthetase by acivicin made it a candidate that could be used to also inhibit the CTP synthetase of *Trypanosoma brucei,* a proposed drug target.[71] Treatment of infected mice with acivicin inhibited CTP-synthetase and reduced *Trypanosoma brucei* proliferation.[72] The inhibitory effect of acivicin on CTP-synthetase of *Trypanosoma brucei* could be increased by exchanging the chlorine for bromine resulting in a 12 fold increase in inhibition.[73]

Another study on acivicin which focused on the electrophile and its reactivity revealed new facts. In this work the chlorodihydroisoxazole moiety and the exchange of chlorine for bromine inspired a set of ABPs that were studied in *Bacillus subtilis* and revealed that a diverse set of aldehyde dehydrogenases were their preferred targets.[74] These findings were new because no link between acivicin and aldehyde dehydrogenases had previously been reported. This opened a possible new area of acivicin research.

2.1.2 Aldehyde Dehydrogenases

Aldehyde dehydrogenases describe a group of enzymes involved in conversion of aldehydes to the corresponding carboxylic acids using the cofactors NAD and NADP. In cells, aldehydes are generated during several physiological processes such as lipid peroxidation, glycolysis, amino acid catablolism and metabolism of several neurotransmitters (GABA, serotonine, adrenaline, noradrenaline and dopamine).[75-80] Apart from the aldehydes that are produced during metabolism, there are also aldehydes derived exogenously: xenobiotics and drugs, e.g.

alcohol that is converted to acetaldehyde or cyclophosphamide, or isofosfamide that generates acrolein. Other sources of aldehydes are smog, cigarette smoke or exhaust fumes. Aldehydes posses strong electrophilic properties and are highly reactive towards several cellular targets like glutathione, nucleic acids and protein amino acids leading to enzyme inactivation, cellular homeostasis or even DNA damage.[81-83] While some aldehydes like retinal play important roles in physiological processes, many aldehydes demand careful regulation and detoxification because of their cytotoxicity and carcinogenicity.

This task is fulfilled by the aldehyde dehydrogenase superfamily that can be found in nearly all organisms. Apart from their protective roles in oxidizing cytotoxic aldehydes, there are additional functions of aldehyde dehydrogenases reported, such as binding of small molecules and hormones, production of NAD(P)H, UV light absorption and scavenging of hydroxyl radicals.[84-88] Mutation in certain enzymes leading to loss of function are associated with several diseases. This superfamily consist of several families with subfamilies containing multiple isoforms and can be found in several subcellular locations, including the cytosol, nucleus, mitochondria and endoplasmatic reticulum.[89, 90] Their distribution in organs and tissue as well as their expression levels vary depending on the enzyme family and subfamily.[80] All of them are reported to use aldehydes as substrates. A proposed mechanism (see figure 5) begins with the activation of a nucleophilic cysteine through deprotonation after cofactor binding; this activated thiol forms a hemithioacetal by attacking the aldehyde carbonyl.[91-93] An asparagine stabilizes the oxyanion, facilitating the hydrogen transfer to the cofactor $NAD(P)^+$, resulting in an *S*-thiocarbamate. This is hydrolyzed by a water molecule and the resulting carboxylic acid and $NAD(P)H/H^+$ are released. Binding of the cofactor initiates activation of the cysteine by deprotonation and a new cycle starts again.[94]

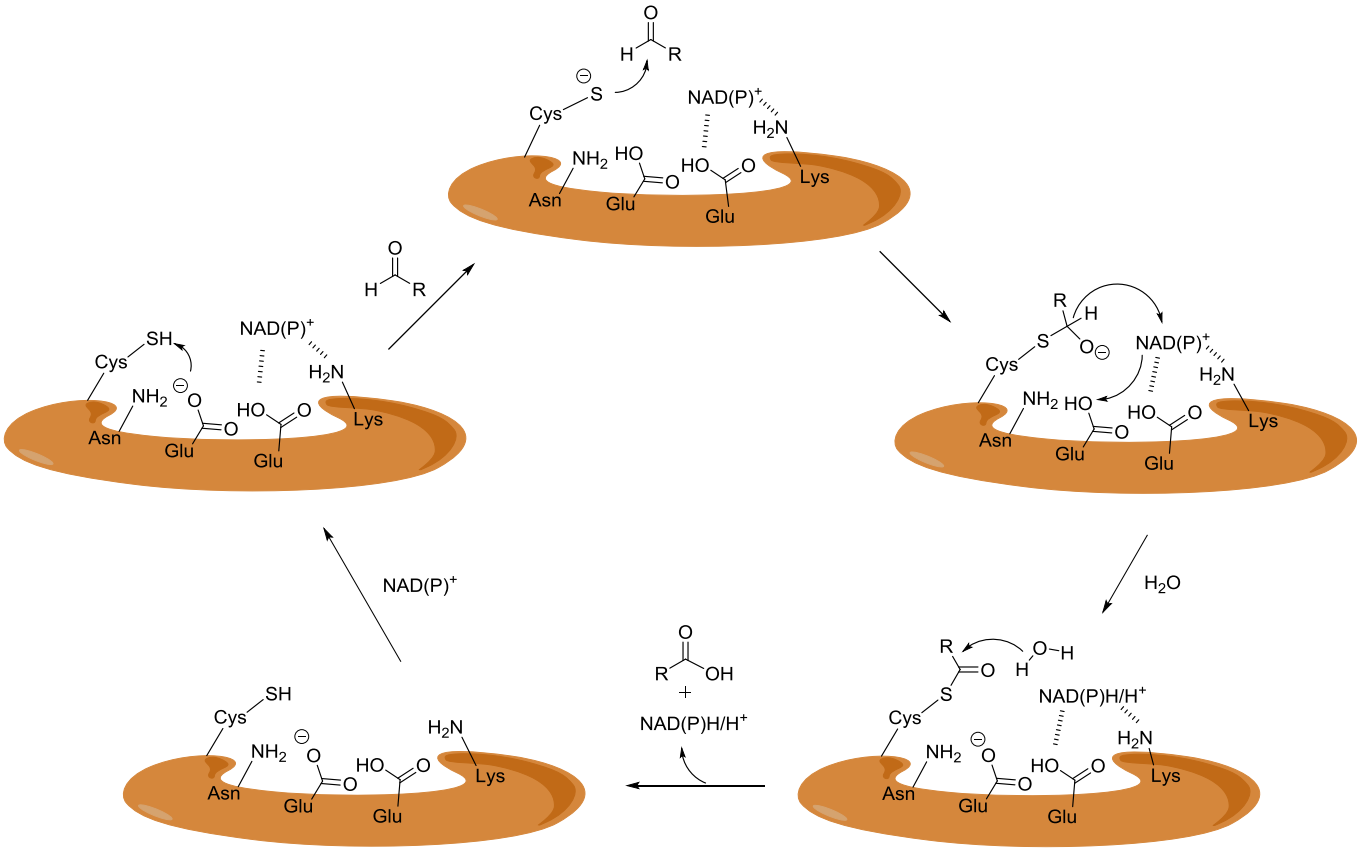

Figure 5. Mechanism of aldehyde dehydrogenases mediated oxidation of an aldehyde to a carboxylic acid. After binding of the cofactor NAD(P)+ the cysteine is activated and forms a hemithioacetal with the aldehyde. A hydrogen transfer to the cofactor forms an *S*-thiocarbamate which is hydrolyzed by a water molecule, releasing NAD(P)H/H+ and the carboxylic acid. Upon binding of a new cofactor the cycle can start again.

To date, there are 19 putative functional genes known for human aldehyde dehydrogenases, which can be clustered in 11 families and 4 subfamilies with specific functions.[95, 96] This allows a classification and systematic nomenclature of enzymes of this superfamily.

Family	Gene	Location	Substrates
ALDH1	ALDH1A1	Cytosol	Retinal, acetaldehyde, lipidperoxidation derived aldehydes
	ALDH1A2	Cytosol	Retinal
	ALDH1A3	Cytosol	Retinal
	ALDH1A7	Cytosol	Retinal
	ALDH1B1	Mitochondria	Acetaldehyde, lipidperoxidation derived aldehydes
	ALDH1L1	Cytosol	10-Formyltetrahydrofolate
	ALDH1L2	Cytosol	Unknown
ALDH2	ALDH2	Mitochondria	Acetaldehyde, nitroglycerin
ALDH3	ALDH3A1	Cytosol, nucleus	Medium-chain aliphatic aldehydes, aromatic aldehydes
	ALDH3A2	Microsomes, peroxisomes	Long-chain aliphatic aldehydes
	ALDH3B1	Mitochondria	Lipidperoxidation derived aldehydes
	ALDH3B2	Mitochondria	Unknown
ALDH4	ALDH4A1	Mitochondria	Pyrroline-5-carboxylate
ALDH5	ALDH5A1	Mitochondria	Succinic semialdehyde
ALDH6	ALDH6A1	Mitochondria	Methylmalonate semialdehyde
ALDH7	ALDH7A1	Mitochondria, cytosol	Betaine aldehyde, lipidperoxidation derived aldehydes
ALDH8	ALDH8A1	Cytosol	Retinal
ALDH9	ALDH9A1	Cytosol	γ-Aminobutyraldehyde, aminoaldehydes
ALDH16	ALDH16A1	Unknown	Unknown
ALDH18	ALDH18A1	Mitochondria	Glutamic γ-semialdehyde

Table 1. Human ALDHs divided up in families with location and major known substrates.[89, 90]

Aldehyde dehydrogenases have a broad spectrum of biological activity ranging from metabolism of important signal molecules to protection from toxic substances. ALDHs are of major importance in cancer research. Cancer stem cells show high aldehyde dehydrogenase activity. ALDH1A1 in particular was regarded as a significant marker for cancer stem cells.[97-99] But more studies revealed additional dehydrogenases to be highly active in cancer stem cells, including ALDH1A2, ALDH1A3, ALDH1A7, ALDH2, ALDH3A1, ALDH4A1, ALDH5A1, ALDH6A1 and ALDH9A1.[98, 100] To date ALDH1A1 and ALDH3A1 are explicit cancer stem cell markers. High expression of aldehyde dehydrogenases is linked to enhanced population function and resistance to cytotoxic drugs; these features make aldehyde dehydrogenases interesting candidates for cancer research.

2.1.3 Aim of this Study

ABPP studies in bacteria with acivicin inspired probes revealed a set of aldehyde dehydrogenases as preferred targets. However no studies on human proteome with these probes has yet been done nor has the target preference of acivicin for aldehyde

dehydrogenases been studied. The scope of this work was to conduct ABPP studies on human/rodent proteome with the already reported probes as well as new probes, directly synthesized from acivicin. All probes were compared with acivicin in terms of bioactivity, target preference and target enzyme inhibition. New target enzymes of acivicin were further investigated for their role in antitumor activity.

2.2 Results and Discussion

2.2.1 Acivicin Based Probes

To convert the compound of interest into an activity-based probe (ABP) it is necessary to attach an alkyne tag. This alkyne tag is needed for further functionalization via click-chemistry. Although in need, this incorporation bares the disadvantage of changing the structure of the compound and comes with a possible loss or change of the biological activity or target specificity.

Acivicin offers two possibilities for an attachment of an alkyne tag, the amine and the carboxyl group. The amine was converted to the amide using the *N*-hydroxy-succinimid ester of hexynoic acid, to give ACV1.

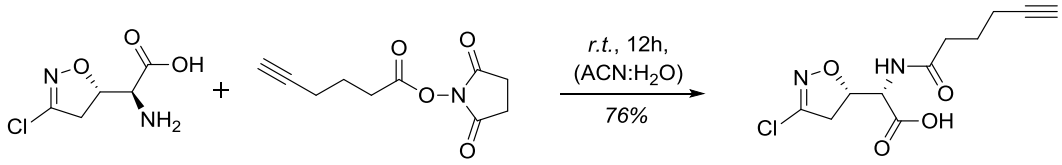

Scheme 1.Synthesis of ACV1.

The reaction gave a clean product after HPLC purification in good yield (78 %). To attach an alkyne handle to the carboxyl group a direct coupling of propargylamine with various coupling reagents (EDC and HOBt, HATU and HOBt) resulted in a mixture of acivicin functionalized with propargylamine (ACV2) and acivicin dimers.

An alternative strategy was to protect the amine at first with a Boc-group and subsequently couple the propargylamine using peptide coupling reagents, followed by deprotection of the Boc-group. For the coupling, COMU combined with Oxyma Pure, HATU and Pybop that were combined with HOBt were tested. COMU together with Oxyma Pure gave the best results in terms of yield and purification. The boc-protected ACV2 was deprotected with TFA and purified by HPLC again to give the probe ACV2 in a medium overall yield (59 %).

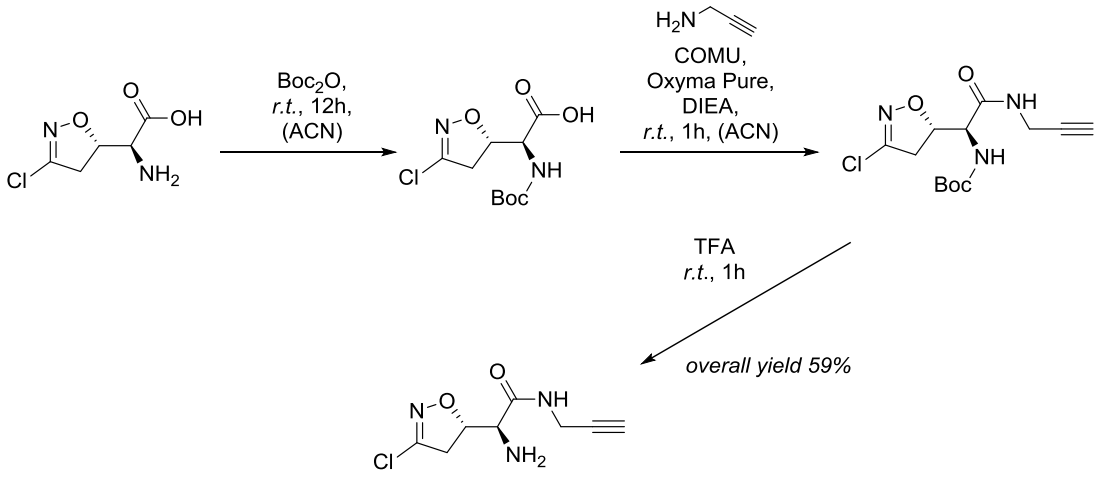

Scheme 2. Synthesis of ACV2.

For further characterization of an electrophilic natural product, it is possible to take solely the electrophile and attach an alkyne tag. This electrophile can be decorated with different residues. An additional possibility for acivicin is the exchange the chlorine of the chlorodihydroisoxazole by bromine and thereby enhance the reactivity. This was employed to acivicin and a better inhibition of CTP-synthase of *Trypanosoma brucei* was achieved.[73] A library of bromodihydroisoxazole probes was synthesized by *Dr. Ronald Frohnapfel* prior to this work.[74] The synthesis starts with the formation of glyoxylic acid aldoxime from glyoxylic acid and hydroxylamine. With bromine, the glyoxylic acid aldoxime formed dibromoformaldoxime that gave the dihydrobromoisoxazole via a dipolar cycloaddition with allylalcohol. By varying the alkene, different residues can be incorporated (e.g. buten-1-ol). The last step is an ester bond formation with hexynoic acid chloride to attach the alkyne tag.

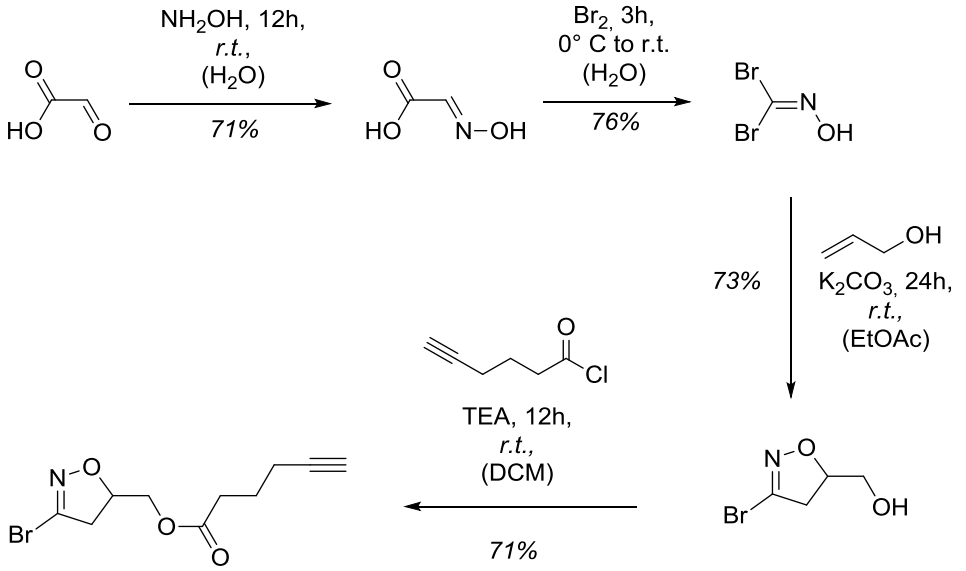

Scheme 3. Synthesis route for ACV1.

With the probes of these synthesis (ACVL series) and the two natural product derived probes ACV1/-2) a broad library halodihydroisoxazole probes was established.

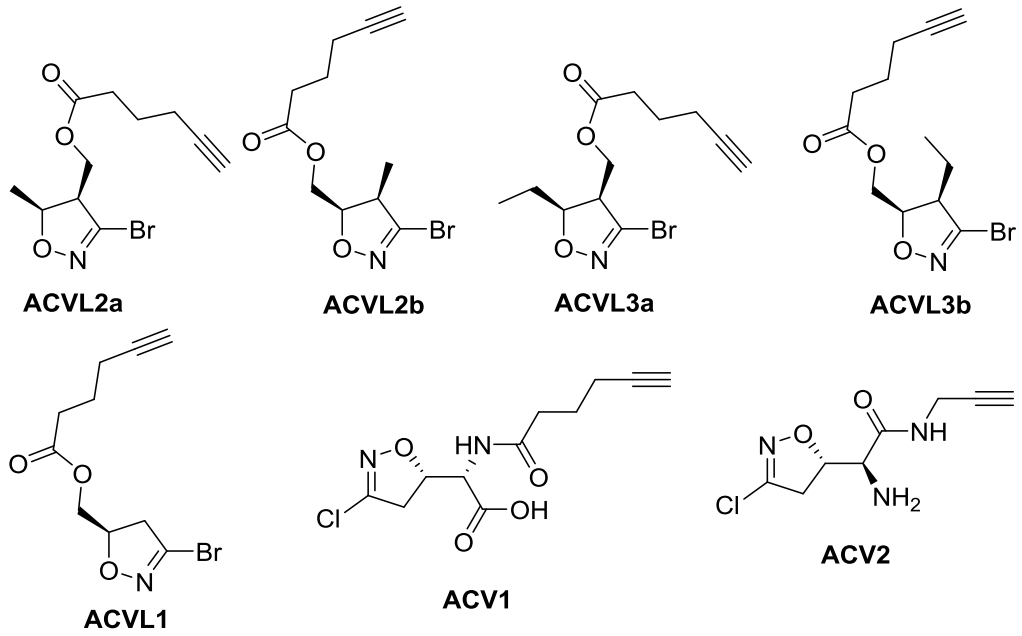

Figure 6. Probe library of acivicin inspired probes and probes obtained from the natural product.

The probe library contains five probes containing bromodihydroisoxazole as an electrophilic unit. The bromodihydroisoxazole moiety is decorated with methyl, ethyl or no substituent. The two regio isomers with methyl and ethyl substituents were also members of this library. Two probes were derived directly from modifying the natural product carrying a chlorodihydroisoxazole as electrophilic moiety.

2.2.2 Bioactivity of Acivicin and Probes

After the successful synthesis of the probes, the next step was to characterize the bioactivity of probes compared to the corresponding natural product. For this purpose an assay monitoring cell growth was performed. In this assay crystal violet is used to stain cells after cell fixation on their growth surface. Crystal violet is a histological stain that is used to stain all kind of cells and it can also be used to stain Gram positive bacteria.

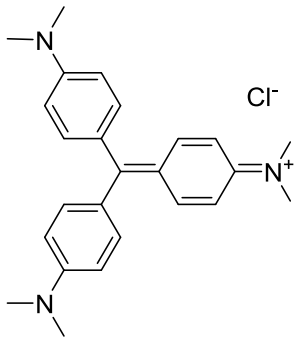

Figure 7. Crystal violet.

After staining the cells are lysed and the attached crystal violet is dissolved and can be measured by absorption spectroscopy.

For this purpose the cell line HepG2, a hepatocellular carcinoma cell line of human origin, was chosen to compare the experimental data from literature of the bioactivity study of acivicin on rat hepatoma cells.[48] HepG2 cells were incubated with various concentrations of acivicin, ACVL1, ACVL2a, ACVL2b, ACV1 and ACV2 for up to five days, with determining the crystal violet intensity after each day. By plotting the intensity over time, cell growth was monitored.

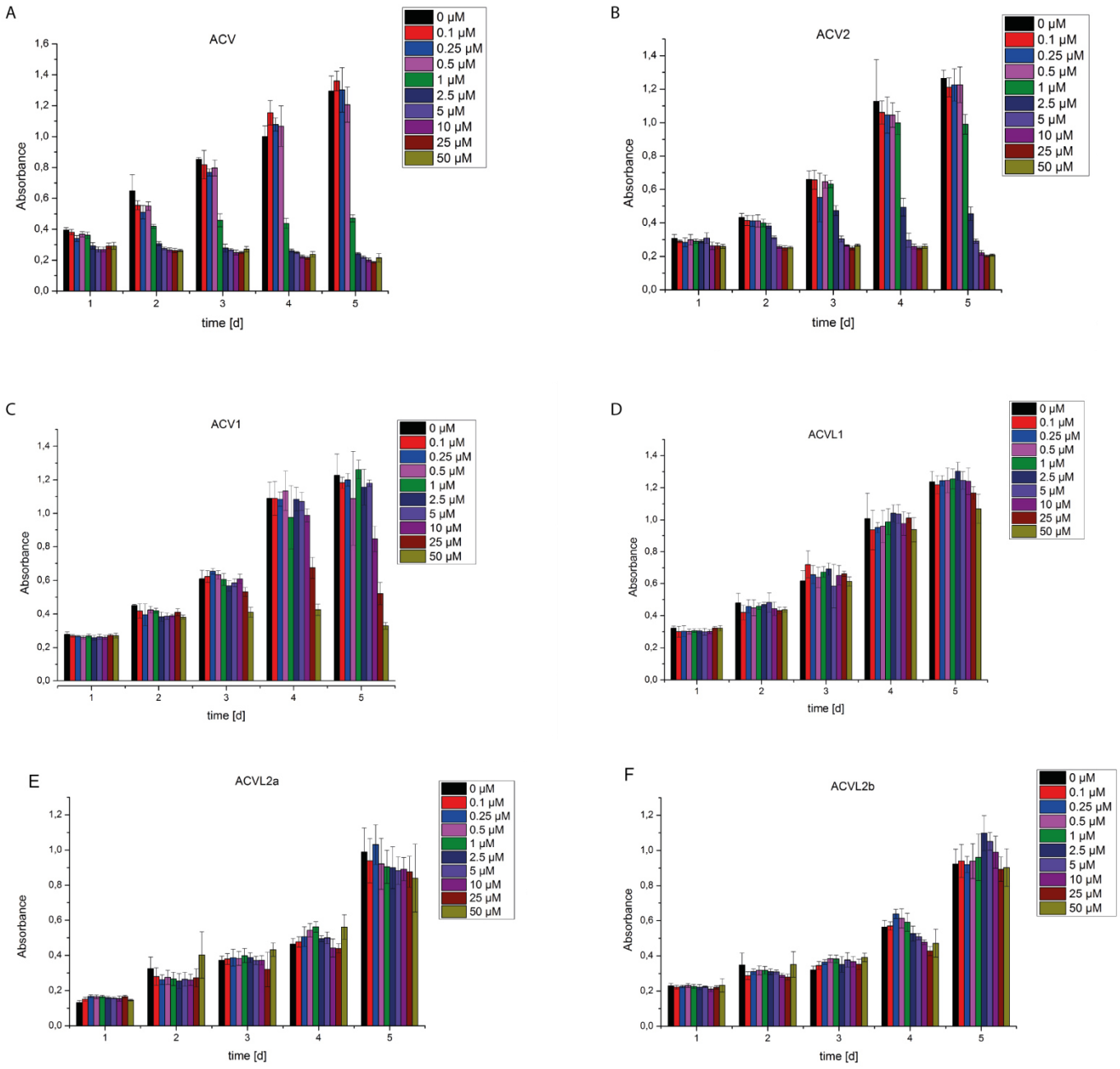

Figure 8. Growth curves of HepG2 cells with incubation of acv and acv library probes for 5 days at various concentrations. Error bars represent standard deviation of the mean form quintuplicates. Experiments were carried in at least two independent trials (figure adapted from[101] - reproduced by permission of The Royal Society of Chemistry)

The growth curves show no growth inhibition for the ACVL-series (1, 2a, 2b). For acivicin and ACV2 growth inhibition can be observed for concentrations down to 5 µM and for acivicin down to 2.5 µM. The values for ACV2 and acivicin are quite close indicating a similar potency towards cancer cells. For ACV1 an inhibition was also observed but at higher concentrations with growth inhibition starting at a concentration of 25 µM ACV1.

This assay also gives the possibility to determine EC_{50} values for each day of incubation. Therefore absorptions for each concentration are set relative to the DMSO control and plotted against the concentration on a logarithmic scale. A sigmoidal curve is fitted and EC_{50} values are determined from this curve.

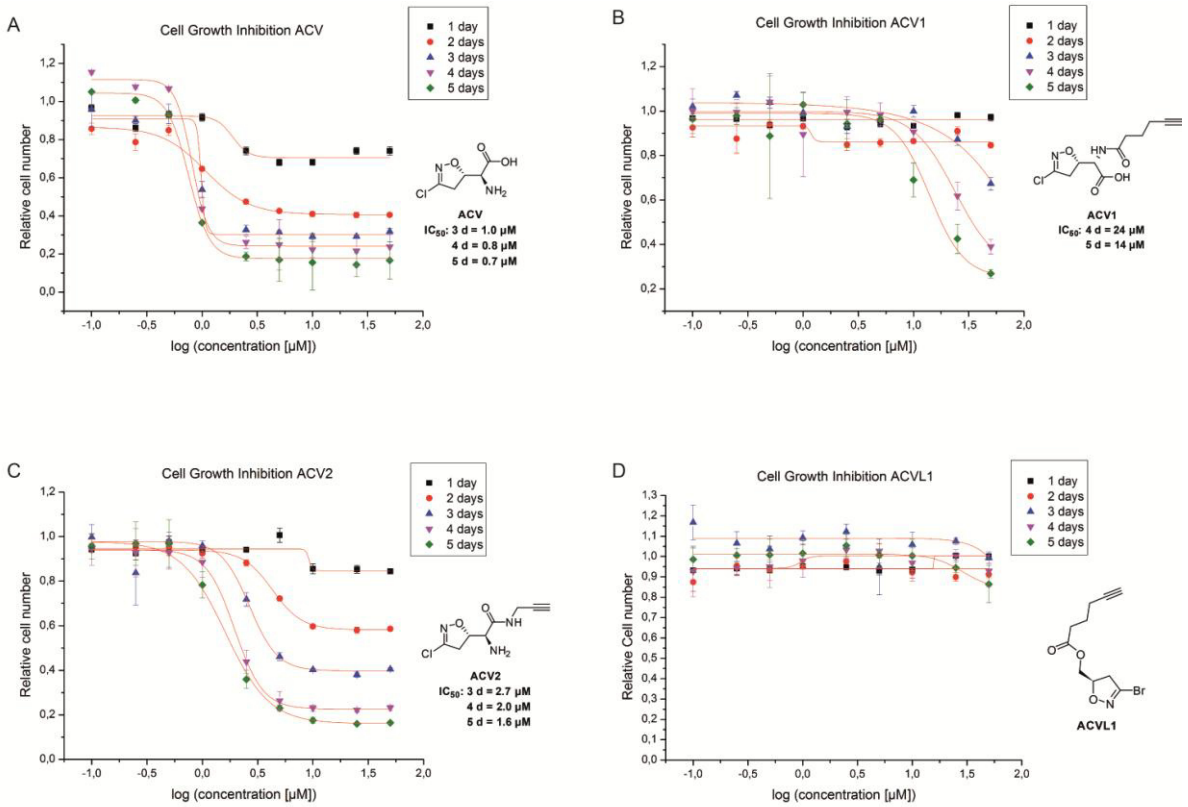

Figure 9. Growth assay curves plotted for each day of acv and probe library on HepG2 cells to determine the EC_{50} for each day upon incubation. Error bars display standard deviation of the mean from quintuplicates and measurements were carried out in at least two biological replicates (figure taken from [101] - reproduced by permission of The Royal Society of Chemistry).

While for the ACVL series no EC_{50} values were obtained, the EC_{50} values decreased over time for acivicin, ACV1 and ACV2. ACV1 reduced cellular growth after five days with an EC_{50} of 14 µM (Figure 2). ACV2 already inhibited cell growth with significant effects after two days. The EC_{50} after five days decreased to 1.6 µM which is about 2-fold above the EC_{50} of the natural product acivicin (0.7 µM). This result is in agreement with the IC_{50} reported for ACV on rat hepatoma cells (0.5 µM after 7 days).[52]

An interesting point was that acivicin, as well as ACV1 and ACV2, needed a certain amount of time to develop their anticancer potential. This in agreement to reported results from rat hepatoma cells, were upon the third day of incubation an effect was visible. This could be due

to the fact that acivicin and presumably ACV1 and ACV2 compete with amino acids for cellular uptake via transporters.[102, 103]

2.2.3 Target Identification of Acivicin Probes

After characterization of the bioactivity, the next step was to identify the protein targets of each probe. The ABPP approach was used for this task with mass spectrometrical identification. In a first attempt mouse liver was investigated with acivicin probes. In the next step HepG2 cells followed as a system for target identification.

2.2.3.1 Target Identification in Mouse liver

The liver is the organ where drug metabolism and detoxification takes place. It provides high amounts of enzymes from the cytochrome P450 superfamily, several proteases and dehydrogenases and it also represents a good system to compare the results obtained from the study on rat hepatoma cells.

Before the pull down was carried out the optimal concentration for the labeling had to be determined. Therefore mouse liver lysate was incubated with increasing concentrations for 1 h at room temperature and afterwards rhodamine azide was attached by click-chemistry. The lysate was separated by SDS-PAGE and analyzed by fluorescence scan.

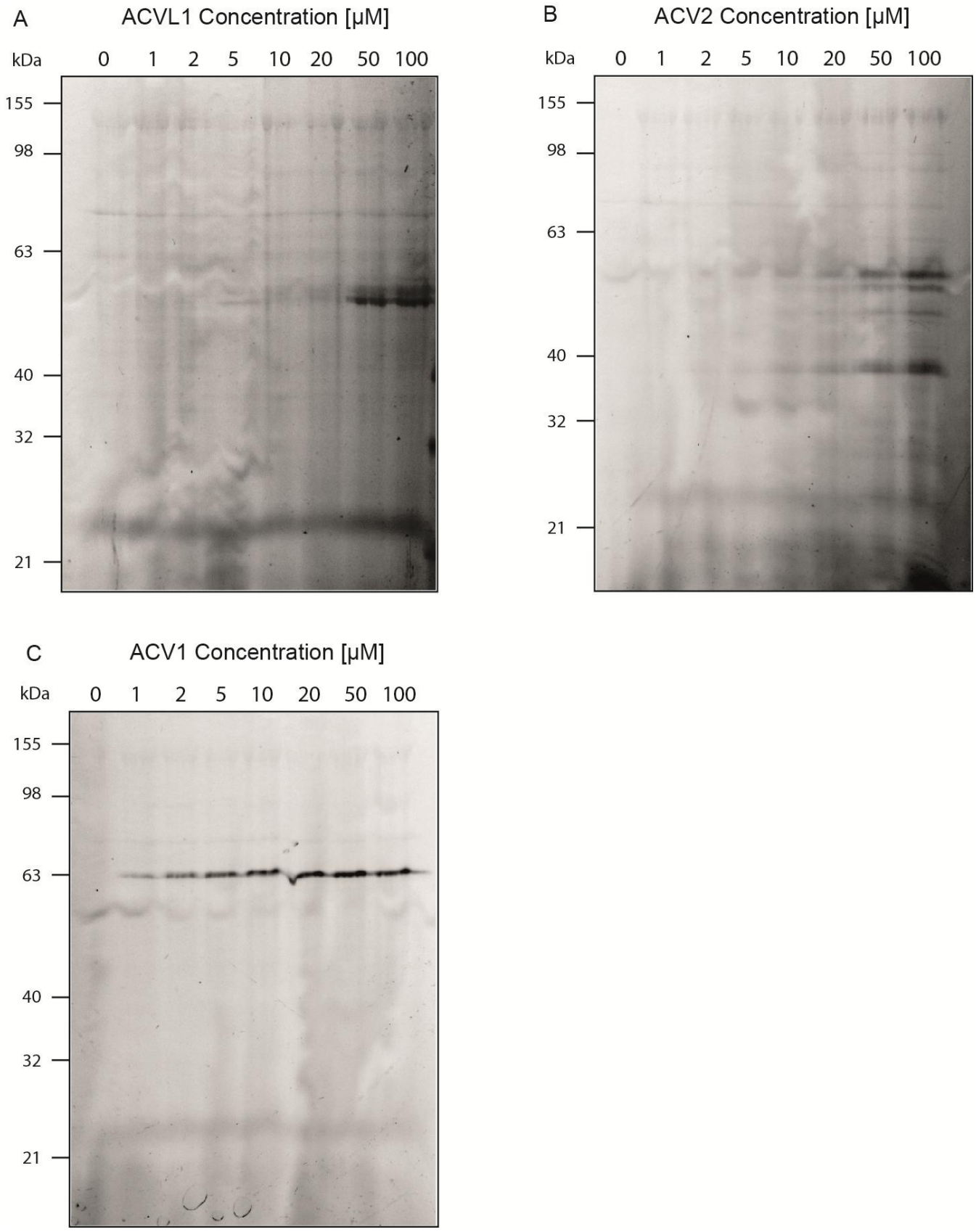

Figure 10. Fluorescence scan of an SDS-PAGE of mouse liver lysate incubated with acv-library probes at different concentrations for one hour and subsequent attachment of rhodamine azide via click chemistry (figure taken from [101] - reproduced by permission of The Royal Society of Chemistry).

For the labeling with the acivicin a very distinct labeling with low background probes in general was observed. For the ACVL-series a concentration of 50 µM gave good results, whereas the ACV1 probe a labeling at even lower concentrations of 5 µM was visible, with saturation of the signal at 10 µM. The labeling of ACV2 however was weaker and a concentration of 100 µM was necessary to observe a clean labeling.

With the optimal concentration established, the acivicin probe library was incubated with mouse liver lysate to compare the labeling pattern of the probe library. The proteins were again analyzed after attachment of rhodamine azide by SDS-PAGE and a fluorescence scan.

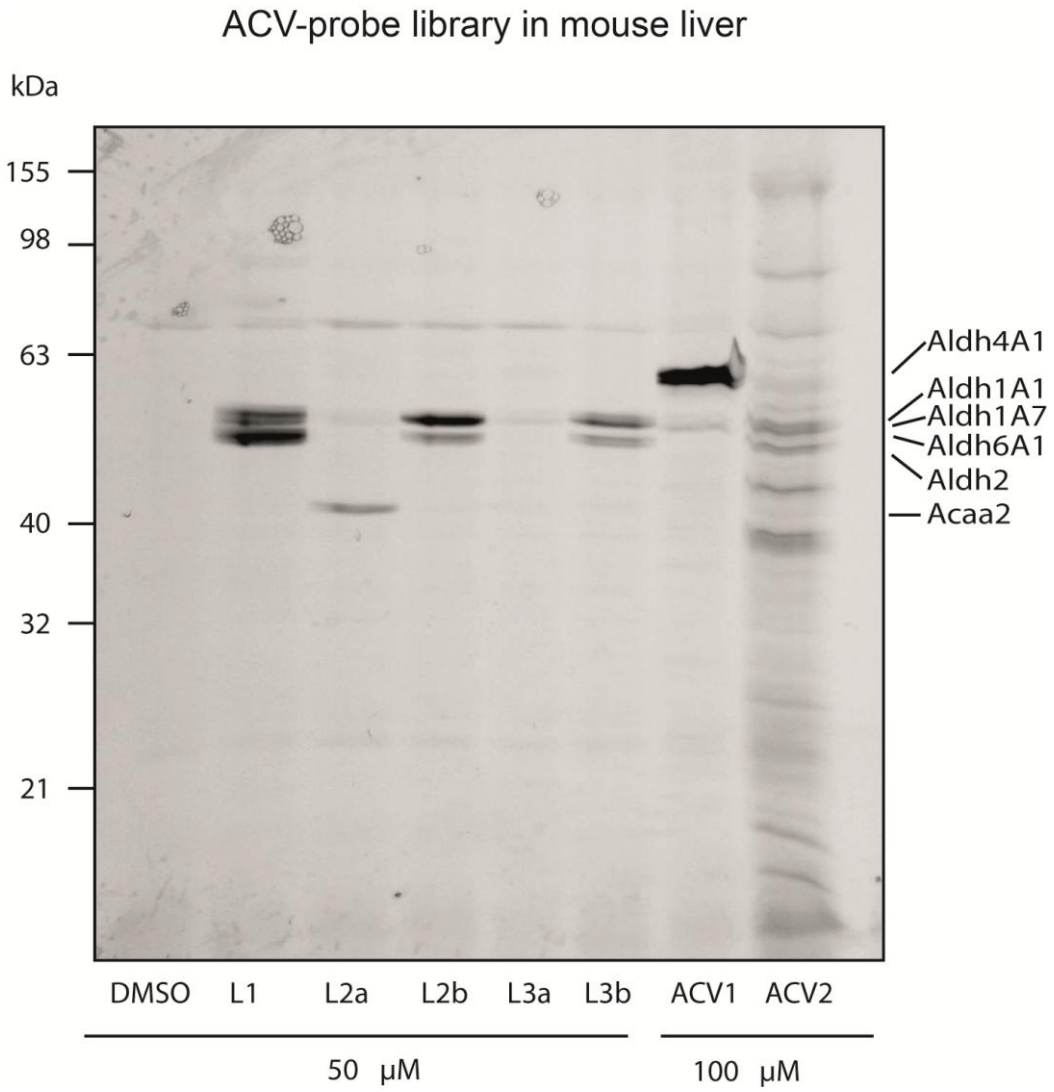

Figure 11. Fluorescence scan of mouse liver lysates incubated with acv-probe library at optimal concentrations (figure taken from [101] - reproduced by permission of The Royal Society of Chemistry).

Comparing the probes by their labeling pattern it was observed that the probes ACVL1, ACVL2b, ACVL3b showed a preference for three bands in the region of ~55 kDa as well as

the ACV2. For the regioisomers ACVL2a,-3a a preference for a band at ~40 kDa was visible. A decreasing labeling intensity from ACVL1 to ACVL3b at the same concentration was observed. This might result from residues getting bigger and therefore bulkier to access the active site. While ACVL1, beside the ester group connecting the hexynoic acid to the ring, had no substituent on the ring, ACVL2a/-2b carried additionally a methyl group and ACVL3a/-3b an ethyl group. These findings agreed with the findings from studies made in bacteria [74]. ACV1 showed labeling of one band (~65 kDa), that differed from the labeling pattern of the other probes of the library.

In the next step, the targeted proteins were identified by mass spectrometry. Therefore lysate was again incubated with probe but this time a trifunctional linker bearing a rhodamine and a biotin was attached by click-chemistry. With the biotin attached, the labeled proteins were enriched on avidin beads and afterwards analyzed by SDS-PAGE and fluorescence scan (see figure 2). The visualized bands were excised and underwent an in-gel digest for subsequent mass spectrometrical analysis following already established protocols.[104, 105] The peptides were separated via reversed phase chromatography prior to mass spectrometry.

The resulting peptides and the corresponding sequence, obtained through fragmentation methods CID (collision-induced dissociation) and HCD (higher-energy collisional dissociation), were searched against database proteome (in this case mus musculus (mouse) fasta file obtained from uniprot) using the SEQUEST algorithm and the software Thermo Proteome Discoverer. The SEQUEST algorithm correlates measured MS/MS spectra with theoretical peptides obtained from an *in silico* digest of the database proteome.[8] The confidence of the identity of a peptide can be quantified through a score that is calculated in two steps. Based on the length of a continuous y/b ion sequence identified from the measured spectrum, a preliminary score (*Sp*) is calculated. Through this process the top 500 peptides are selected for further calculation applying the correlation function. This function gives scores based on the presence of significant peaks from the measured spectrum corresponding to the expected y/b ion peaks in each theoretical spectrum in the database (see figure 12).[106, 107] The obtained peptides are then assigned to the corresponding proteins. Additional statistical values like the number of peptide-spectrum match (PSM) which displays the number of peptides identified in a search process strengthen the confidence as well as searches against decoy databases to eliminate false positive peptides.[108]

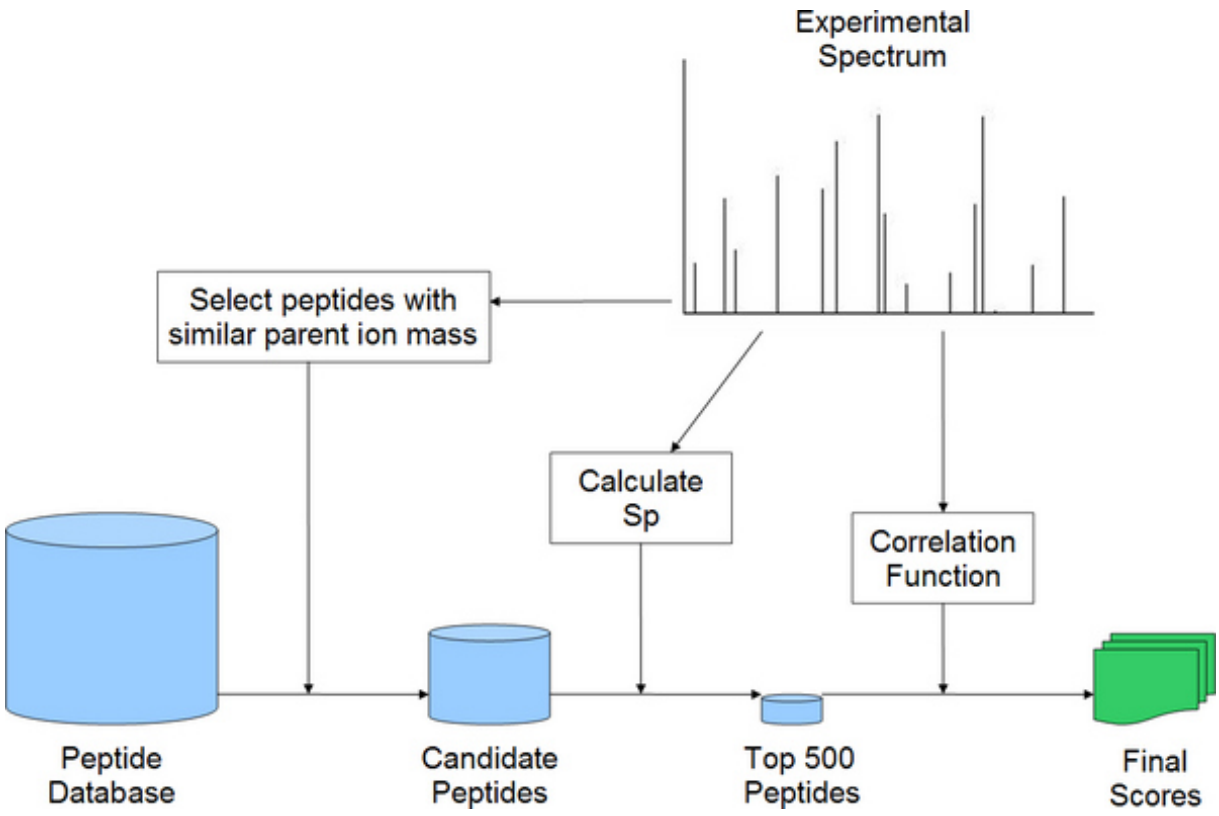

Figure 12. Simplified SEQUEST workflow (figure taken from [107]).

The SEQUEST algorithm identifies a lot of proteins, even with decoy database search applied. Especially high resolution mass spectrometers like orbitrap hybrid mass spectrometers combined with nano HPLC are very sensitive. E.g. one excised band from a pull down can, depending on the molecular weight and proteome, identify around 50 different proteins (with isoforms grouped for one protein hit). To identify the targeted protein or proteins of the probe the background proteins from each band must be eliminated. This was done by adding a control lacking the probe and therefore containing proteins binding unspecific to agarose or biotinylated proteins. In an ideal case the targeted proteins are identified only in the samples that was incubated with the probe and these targeted proteins are missing in the corresponding control that was incubated with the equal amount of DMSO. But as mass spectrometry is very sensitive and/or proteins can be high abundant, the characterization of the target only based on identification is not sufficient. Therefore a semi quantitative approach was applied by using the area of the precursor ions (peptide) that is determined from the area of the precursor ion from the ion chromatogram. The values for each peptide summed up give a value for the protein relative to the other proteins identified and quantified in the same sample. To determine an enrichment factor the area values of one protein from the probe sample and the control sample have to be set in relation by dividing the

area obtained from the sample incubated with probe (termed probe) by the area obtained from the control sample (termed DMSO).

$$Ratio = \frac{Area\ (Probe)}{Area\ (DMSO)}$$

Formula 1. Semi quantification based on determined areas from ion chromatogram.

A positive hit was considered by a ratio higher than 2 for a protein. These methods indentified for ACVL2b and ACVL3b and ACV2 three members of superfamily of aldehyde dehydrogenases, Aldh1A1, Aldh2 and Aldh3A1. ACV2 showed a less distinct labeling pattern and additional bands beside the ones similar to ACVL1, -2b and -3b. For these bands no protein hit could be obtained. Aldh1A1, Aldh2 and Aldh3A1 play major roles in detoxification of aldehydes and acetic aldehyde derived from alcohol, while Aldh3A1 and Aldh1a1 are additionally involved in cell differentiation and related to cancer resistance.[87, 109-112] ACV1 revealed Aldh4A1 as the band at ~60 kDa and Aldh6A1 as the weaker band at ~55 kDa. Both dehydrogenases are mitochondrial proteins and fulfill tasks in amino acid metabolisms.[113-115] The ACVL-series labeled dehydrogenases as it was expected from the studies in bacteria, but the newly synthesized probes ACV1 and ACV2 also showed labeling of aldehyde dehydrogenases. This indicates that this enzyme class could be the preferred target of the chloro-/bromodihydroisoxazole electrophile. As an exception to the general trend ACVL2a labeled the thiolase Acaa2 that is in agreement with results from bacterial studies. Acaa2 (3-ketoacyl-CoA thiolase, mitochondrial), describes a mitochondrial acetyltransferase that is involved in fatty acid metabolism.[116-118]

The results from the LC-MS runs gave clear results for each probe and with good enrichment factors (at least above 4).

Probe	Target	Accession	Description	Area				Probe (1)			Probe (2)			DMSO (1)			DMSO (2)			General information			(Area Probe)/(Area DMSO)	
				Probe (1)	Probe (2)	Control (1)	Control (2)	Score	# Peptides	# PSM	Score	# Peptides	# PSM	Score	# Peptides	# PSM	Score	# Peptides	# PSM	# AAs	MW [kDa]	Sequence coverage	(1)	(2)
ACVL2a	Acaa2	IPI00226430.2	3-ketoacyl-CoA thiolase, mitochondrial	5,741E8	8,408E8	0,000E0	1,965E8	133,1	15	38	67,6	9	21				34,6	7	10	397	41,8	56,4	100,00	4,28
ACVL2b	Aldh1A7	IPI00336362.2	Aldehyde dehydrogenase, cytosolic 1	9,488E8	3,334E8	7,571E7	6,715E7	44,4	11	15	31,3	8	11	21,5	2	6	7,0	2	2	501	54,6	39,7	12,53	4,97
	Aldh2	IPI00111218.1	Aldehyde dehydrogenase, mitochondrial	2,667E9	5,659E9	3,164E7	1,029E8	117,5	14	39	182,1	20	59	11,7	2	4	10,7	4	4	519	56,5	52,4	84,29	55,00
ACVL2b	Aldh1A1	IPI00626662.3	Retinal dehydrogenase 1	1,409E9	5,290E7	0,000E0	0,000E0	120,3	20	38	5,7	2	2							501	54,4	56,1	100,00	100,00
ACV1	Aldh4A1	IPI00928176.1	aldehyde dehydrogenase 4A1 precursor	1,893E9	1,655E9	4,052E8	3,589E8	130,7	13	40	153,4	14	49	83,6	14	25	97,8	14	29	562	61,8	39,7	4,67	4,61
ACV1	Aldh6A1	IPI00461964.3	Methylmalonate-semialdehyde dehydrogenase [acylating], mitochondrial	7,048E8	3,094E9	0,000E0	6,786E8	49,3	10	18	237,8	19	71				71,2	13	22	535	57,9	49,7	100,00	4,56
ACV2	Aldh1A1	IPI00626662.3	Retinal dehydrogenase 1	5,993E9		2,977E8		273,9	25	82				90,0	15	29				501	54,4	55,7	20,13	100,00

Table 2. MS hits of *in vitro* labeling of mouse liver with acivicin probes.

2.2.3.2 Target Identification in HepG2 Cells

After a successful target identification of acivicin probes in mouse liver, the next step was to investigate the target enzymes in living cells. For this purpose an *in situ* incubation of HepG2 cells with acivicin probes was carried out. HepG2 cells are derived from human hepatocellular carcinoma and therefore represent a good match with the *in vitro* labeling results of the mouse liver proteome and continued the studies of acivicin probes on the HepG2 cell line. This considers that a lysate never completely mimics a whole cell and labeling in living cells and lysate can differ.

For in situ labeling, the optimal concentration for each probe from the mouse liver labeling experiments were adjusted in PBS and the cells incubated for 2 h. After harvesting and lysis, the cells underwent the standard ABPP protocol. The analytical gel of the HepG2 labeling (figure 13) revealed a certain similarity with the *in vitro* labeling of the mouse liver lysate (figure 11). There was a preference of the ACVL1 and ACVL2b series for targets around the molecular weight of 55 kDa with ACV2 showing a weak labeling in this area. ACVL2a showed labeling at the lower molecular weight region around 40 kDa. For ACV1, a single pattern with one unique band at 60 kDa was observed again. Whereas for ACV2, labeling was more promiscuous.

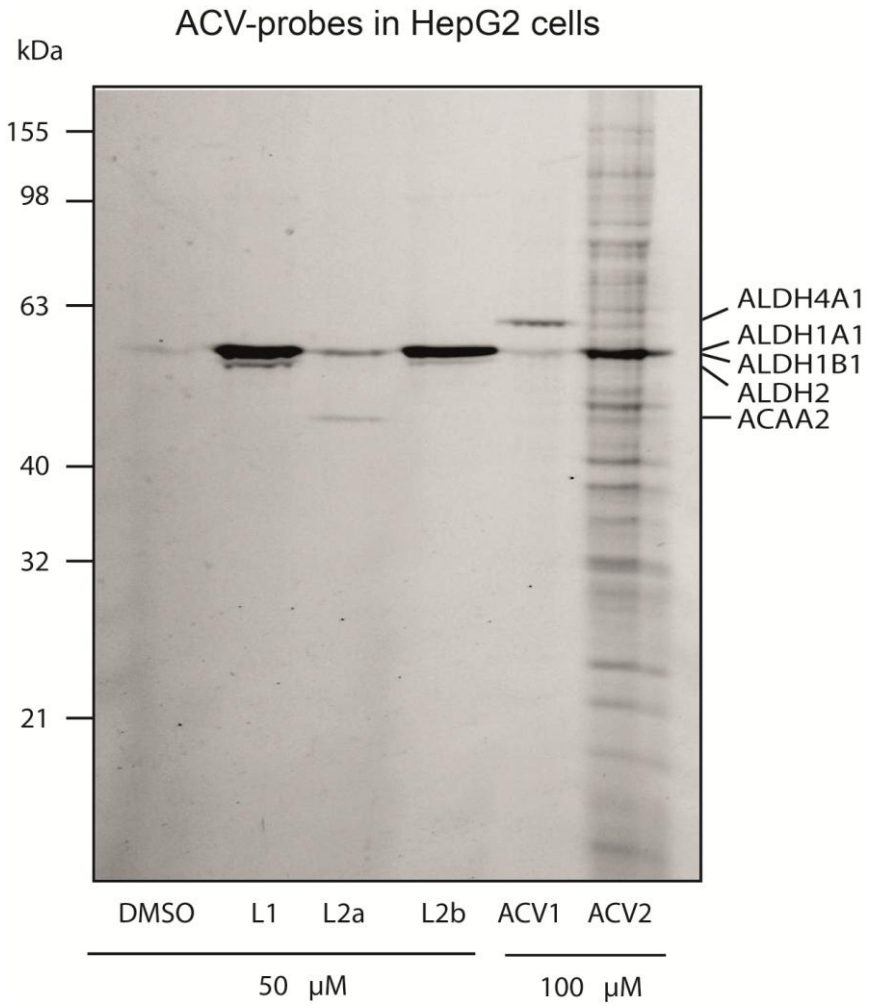

Figure 13. Fluorescence scan of HepG2 cells in situ labeled with acv probe library (figure taken from [101] - reproduced by permission of The Royal Society of Chemistry).

As labeling in PBS does not reflect physiological conditions, an *in situ* labeling of HepG2 with probes supplemented in media was additionally carried out. PBS could cause stress on cells and thereby effect the protein expression pattern. For the ACVL probe series this labeling procedure worked well using the same concentrations compared to PBS. But no labeling was observed for ACV1 and ACV2 under these conditions. Only an increase of the concentration from 100 µM to 200 µM, as well as extending the incubation time from 2 h to 3.5 h in conditioned media gave a labeling of comparable intensity. A possible reason could be again the uptake of these two probes by amino acid transporters and therefore competition with amino acids of high concentration (e.g. 2 mM for L-glutamine or 115 µM for L-arginine). The pattern observed in media was similar to that observed in PBS with preferences in the ~55 kDa area for ACVL1, -2b and ACV2. ACVL2a showed a band above 40 kDa and ACV1 a single band at 60 kDa (see figure 14). For ACV2 the labeling in this experiment was

less promiscuous but an additional band occurred weakly at the 60 kDa area, to which will be referred later.

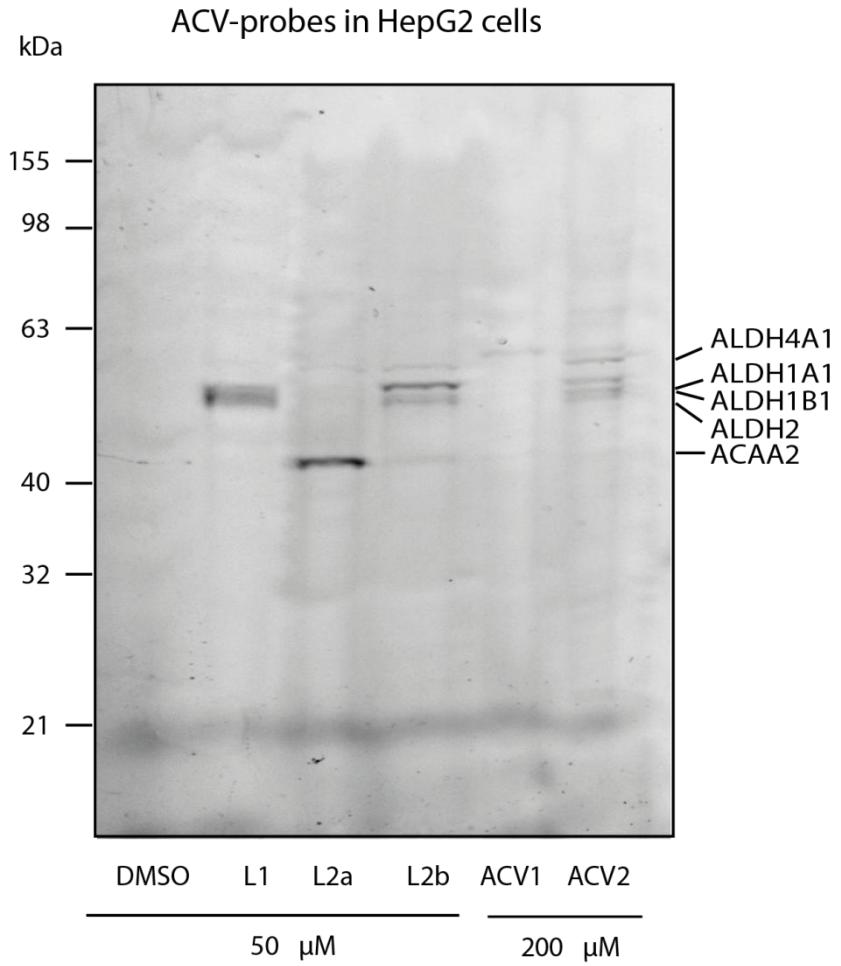

Figure 14. Fluorescence scan of in-situ labeling of HepG2 cells incubated with acivicin probes supplemented in conditioned media (figure taken from [101] - reproduced by permission of The Royal Society of Chemistry).

These results enabled a more sophisticated technique for confirmation of the identified targets. Studies on whole cells enable the use of stable isotope labeling (SILAC). This method allows direct quantification through mass spectrometric analysis. For this purpose, HepG2 cells were cultivated with media supplemented with lysine and arginine that are labeled with different isotopes and can be paired in up to three different categories (heavy, medium and light). These amino acids are incorporated in all proteins and allow to study different conditions of up to three cell lines next to each other based on relative quantification of the precursor peptides using mass spectrometry.[119] For implementation of SILAC in the ABPP workflow, cells labeled with "medium" amino acids served as DMSO control and "heavy" labeled cells were additionally labeled with probes. After lysis both lysates were combined and ABPP pull down was applied following mass spectrometry.

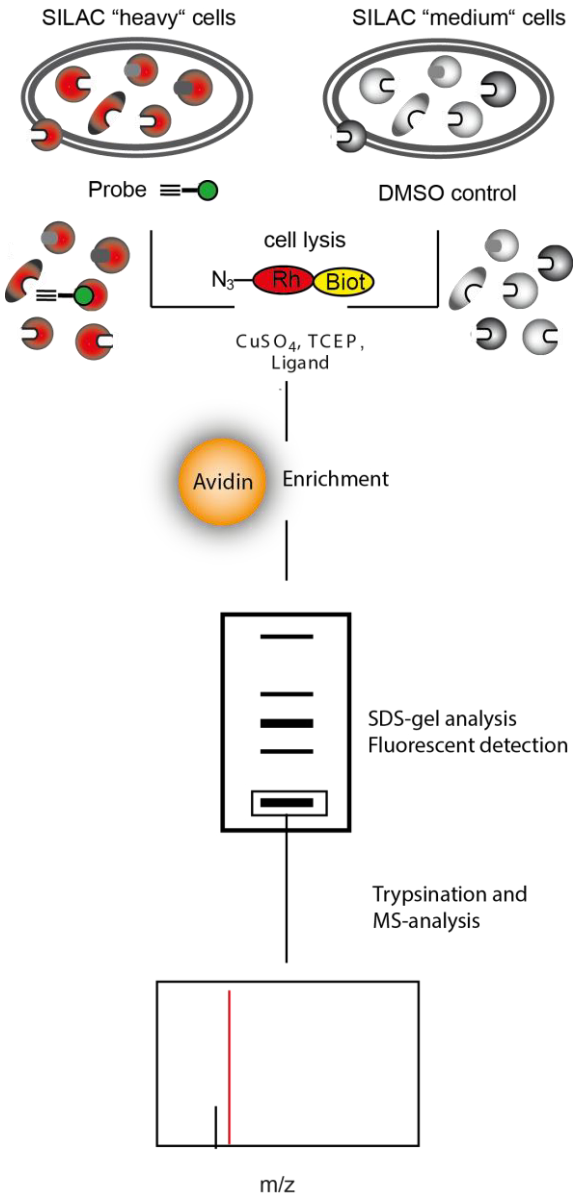

Figure 15. SILAC labeling implemented in ABPP workflow (figure adapted from [101] - reproduced by permission of The Royal Society of Chemistry).

A preparative approach using the trifunctional linker followed using the standard ABPP approach and the SILAC approach followed. The preparative analysis showed a good enrichment of the proteins and analysis of the bands on mass spectrometrical level revealed a quite similar targets compared to the results of the mouse liver lysate screening.

Probe	Target	Accession	Description	Area				Probe (1)			Probe (2)			DMSO (1)			DMSO (2)			General information			(Area Probe)/(Area DMSO)	
				Probe (1)	Probe (2)	Control (1)	Control (2)	Score	# Peptides	# PSM	Score	# Peptides	# PSM	Score	# Peptides	# PSM	Score	# Peptides	# PSM	# AAs	MW [kDa]	Sequence coverage	(1)	(2)
ACVL1	ALDH1A1	IPI00218914.5	Retinal dehydrogenase 1	2,042E9	1,136E10	0,000E0	5,380E7	419,2	29	132	652,5	28	208				12,9	4	4	501	54,8	74,7	100,00	211,15
ACVL1	ALDH1A1	IPI00218914.5	Retinal dehydrogenase 1	6,630E9	6,114E8	1,341E9	6,403E7	253,8	25	80	114,2	18	37	141,5	21	38	30,6	8	9	501	54,8	63,1	4,94	9,55
	ALDH2	IPI00006663.1	Aldehyde dehydrogenase, mitochondrial	1,571E10	1,546E9	4,902E8	3,117E8	916,4	28	284	315,7	22	97	107,1	17	31	148,6	20	45	517	56,3	62,5	32,05	4,96
	ALDH1B1	IPI00103467.5	Aldehyde dehydrogenase X, mitochondrial	1,701E10	4,413E8	4,268E8	0,000E0	989,6	23	294	86,9	10	25	90,2	12	25				517	57,2	44,9	39,85	100,00
ACVL2a	ACAA2	IPI00001539.8	3-ketoacyl-CoA thiolase, mitochondrial	1,286E9	2,400E8	6,163E8	0,000E0	126,7	12	33	100,6	14	26	48,8	11	13				397	41,9	60,7	2,09	100,00
ACVL2b	ALDH1A1	IPI00218914.5	Retinal dehydrogenase 1	8,747E8	3,903E9	6,403E7	1,341E9	176,2	25	54	220,1	26	65	30,6	8	9	141,5	21	38	501	54,8	73,1	13,66	2,91
	ALDH2	IPI00006663.1	Aldehyde dehydrogenase, mitochondrial	1,383E9	1,026E10	3,117E8	4,902E8	298,0	23	91	793,3	25	264	148,6	20	45	107,1	17	31	517	56,3	71,8	4,44	20,93
ACV1	ALDH4A1	IPI00217871.4	Delta-1-pyrroline-5-carboxylate dehydrogenase, mitochondrial	1,686E10	2,308E9	9,642E7	4,699E7	664,3	27	215	205,7	19	68	17,5	5	5	39,9	8	13	563	61,7	63,6	174,86	49,12
ACV2	ALDH1A1	IPI00218914.5	Retinal dehydrogenase 1	7,037E8		6,403E7		182,2	21	59				30,6	8	9				501	54,8	58,5	10,99	
ACV2	ALDH1A1	IPI00218914.5	Retinal dehydrogenase 1	7,037E8	2,824E9	3,536E8	5,380E7	182,2	21	59	136,9	18	39	120,4	18	38	12,9	4	4	501	54,8	61,5	1,99	52,49
	ALDH2	IPI00006663.1	Aldehyde dehydrogenase, mitochondrial	2,728E8	1,011E9	0,000E0	0,000E0	40,6	10	14	109,7	15	32							517	56,3	45,5	100,00	100,00

Table 3. MS hits from ABPP experiments of HepG2 cells incubated with acivicin probe library.

Probe	Target	Accession	Description	Ratio Probe / Control	General information		
					# AAs	MW [kDa]	Sequence coverage
ACVL1	ALDH1A1	IPI00218914.5	Retinal dehydrogenase 1	10,4	501	54,8	41,1
ACVL1	ALDH2	IPI00006663.1	Aldehyde dehydrogenase, mitochondrial	2,6	517	56,3	22,2
	ALDH1B1	IPI00103467.5	Aldehyde dehydrogenase X, mitochondrial	7,8	517	57,2	16,6
ACVL2b	ALDH1A1	IPI00218914.5	Retinal dehydrogenase 1	7,6	501	54,8	21,6
ACV1	ALDH4A1	IPI00217871.4	Delta-1-pyrroline-5-carboxylate dehydrogenase, mitochondrial	2,9	563	61,7	28,2
ACV2	ALDH1A1	IPI00218914.5	Retinal dehydrogenase 1	5,7	501	54,8	41,1

Table 4. MS hits from SILAC-ABPP of HepG2 cells incubated with acivicin probe library.

For ACVL1, ACVL2b and ACV2 the aldehyde dehydrogenases ALDH1A1 and ALDH2 were identified. ACVL1 and ACVL2b also identified ALDH1B1 as preferred target enzyme. For ACVL2a, ACAA2 was identified and for ACV1, ALDH4A1 turned out to be its target. Many enzymes represent homologues from the identified targets from mouse tissue.

The two identified members of the ALDH1 family are present in many tissues. In general, enzymes of this subfamily occur in cytosol, except ALDH1B1 which is a mitochondrial protein. For ALDH1A1 retinal is the major substrate and therefore this enzyme plays important roles in differentiation and development processes in retinoid depending tissues, e.g. neurons, and during embryonal development.[120-125] A decreased level of ALDH1A1 was observed in dopaminergic neurons of Parkinson's disease patients and in patients suffering from schizophrenia.[126, 127] Both enzymes ALDH1A1 and ALDH1B1 play an important role in defending oxidative stress by metabolizing lipid-peroxidation derived aldehydes.[128] Furthermore they play a key role in detoxifying acetaldehyde, that derived from ethanol and lower dehydrogenase activity is associated with higher alcohol sensitivity.[129-132] Another important fact is increasing drug resistance of tumor cells that is accompanied with high expression of ALDH1A1, as it was shown for ifosfamide and cyclophosphamide.[133, 134]

ALDH2, which represents the only enzyme of the ALDH2 family, is located in mitochondria and expressed in various tissues, including liver, heart, lung kidney and brain. The main role of this enzyme is detoxifying ethanol derived acetaldehyde by oxidizing it to acetic acid.[135] Less active mutants of this enzyme are described, with one resulting in an inactive mutant. This inactive mutant is common among people of Asian descent and leads to alcohol flush reaction upon consumption, because of accumulation of toxic acetaldehyde.[136, 137] Beside acetaldehyde conversion, ALDH2 shows also nitrate reductase activity and is needed to activate nitroglycerin, that is used for treating cardiac arrest or angina pectoris. Here again the inactive mutant leads to a less effective treatment.[138]

ALDH4A1 is a mitochondrial enzyme, that is expressed in liver, skeletal muscle, kidney, heart, brain, placenta, lung and pancreas.[139] The substrate is pyrroline-5-carboxylate, that is converted to glutamate, preventing accumulation of pyrroline-5-carboxylate.[140, 141] For type II hyperprolinemia, a mutation of ALDH4A1 is reported, that inactivates ALDH4A1 leading to high levels of pyrroline-5-carboxylate in blood.[142, 143] People suffering from type II hyperprolinemia, show seizures, convulsions and mental retardation. This effect results from high levels of pyrroline-5-carboxylate that inactivates pyridoxal phosphate, an important cofactor needed for many biosyntheses, especially of neurotransmitters (e.g. GABA,

serotonin, noradrenaline) and, if inactivated, causes harmful effects.[144, 145] The deactivation of pyridoxal phosphate happens through a Knoevenagel-type condensation.

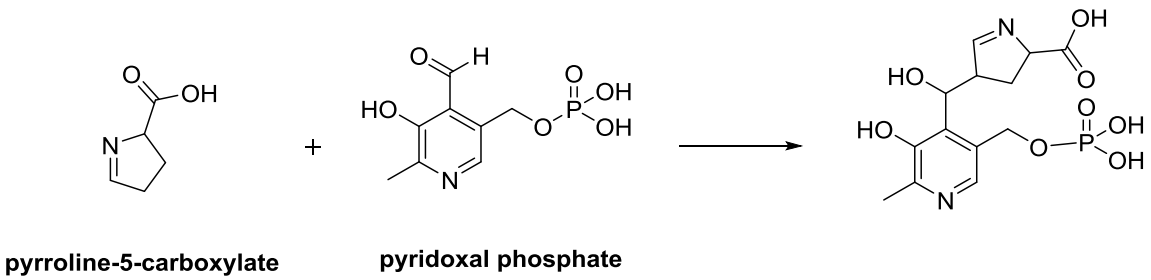

pyrroline-5-carboxylate **pyridoxal phosphate**

Scheme 4. Deactivation of pyridoxal phosphate by pyrroline-5-carboxylate.

Beside proline metabolism ALDH4A1 oxidizes short and medium chain aldehydes and therefore may play a role in protection from lipid peroxidation derived aldehydes.[146, 147] ALDH4A1 is inducible by p53 and is thought to play a role in DNA repair, due to upregulation upon DNA damage.[147] A knockdown of ALDH4A1 enhances susceptibility on p53 mediated apoptosis.[147]

The only non dehydrogenase identified protein in this experiments ACAA2, describes a mitochondrial acyltransferase.[148, 149] This protein is involved in lipid metabolism and is described to attenuate BNIP3 induced apoptosis.[150, 151]

2.2.3.3 Long Term Labeling

The standard labeling procedure already gave a good insight into target specificity of the acivicin probes. Beside these facts, some questions remained, like the fact that ACVL1 and ACVL2b label ALDH1A1 and ALDH2 stronger than ACV2 implying that they would inhibit these enzymes stronger but showed no biological effect. To answer this question an ABPP experiment was designed that reflected the results from the cell growth assay. The key was to set up the same incubation times for the probes on HepG2 cells for ABPP experiments as for the cell growth assay.

For this experiment the two probes that showed a biological effect, ACV1 and ACV2, were taken and their concentration was reduced to a concentration where inhibition of cell growth was observed. This resulted in 10 µM for ACV2 and 25 µM for ACV1 supplemented to the media and the HepG2 cells were incubated up to five days in media containing ACV1 and ACV2.

Carrying out this experiment on an analytical scale revealed a single band for ACV1 in the range of 60 kDa, that was already identified as ALDH4A1 in the standard ABPP experiments. In contrast to previous experiments, this band did not occur in the soluble fraction, but in the insoluble fraction. For ACV2 an already known pattern was visible around the area of 55 kDa and an additional band at 60 kDa appeared with high intensity (see figure 16). The distinct labelings increased in intensity with longer incubation times. The reason for the increasing intensity could be a slow uptake of the probes or an induction of expression of the addressed enzymes.

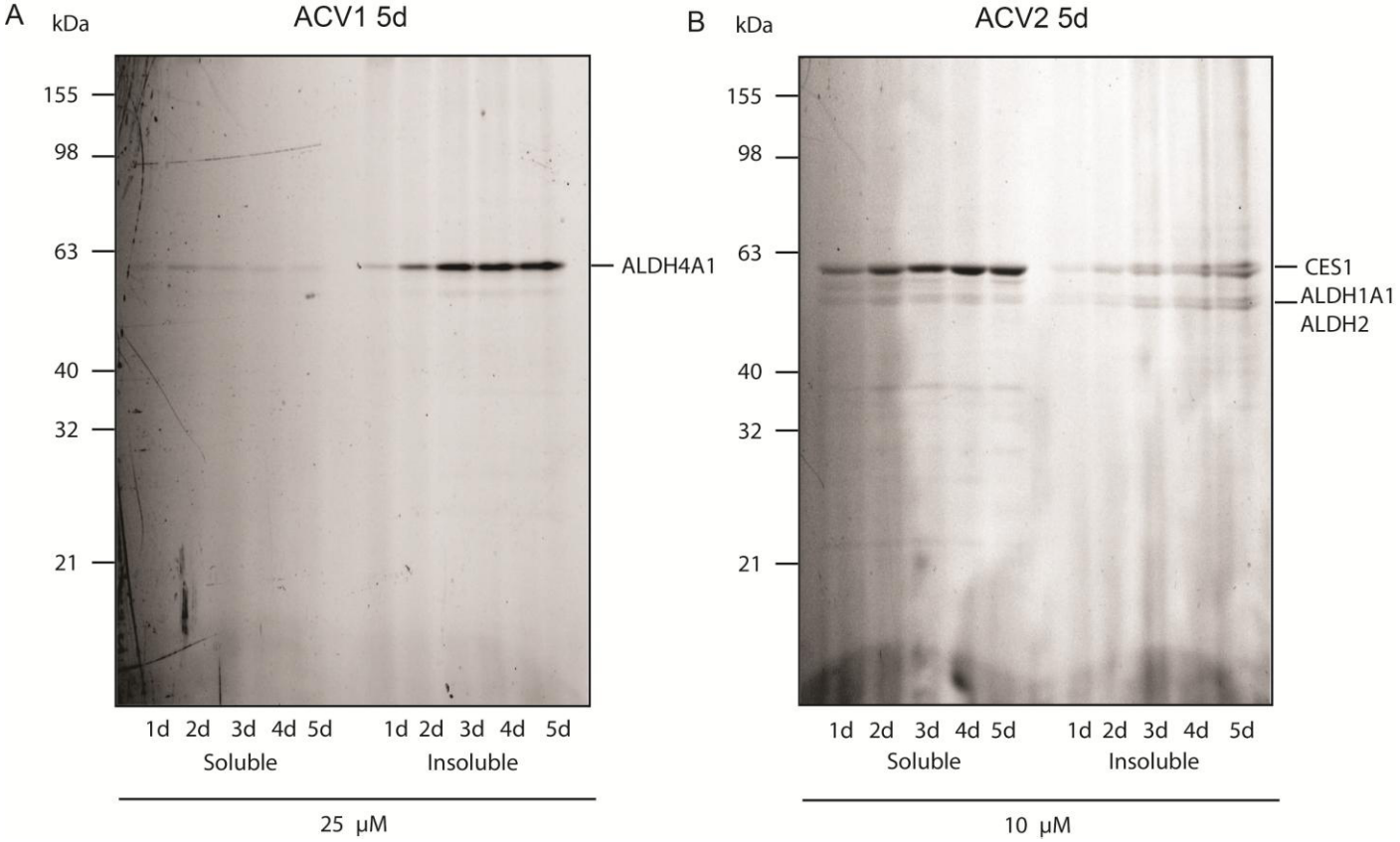

Figure 16. Fluorescence scan of HepG2 cells labeled *in situ* for up to five days with ACV1 and ACV2 (figure taken from [101] - reproduced by permission of The Royal Society of Chemistry).

The following preparative enrichment with the trifunctional linker using ABPP pull down revealed for ACV2 the targets ALDH1A1 and ALDH2 and a new target with CES1 for the 60 kDa band (see table 5). CES1 is serine hydrolase and represents a new enzyme class among the target enzymes. The active site of ALDHs and ACAA2 have a nucleophilic cysteine that is normally responsible for attacking electrophiles, whereas serine hydrolases contain a nucleophilic serine.

CES1 is a major serine hydrolase in the liver and is also expressed throughout various tissues.[152, 153] It is involved in cholesterol and lipid metabolism, hydrolysis of xenobiotics and drugs, e.g. cocaine and heroin, but the complete function remains unknown.[154, 155] CES1 is upregulated upon HCV infection in cells, being important for virus replication and deficient CES1 is associated with lymphoma, rheumatoid arthritis and arteriosclerosis.[156-161] It is mainly regarded for interaction with small molecules rather than diseases because of the metabolic function. In a recent study, it was shown that the inhibition of CES1 by organophosphorous compounds leads to hypertriglyceridemia.[162]

Probe	Target	Accession	Description	Area				Control day 1			Control day 5			ACV2 day 1			ACV2 day 5			General information			(Area Probe)/(Area DMSO)	
				ACV2 day 1	ACV2 day 5	Control day 1	Control day 5	Score	# Peptides	# PSM	Score	# Peptides	# PSM	Score	# Peptides	# PSM	Score	# Peptides	# PSM	# AAs	MW [kDa]	Sequence coverage	(day 1)	(day 5)
ACV2	ALDH1A1	IPI00218914.5	Retinal dehydrogenase 1	4,490E8	5,250E8	1,635E8	2,353E8	70,5	18	23	77,7	15	24	68,9	16	23	92,0	16	31	501	54,8	56,9	2,75	2,23
	ALDH2	IPI00006663.1	Aldehyde dehydrogenase, mitochondrial	1,654E8	3,199E8	8,303E6	3,508E7	6,3	2	2	22,3	5	8	50,3	14	17	59,6	14	21	517	56,3	38,5	19,92	9,12
ACV2	CES1	IPI00607693.2	liver carboxylesterase 1 isoform c precursor	1,131E9	1,513E9	1,043E8	4,298E7	39,7	12	12	32,3	10	10	157,4	20	49	249,2	25	80	566	62,4	51,1	10,84	35,20

Table 5. MS hits of HepG2 cells incubated with ACV2 up to five days.

An experiment with ACV2 incubation on HepG2 cells at 10 µM concentration with shorter time intervals with 2 h, 4 h, 6 h, 8 h, 24h and 48 h could reveal that at least 4 h incubation was essential for visual appearance of labeling.

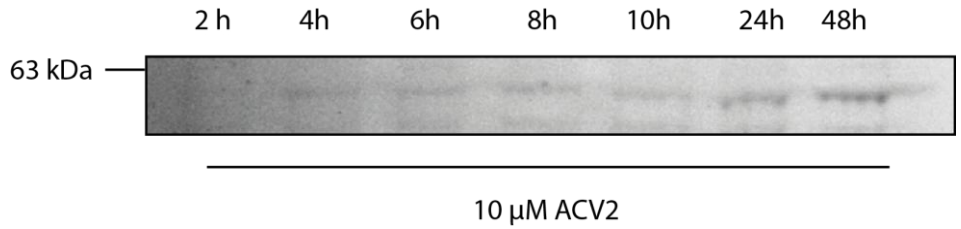

Figure 17. Fluorescence scan of time resolved incubation of ACV2 with HepG2 cells.

The preparative enrichment for ACV1 was not successful even after several trials including 2 M and 4 M urea in PBS. Therefore an alternative route for target identification was applied. The similar height of the band of ACV1 in the five day labeling and in the standard ABPP labeling as well as the high specificity of ACV1 for ALDH4A1 from concentration dependent labeling indicated, that the target enzyme of the long term labeling was also ALDH4A1. To verify this assumption the HepG2 cells were labeled in the same manner as before in an analytical scale and rhodamine azide was attached by click chemistry. After SDS-PAGE fluorescence readout the gel was blotted on a PVDF membrane and analyzed by western blot using a primary antibody against ALDH4A1 and a secondary antibody carrying HRP for chemoluminescence detection. The membrane was first analyzed by fluorescence imaging visualizing the rhodamine and subsequently afterwards, the antibody was detected by chemoluminescence using HRP substrate. The bands detected by both methods were of the same molecular weight and of the same shape proving ALDH4A1 as the target protein of ACV1.

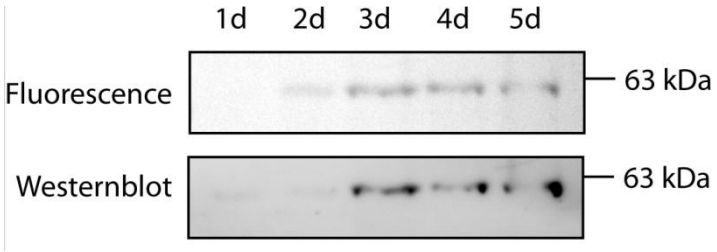

Figure 18. Fluorescence scan of rhodamine and chemo luminescence scan against HRP of HepG2 cells labeled in situ with ACV1 for up to five days (figure taken from [101] - reproduced by permission of The Royal Society of Chemistry).

For the next step, the question remained whether protein expression of ALDH4A1 and CES1 is induced or affected upon treatment with ACV1 and ACV2. An induction seemed unlikely since both proteins are reported to be present in liver tissue, with CES1 belonging to the high abundant proteins. For this purpose HepG2 cells were incubated with 25 µM ACV1 and 10 µM ACV2 for up to five days and expression levels of CES1 and ALDH4A1 were monitored by western blot. This analysis showed no alteration of CES1 and ALDH4A1 expression levels upon treatment with ACV1 and ACV2.

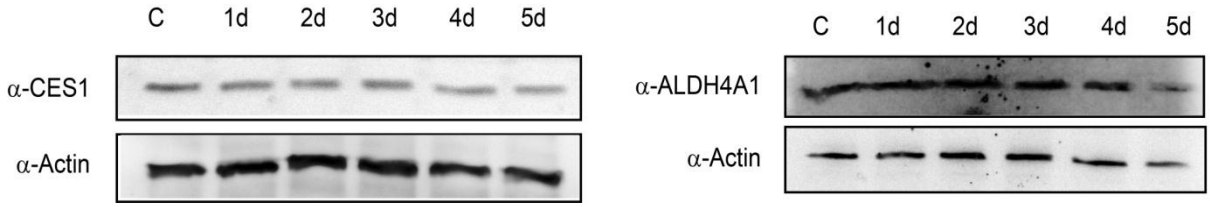

Figure 19. Western blot analysis of CES1 and ALDH4A1 with treatment of ACV1 and ACV2 for up to 5 days (figure taken from [101] - reproduced by permission of The Royal Society of Chemistry).

2.2.4 Confirmation of Aldehyde Dehydrogenases and ACAA2 as Target Enzymes

For confirmation of the ALDHs as target enzymes of the acivicin probes recombinant expression in *E. coli* was used. Therefore the target genes were cloned into a vector suitable for this purpose. In this work the genes used were cloned into vectors using the Gateway® system. This system uses the recombination system of phages and requires special vector systems containing the recombination sites.[163]

The cDNAs of ALDH2, ALDH1B1, ALDH4A1, ACAA2, were commercially available in pDONOR vectors and recombined via LR clonase into the pDest007 Vector. This inducible vector contained an *N*-terminal strepII tag for affinity purification. After recombination, the clones were transformed into *E. coli* BL21 Solu®. The ALDH1A1, cloned into pDest007, was kindly provided by Dr.Tanja Wirth from her previous work and transformed into *E. coli* BL21 DE3, that provided sufficient soluble protein.

The inducible expression in *E. coli* provides both a good control and the protein in a complex proteome. To verify the selectivity of a probe for a certain enzyme, it was necessary to provide the desired enzyme in a complex proteome mixture, to exclude unspecific reactivity towards this enzyme. For confirmation of ALDH1A1, ALDH2, ALDH1B1, the probe ACVL1 was used, ACVL2a was used for confirming ACAA2 and for ALDH4A1 the ACV1 probe

was used. The bacteria were cultivated in LB media, with one sample inducing the expression and one sample without induction as control. After expression, the cells were incubated with the corresponding probe and, after attachment of rhodamine azide, analyzed by SDS-PAGE fluorescence readout.

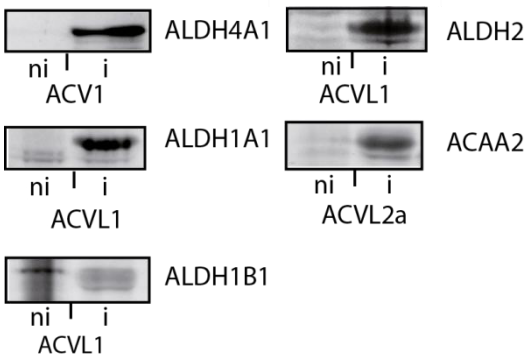

Figure 20. Fluorescence scan of the confirmation of target enzymes ALDH4A1, -1A1, -1B1, -2 and ACAA2 overexpressed in *E. coli* using ABPP of the respective probes. One culture was not induced while the other culture overexpression was induced (figure adapted from [101] - reproduced by permission of The Royal Society of Chemistry).

All identified proteins proofed to be hits of the probes as the induced target proteins gave a labeling while in the non induced bacteria no labeling was observed.

For additional studies, the proteins ALDH1A1 and ALDH4A1 were purified using the Strep II tag. ALDH1A1 was obtained in good yields and very pure while the expression of the ALDH4A1 gave low yields but pure protein. Different strategies, from overexpression at low temperatures overnight, expression using poor media, coexpression of pTGROE, an *E. coli* chaperone, as well as the expression of the proteins fused with TRX or MBP, didn't increase the amount of soluble proteins.[164, 165] For ALDH4A1 overexpression in *E. coli* BL21 Solu® in poor media (M9 medium) over night at 20 °C gave the best results, while ALDH1A1 was overexpressed in *E. coli* BL21 DE3 in LB medium over night at 20 °C.

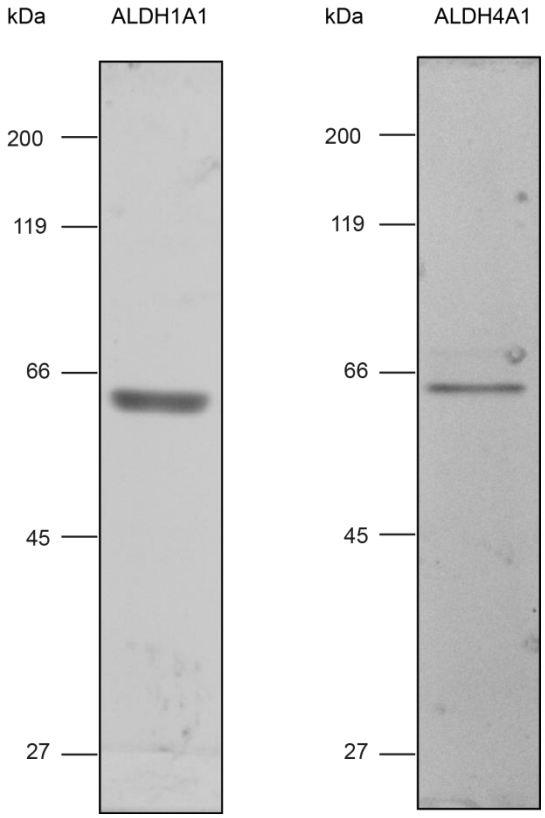

Figure 21. Coomassie stained SDS-PAGE auf purified ALDH1A1 and ALDH4A1.

2.2.5 Competitive Labeling

After confirmation of the ALDHs as targets of the probes by labeling the overexpressed enzymes, the question arose, if the targets were probe specific or if these ALDHs were also targets of the natural product. This question is mandatory since none of the reported targets were identified for acivicin before. A simple approach to answer this question is to do a competitive labeling experiment. The lysate is preincubated with the natural product at various concentration varying from deficient to excess concentration compared to the concentration of the probe. In case of competition, the resulting labeling intensity after attachment of rhodamine azide and SDS-PAGE, should decrease with increasing concentration of the natural product.

For identification the probes that gave the strongest labeling were used against the natural product. In mouse liver lysates ACVL1 was tested to confirm Aldh1a1, Aldh2 and Aldh1a7 as acivicin target and ACV1 was tested to confirm Aldh4a1 as a target of acivicin.

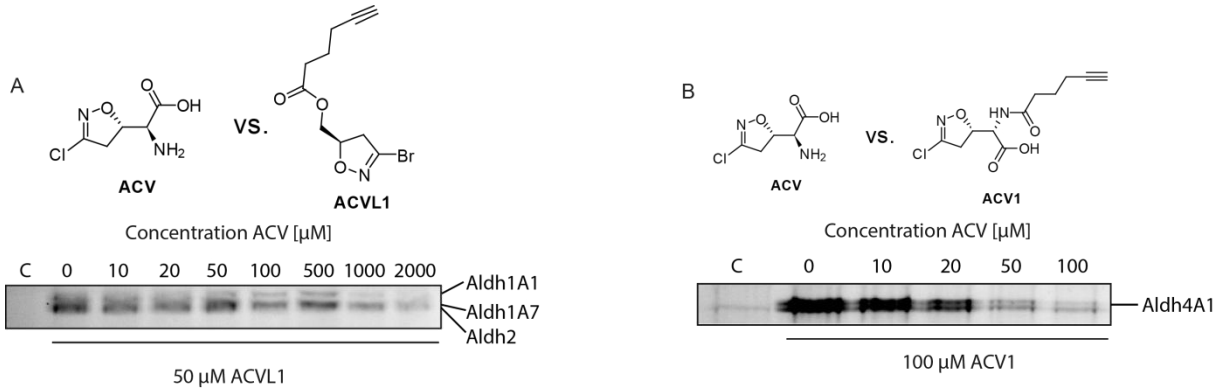

Figure 22. Fluorescence scan of A) acivicin competing with ACVL1 and B) acivicin competing with ACV1 in mouse liver lysate for the target enzymes Aldh1A1, -1A7 and -2 (ACVL1) and Aldh4A1 (ACV1) (figure taken from [101] - reproduced by permission of The Royal Society of Chemistry).

Acivicin displayed a high specificity for Aldh4a1, while a complete decrease of the band was already achieved with equimolar concentrations making it a target of the natural product. This target of acivicin was so far unknown. In contrast to ACV1, ACVL1 still showed labeling for Aldh1a1, Aldh2 and Aldh1a1 at an equimolar ratio. At a 40 fold excess of acivicin and at a concentration of 2 mM a decrease in intensity was observed, making these enzymes no target of acivicin.

For the human enzymes, the lysate of HepG2 was used and ACVL1 and ACV1 in similar manner as in the mouse liver lysate. ACVL1 was used to investigate ALDH1A1, ALDH2 and ALDH1B1 and ACV1 was used for ALDH4A1.

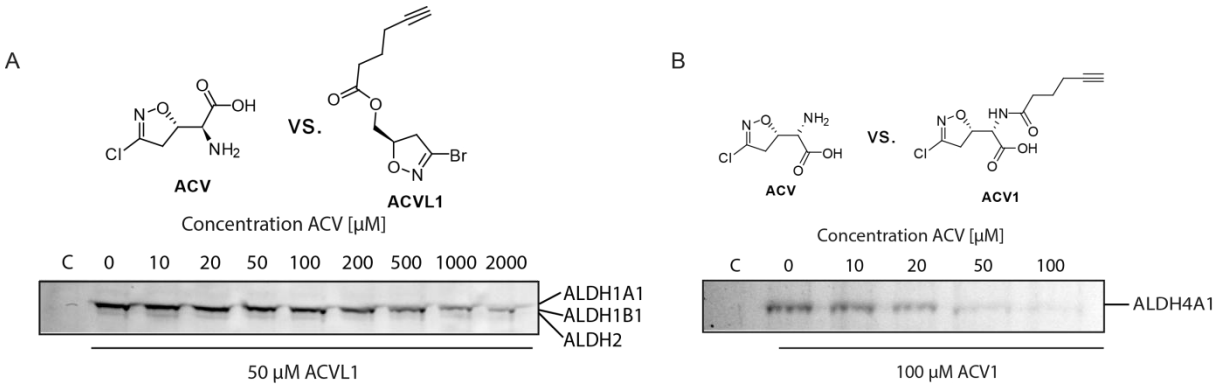

Figure 23. Fluorescence scan of A) acivicin competing with ACVL1 and B) acivicin competing with ACV1 in HepG2 lysate for the target enzymes Aldh1A1, -1B1 and -2 (ACVL1) and Aldh4A1 (ACV1) (figure adapted from [101] - reproduced by permission of The Royal Society of Chemistry).

The results for HepG2 were similar to the ones obtained from mouse liver, indicating ALDH4A1 as a new target of acivicin and ALDH1A1, ALDH2 and ALDH1B1 being no

targets of acivicin, with only slight decreasing intensity at high ratios at concentrations far above clinical relevance (over 50 µM).[43]

ALDH4A1 was further confirmed as a target of acivicin via mass spectrometry by using ABPP-SILAC approach. For this experiment HepG2 cells were labeled with heavy and medium isotopes. The heavy labeled cells were treated with ACV1 in PBS for 2h at 100 µM and the medium labeled cells were treated with 100 µM acivicin and 100 µM ACV1 prior to ABPP pull down. The experiments were carried out in triplicates including one label switch (heavy cells were treated with acivicin and ACV1 and medium cells with ACV1). With this method a competition for the binding between acivicin and ACV1 was read out via mass spectrometry, which proofed ALDH4A1 a target of acivicin (see table 6).

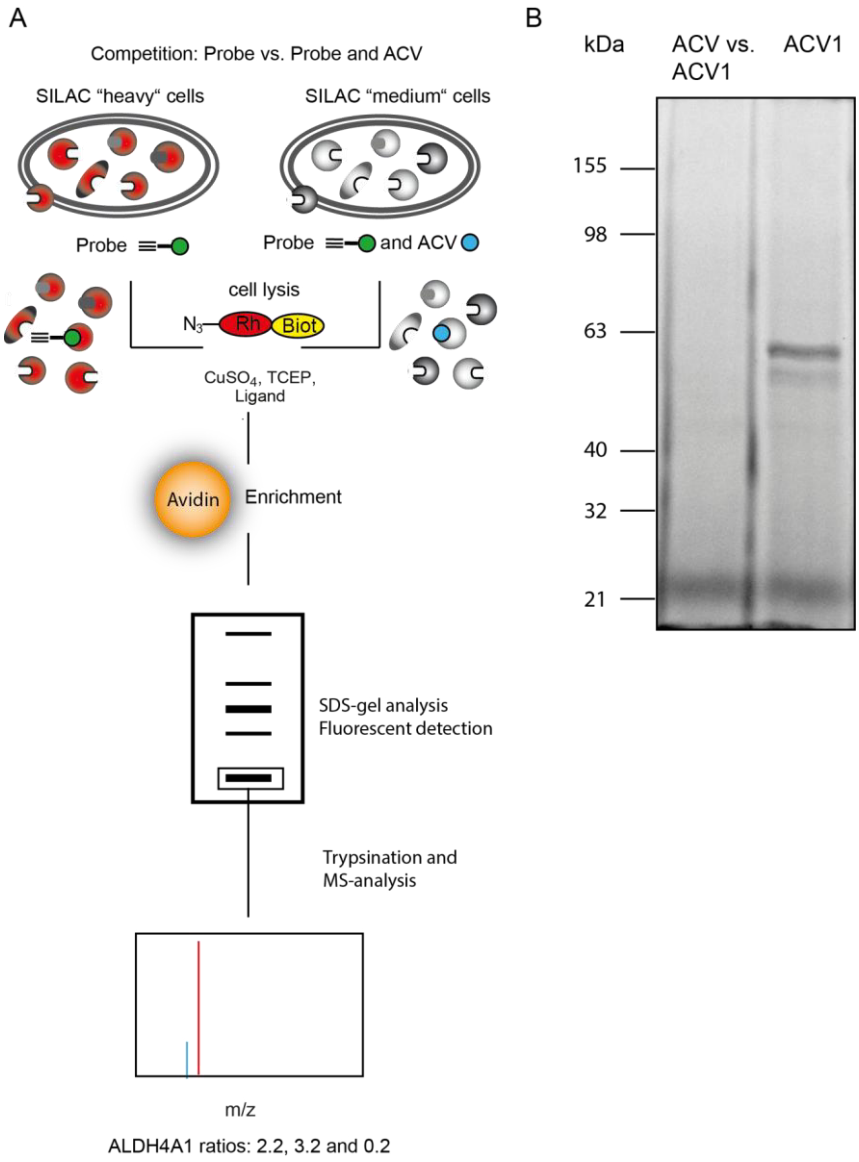

Figure 24. A) Workflow competitive ABPP labeling with implemented SILAC. B) fluorescence scan of SILAC HepG2 that underwent competitive ABPP labeling (figure adapted from [101] - reproduced by permission of The Royal Society of Chemistry).

Probe	Target	Accession	Description	1	2	3 (label switch)	General information		
				Ratio ACV1 / (ACV1+ACV)	Ratio ACV1 / (ACV1+ACV)	Ratio (ACV1+ACV) / ACV1	# AAs	MW [kDa]	Sequence coverage
ACV1	ALDH4A1	IPI00217871.4	Delta-1-pyrroline-5-carboxylate dehydrogenase, mitochondrial	2,2	3,2	0,2	563	61,7	33,2

Table 6. MS hits from SILAC labeled HepG2 cells incubated with ACV1 and acivicin and ACV1 in competition.

2.2.6 Inhibition of Aldehyde Dehydrogenases

For a deeper characterization of the probes and acivicin an inhibition assay was carried out. Aldehyde dehydrogenases can be investigated with an assay, that is used generally for aldehyde dehydrogenases. In this assay, propionic aldehyde is oxidized to propionic acid, while converting NAD^+ to NADH, that can be observed by absorption spectroscopy.

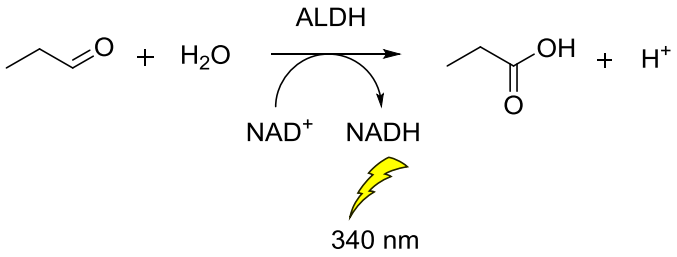

Scheme 5. Conversion of propionic aldehyde to propionic acid through ALDH using NAD^+.

The slopes from the conversion of NAD^+, for each inhibitor concentration used, were extracted and plotted against these concentrations. Plotting the concentrations on a logarithmic scale, a sigmoidal curve was fitted to the plot. From this curve the IC_{50} was extracted from the fitted curve. For ALDH1A1 the probes ACVL1, ACV2 and acivicin were tested and ALDH4A1 was tested against ACV1, ACV2 and acivicin.

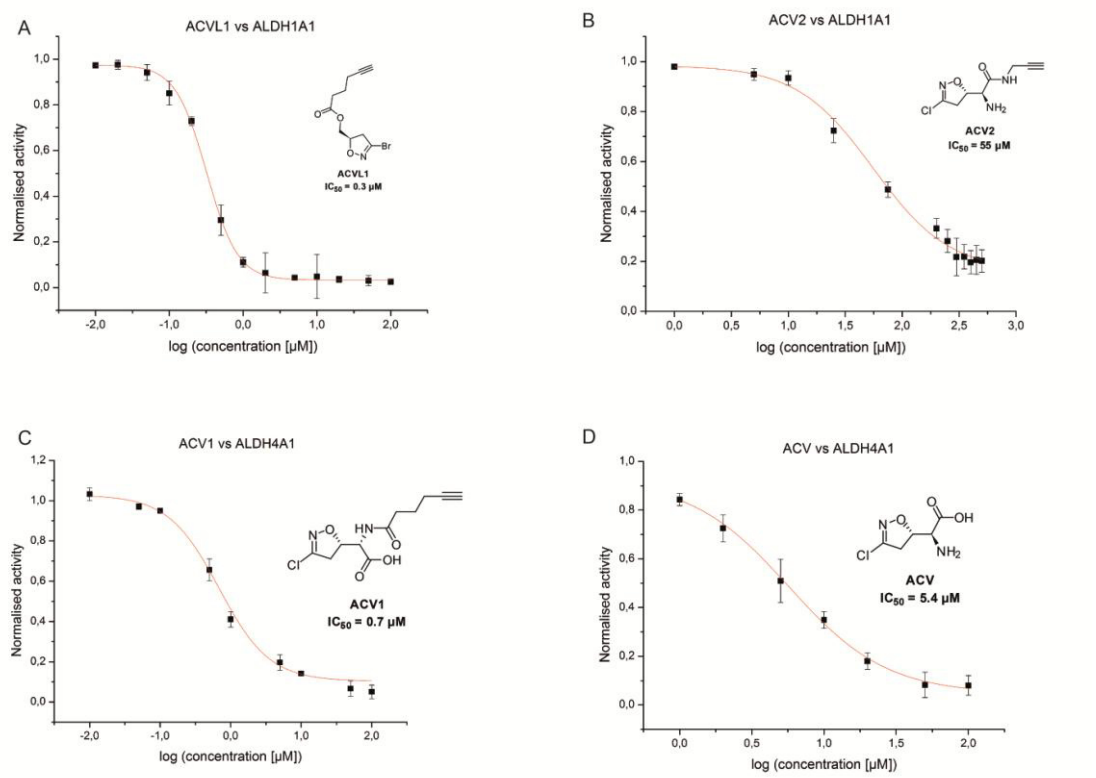

Figure 25. Measurement of IC_{50} value through ALDH activity assay for the compounds ACVL1 (A), ACV2 (B), ACV1 (C) and ACV2 (D) for the dehydrogenases ALDH1A1 (A and B) and ALDH4A1 (C and D). Each compound was tested in two independent trials in triplicates (figure taken from [101] - reproduced by permission of The Royal Society of Chemistry).

ACVL1 inhibited the enzyme ALDH1A1 with an IC_{50} of 0.3 µM, whereas ACV2 showed a much weaker inhibition with an IC_{50} of 55 µM. This reflects very good the intensities from the labeling studies (figure 10), where ACV2 needed higher concentrations for a sufficient labeling. ACV1 showed a good inhibition of ALDH4A1(IC_{50} of 0.7 µM) as well as acivicin (IC_{50} of 5.4 µM), as it was expected.

Acivicin did not show inhibition of ALDH1A1 even at very high concentrations of up to 500 µM, making ALDH1A1 not a target enzyme of acivicin, like it is the case for ACV2 and ALDH4A1.

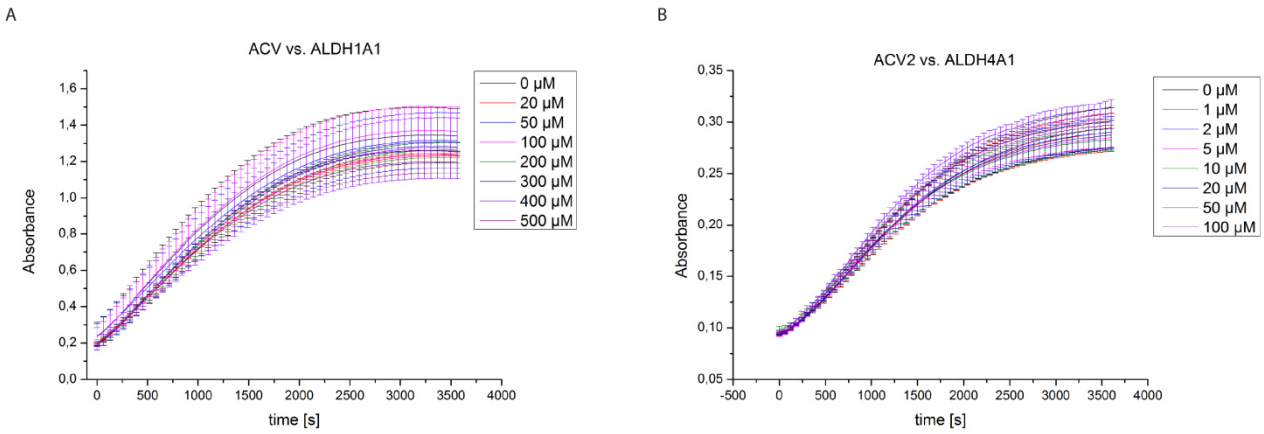

Figure 26. Conversion of ALDH4A1 upon treatment with acivicin (A) and ACV2 (B) showing no inhibition (figure adapted from [101] - reproduced by permission of The Royal Society of Chemistry).

This fact was not surprising since no labeling of ALDH4A1 by ACV2 occurred. The results obtained from the ALDH-assay reflected the results obtained from the competitive labeling experiments (figure 20 and 21) and additionally confirm ALDH4A1 as a target of acivicin.

2.2.7 Confirmation of CES1 as Target Enzyme

Time dependent labeling of ACV2 in HepG2 revealed an increasing intensity of the CES1 band. The reason of this developing signal over time was still unclear and a confirmation of CES1 as a target was also in need. To confirm CES1 as a target, recombinant CES1 was purchased and added to A549 lysate to embed it in a complex proteome mixture and additionally in PBS. After incubation with ACV2, rhodamine azide was attached for fluorescence readout. FP probe, which specifically labels active serine hydrolases, was used as a positive control.

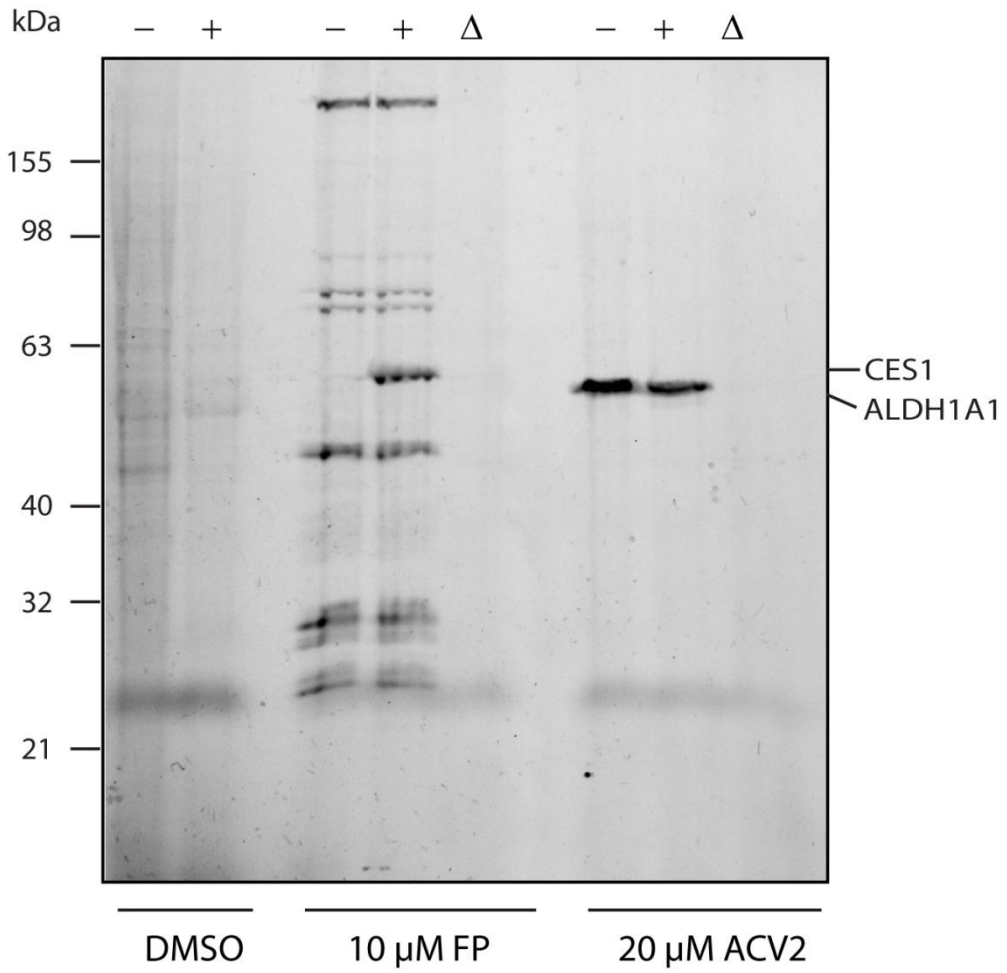

Figure 27. Labeling of recombinant CES1 in A549 lysate. Incubation with FP showed the expected result with labeled CES1 that was spiked in A549 lysate (+). ACV2 shows no labeling on CES1 but a strong labeling of ALDH1A1 which is below the CES1 signal. The heat control (Δ) shows no unspecific binding of both probes (figure taken from [101] - reproduced by permission of The Royal Society of Chemistry).

In this experiment the additional CES1 added to an A549 lysate was visible when labeled with FP, indicating an active enzyme. For ACV2 no labeling of CES1 was visible. A strong band at 55 kDA was labeled by ACV2 in A549 lysate in both lanes, with and without CES1 added. This band represents ALDH1A1, which is highly expressed in A549 lysates and was labeled by ACV2, as already confirmed before (see chapter 2.2.3.2). The absent labeling could indicate that CES1 was an unspecifically enriched protein by the protocol, but on the other hand the MS identification of CES1 was explicit. To verify this assumption another point had to be considered. The fact that a minimum incubation time of four hours was necessary and an incubation of 24 hours gave a satisfactory signal, revealed that the inhibition of CES1 by ACV2 could also be a very slow process.

For further investigation, the incubation time was extended to 24 hours and one sample was incubated for 24 hours without the probe and subsequently incubated with the probe. This experiment was done to cover the possibility that the enzyme could be activated by the lysate.

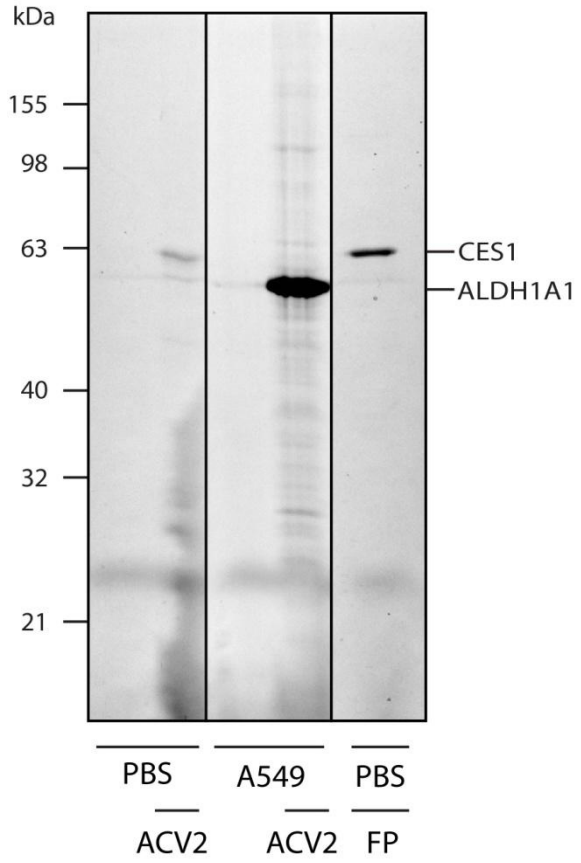

Figure 28. Labeling of recombinant CES1 in PBS and A549 lysates with incubation for 24 hours. In A549 lysates a strong labeling of ALDH1A1 by 20 µM ACV2 was observed but no labeling of CES1 in comparison to the positive control of CES1 labeled with 10 µM FP. Only weak labeling of CES1 in PBS by 20 µM ACV2 can be observed (figure taken from [101] - reproduced by permission of The Royal Society of Chemistry).

From these experiments it was obvious that no direct labeling of CES1 by ACV2 occurred. Only a weak labeling of CES1 in PBS by ACV2 was seen, but its intensity was weaker than CES1 labeled with FP under same conditions. The second experiment indicated clearly that no direct labeling of CES1 by ACV2 was performed. This concluded that a whole cell was needed to achieve a labeling of CES1 by ACV2.

2.2.8 CES1 Inhibition Assay

To confirm the obtained results for CES1 labeling, CES1 was also investigated for inhibition with a standard assay for esterase activity. Esterases hydrolyze 4-nitrophenylacetate to give 4-nitrophenol that can be monitored at 410 nm with absorption spectroscopy.

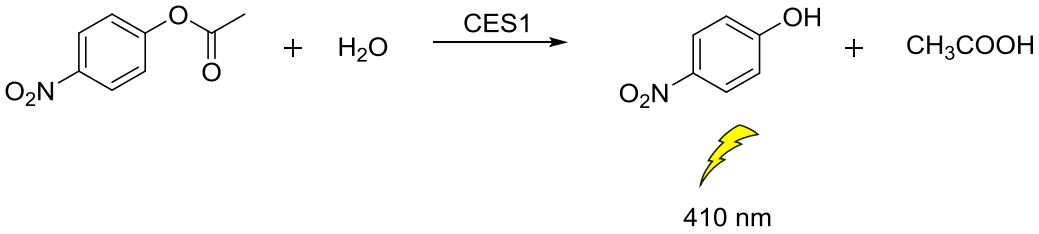

Scheme 6. Conversion of 4-nitrophenylacetate by CES1.

Recombinant CES1 was incubated with 4-nitrophenol acetate and different concentrations of ACV2. Different preincubation times for ACV2 were tested ranging from one hour to four hours, to respect results obtained by labeling of CES1 after at least 4 hours.

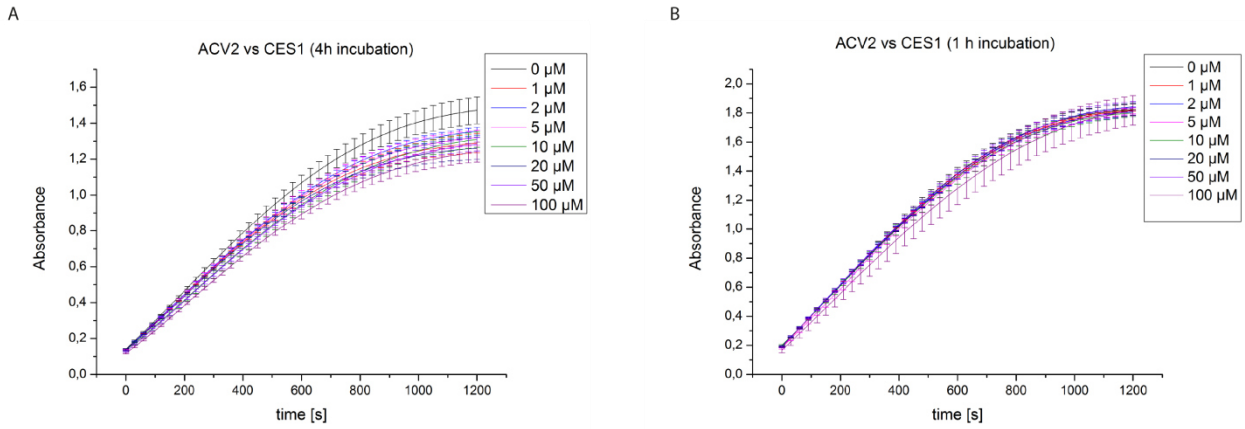

Figure 29. Conversion of CES1 upon incubation of ACV2 for A) 4 hours and B) 1 hour showing no inhibition (figure adapted from [101] - reproduced by permission of The Royal Society of Chemistry).

The results showed only conversion with no inhibition by ACV2. Even very high concentrations or long incubation times led to no significant decrease. A very slight decrease could be observed for an incubation of four hours, but this decrease is not sufficient to determine an IC_{50} value. In HepG2 cells labeling was already obtained at 10 µM but concentrations for ACV2 in this assay ranged up to 100 µM with no inhibition.

2.2.9 Immunoprecipitation of CES1

Given the fact, that CES1 was only labeled after longer incubation of the Cell with ACV2 and no direct labeling of recombinant protein was achieved, brought in the possibility that the probe might get altered during incubation and therefore the adduct on CES1 became interesting. The challenge of directly isolating the probe-protein adduct, resulted in a new strategy to answer this question. The new strategy consisted of CES1 labeling inside the cell following a pull down for analysis. A suitable method is to use immunoprecipitation, as CES1 is a common protein and antibodies, sufficient for immunoprecipitation, are widely available. The immunoprecipitation uses the affinity of the antibody towards the enzyme and the affinity of the antibody towards immunoglobulin, that is coupled to a resin. There are different ways to operate. The first one is to form the immunocomplex with the antigen and couple this immunocomplex to the immunoglobulin. Another method is to couple the antibody to the resin an form the immunocomplex afterwards. A recently developed method uses lysine residues and couples those on aldehyde functionalized resin via reductive amination. This offers the possibility to reuse the antibody after elution and the antibody is not eluted, too, making the sample more pure for following analysis.

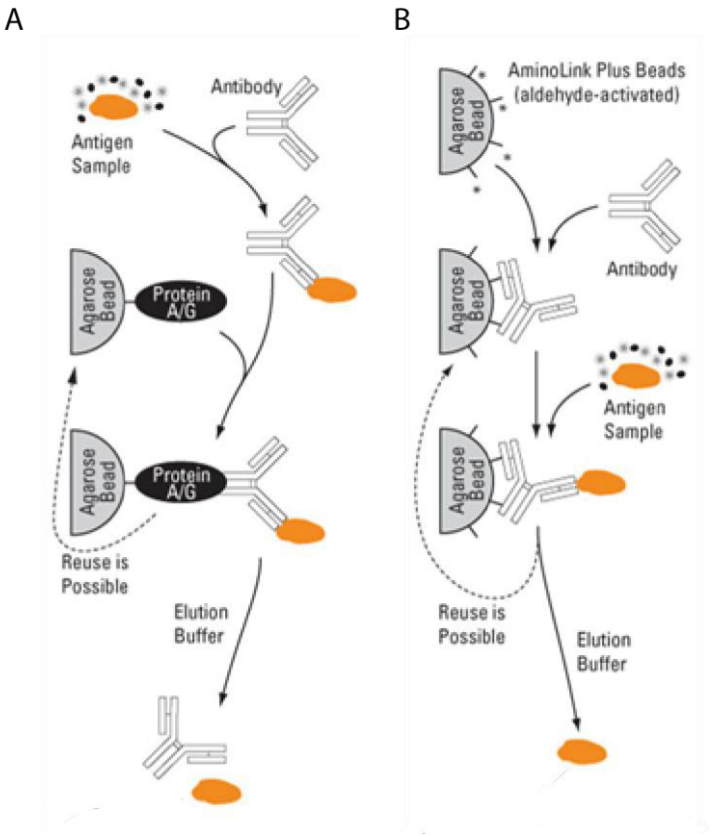

Figure 30. A) Immunoprecipitation performed by formation of the immunocomplex before binding to the immunogloblulin coupled to solid phase. B) Immunoprecipitation with the anribody coupled to the resin via reductive amination before formation of the immunocomplex. (reproduced and modified by permission of Thermo Fisher Scientific)

For the pull down of CES1 from HepG2 the strategy of forming the immunocomplex followed by immobilization on the resin and the strategy of the covalently attached antibody were used. The HepG2 cells were incubated with ACV2 for 48 hours and afterwards the pull down was performed.

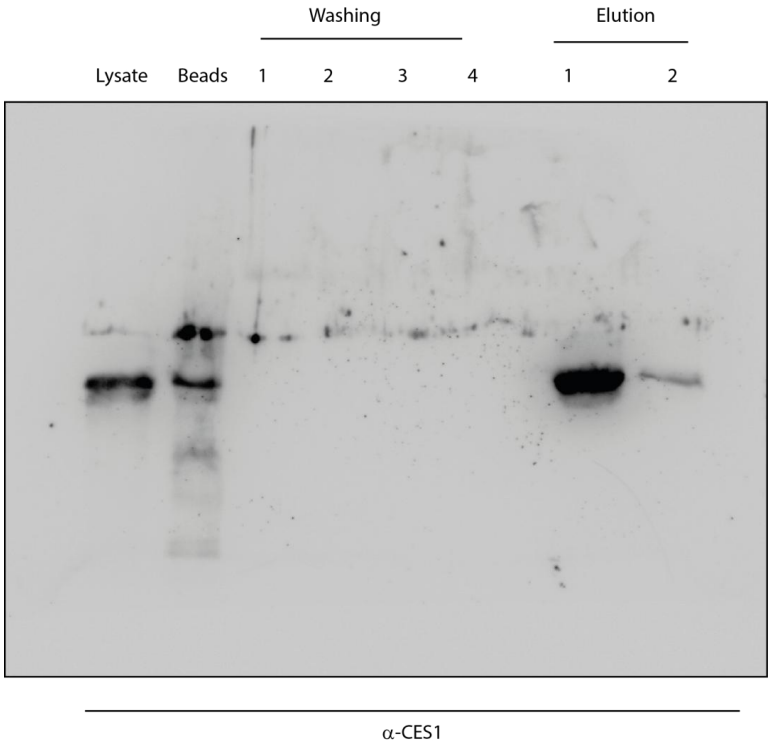

Figure 31. Western blot of Immunoprecipitation of CES1 from HepG2 that were incubated with ACV2 for 48 hours. Samples from all steps were analyzed starting with lysis, incomplete elution from beads, four washing steps and two elution steps.

The western blots showed a successful pull down with both applied methods, unfortunately the reuse of the covalently attached antibody was not possible. Despite the successful pull down, there was never enough material to conduct intact protein mass spectrometry. This result and the fact that the specificity of an antibody is a general problem led to the conclusion, that this approach was not capable to elucidate the ACV2 originating CES1 labeling.

2.2.10 Metabolic Labeling

As the IP was unable to show the ACV2 and CES1 protein adduct, it was reasonable to change the strategy. The alternative strategy was an recombinant overexpression but in this case in eukaryotic cell lines rather than using *E. coli*. To follow this strategy, the custom synthesized CES1 gene was recombined into the pT-REx-DEST30 vector using Gateway® cloning. The pTrex DEST30, which is a shuttle vector working in different expression hosts, contains no affinity tag and uses a cmv promoter system. After transfection using Liprofectamine 2000 two possible procedures follow. The transient transfection, that gives

stable protein expression up to three days until the plasmid is excreted again or the stable expression, where cells are treated with selection marker (in this case neomycin) over weeks to get only cells carrying the plasmid. Stable cells are clonally selected and tested for expression. The advantage of this method is to have cells expressing the protein of interest over many passages. Disadvantages are the complex and long process until a good clone is identified. The advantage of transient expression is the simpler procedure of the experiment but the expression is only stable for a up to three days. For the expression of CES1, the stable expression gave only poor results with stable cell lines towards selection, but poor expression For transient expression, the embryonic kidney derived cell line HEK293T and the widely known HeLa cell line were chosen. The transfection for HEK293T worked better than for HeLa.

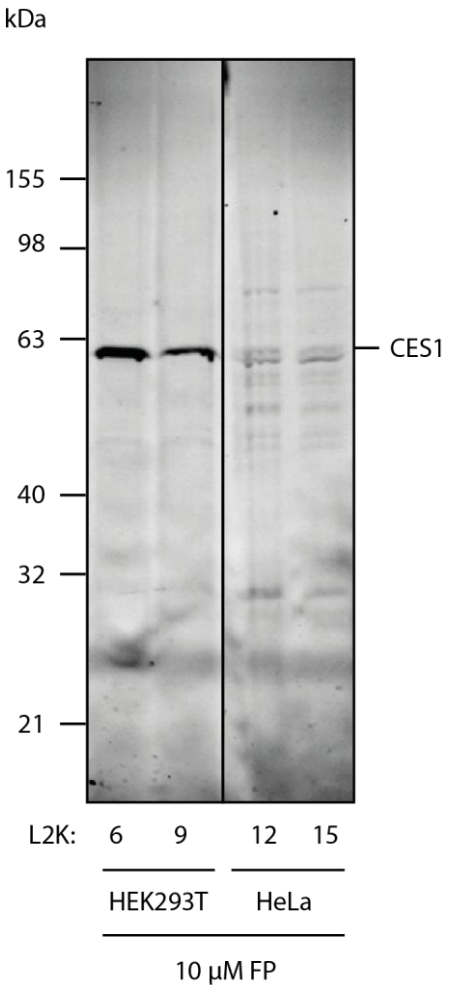

Figure 32. Fluorescence scan of HEK293T and HeLa cells transfected with CES1 using different amounts of lipofectamine 2000.

The stability for three days and the good expression in HEK293T, gave the possibility to conduct a metabolic labeling of CES1. Therefore the cells were transfected with CES1 on

pTREx-DEST30 and incubated for 24 hours. ACV2 was added to the media and incubated for additional 48 hours. This gave the cells enough time to start the expression of CES1 and the two days of incubation were sufficient for ACV2 uptake and metabolism, as experiments in HepG2 cells already showed.

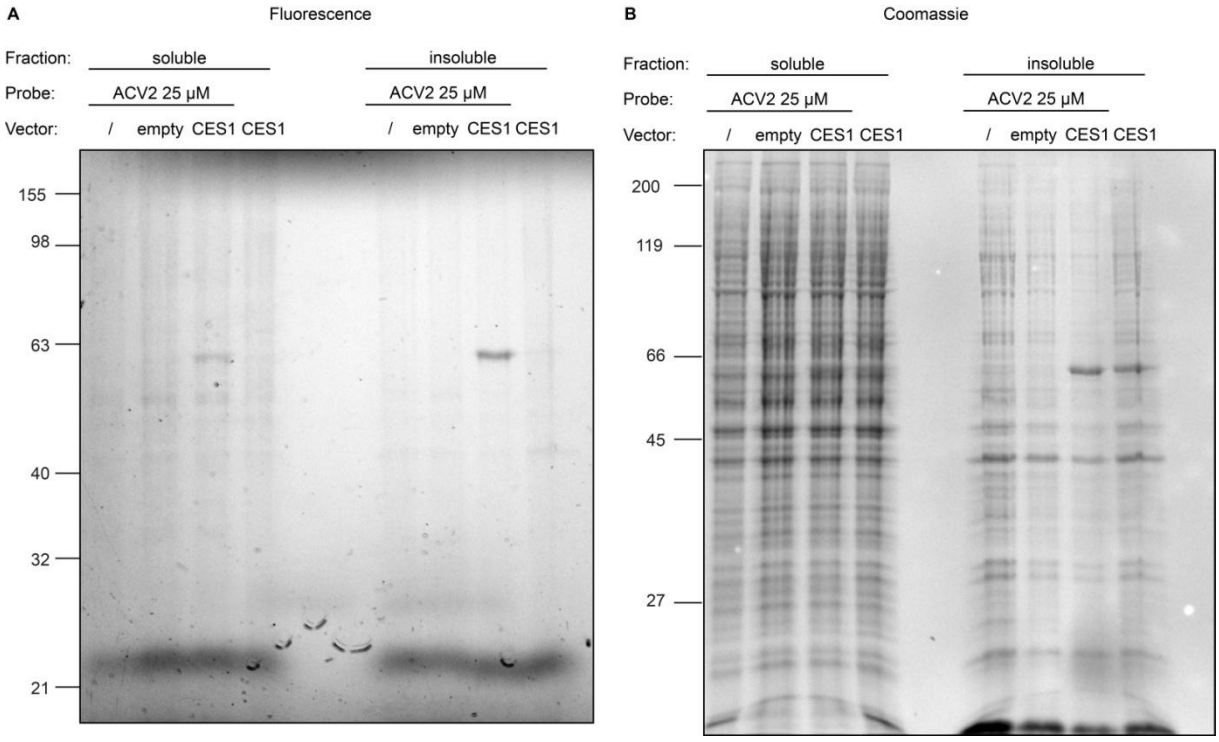

Figure 33. A) Fluorescence scan of metabolic labeling of ACV2 by HEK293T cells overexpressing CES1, with control lacking the plasmid, empty vector control and HEK293T cells overexpressing CES1 without ACV2. B) Corresponding coomassie gel (figure taken from [101] - reproduced by permission of The Royal Society of Chemistry).

This experiment clearly showed that the whole cell is necessary for ACV2 to label CES1 upon incubation. Additionally this experiment confirmed CES1 as a target of ACV2. This experiment indicated that ACV2 is metabolized after uptake and subsequently labels CES1.

A competitive metabolic labeling of acivicin and ACV2 was carried out to identify if CES1 is also a target of the natural product. For this experiment CES1 was transfected into HEK293T cells and acivicin at various concentration and ACV2 at constant concentration was added 24 hours after transfection and incubated for 48 hours.

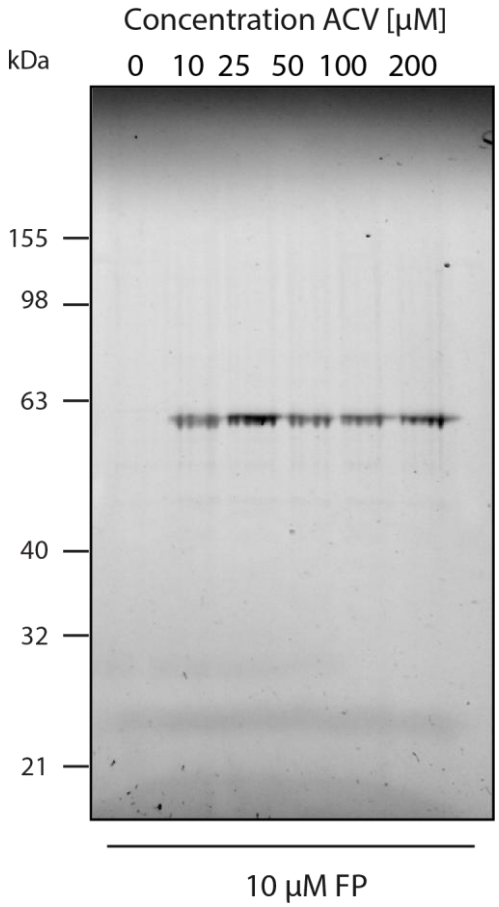

Figure 34. Fluorescence scan of HEK293T transfected with CES1 and incubated with increasing concentrations of acivicin for 48 h and subsequent *in vitro* labeling with FP.

This experiment showed no decreased labeling of CES1 under the influence of acivicin. The similar experiment with HepG2 cells gave the same result. This indicated CES1 as a probe specific target. Nevertheless it showed a possible metabolization of acivicin, that could be interesting for elucidating the mode of action. To get an insight in the metabolism of ACV2, and thereby also possible metabolism of acivicin that is discussed, the identification of the metabolite of ACV2 bound to CES1 needed to investigated.[43]

2.2.11 Overexpression and Pull Down of CES1

The indication of a metabolism of ACV2 emphasized the question of the structure of the metabolite or the adduct on CES1. IP could not reveal the additional mass due to not providing enough material but with the established recombinant expression there is a system were enough protein can be produced. Another useful possibility was to add a 10 his tag to the *C*-terminus via PCR and purify the protein via affinity chromatography. The *C*-terminal

modification was a consequence of the 12 *N*-terminal amino acids being cleaved to give the mature protein. After successful scale up of the transfection and purification via FPLC, a pure protein in sufficient quantities was obtained carrying the modification and to conduct intact protein mass spectrometry.

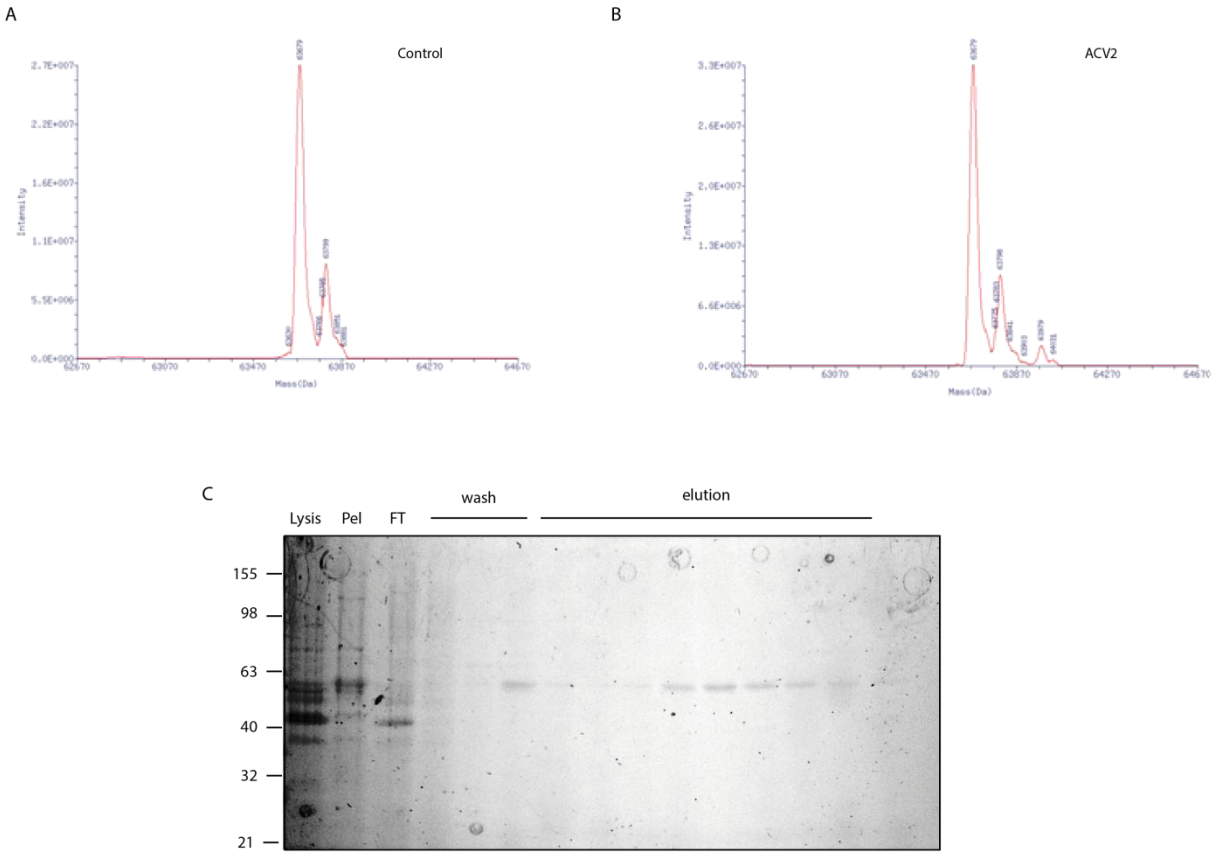

Figure 35. A) Deconvoluted mass of purified recombinant CES1. B) Deconvoluted mass of purified recombinant CES1 carrying metabolized ACV2. C) Fluorescence gel of different fractions from purification of CES1 carrying metabolized ACV2.

The additional mass identified from labeled CES1 towards unlabeled CES1 was, 180 kDa, but the amount of labeled CES1 was too small to give an exact answer. For a clear analysis of the adduct the content of labeled CES1 has to be increased. Higher amounts of ACV2 proofed to be toxic after the stress of transfection. A batch purification to obtain labeled CES1 from the insoluble fraction did not improve the content of labeled protein. To address this problem the amount of CES1 expressed upon transfection has to be reduced to increase the amount of labeled CES1 within the cell. Additional experiments that solve this problem need to be carried out.

2.2.12 Active Site Determination of ALDH4A1 and CES1

Although ALDH4A1 and CES1 were confirmed as targets, the mechanism of inhibition remained unknown. To identify the mechanism of inhibition side directed mutagenesis was carried out to exchange the nucleophilic amino acids of the active site by alanine. For CES1 the nucleophilic serine 221 and for ALDH4A1 the cysteine 348 were exchanged by alanine. Primers were designed using QuikChange Primer Design from Agilent Technologies. The mutations were incorporated by PCR and the obtained ALDH4A1 C348A was transformed into *E. coli* BL21 Solu® and CES1 S221A was transfected into HEK293T. ABPP experiments for ALDH4A1 with ACV1 were carried out in bacteria to compare the created mutant with the wild type as already described. For CES1 a metabolic labeling was conducted to compare wild type with mutant.

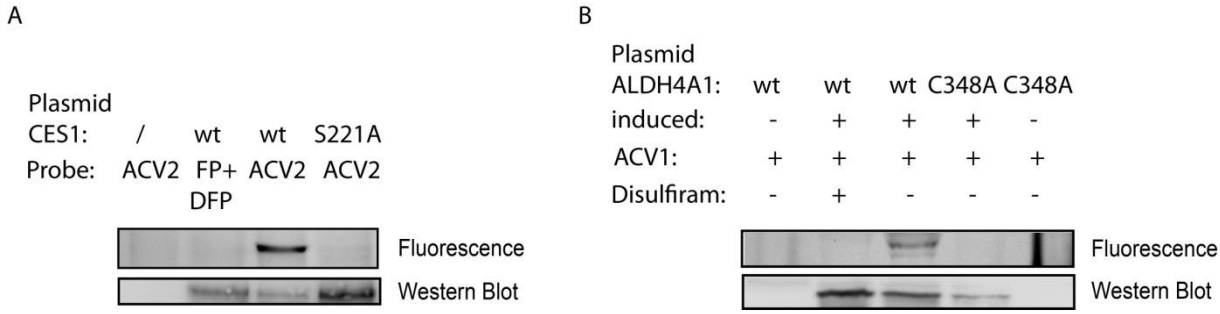

Figure 36. A) Labeling and western blot analysis of HEK293T cells and HEK293T cells overexpressing CES1 and S221A mutant. ACV2 was incubated for 48 h with both cell lines HEK293T cells and HEK293T cells overexpressing CES1 and in addition S221A mutant. CES1 overexpressed in HEK293T was incubated with 10 µM DFP (diisopropyl fluorophosphonate, a serine protease inhibitor) for 15 min and afterwards with 10 µM FP (fluorophosphonate probe, a serine hydrolase specific probe) (lane 2) (figure taken from [101] - reproduced by permission of The Royal Society of Chemistry).

The experiments showed that labeling was absent in both mutants indicating that ACV1 or the ACV2 derived metabolite binds to the nucleophilic amino acid of the active site.

2.2.13 siRNA Knockdown of ALDH4A1 and CES1

With ALDH4A1 a new target of acivicin and with CES1 a metabolism associated target of ACV2 have been identified. Among proteins that are related to cancer these two proteins remain unknown. In fact, both enzymes are related to metabolism. ALDH4A1 catalyzes the conversion of pyrrolidine-5-carboxylate to glutamate and CES1 hydrolyses various esters

especially of drugs but their cancer related function has yet been determined. To test these new targets for cell growth inhibition, the siRNA approach was applied. This widely used technique reduces gene expression by applying short RNA strands of 20-25 bp length at the mRNA level. After introduction into cells the double strand siRNA binds to Dicer (an RNAse III family member) that cuts the double strand RNA into pieces of 20-25 bp. This short RNA then binds to an argonaut protein where the guide strain remains bound to the argonaut forming the RNA induced silencing complex (RISC), while the other strain is digested. The RISC binds to the targeted mRNA and the argonaut catalyses the cleavage of mRNA, which gets degraded.

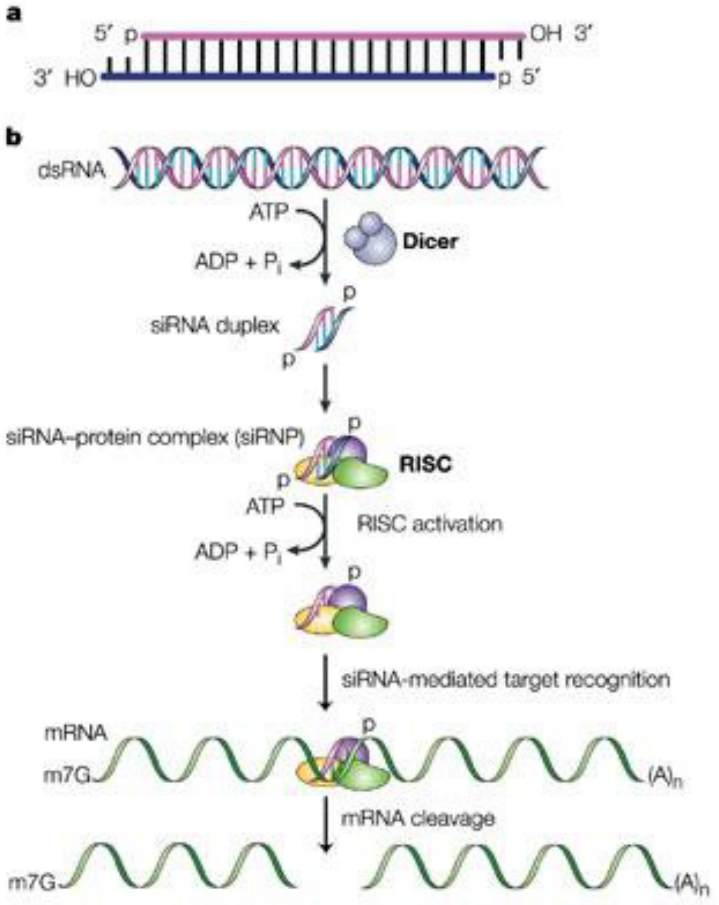

Figure 37. a) Short interfering siRNA as double strand siRNA. b) The siRNA pathway with double stranded siRNA that is cleaved by Dicer into siRNA in an ATP dependent reaction. These siRNAs are then incorporated into the RNA-inducing silencer complex (RISC). Once unwound, the single stranded antisense strand guides the RISC to the messenger RNA that has a complementary sequence which results in the endonucleolytic cleavage of the target mRNA (reprinted by permission from Macmillan Publishers Ltd: Nature reviews. Molecular cell biology [166], copyright 2003).

This provides a transient knockdown of the gene expression of the desired protein. After transfection of siRNA with Lipofectamine RNAimax®, the knockdown stability was tested using western blot analysis. The knockdown of ALDH4A1 was achieved 1 day after transfection and remained stable for up to 4 days. For CES1 the knockdown was also successful one day after transfection but less effectiv than ALDH4A1 and CES1 levels increased again on day four after transfection. After establishing stable knockdowns cell growth assay followed. To obtain information on this, cell growth was observed with crystal violet staining, after knockdown, for four days. The knockdown of ALDH4A1 inhibited cell growth significantly, whereas CES1 also reduced cell growth but less compared to ALDH4A1. This showed that the major targets ALDH4A1 of ACV1 and CES1 of ACV2, are involved in cell growth inhibition on HepG2.

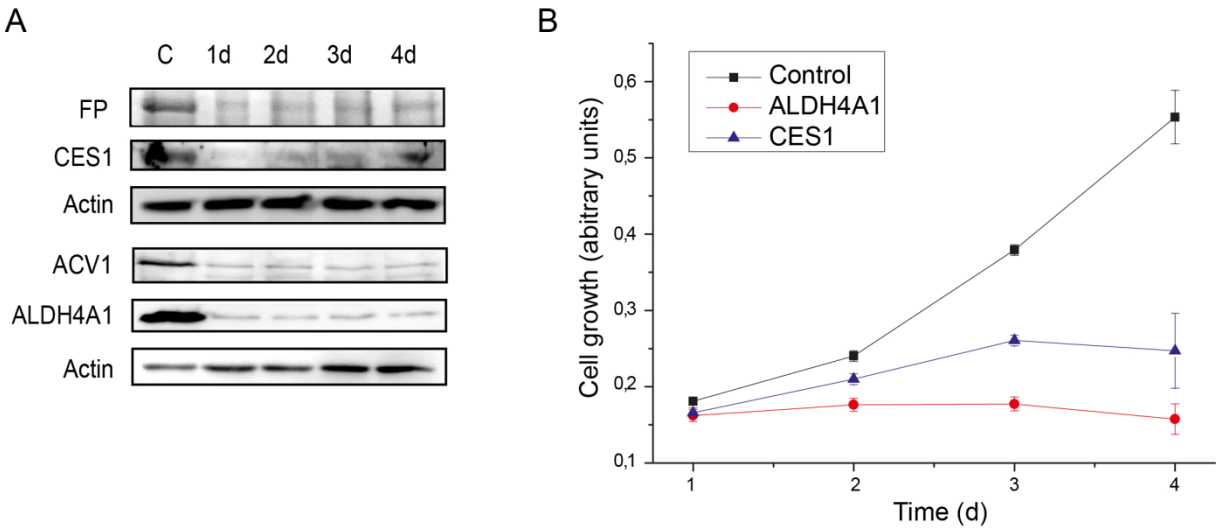

Figure 38. A)Western blot and fluorescence analysis of knockdown efficiency for CES1 and ALDH4a1 in HepG2 cells, including actin as loading control. B) cell growth assay of HepG2 cells upon with knock downs of CES1, ALDH4A1 and a control only containing transfection reagents (figure adapted from[101] - reproduced by permission of The Royal Society of Chemistry).

2.2.14 Conclusion and Outlook

The acivicin inspired probes of the ACVL series, except ACVL2a/-3a, show a preference for aldehyde dehydrogenases (ALDH1A1, -1B1 and -2) as expected from previous studies. The acivicin derived probe ACV2 showed the same preference but with a weaker intensity. The intensity decreased with bigger residues on the bromodihydroisoxazole moiety. These probes

showed a distinct selective labeling and provide good tools for visualization of ALDH1A1, -1B1 and -2. Especially ACVL1, which showed the strongest labeling, is easy accessible through synthesis and therefore represents the best visualization tool among those probes. In bioactivity studies the probes of the ACVL series showed no growth inhibition but ACV2 showed a growth inhibition close to the natural product acivicin. This indicates that an inhibition of these three ALDHs by these probes is not sufficient. One the other hand ACV2 showed only weak labeling of ALDHs, but by extending labeling times the additional target CES1 was labeled. A knockdown of CES1 resulted in growth reduction. The labeling of CES1 was metabolically derived, as no direct labeling of CES1 was possible with ACV2. A labeling of transiently expressed CES1 after extended incubation of whole cell with ACV2 finally approved the metabolic conversion of this probe. The labeling occurs on the active site as mutagenesis studies revealed. CES1 was a probe specific target as well as ALDH1A1, -1B1 and -2, but the fact that ACV2 is metabolically converted stands in line with the hypothesis of a metabolic conversion of acivicin into a neuroactive metabolite.[43]

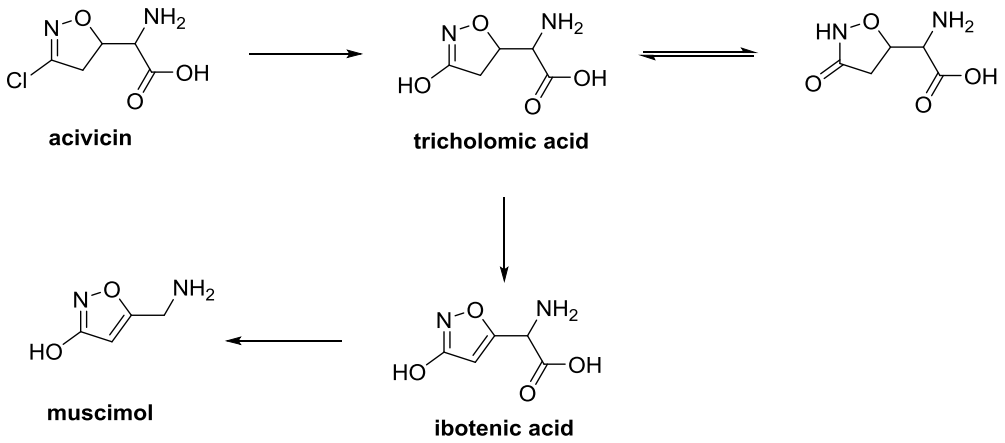

Scheme 7. Possible conversion of acivicin.

The pull down and identification of the covalently bound CES1 was not possible so far and needs to be optimized in future studies. The characterized adduct of metabolically converted ACV2 could explain possible conversion of acivicin and simplify the elucidation via metabolomic studies.

Beside these findings, ACV1 showed a preference for ALDH4A1 which was not observed by other probes used in this work. ACV1 showed growth inhibition but to a lesser extent than ACV2 and acivicin. ALDH4A1 could be labeled directly by ACV1, but longer labeling times showed an alteration of structure as labeled ALDH4A1 became insoluble. Competitive labeling and inhibition assays revealed ALDH4A1 as a target of the natural product acivicin.

ALDH4A1 represents a new identified target of acivicin that also showed growth inhibition of tumor cells upon siRNA knock down. The inhibition of ALDH4A1 happens by inactivation of the active site cysteine. The alteration of neurotransmitter biosynthesis that is affected by inactivation of ALDH4A1 could serve as an explanation for the neurological side effects of acivicin. But ALDH4A1 seems to play an additional role as the growth reduction of tumor cells showed. Studies in glioblastoma cells revealed a higher susceptibility to p53 mediated apoptosis upon inhibition of ALDH4A1 expression. Future work will elucidate the role of ALDH4A1 in growth arrest or apoptosis in relation with p53.

3 Uterine Fibroids

3.1 Special Introduction

3.1.1 Uterine Fibroids

Uterine fibroids (also termed leiomyma or myoma), are benign smooth muscle tumors, that represent the most common gynecological tumors in women of reproductive age. Their prevalence ranges up to 77% among gynecological tumors with an occurrence in 70-80% of women reaching the age of 50.[167-171] Although benign tumors, myomas negatively affect women's life quality with their severe symptoms of heavy, irregular and prolonged menstrual bleeding, anemia, abdominal pain and infertility. Recurrent abortion and preterm labor is also associated with uterine fibroids.[172]

Due to their frequent occurrence, uterine fibroids became objects to clinical research but their clear pathogenesis and etiology still remains unknown. As they normally occur after menarche and regress following menopause, an effect of estrogens and progesterones seems evident. Several studies confirmed this assumption by showing that these hormones promote tumor growth.[167, 173-178] Furthermore, gene polymorphism, epigenetics, familial disposition, oncogenic viruses as well as miRNA deregulation are additionally discussed to trigger myoma development, but contemplation of these factors could not give a clear answer up to date.[179-185]

The benign tumors are derived from uterine smooth muscle cells (myometrium) and consist of large amounts of collagen, fibronectin and proteoglycan, which are typical components of the extracellular matrix.[171, 186] A thin pseudocapsule of areolar connective tissue and compressed muscle fibers are surrounding these tumors.[187] Uterine fibroids are classified in three categories by their location in the uterus (see figure 39) giving subserous, intramural or submucous myoma.

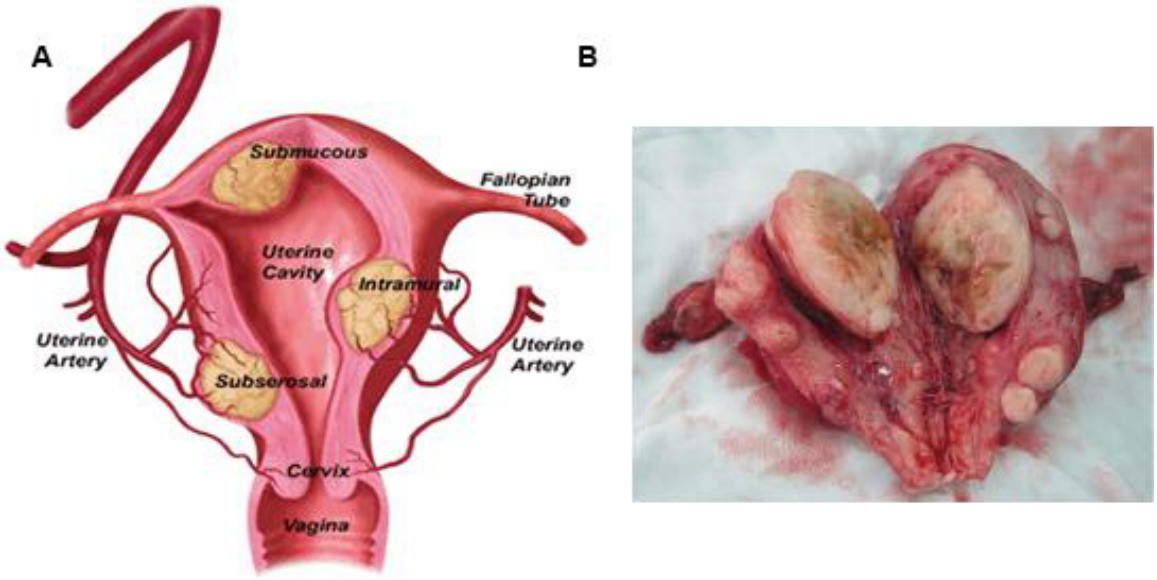

Figure 39. A) Schematic view of the uterus (figure taken from [188])with different types of uterine fibroids and B) picture of an uterus with multiple uterine fibroids after a hysterectomy (figure taken from [189]).

Myomas can occur as single tumors but often multiple tumors are found in one uterus. Analysis of these multiple tumors has shown, that each tumor from the same uterus can have different cytogenetic changes, indicating an independent development.[190] This assumption was confirmed by several x-inactivation studies, showing the monoclonality of each tumor from the same uterus.[191-194]

The size of myoma can vary a lot, even multiple myoma can have size variations ranging from a few millimeters to bigger than 30 centimeters.[195] This could reflect different date of development, with all tumors bearing the same general growth potential, but studies showed that even small myoma can stop growing.[196] Indeed studies showed different growing speeds of different tumors, with bigger tumors that grow faster than smaller tumors.[196, 197] But more surprising was the finding that within multiple myomas, some myomas grow faster than the others.[197] This endogenous growth control differentiates myomas from malignant neoplasms, that do not possess any growth control. For benign and premalignant tumors, growth inhibition is very often caused by oncogene-induced-senescence (OIS) and could possibly explain the growth arrest of myomas.[198-202]

Cellular senescence describes an irreversible cell cycle arrest in the G1 phase, while cells stay metabolically active but are incapable of DNA replication.[203] OIS describes the fact, that senescence is caused by activated oncogenes or oncogenic viruses, that activate p14(Arf) and p16(Ink4a), known cell cycle inhibitors, resulting in an activation of a tumor-suppressor-network, leading to senescence or apoptosis.

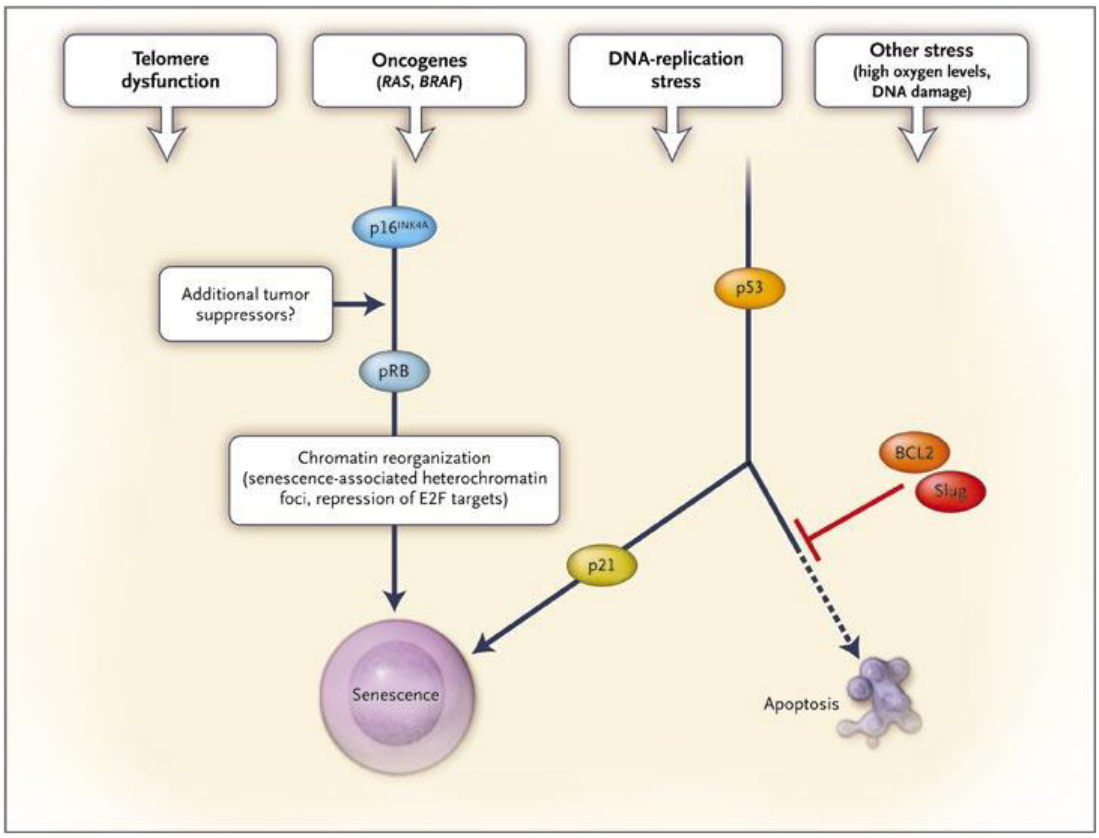

Figure 40. Tumor suppressor networks activated by different types of stress (reproduced with permission from [198], Copyright Massachusetts Medical Society). Stress induces higher levels of p16 (Ink4a) leading to accumulation of tumor suppressor protein retinoblastoma (pRB), which binds to several downstream effectors like E2F. This inactivates DNA replication and transcription leading to senescence. The other major tumor suppressor network is the activated p53 pathway. Different factors can activate the antiproliferative gene p21, survival factors like BCL2 or Slug leading to senescence or proapoptotic genes resulting in apoptosis.

OIS represents a critical step in the premalignant tumor during the development into an malignant tumor were the described tumor suppressor pathways are inactive. Upon an oncogenic mutation, a cell can react in three different ways. First, there is an antiproliferative reaction leading to apoptosis or senescence. The second possibility is a lesion (abnormal tissue) caused by no reaction on the mutation, but this lesion can later develop senescence or apoptosis. And the last possibility is uncontrolled growth linked with additional mutations (see figure 41). The state of senescence represents a very stable state, where cells can stay for decades, but in rare cases these cells can undergo additional mutations and transform into a malignant tumor.

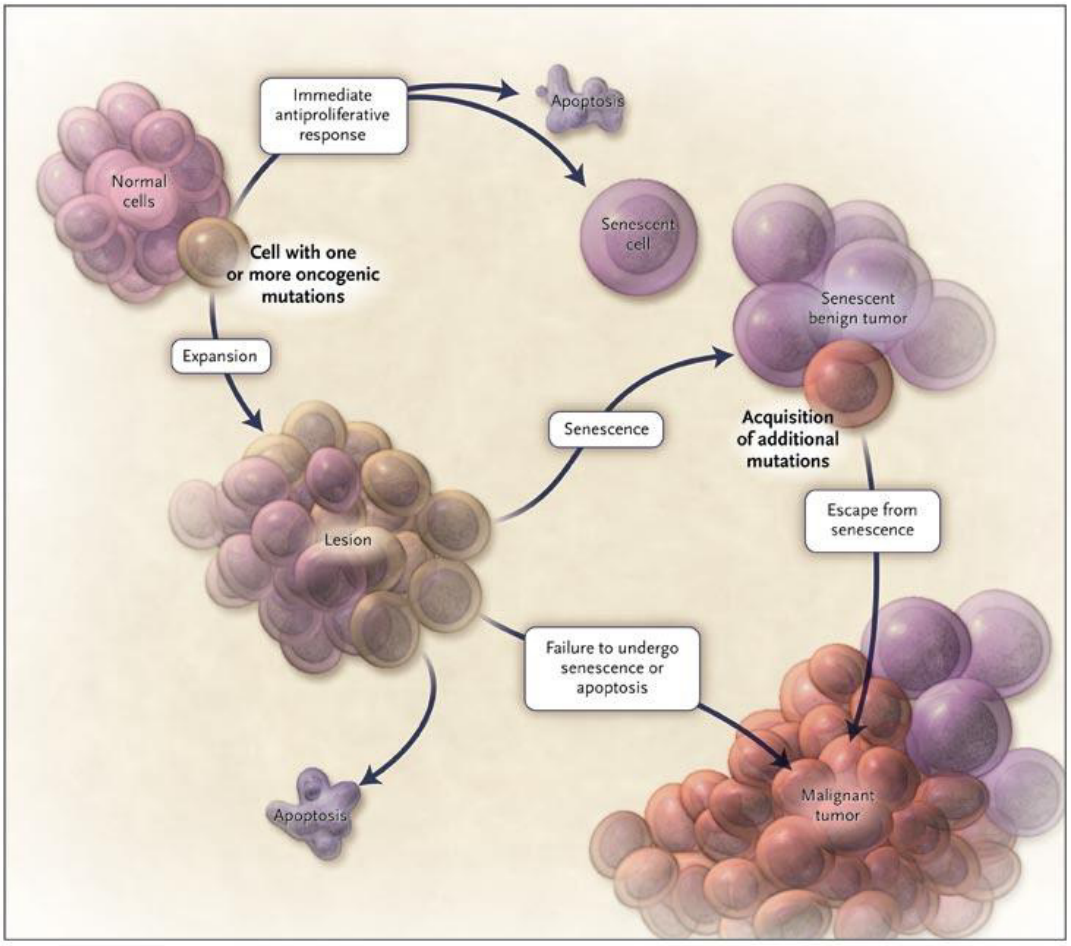

Figure 41. Tumor progression model with three different responses on oncogenic mutations (reproduced with permission from [198], Copyright Massachusetts Medical Society). An antiproliferative response leading to apoptosis or senescence, production of a lesion which can either promote senescence or apoptosis or transform into a malignant tumor with absent defense mechanisms. Cells in senescence state can undergo a malignant transformation.

Recent findings suggest that senescence plays a key role in myoma growth as tumors showed more than 50% of β-galactosidase positive cells , which is a senescence associated marker.[204]

Another model for myoma development recently evolved, suggesting that myomas arise from deregulated stem cells.[205-208] The uterus undergoes several hormone controlled changes (menstruation, pregnancy), which also includes myometrial smooth muscle cells. During these changes cells in the uterine tissue are constantly renewed from these stem cells and this offers a possibility for mutations. Such a mutation was found in the mediator complex subunit 12 (MED12) in uterine fibroids affecting its function.[209] This results in high levels of high-mobility group AT-hook 2 (HMGA2), which are also observed in uterine fibroids and inhibit senescence and self renewal by down regulating p14(Arf).[210, 211] This mutation is also

linked to an alteration of β-catenin and TGF-β signaling, which regulates cell cycle, proliferation, senescence, formation of extracellular matrix, differentiation of stem cells and cell renewal.[210, 212-215]

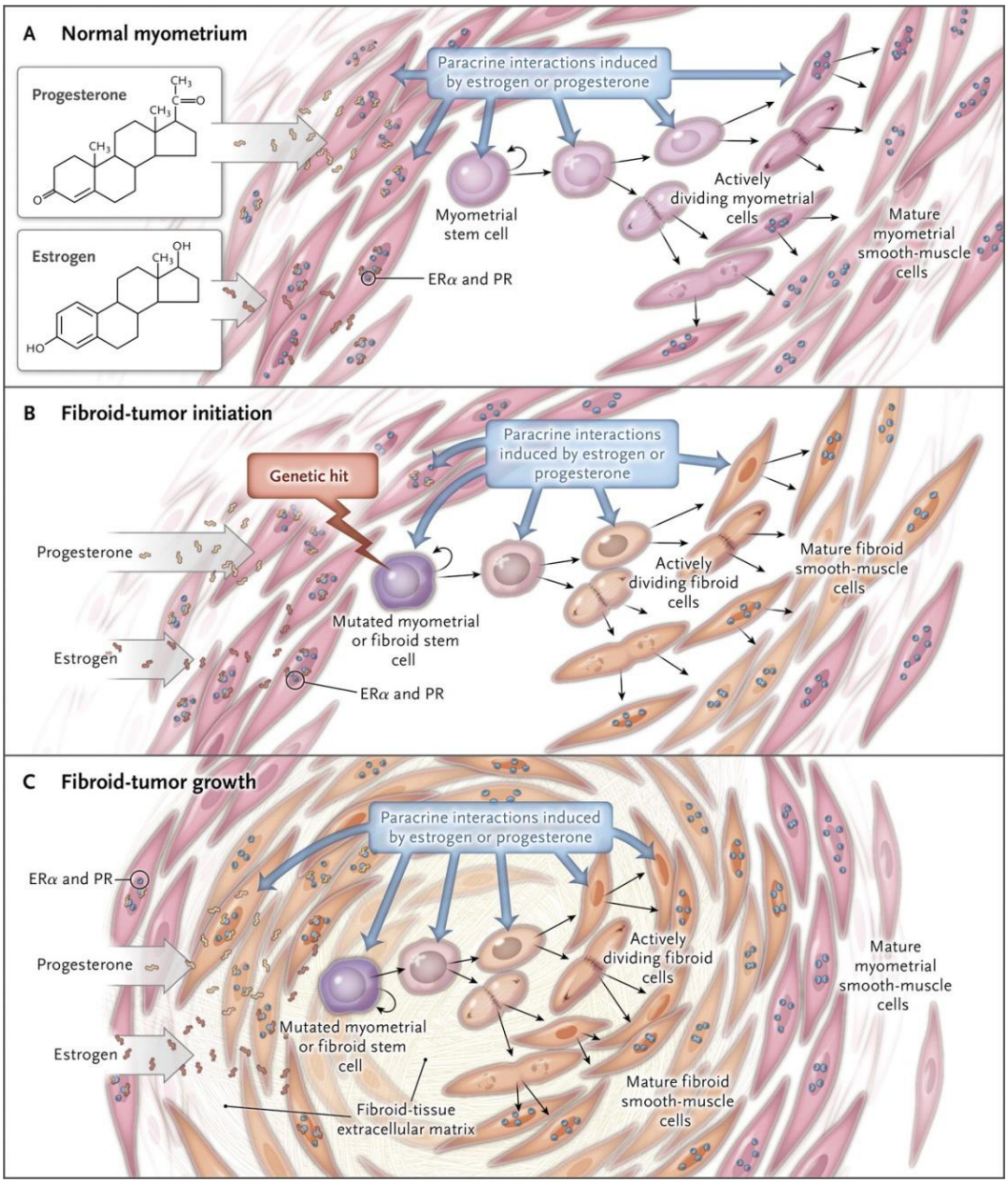

Figure 42. Tumorigenesis of uterine fibroids (reproduced with permission from [205], Copyright Massachusetts Medical Society) A) Progesterone and estrogene mediate stem cell differentiation into myometrial cells that develop into mature myometrial smooth-muscle cells. These have estrogene and progesterone receptors, which in turn activate paracrine factors like WNT ligands that induce stem cell proliferation and renewal. B) HMGA2 mutation (genetic hit) differentiates stem cell into a fibrotic cell, that can start self renewal and divide in an uncontrolled fashion until developing into a mature fibroid smooth-muscle cell. Estrogene and progesterone receptors on this cells induce the mutated stem cell again. C) Benign tumor formation of the mutated stem cell within myometrial tissue with extracellular matrix formation within the tumor.

Despite the tremendous progress in this field, the growth and etiology of myoma still provides many open questions. Without answers to these questions, a new medication on myomas is hard to develop. Current treatment of myoma involve surgery, mainly hysterectomy, where the complete uterus is removed, resulting in immediate cure of the symptoms and prevention of the recurrence. On the other hand it bears all risk that come with surgeries in general and additionally this option might be mostly inacceptable for women of reproductive age. Myomectomy is an alternative surgical option using laparoscopically approach, to excise the tumor. The benefit of this method is to retain the fertility but the main disadvantage is the recurrence of myomas. Another minimal invasive option is the uterine artery embolization, where particulate embolic agents are delivered through the uterine arteries to block the blood vessels of the myomas.[216, 217] This method also remains the possibility of pregnancy but returning symptoms are reported very often as well as miscarriage, preterm labor, postpartum hemorrhage.[187]

In contrast to surgical methods, medical treatment showed only success on short-terms. Gonadotropin-releasing hormone analoga (GnRHa) are a widely used medication in presurgical treatment. They effectively reduce the tumor size, making surgery easier, but go in hand with menopausal symptoms and longterm treatment showed bone demineralization. GnRHa treatment leads to a reduction of angiogenesis and increases apoptosis and reduces the inflammatory reaction in myoma lesions.[218] While myomas possess GnRH receptors, a direct effect of these receptors on tumor growth is also discussed as a possible mechanism of action.[219, 220] However an offset of GnRHa treatment induces regrowth of the tumors to their pretreatment size and the side effects of GnRHa treatment make it inacceptable for long-term treatment.

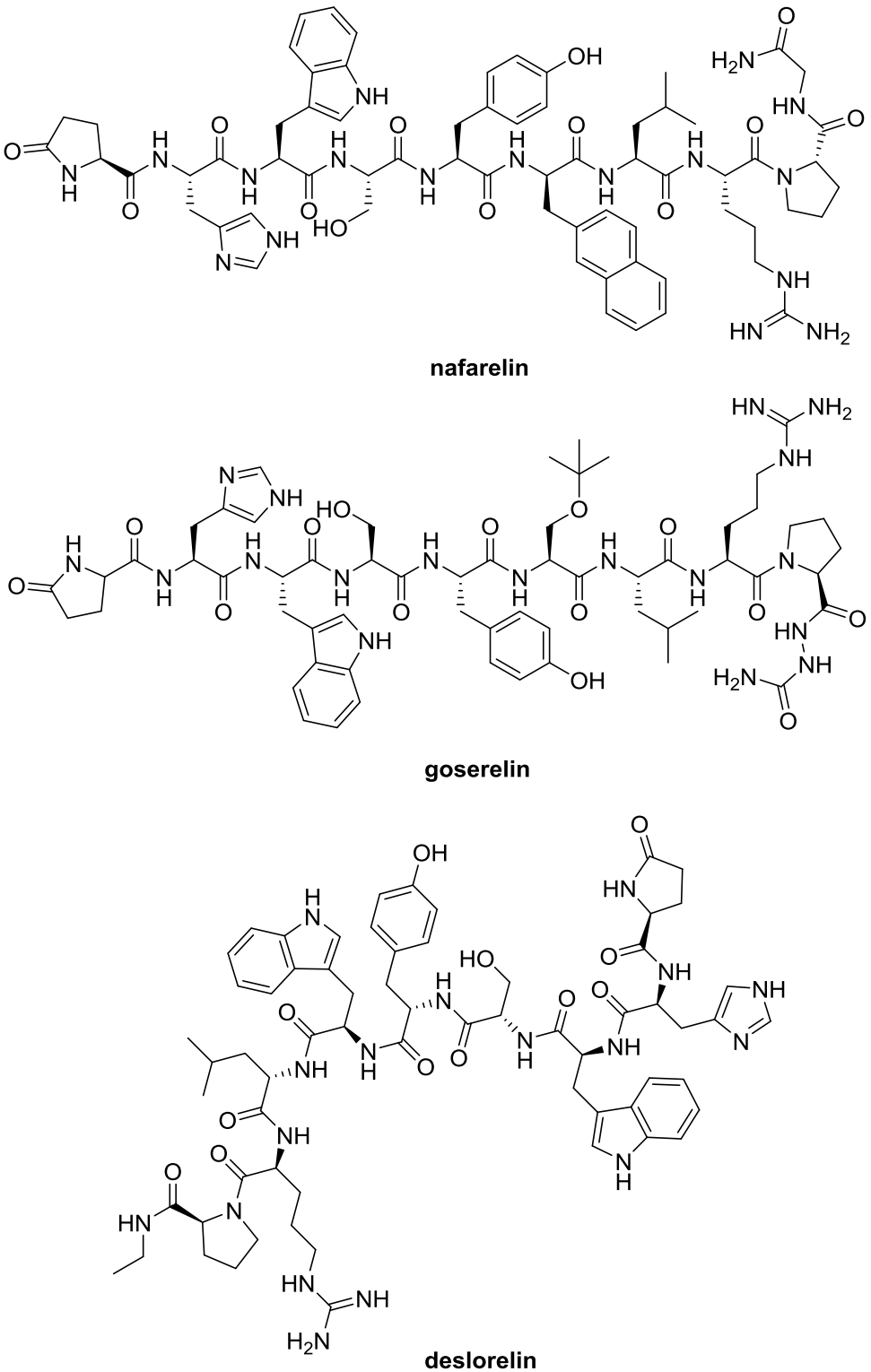

Figure 43. Structures of the gnrh-antagonists nafarelin (Synarel), goserelin (Zoladex) and deslorelin (Ovuplant).

The unsatisfying results for long-term medical treatment and only surgical methods remaining for cure with all its disadvantages, indicates that there is a need for new medical treatment upon these tumors. The fact that their etiology is still only poorly understood, makes it a big challenge. One possible approach is the observation on proteomic level, especially on active

enzymes that could be involved in many development processes of myomas and are accessible for selective inhibitor. Serine hydrolases present such an enzyme class. Until today no such study has been performed.

3.1.2 Serine Hydrolases and MetAP2

Serine hydrolases comprise a large and widely distributed class of enzymes involved in many physiological and pathological processes. In humans, serine hydrolases constitute even 1 % of the predicted protein products and include proteases, lipases, thioesterases, esterases and pepidases, making the serine hydrolases a highly diverse enzyme class.[221] Processes where serine hydrolases are involved span from blood clotting, digestion, nerve signaling, inflammation, to pathological conditions such as cancer, drug resistance, neurodegenerative diseases, cardiovascular alterations, allergies and vital roles in virus life cycles.[160, 222-234] These huge number of involved processes is the reason, why serine hydrolases gained huge biomedical interest and are object to pharmaceutical research.

All serine hydrolases share a nucleophilic serine that is used to cleave ester or amide bonds. The cleavage occurs through a covalent acyl-serine intermediate formed by an attack of a base activated serine on the carbonyl group. That intermediate is cleaved by water hydrolysis.

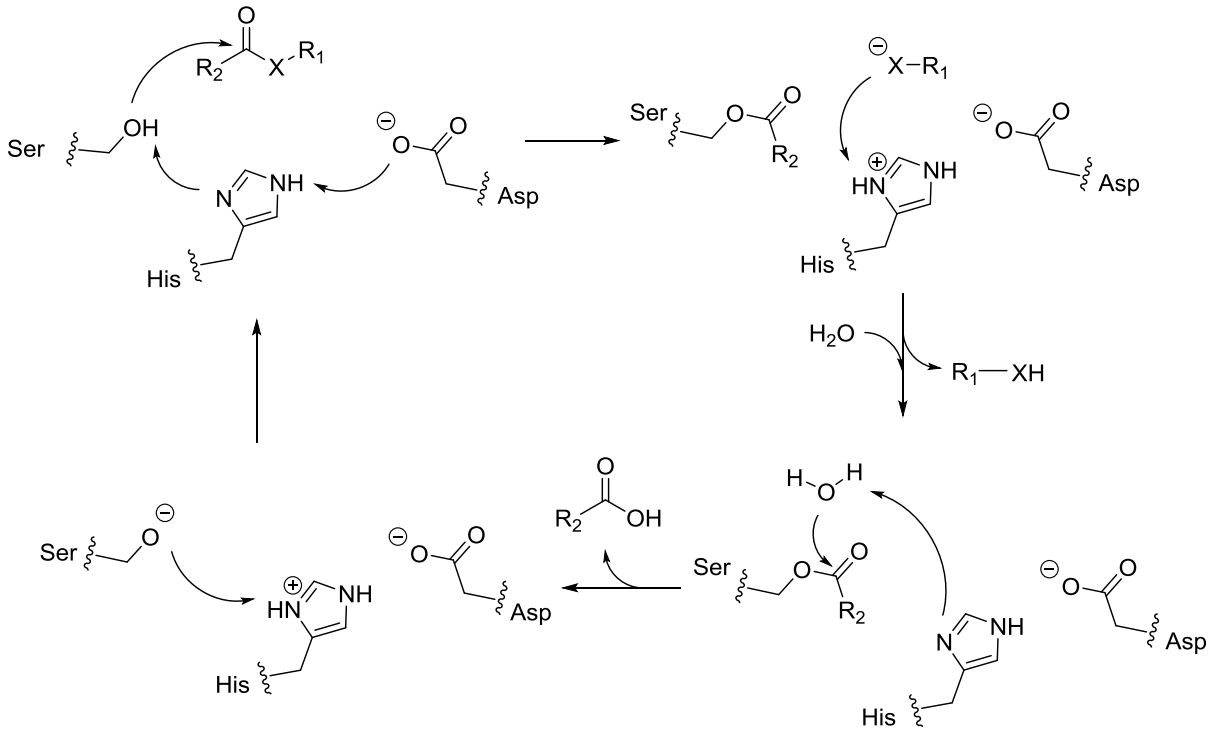

Figure 44. Catalytic cycle of a serine hydrolase.

Approximately 240 human serine hydrolases are to date known and are subdivided in two groups.[235] One subgroup contains the serine proteases, which cleave peptide bonds and are expressed is inactive precursors, so called zymogens.[236] These zymogens are activated by specific cleavage upon stimulation and inactivated by specific endogenous inhibitors.[237, 238] The other subgroup, termed metabolic serine hydrolases, display a more diverse set of substrates and hence a more diverse set of structures. The metabolic serine hydrolase subfamily contains lipases, esterases, thioestereases, peptidases and amidases.[239, 240] Aside with the catalytic triad, that is found in the majority of the metabolic serine hydrolases, there are also Ser-Asp and Ser-Lys Dyads used by some lipases and amidases.[235]

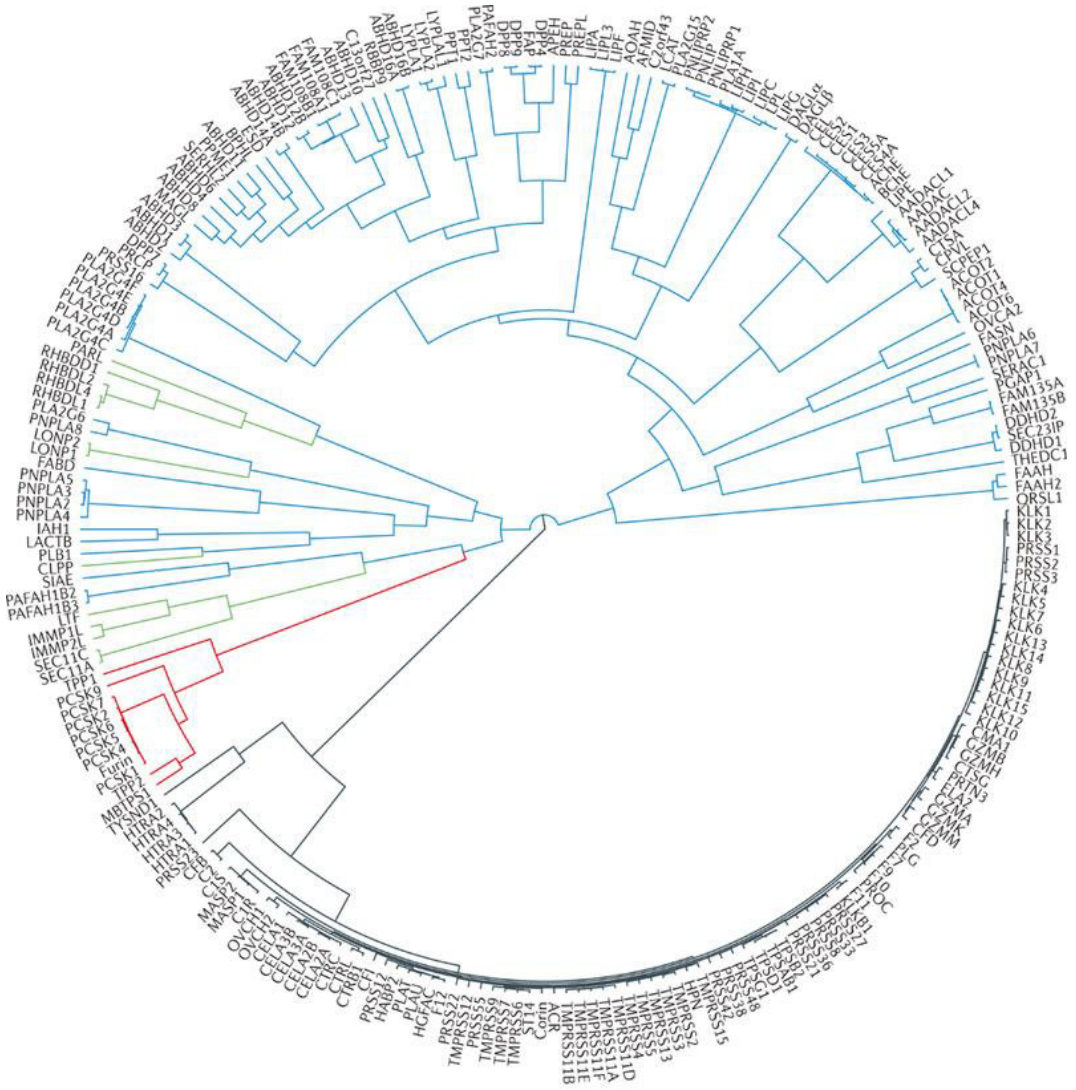

Figure 45. Dendrogram showing over 200 predicted and known serine hydrolases and their relationship (reprinted by permission from Macmillan Publishers Ltd: Nature reviews. Drug discovery [235], copyright 2012). Grey lines represent chymotrypsin like enzymes, blue lines stand for metabolic serine hydrolases, subtilisin like enzymes are depicted in red and the green lines show other small serine hydrolases.

Prominent serine hydrolases are trypsin, a well known enzyme involved in digestion or thrombin and factor Xa that plays an important role in blood clotting, acetylcholinesterase, that is important for synaptic transmission and dipeptidyl peptidase 4, that plays a role in glucose metabolism.

Some enzymes are already considered as therapeutic targets with inhibitors that are already in clinical use. Argatroban and Dabigatran are two inhibitors of thrombin and used for treatment of thrombosis.[241, 242] The same indication can be treated with rivaroxoban, this time targeting factor Xa.[243] For the treatment of dementia caused by Alzheimer's disease, acetylcholin esterase is inhibited by e.g. rivastigmine or the natural product galantamine.[244, 245] Obesity can be treated with the lactone orlistat, that addresses lipases in order to block the uptake of lipids.[246] Another diet associated disease, type 2 diabetes, can be treated by addressing dipeptidyl peptidase 4, that is achieved by using e.g. saxagliptin or linagliptin during therapy.[247, 248] This is a very diverse set of indications, that can already be treated with serine hydrolase inhibitors and even more small molecules that target these enzymes are already in clinical evaluation process.

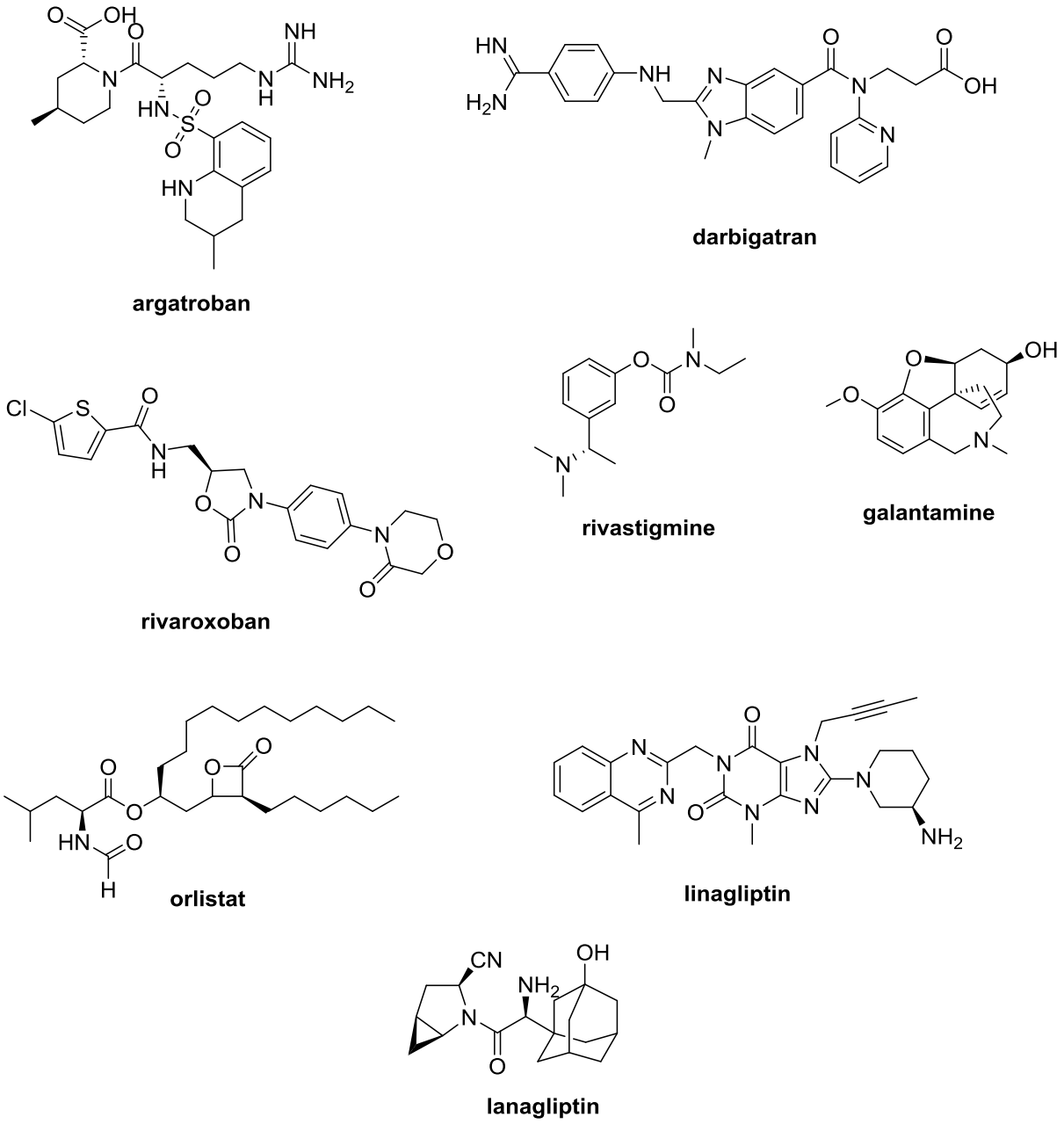

Figure 46. Serine hydrolase inhibitors in clinical use.

But not only serine hydrolases represent an interesting class regarding human pathology. Their close relatives cysteine-, aspartic-, threonine- and metalloproteases are also enzymes of high interest concerning therapies. The HIV1 protease is an aspartic protease and the drug target of retroviral drugs.[249] Cysteine proteases play important roles in apoptosis and threonine proteases contain parts of the proteasome complex, a vital enzyme in eukaryotic cells. The metalloproteases gained huge attention, especially when related to cancer.[32, 250, 251] They are linked with tumor growth, tissue remodeling and basal membrane degradation facilitating tumor metastasis.[252]

A member of this family, the methionyl aminopeptidase 2, gained interest during the last 20 years. This enzyme belongs to methionyl aminopeptidase subfamily, that consists of two proteins and is known to bind 2 cobalt or manganese ions.[253, 254] Methionyl aminopeptidase catalyzes selectively the removal of the initiator methionine residue from nascent proteins during maturation and therefore regulates processes like protein turnover, protein targeting, and cell proliferation.

The reason why MetAP2 gained interest, was the finding that it is the single target of fumagillin and its variants.[255] Studies in cells, down regulating MetAP2, showed reduced angiogenesis as well as reduced cell proliferation and studies in rats revealed tumor growth inhibition and metastasis.[256, 257] These findings indicate a major role in angiogenesis and cell proliferation. In a recent investigations it was found that MetAP2 is also relevant for treatment of obesity and MetAP2 inhibitors are currently tested in clinical trials.[258]

Results and new findings on proteases, especially serine hydrolases and MetAP2, show the great value of these enzymes for future research. By elucidating their roles in the cells, which is not yet fulfilled and the fact, that inhibitors can be designed on these classes, makes these classes promising candidates for future pharmaceutical research and diagnosis.

3.1.3 Aim of this Study

The unsatisfying therapies available for myoma present an urgent need for medical therapies. Medical treatment of myomas to date only consists of hormonal therapy with relapse upon stopping treatment. Serine hydrolases and MetAP2 are involved in tissue regulation and extracellular matrix remodeling. For these enzymes a wide range of inhibitors is already available. Here these enzymes were studied in myoma tissue and healthy myometrium tissue using the ABPP approach. A comparison of enzyme activities in healthy and tumor tissue in several patients was investigated.

3.2 Results and Discussion

3.2.1 Establishing Fluorophosphonate probe

To identify serine hydrolases a probe is needed that broadly labels the big serine hydrolase family. The fluorophosphonate probe (FP) already proved its ability to broadly label serine hydrolases.[19] The design of this probe is inspired by protease inhibitors like diisopropylfluorophosphonate or chemical warfare gases like e.g. sarin.

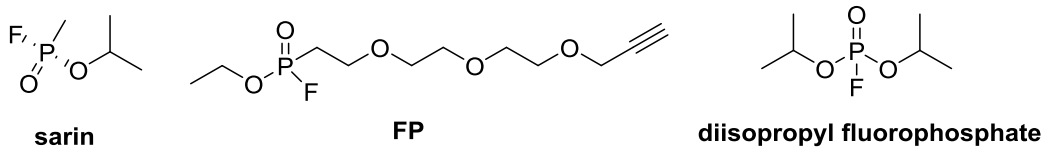

Figure 47. Fluorophosphonates sarin, the fluorophosphonate probe and diisopropyl fluorophosphponate.

With the fluorophosphonate moiety, FP bares a very potent electrophile. A PEG linker enhancing cell permeability connects the electrophile with an alkyne for further click chemistry modification. First labeling attempts with the commercially available FP were done with HCT116 cells that were incubated with 10 µM FP for one hour, followed by attachment of rhodamine using click chemistry and analysis by fluorescence readout of the SDS-PAGE. Together with *in situ* labeling experiments of HCT116 cells, porcine trypsin was incubated with 10 µM FP with the same treatment and analysis as a positive control (see figure 48).

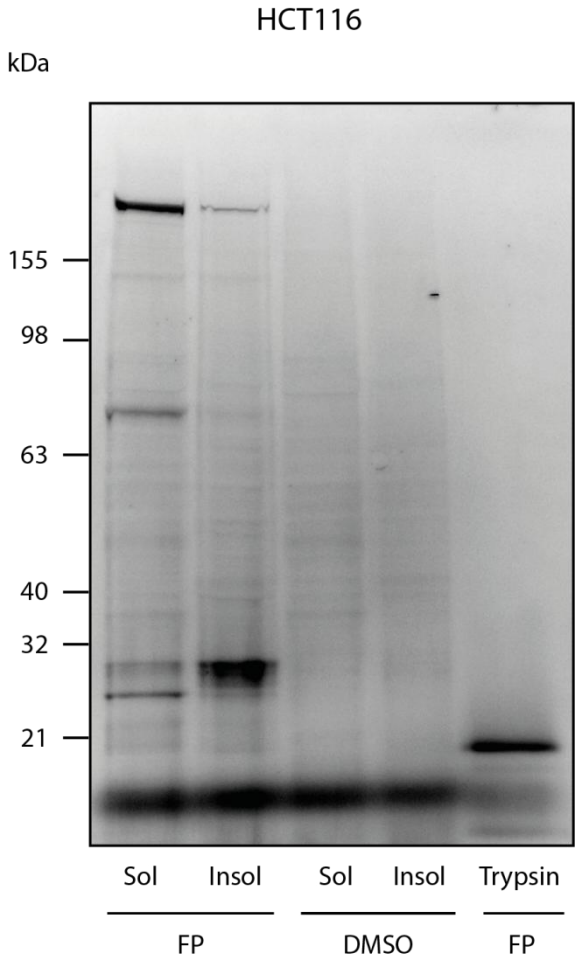

Figure 48. Fluorescence scan of SDS-PAGE of HCT116 cells labeled with FP after attachment of rhodamine azide.

The observed labeling pattern proved the probe and protocol applied as appropriate. The labeling is clear and distinct with low background. With these results in hand FP labeled HCT116 lysates underwent LC-MS analysis by first coupling biotin-azide to FP labeled protein followed by enrichment with streptavidin and tryptic digest on the beads, with subsequent analysis using liquid chromatography and MS/MS analysis. Hits were defined by a ratio of the measured peak area of the labeled proteome divided by the proteome incubated with the same volume of DMSO as described above. MS analysis identified following proteins as shown in the following table 7.

Target	Accession	Description	Area				Probe (1)			Probe (2)			DMSO (1)			DMSO (2)			General information			(Area Probe)/(Area DMSO)	
			Probe (1)	Probe (2)	Control (1)	Control (2)	Score	# Peptides	# PSM	Score	# Peptides	# PSM	Score	# Peptides	# PSM	Score	# Peptides	# PSM	# AAs	MW [kDa]	Sequence coverage	(1)	(2)
FAS	IPI00026781.3	Fatty acid synthase	1,497E9	2,096E8	5,415E8	6,404E7	226,34	39	69	41,81	8	13	146,43	31	46	20,27	4	6	2511	273,3	30,39	2,77	3,27
APEH	IPI00337741.4	Acylamino-acid-releasing enzyme	5,271E7	6,384E7	0,000E0	0,000E0	27,99	6	8	17,50	3	5	0,00	0	0	0,00	0	0	732	81,2	8,47	100	100
PREP	IPI00008164.2	Prolyl endopeptidase	2,039E8	1,027E8	7,201E7	0,000E0	11,07	3	4	8,18	2	3	5,40	2	2	0,00	0	0	710	80,6	8,70	2,83	100
PREPL	IPI00880064.4	Isoform 4 of Prolyl endopeptidase-like	1,691E8	2,340E8	0,000E0	0,000E0	10,82	2	5	8,52	2	4	0,00	0	0	0,00	0	0	638	73,3	6,75	100	100
CPVL	IPI00301395.4	Probable serine carboxypeptidase CPVL	3,06E+08	1,46E+08	0,00E+00	0,000E0	15,54	4	5	10,52	2	3	0,00	0	0	0,00	0	0	476	54,1	9,03	100	100
ABHD10	IPI00020075.4	Abhydrolase domain-containing protein 10, mitochondrial	4,809E7	2,572E9	0,000E0	3,558E7	4,92	2	2	103,95	15	33	0,00	0	0	12,64	2	4	306	33,9	57,52	100	72,30
ABHD11	IPI00171152.2	Isoform 4 of Abhydrolase domain-containing protein 11	8,675E7	2,880E8	0,000E0	0,000E0	22,49	4	8	33,40	5	10	0,00	0	0	0,00	0	0	308	33,8	21,75	100	100
SCPEP1	IPI00477895.3	Isoform 2 of Retinoid-inducible serine carboxypeptidase	1,882E8	4,943E8	1,127E6	1,674E8	18,30	4	6	50,12	8	15	9,32	2	2	47,58	7	14	296	32,9	38,76	166	2,95
PAFAH1B2	IPI00026546.1	Platelet-activating factor acetylhydrolase IB subunit beta	2,015E8	1,64E+08	0,000E0	0,000E0	28,18	2	10	14,30	3	4	0,00	0	0	0,00	0	0	229	25,6	12,23	100	100
PAFAH1B3	IPI00014808.1	Platelet-activating factor acetylhydrolase IB subunit gamma	3,392E7	1,24E+08	0,000E0	0,000E0	10,86	3	4	10,01	4	4	0,00	0	0	0,00	0	0	231	25,7	17,32	100	100
LYPLA2	IPI00646978	Lysophospholipase II	4,511E8	1,123E8	0,000E0	0,000E0	23,25	6	8	4,9	2	2	0,00	0	0	0,0	0	0	231	24,7	36,54	100	100

Table 7. Protein hits from HCT116 incubated *in situ* with FP.

A total of 11 serine hydrolases were identified with different molecular weights. The different protein hits were assigned to bands that showed up in the fluorescence scan. One would expect a higher number of serine hydrolases from this lysates, but no prefractionation (e.g. preparative SDS-PAGE) was done. These findings indicate that the FP-probe and the protocol worked properly and could be used for further experiments.

3.2.2 Homogenization of Myoma and Myometrium Tissue

Labeling of tissue is only enabled by the *in vitro* labeling approach. Samples were purchased from Alcedo or obtained from the tissue collection of Bayer Schering Pharma (now Bayer HealthCare) and were derived from women that underwent hysterectomy. Homogenization of uterine fibroids bears several challenges and is an important step towards ABPP studies. As mentioned above uterine fibroids, like the surrounding tissue contain high amounts of fibronectin and collagen making them very stable tissues. Therefore a more rigid treatment for homogenization is needed, than for instance is needed for liver tissue, to deliver satisfying protein yields. The disadvantage of applying high force during tissue homogenization is the consequence of protein denaturation. This is incompatible with the subsequent ABPP protocol. For uterine fibroids a balance of high yields and a high amount of native protein was needed. This was achieved by using a bead mill with ceramic beads of different diameters. This method offered good protein yields together with native proteins. Detergents and high salt buffers also improved yields and were implemented in the homogenization process. For an adequate comparison, only tissue from one sample was used for all experiments and the same protein amount was loaded on each gel (see figure 49).

A

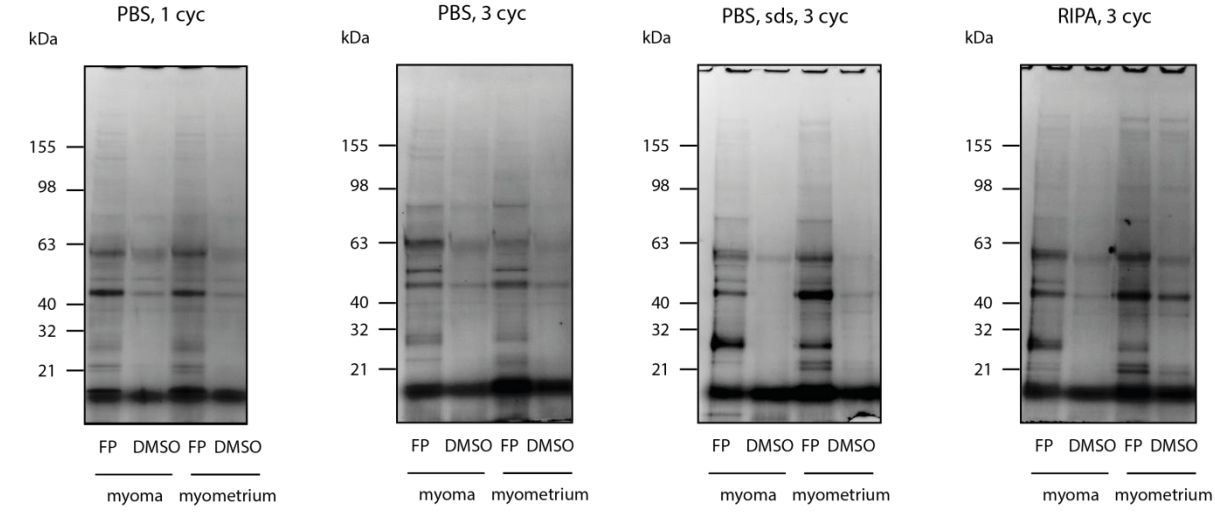

B

	yield [%]			
tissue	myoma		myometrium	
sample	FP	DMSO	FP	DMSO
PBS, 1 cyc	2,1	2,11	3,88	3,21
PBS, 3 cyc	2,92	3,03	3,66	3,31
PBS, sds, 3 cyc	3,76	3,44	3,97	4,11
RIPA, 3 cyc	3,94	3,52	4,6	4,08

Figure 49. A) Fluorescence scans of homogenized tissue under different conditions. B) Protein yields calculated from the amount of tissue used for homogenization.

In general, all methods resulted in labeling, while the addition of SDS enhanced both protein yield and the signal to noise ratio of the labeling. The ripa buffer gave an equal result regarding yield but the labeling compared to the background signal was weaker. The increase of homogenization cycles provided a great improvement on protein yields. These findings provided a robust protocol for further in dept ABPP studies on uterine fibroids.

3.2.1 Labeling of Myoma and Myometrium Tissue with Fluorophosphonate Probe

With the established protocol for homogenization and labeling of myoma and myometrium a total of 9 samples from different patients was analyzed by the ABPP approach. The initial studies were done on small analytical scale using rhodamine azide following protocol on preparative scale where enrichment was done using a trifunctional linker, carrying biotin and rhodamine. The analytical scale experiments additionally offer a good control for the whole enrichment process when applied on the same gel like the preparative samples for band

excision (see figure 50). A problem of serine hydrolases in terms of ABPP is their low abundance resulting in a weak fluorescence readout. This can be overcome by the fluorescence readout of the samples after the enrichment protocol.

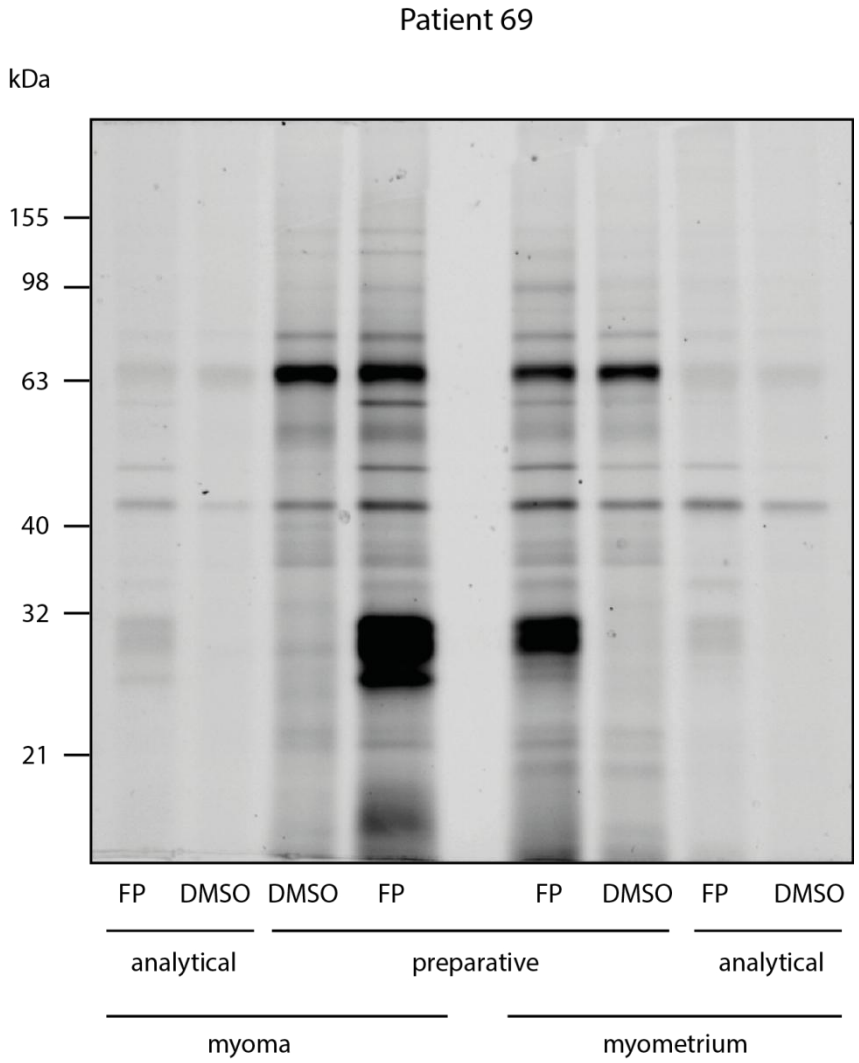

Figure 50. Fluorescence gel of paired myoma and myometrium samples of patient 69 incubated with FP, with analytical samples flanking the preparative samples from avidin enrichment.

The labeling pattern of the myoma and myometrium gave good signal to noise ratio over a wide range of molecular weight. The fluorescence intensity of the enriched samples is, as expected, higher than the analytical samples. Very strong labeling occurs in the areas of ~30 kDa, ~40 kDa and ~60 kDa, with the later ones occurring with almost equal intensity in the DMSO control. The bands of ~40 kDa and ~60 kDa revealed to be actin and serumalbumin, that were labeled due to high abundance. The MS analysis of myoma and myometrium tissue of one patient revealed a big set of serine hydrolases in the sample of this patient (see table 8). Positive protein hits were defined as described above by dividing the

area obtained for a protein the FP sample by the area for a protein obtained by the control sample.

Myoma

Target	Accession	Description	Area		FP			DMSO			General information			(Area FP)/(Area DMSO)	(Area Myoma)/(Area Myometrium)
			FP	DMSO	Score	# Peptides	# PSM	Score	# Peptides	# PSM	# AAs	MW [kDa]	Sequence coverage		
CFB	IPI00921523.1	Isoform 1 of Complement factor B (Fragment)	5,25E+07	1,13E+07	16,18	4	6	8,37	2	3	764	85,5	6,15	4,65	0,77
CES1	IPI00942507.4	Liver carboxylesterase 1	3,01E+08	0,00E+00	241,74	14	76	0,00	0	0	567	62,5	25,93	100	7,93
ACOT1	IPI00333838.1	Acyl-coenzyme A thioesterase 1	5,48E+08	0,00E+00	91,88	11	32	0,00	0	0	421	46,2	29,22	100	14,44
ACOT2	IPI00220906.6	Acyl-coenzyme A thioesterase 2, mitochondrial	3,76E+08	0,00E+00	75,15	10	26	0,00	0	0	483	53,2	22,77	100	9,89
ABHD10	IPI00020075.4	Abhydrolase domain-containing protein 10, mitochondrial	5,66E+07	0,00E+00	8,31	3	3	0,00	0	0	306	33,9	13,07	100	100
ESD	IPI00411706.1	S-formylglutathione hydrolase	2,65E+07	6,60E+06	23,71	3	7	6,52	2	2	282	31,4	15,25	4,02	0,79
TPSAB1	IPI00472739.1	Isoform 2 of Tryptase alpha/beta-1	2,50E+09	8,36E+07	300,48	9	91	11,81	2	4	266	29,5	31,58	29,93	1,77
TPSB2	IPI00419942.2	Tryptase beta-2	9,01E+08	3,27E+07	298,48	8	87	10,54	2	4	275	30,5	30,55	27,59	0,81
TPSD1	IPI00376200.3	Isoform 2 of Tryptase delta	1,51E+09	0,00E+00	143,16	3	38	0,00	0	0	233	25,6	10,73	100	100
CTSG	IPI00028064.1	Cathepsin G	7,72E+08	0,00E+00	76,81	6	27	0,00	0	0	255	28,8	25,1	100	100
CMA1	IPI00013937.1	Chymase	3,98E+08	9,60E+06	162,49	7	52	9,79	3	3	247	27,3	30,77	41,45	29,47

Myometrium

Target	Accession	Description	Area		FP			DMSO			General information			(Area FP)/(Area DMSO)	(Area Myoma)/(Area Myometrium)
			FP	DMSO	Score	# Peptides	# PSM	Score	# Peptides	# PSM	# AAs	MW [kDa]	Sequence coverage		
DPP4	IPI00018953.1	Dipeptidyl peptidase 4	1,40E+07	0,00E+00	9,93	2	3	0,00	0	0	766	88,2	3	#DIV/0!	0
FAP	IPI00295461.4	Isoform 1 of Seprase	8,98E+07	0,00E+00	27,60	5	9	0,00	0	0	760	87,7	7,76	100	0
CFB	IPI00921523.1	Isoform 1 of Complement factor B (Fragment)	5,25E+07	1,13E+07	16,18	4	6	8,37	2	3	764	85,5	6,15	4,65	0,77
F12	IPI00019581.2	Coagulation factor XII	1,42E+07	0,00E+00	10,14	3	3	0,00	0	0	615	67,7	7,97	100	0
CES1	IPI00942507.4	Liver carboxylesterase 1	3,79E+07	0,00E+00	18,06	6	6	0,00	0	0	567	62,5	12,87	100	7,92
ACOT1	IPI00333838.1	Acyl-coenzyme A thioesterase 1	3,80E+07	5,90E+06	25,72	5	9	0,00	0	0	421	46,2	13,54	100	14,44
ACOT2	IPI00220906.6	Acyl-coenzyme A thioesterase 2, mitochondrial	3,80E+07	0,00E+00	22,90	4	8	0,00	0	0	483	53,2	9,11	100	9,89

ESD	IPI00411706.1	S-formylglutathione hydrolase	8,32E+06	1,28E+06	16,00	4	5	7,07	2	2	282	31,4	19,5	6,50	0,79
TPSAB1	IPI00472739.1	Isoform 2 of Tryptase alpha/beta-1	1,11E+09	0,00E+00	163,47	7	51	0,00	0	0	266	29,5	26,32	100	1,77
TPSB2	IPI00419942.2	Tryptase beta-2	9,07E+08	0,00E+00	112,67	5	43	0,00	0	0	275	30,5	25,45	100	0,81
CMA1	IPI00013937.1	Chymase	1,35E+07	0,00E+00	5,92	2	2	0,00	0	0	247	27,3	10,93	100	29,47

Table 8. Protein hits for patient 69 including determined ratios for FP-labeled samples versus control and myoma samples versus myometrium samples. In the case of a protein only occuring in the labeled sample or the myoma the ratio value was set to 100.

The facts that hormones influence myoma growth and that the menstrual cycle is also hormonal driven was also considered. The uterine cycle describes the renewing of the endometrium during menstruation and divides up in three phases. It starts with the menstruation or desquamation of damaged endometrium followed by the proliferative phase in which the endometrium, induced by estrogen, grows while in its last phase, the secretory phase, the thickness of the endometrium reaches its peak and transforms by induction of progesterone into secreting tissue that supports early pregnancy. Although this transformations take place in the endometrium the serine hydrolase activity pattern in myoma or myometrium could be affected as well. To address this issue, samples from the proliferating, secretory phase were analyzed, while samples from the menstruation or desquamation phase were not available. When working with patient samples there is always the possibility that these samples can differ from each other. This brings in an additional variant to the analysis of myoma and myometrium that has to be taken in consideration. For a better overview preparative labeling pattern from different patients were merged together, the myoma and myometrium lanes from each patient separated and grouped to give an overview on myoma and myometrium labeling pattern throughout all patients (see figure 51). All patient samples were analyzed in the same way as described above (see figure 50 and table 8) and gels and protein hits for each patient sample can be found in the appendix.

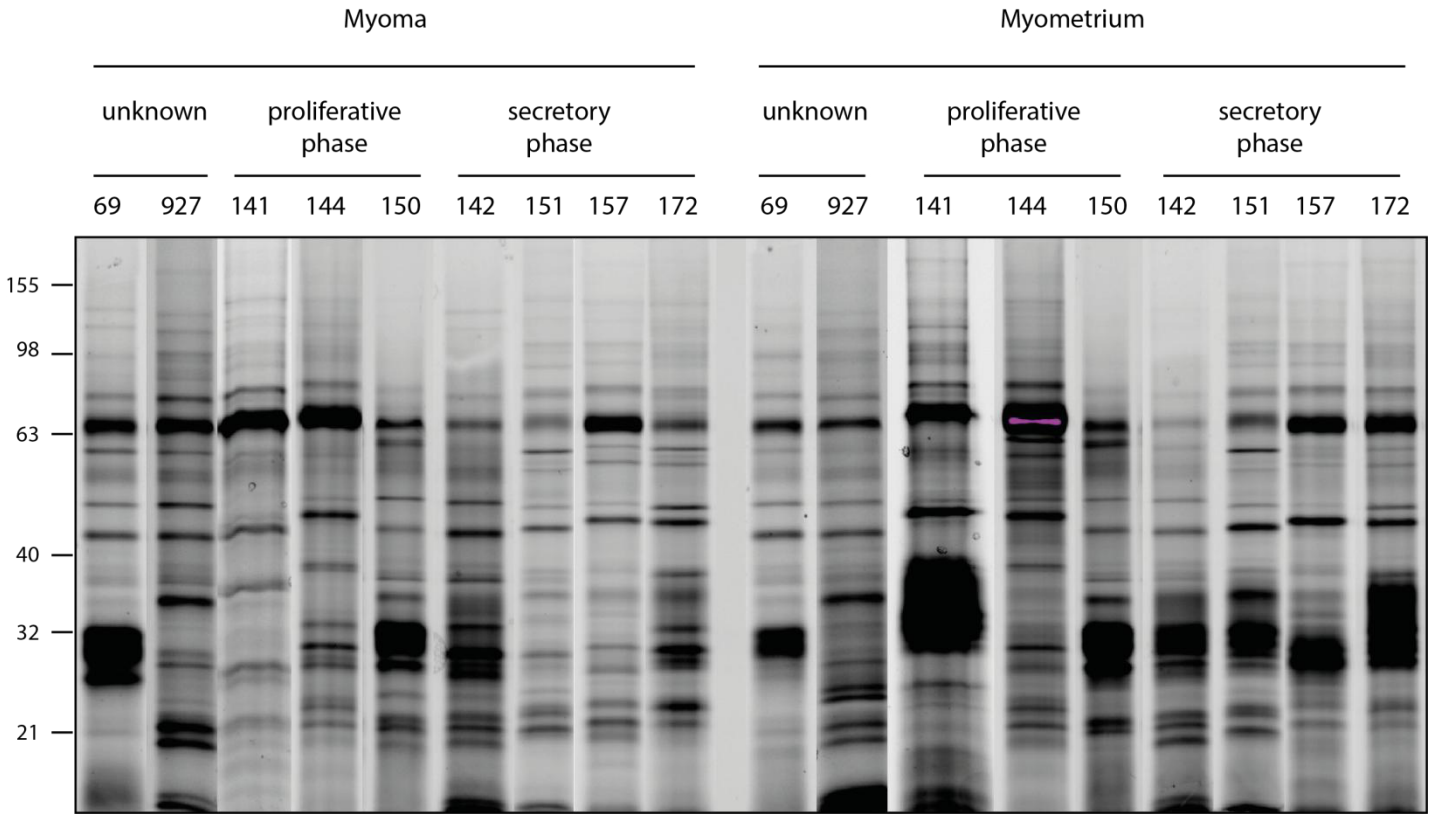

Figure 51. Fluorescence scans preparative scale gels of 9 patients merged together.

The analysis of 9 different patient samples revealed certain similarities that occurred with different intensities but also differences in the labeling pattern. A general difference within cycle phases could not be observed. In myoma samples there was no enzyme or enzymes observed that solely occurred on myoma or were more active in myoma throughout all patients. On the opposite site there was a trend of enzymes around the 30 kDa area that tended to be more active in the myometrium. The mass spectrometrical analysis over all 9 patients revealed 32 active serine hydrolases (table 8). The serine hydrolases Acyl-coenzyme A thioesterase 1 (ACOT1) and 2 (ACOT2), S-formylglutathione hydrolase (ESD), tryptase alpha/beta-1 (TPSAB1), tryptase beta-2 (TPSB2) and Tryptase delta (TPSD1) were active in all patient samples. The serine hydrolases active in at least five patients were complement factor I (CFI), acylamino-acid-releasing enzyme (APEH), Prolyl endopeptidase (PREP), coagulation factor XII (F12), carboxylesterase 1 (CES1), lysosomal protective protein (cathepsin A, CTSA), abhydrolase domain-containing protein 10 (ABHD10), cathepsin G (CTSG), chymase (CMA1) and platelet-activating factor acetylhydrolase IB subunit beta (PAFAH1B2). The hydrolases prothrombin (F2), carboxypeptidase vitellogenic-like (CPVL) and platelet-activating factor acetylhydrolase IB subunit alpha (PAFAH1B1) were active in less than five patients but were active in at least three patients. The last group showed only activity in one or two patients and included dipeptidyl peptidase 4 (DPP4), seprase (FAP),

complement factor B (CFB), Dipeptidyl peptidase 2 (DPP2), acyl-protein thioesterase 1 (LYPLA1), Protein phosphatase methylesterase 1 (PPME1), neutrophil elastase (ELA2), alpha/beta hydrolase domain-containing protein 14B (ABHD14B), platelet-activating factor acetylhydrolase IB subunit gamma (PAFAH1B3), myeloblastin (PRTN3), isoamyl acetate-hydrolyzing esterase 1 (IAH1) homolog, putative hydrolase RBBP9 (RBBP9) and lysophospholipase-like protein 1 (LYPLAL1). This group contains highest number of serine hydrolases. This could be due to sample specific proteins or the fact that these proteins are low abundant. Serine hydrolases with a mass above 65 kDa showed in general lower abundance than compared to homologues with masses below 65 kDa.

From the visual analysis (see figure 51) first hints on different activities were detected that were confirmed by the analysis of the mass spectrometrical data. But identification alone is not sufficient. A comparison of enzyme activity in both healthy and tumor tissue can be assigned. For this purpose the results for protein hits from both myometrium and myoma were compared regarding their intensity. A similar approach as for the identification of protein hits was used but instead of dividing the area of the probe sample by the area of the control sample, the area of the myoma sample was divided by the area of the myometrium sample.

$$Ratio = \frac{Area\ (Myoma)}{Area\ (Myometrium)}$$

Formula 2. Semi quantification of enzyme activity in different tissue based on determined areas from ion chromatogram.

This enabled a direct readout of proteins regarding occurrence and intensity (see table 8 and figure 52).

						(Area Myoma)/(Area Myometrium)								
					Localization			IM	IM		IM		SS	IM
Target	Accession	Description	General information		Cycle phase	unknown		proliferative phase			secretory phase			
			# AAs	MW [kDa]	Patient	69	927	141	144	150	142	151	157	172
DPP4	IPI00018953.1	Dipeptidyl peptidase 4	766	88,2		0	0,68							
FAP	IPI00295461.4	Isoform 1 of Seprase	760	87,7		0	2,07							
CFB	IPI00921523.1	Isoform 1 of Complement factor B (Fragment)	764	85,5		0,77								
APEH	IPI00337741.4	Acylamino-acid-releasing enzyme	732	81,2			0,22		0,88			0,87	1,38	1,25
PREP	IPI00008164.2	Prolyl endopeptidase	710	80,6			1,8	0	1,27			1,47	2,51	1,37
F2	IPI00019568.1	Prothrombin (Fragment)	622	70,0			0	0					0,31	
F12	IPI00019581.2	Coagulation factor XII	615	67,7		0	0					0,86	1,01	0
CFI	IPI00291867.4	Complement factor I	583	65,7			0	0,58	0,84	0,48		0		
CES1	IPI00942507.4	Liver carboxylesterase 1	567	62,5		7,93	100	100	0			0,59		
CTSA	IPI00021794.8	Lysosomal protective protein	480	54,4			100		2,25	0,46	100			100
CPVL	IPI00301395.4	Probable serine carboxypeptidase CPVL	476	54,1					0	100	5,33			
DPP2	IPI00296141.4	Dipeptidyl peptidase 2	492	54,3					0,57					
ACOT1	IPI00333838.1	Acyl-coenzyme A thioesterase 1	421	46,2		14,44	100	1,04	0,17	1,13	1,76	0,9	1,73	1,58
ACOT2	IPI00220906.6	Acyl-coenzyme A thioesterase 2, mitochondrial	483	53,2		9,89	7,56	1,2	0,16	100	1,65	0,93	1,75	1,62
PPME1	IPI00007694.5	Protein phosphatase methylesterase 1	386	42,3					100		100			
ABHD10	IPI00020075.4	Abhydrolase domain-containing protein 10, mitochondrial	306	33,9		100		0	3,07	0,83	4,97	0	0	2,44
ABHD14B	IPI00063827.1	Isoform 1 of Abhydrolase domain-containing protein 14B	210	22,3						1,03	0			
ESD	IPI00411706.1	S-formylglutathione hydrolase	282	31,4		0,79	3,01	0,34	0,75	1,55	1,77	0,83	1,09	1,03
TPSAB1	IPI00472739.1	Tryptase alpha/beta-1	266	29,5		1,77	0	0	0,86	0,93	0,42	0,01	0	0,41
TPSB2	IPI00419942.2	Tryptase beta-2	275	30,5		0,81	0	0	0,85	0,92	0,32	0,01	0	0,43
TPSD1	IPI00419573.3	Isoform 1 of Tryptase delta	242	26,6		100	0	0	0	0,91	0,36	0	0	0,31
CTSG	IPI00028064.1	Cathepsin G	255	28,8		100	0		100	0	1,19	0	0	0,41
CMA1	IPI00013937.1	Chymase	247	27,3		29,47				0	0,33	0	0	0
PAFAH1B1	IPI00218728.4	Isoform 1 of Platelet-activating factor acetylhydrolase IB subunit alpha	410	46,6							100	0,73	1,22	

PAFAH1B2	IPI00026546.1	Platelet-activating factor acetylhydrolase IB subunit beta	229	25,6			0	1,64	0,4	100	1,23	0,42	1,04
PAFAH1B3	IPI00014808.1	Platelet-activating factor acetylhydrolase IB subunit gamma	231	25,7				100			100		
LYPLAL1	IPI00059762.5	Isoform 1 of Lysophospholipase-like protein 1	237	26,3				100					100
ELA2	IPI00027769.1	Neutrophil elastase	267	28,5		0							
PRTN3	IPI00027409.1	Myeloblastin	256	27,8		0							
RBBP9	IPI00034181.1	Isoform 1 of Putative hydrolase RBBP9	186	21,0				100	100				
IAH1	IPI00419194.2	Isoamyl acetate-hydrolyzing esterase 1 homolog	248	27,6				100					
LYPLA1	IPI00514320.4	Acyl-protein thioesterase 1	565	62,8						100			

Table 9. Protein hits from 9 paired myoma and myometrium patient samples comparing activities of confirmed protein hits in myoma and myometrium tissue, from different cycle phases and different localizations as far as known. IM stands for intramural and SS stands for subserosal myoma. For proteins only active in myoma the value was set to 100 and proteins only active in myometrium were set to 0. Other values were derived by dividing the areas for the specific protein from the different tissues. No entry means not detected in this patient.

The activity of a serine hydrolase in myoma and myometrium in a patient could be equal, more active in myoma/myometrium or only active in myoma/myometrium. By applying these criteria to the results obtained and converting it to a color code a heat map was generated to facilitate the readout of this data.

Target			IM	IM		IM		SS	IM	Localization
	unknown		proliferative phase			secretory phase				Cycle phase
	69	927	141	144	150	142	151	157	172	Patient
DPP4	0	0,68								
FAP	0	2,07								
CFB	0,77									
APEH		0,22		0,88			0,87	1,38	1,25	
PREP		1,8	0	1,27			1,47	2,51	1,37	
F2		0	0					0,31		
F12	0	0					0,86	1,01	0	
CFI		0	0,58	0,84	0,48		0			
CES1	7,93	100	100	0			0,59			
CTSA		100		2,25	0,46	100			100	
CPVL				0	100	5,33				
DPP2				0,57						
ACOT1	14,44	100	1,04	0,17	1,13	1,76	0,9	1,73	1,58	
ACOT2	9,89	7,56	1,2	0,16	100	1,65	0,93	1,75	1,62	
PPME1				100		100				
ABHD10	100		0	3,07	0,83	4,97	0	0	2,44	
ABHD14B					1,03	0				
ESD	0,79	3,01	0,34	0,75	1,55	1,77	0,83	1,09	1,03	
TPSAB1	1,77	0	0	0,86	0,93	0,42	0,01	0	0,41	
TPSB2	0,81	0	0	0,85	0,92	0,32	0,01	0	0,43	
TPSD1	100	0	0	0	0,91	0,36	0	0	0,31	
CTSG	100	0		100	0	1,19	0	0	0,41	
CMA1	29,47				0	0,33	0	0	0	
PAFAH1B1						100	0,73	1,22		
PAFAH1B2			0	1,64	0,4	100	1,23	0,42	1,04	
PAFAH1B3				100			100			
LYPLAL1				100					100	
ELA2		0								
PRTN3		0								
RBBP9				100	100					
LYPLA1						100				
IAH1				100						

Only active in myometrium
More active in myometrium
Equal active
More active in myoma
Only active in myoma

Figure 52. Heat map of protein hits comparing their activity in myoma and myometrium. Enzymes only active in myoma were set to the value 100 and enzymes only active in myometrium were set to 0. Equal activity ranged from 0.5 to 2. Values in between were defined as more active in myoma/myometrium. No entry means no detection in this patient.

The analysis of the relative activity profile gave conclusions on the activity in the healthy tissue compared to tumor tissue. Many enzymes were only found in a small number of patients and are not significant enough for a general characterization of myoma and myometrium tissue, but should be still regarded as interesting enzymes for characterization, e.g. for targeted approaches, since they mainly show low abundance and could be below the detection limit. Enzyme showing these limitations were DPP4 and FAP, that were only found in 2 patients but with no clear tendency regarding activity in one of both tissues types. CFB and DPP2 showed only activity in one patient with an equal activity. The enzymes IAH1, LYPLA1, were active in one patient and PPME1, PAFAH1B3 and LYPLA1 were found in two patients being only active in the myoma. This could be a seen as a hint for enzymes only active in myoma, but these enzymes again showed low abundance making them hard to detect. By only occurring in only up to two patients, these hits were lacking significance throughout several patients. ELA2 and PRTN3 showed similar characteristics, except being only active in myometrium. F2 appeared in three patients only active in myometrium and a tendency of higher myoma activity was shown by CFI (three of five patients) and F12 (three of four patients). CPVL and PAFAH1B1 were detected in three patients but showed no clear tendency towards activity in one of the two tissue types, as did ABHD14B that was only found in two patients.

CES1 and CTSA showed a tendency to be more active in myoma, while the tendency was clearer for CTSA (four of five patients) than for CES1 (three of five patients) but their significance throughout all patients is still low. PAFAH1B2 was also detected in five patients but a clear tendency towards activity in one of both tissues was not found.

ACOT1, ACOT2 and ESD were always detected in all patients showing no tendency to be more active in one of both tissues. ABHD10 was found in eight patients also showing no tendency to be more active in myometrium or myoma.

TPSAB1, TPSB2 and TPSD1 were detected in all patients and belong to the high abundant serine hydrolases. They showed a higher activity in myometrium in six of nine patients and for TPSD1 in seven of nine, with one sample only occurring in myoma. All patients with samples from the secretory phase showed a higher activity for these enzymes in myometrium while in two of three patients with samples from the proliferative phase showed an equal activity. These patients (144 and 150) on the other hand showed activity of RBBP9 in myoma. Although RBBP9 was only detected in two patients, the fact that these patients samples were taken during the proliferative phase and the inverse activity compared to TPSAB1 and TPSB2

in these patients and the additional fact that the sample 141 was only slightly proliferating already turning to the secretory phase highlighted the role of this enzyme.
CMA1 and CTSG showed a higher activity in mainly myometrium. This was the case for CMA1 in five of six patients. CTSG showed in five of eight patients a higher activity in myometrium while both enzymes showed in the majority of all patients only active in myometrium. This activity pattern showed similarity to the three tryptases TPSAB1, TPSB2 and TPSD1 but a relation to cycle phases was not detected.

3.2.2 Functions of Differentially Active Serine Hydrolases

From the 9 patients analyzed, the enzymes TPSAB1, TPSB2, TPSD1, CMA1, CTSG, CES1, CTSA and RBBP9 showed a different activity profile in healthy and tumor tissue. These enzymes comprise various tasks and are involved in complex processes.
The serine proteases TPSAB1, TPSB2, TPSD1 and CMA1 are typical enzymes for mast cells, a cell type discovered by Paul Ehrlich in the late 19th century. This indicates the presence of mast cells in myometrium. Among the proteases CMA1, TPSAB1 and TPSB2 are well studied, while TPSD1 was long believed to be a pseudogene but was later characterized in various tissues.[259, 260] Mast cells occur in various tissues and organs including heart, lung, skin, digestive system, smooth muscle tissue and are involved in a number of processes and diseases like inflammation, wound healing, tissue remodeling, allergies, arteriosclerosis, arthritis, tumorigenesis and autoimmune diseases.[261-264] The processes were mast cells are involved are mainly induced by the secretion of the mast cell specific proteases TPSAB1, TPSB2, TPSD1 and CMA1. Beside tissue degradation through their protease activity, these mast cell proteases also activate tissue-resident macrophages, as well as several matrix metalloproteinases (MMP) for the degradation of extracellular matrix.[233] Mast cell proteases also influence tissue remodeling through activation of procollagenases or the activation of transforming growth factor beta (TGF-β) which counteracts the MMP-dependent extracellular tissue degradation.[233, 265, 266] The three tryptases (TPSAB1, TPSB2 and TPSD1) cause endothelial cells to produce interleukin-8 and the chemokine ccl2, proinflammatory proteins that recruit leukocytes.[267] CMA1 seems to play a special role among mast cell proteases, since some mast cells lack this protease. CMA1 can modify high-density lipoprotein, altering cholesterol metabolism, enhance the formation of angiotensin II, a peptide hormone that increases blood pressure. It was shown that CMA1 can induce

apoptosis in vascular smooth muscle cells and endothelial cells.[268-271] Additional studies with rat derived aortic smooth muscle cells showed that CMA1 inhibits cell growth and collagen expression induced through TGF-β.[272]

Mast cells are typically identified through the above mentioned tryptases and/or CMA1. Nevertheless the mast cell proteases play a key role. Studies in mice with a knockout of mast cell proteases revealed delayed wound healing on skin injury, revealing their important role in wound healing.[273] But mast cells do not only play a role regarding inflammation/immune processes and autoimmune diseases. They also showed a relevance regarding cancer with effects in both ways, antitumor and tumor progressive, depending on the tumor type and tumor microenvironment.[274] This is something, that can be observed in general. Their ability to stimulate immune responses with its protective role, can on the other side cause severe diseases, as shown for arteriosclerosis.[233] This makes mast cells controversial cells that are not fully understood. Their abilities for tissue remodeling, wound healing and tumor progression make them interesting candidates for further studies on their role in myoma pathology since in myoma tissue mast cell indicating proteases (TPSAB1, TPSB2, TPSD1 and CMA1) were less active or even inactive. The critical role of regulation of mast cell activity is currently discussed in literature. [233, 262, 263]

Along with the four proteases mentioned above CTSG showed a similar activity pattern in myometrium and plays a role in terms of tissue remodeling and defensive system. CTSG is produced mainly by neutrophils, but also occurs in mast cells where it is CTSG secreted along with TPSAB1, TPSB2, TPSD1 and CMA1.[275] CTSG in combination with the other two neutrophil serine proteases PRTN3 and ELA2 plays a major role in the innate immune response and represents the first line of defense against bacterial tissue infection. An activity of all three was only discovered in one patient (patient 927).[276] The functions of CTSG include cleavage of extracellular matrix proteins like collagens or proteoglycans, the conversion of angiotensin I to angiotensin II, cleavage of inflammatory mediators like chemokines and cytokines (CXCLs 5 and 7,CCL 5, 15 and 23, chemerin, interleukines) that recruit leukocytes, activation of platelets [275-279] The participation in inflammation processes like in the case of CMA1 and the mast cell tryptases goes with a controversial role with beneficial and detrimental effects. CTSG together with the two other neutrophil proteases ELA2 and PRTN3 is discussed as a pharmaceutical target due to being involved in diseases like chronic obstructive pulmonary disease (COPD), Crohn's disease, rheumatoid arthritis, cystic fibrosis.[280] CTSG was recently found in endometrial tissue, being highly upregulated in inflammation related endometriosis, a chronic gynecological disorder with

abnormal localization of endometrial tissue outside the uterus.[281] In an another recently published study CTSG together with CMA1 derived from mast cells were described to be key players in abdominal aortic aneurysm.[282]

Together all five enzymes (TPSAB1, TPSB2, TPSD1, CMA1 and CTSG) play an important role in inflammation processes and tissue remodeling and are typical enzymes for mast cells. Those enzymes were mainly active in myometrium indicating a certain role for this tumors. As a part of the immune system they play a controversy role, being part of the immune system as well as the mediator of disease such as diverse autoimmune disorders indicating that regulation of these cells plays a crucial role. Furthermore, studies showed that growth factors play an important role in mediating fibroid growth, including TGF-ß which is regulated by CMA1 as well as angiotensin II, which is regulated by CMA1 and CTSG. That was shown in *in vitro* experiments to enhance myoma proliferation.[186, 283] Furthermore the role of mesenchymal stem cells, which were identified as a side population in myometrium and identified to promote growth of myoma arise interest.[205-207] Mesenchymal stem cells are regulated through TGF-ß, chemokines and cytokines and play an important role in fibrosis.[284-286]

CTSA is a protective protein that is expressed in a variety of tissues and is present in lysosomes, cell membranes and in the extracellular space.[287] CTSA forms together with neuroamidase 1 (NEU1) and ß-galactosidase (GLB1) a multienzyme complex protecting from lysosomal degradation and an absence of CTSA or mutation in this complex is connected with galactosalidosis.[288, 289] These findings and studies in mice show that CTSA plays an important role in diseases or processes that are mediated through NEU1 and GLB1, such as elastic fiber formation and endothelin activation.[290] CTSA also processes bioactive peptides like angiotensin I, substance P, oxytocin and endothelin I.[291-293] Recent findings suggest a role of CTSA in chaperone mediated autophagy, by degrading the lysosome-associated membrane protein type 2a (LAMP2a), an isoform of a receptor that is solely responsible for the induction chaperone mediated autophagy.[294] Additionally, it was shown that CTSA together with NEU1 activates macrophages and also regulates phagocytosis of macrophages.[295-297] These findings are interesting regarding myoma, since CTSA was found mainly in myoma, especially in intramural myomas, as far as classified, which are reported to have a higher accumulation of macrophages compared to otherwise localized myomas.[298] The exact role of CTSA and especially the enzyme complex it is involved in is still not fully understood.

Retinoblastoma-binding-protein 9 (RBBP9) has its name from binding to the tumor suppressor protein retinoblastoma, but it has also serine hydrolase activity. Its substrates are so far unknown.[299] The upregulation of RBBP9 was associated with tumorigenesis of pancreatic cancer cells and the transformation process of endothelial cells.[300-302] Furthermore, RBBP9 was found downregulated in mesenchymal stem cells of patients suffering from amyotrophic lateral sclerosis.[303] For pluripotent stem cells RBBP9 seems to be important to uphold pluripotency as siRNA studies showed.[304] This implicates various functions of RBBP9, while the complete role in the human organism is not yet completely understood. A key mechanism concerning tumor growth was identified by suppression of the TGF-β induced growth arrest.[300] The interference in the TGF-β signaling is interesting since the above mentioned mast cell tryptases and chymase also activate TGF-β. This is important because RBBP9 was only found active in myoma when the mast cell tryptases and chymase showed an equal activity in both myoma and myometrium tissue. Although there is an interesting relationship between these enzymes additional samples must be investigated to confirm these conclusions.

3.2.3 Labeling of Myoma and Myometrium Tissue with Fumagillin

The angiogenesis inhibitor fumagillin with its carboxyl group offers a position for directly modifying the natural product. Probes based on fumagillin were already synthesized including probes that were obtained from ovalicin, an angiogenesis inhibitor related to fumagillin, a spiroepoxide bearing a second epoxide unit. The derivative fumagillin probe lacks the polyene tag with the carboxyl group, that is replaced by an alkane spacer connected to fumagillin through a carbamate, carrying biotin, whereas ovalicin has a similar linker attached.[305, 306]

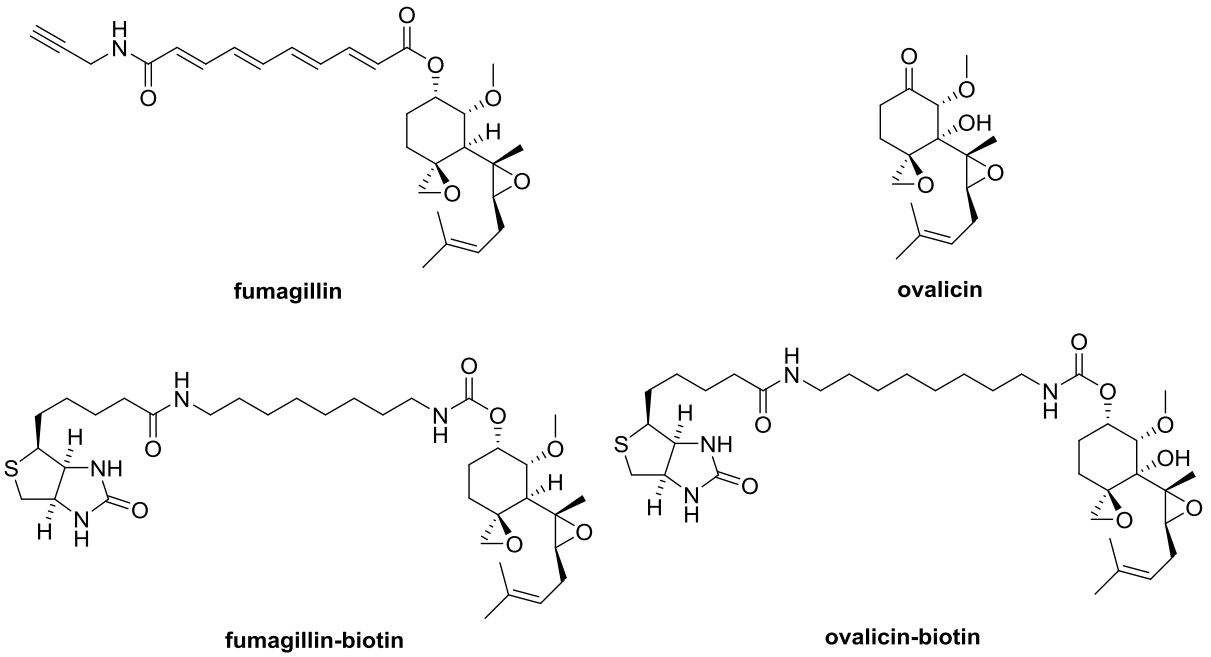

Figure 53. Already established probes build from fumagillin and ovalicin.

In this work, fumagillin was modified carrying the original polyene tag by coupling propargylamine to the carboxyl group via amide coupling. The reaction was carried out using the high performance coupling agents COMU and Oxyma pure. After HPLC-purification the desired product was isolated 20% yield.

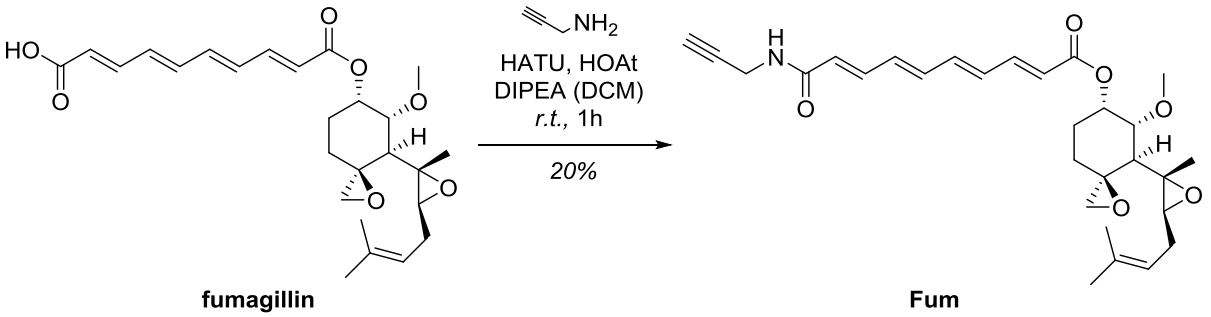

Scheme 8. Synthesis of Fum probe from the natural product fumagillin.

After the successful synthesis the Fum-probe underwent first labeling experiments at various concentrations to find an optimal concentration. For the labeling experiments the breast cancer cell line MDA-MB231 was used. The cells were incubated with the probe for one hour with subsequent attachment of rhodamine-azide using click chemistry.

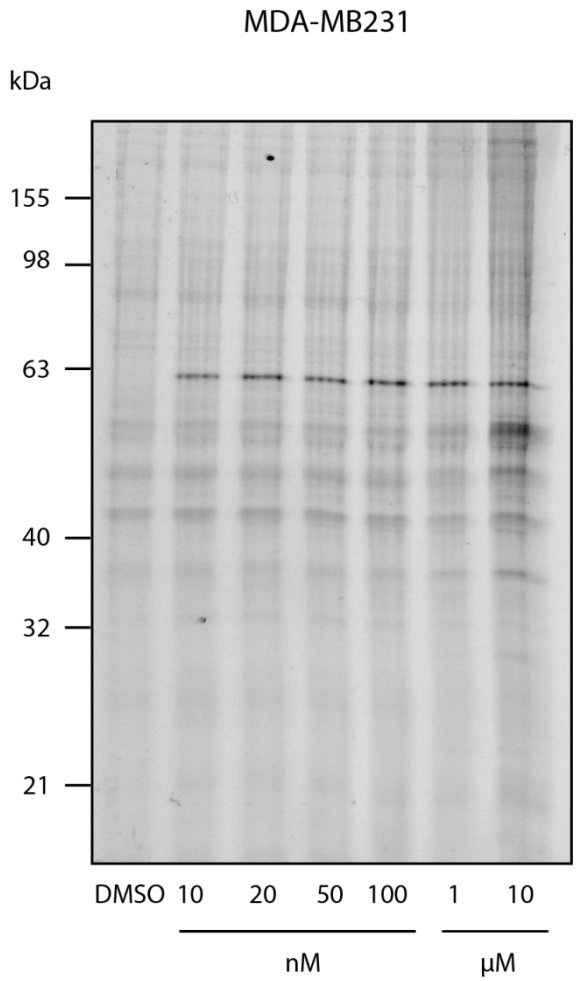

Figure 54. Fluorescence scan of MDA-MB231 labeled with Fum.

The labeling experiments reveal a very sensitive probe that gives a good signal to noise ratio with specific labeling. A saturation of labeling was already achieved using concentrations as little as 10 nM. Labeling experiments on preparative scale and pull down of labeled proteins and LC-MS analysis revealed MetAP2 as the identified hit from that band. Hits were defined by a ratio of the measured peak area of the labeled proteome divided by the proteome incubated with the same volume of DMSO as described above (protein hit can be found in the appendix).

With this successful labeling the next step was to label myoma and myometrium tissue lysates. Lysates were obtained the same way as described above and incubated with 1 µM Fum-probe for one hour with subsequent attachment of rhodamine-azide and fluorescence readout of SDS-PAGE.

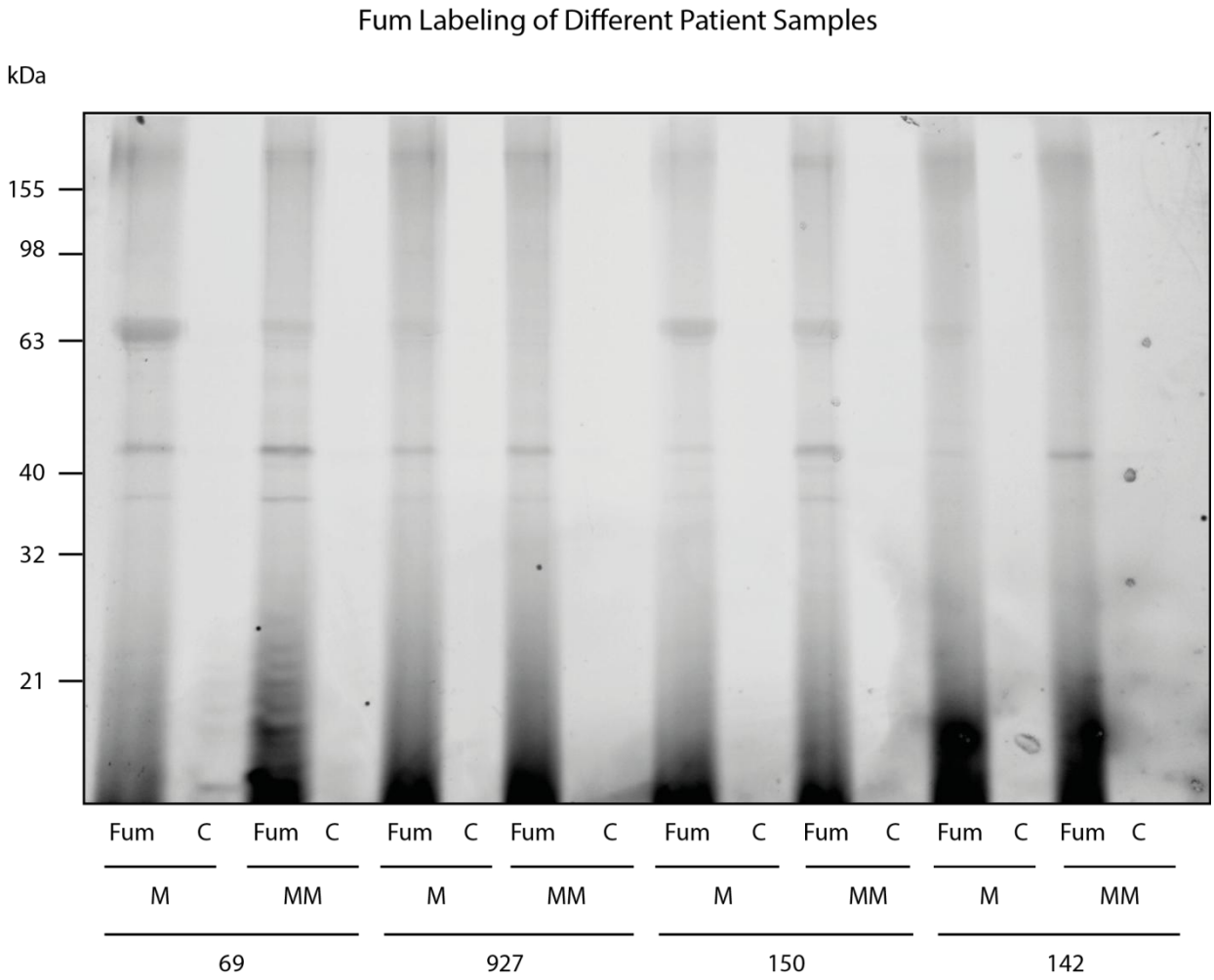

Figure 55. Fluorescence scan of paired myoma and myometrium tissue samples from different patients labeled with Fum. C stands for DMSO control.

These experiments showed a diffuse band at ~60 kDa. This result was obtained using different patient samples. Labeling on preparative scale, with pull down and LC-MS revealed no MetAP2 but serumalbumin, that was labeled due to high abundance. The same issue already occurred while labeling with FP-probe. MetAP2 was not found on several patient samples, so it was regarded as not active in these tissues.

3.2.4 Conclusion and Outlook

In this study a total number of 32 different active serine hydrolases were found in 9 different patient samples of myoma and myometrium tissue. MetAP2 was not active in 4 different patient samples. Among the serine hydrolases TPSAB1, TPSB2, TPSD1, CMA1, CTSG, CES1, CTSA and RBBP9 showed a different activity in myometrium and myoma. In myoma

CES1, CTSA and RBBP9 showed higher activity but not over all patients. So an evident drug target for a possible treatment was not found that way. CTSA like CES1 was active in several myoma tissues but only in three patients for CES1 and four patients for CTSA (with higher activity in myometrium in one patient) being too less evident. Nevertheless the role of these enzymes in myomas or myometrium should be further investigated. RBBP9 was only active in two patients, not being significant. But these patients showed differences in their activity profile for TPSAB1 and TPSB2 as well. both samples were from the proliferative phase indicating a relation of this phase and RBBP9 activity. RBBP9 represents a very interesting target because it is involved in TGF-β signaling by suppressing it. TGF-β stays interesting since it is also activated by the mast cell proteases TPSAB1, TPSB2, TPSD1, CMA1 and CTSA, which in turn showed mainly higher activity in myometrium tissue compared to myoma tissue. All these proteases are related to extracellular matrix degradation and tissue remodeling and could therefore be interesting for elucidation of cellular processes upon myoma formation. For a deeper understanding more patients need to be analyzed, especially to clearly point out the role of RBBP9. The role of TGF-β seems also interesting for future work, because on the one hand there were enzymes found that activate this growth factor but only in healthy tissue. One the other hand RBBP9 was found to be active in tumor tissue that suppresses the TGF-β signaling. This cytokine mainly maintains tissue homeostasis through transcriptional regulation of genes involved in proliferation, cell survival and cytostasis, differentiation, cell motility and the cellular microenvironment. The function of this cytokine is found perturbed in many cancer cells.

4 Experimental Section

4.1 Chemistry

4.1.1 Materials

All chemicals used were of reagent grade or higher and used without further purification. Solvents for reactions were of HPLC-grade and purchased from *Sigma Aldrich*, *Bachem* or *Acros*. Solvents for chromatography and workup purposes were generally of reagent grade and purified before use by distillation. Acivicin was purchased from *Santa Cruz Biotechnology* (*SCBT*). FP-probe was custom synthesized by *SYNCOM Corp*., Groningen, NL; (Syncom #17682) as already described before.[307] ACVL probes were synthesized as described before.[74] Recombinant CES1 was purchased from *Sigma Aldrich*.

^{1}H- and ^{13}C-NMR spectra were recorded on a *Bruker Avance I 360* (360 MHz), a *Bruker Avance I* (500 MHz) or a *Bruker Avance III 500* (500 MHz) NMR-System and referenced to the residual proton and carbon signal of the deuterated solvent, respectively.

HR-ESI-MS, HR-LC-ESI-MS, HR-APCI-MS and HR-LC-APCI-MS mass spectra were recorded with a *Thermo Finnigan LTQ FT Ultra* coupled with a *Dionex UltiMate 3000* HPLC system. ESI-MS and LC-ESI-MS mass spectra were recorded with a *Thermo Finnigan LCQ ultrafleet* coupled with a *Dionex UltiMate 3000* HPLC system.

HPLC analysis was accomplished with a *Waters 2695 separations module*, an *X-Bridge™ C18 3.5 µm OBD™* column (4.6 x 100 mm) and a *Waters 2996 PDA detector*.

HPLC separation was accomplished with a *Waters 2545 quaternary gradient module*, an *X-Bridge™ Prep C18 10 µm OBD™* (50 x 250 mm), an *X-Bridge™ Prep C18 5 µm OBD™* (30 x 150 mm) or an *YMC Triart C18 5 µm* column (10 x 250 mm), a *Waters 2998 PDA detector* and a *Waters Fraction Collector III*.

4.1.2 2,5-Dioxopyrrolidin-1-yl hex-5-ynoate (2)

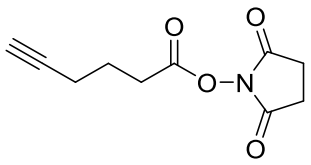

2.21 mL 5-hexynoic acid (20 mmol, 1 eq.) and 2.42 mL *N*-hydroxysuccinimide (21 mmol, 1.05 eq.) were dissolved in 80 mL CH_2Cl_2. 4.33 g DCC (dicyclohexylcarbodiimide) (21 mmol, 1.05 eq.) were subsequently added in portions. The reaction mixture was stirred for 2 h at RT and filtered. The filtrate was washed twice with 50 mL water and the combined aqueous phases were washed with 50 mL CH_2Cl_2. The combined organic phases were dried over Na_2SO_4 and the solvent was removed under reduced pressure. The crude product was purified by column chromatography (silica gel, hexane:ethyl acetate = 6:4) to yield 1.44 g (34%) of an yellowish oil. Data is consistent with that reported in the literature.[308]

R_f (hexane:ethyl acetate = 6:4) = 0.53

^{1}H NMR (500 MHz, Chloroform-*d*) δ (ppm) = 2.84 (d, *J* = 5.7 Hz, 4H), 2.77 (t, *J* = 7.4 Hz, 2H), 2.35 (td, *J* = 6.9, 2.6 Hz, 2H), 2.02 (t, *J* = 2.6 Hz, 1H), 1.96 (p, *J* = 7.1 Hz, 2H).

^{13}C NMR (126 MHz, $CDCl_3$) δ (ppm) = 169.23, 168.30, 82.53, 69.97, 29.77, 25.71, 23.43, 17.71.

4.1.3 (S)-2-((S)-3-Chloro-4,5-dihydroisoxazol-5-yl)-2-(hex-5-ynamido)acetic acid (3, ACV1)

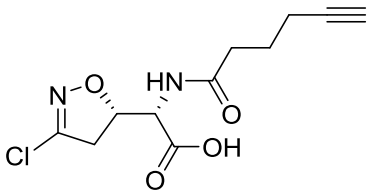

10.0 mg acivicin (0.056 mmol, 1.0 eq.) were dissolved in 600 µL ddH2O and 300 µL acetonitrile. 23.6 mg **2** (0.112 mmol, 2.0 eq.) and 4 µl diisopropylethylamine were added and the solution was stirred for 14 h at RT. The crude product was purified by HPLC (5-60% MeCN, 0.1% TFA, 15 min) to give 9.6 mg (76%) white solid.

HPLC t_R = 10.9 min (5-60% MeCN, 0.1% TFA, 15 min)

^{1}H NMR (500 MHz, Acetonitrile-d_3) δ (ppm) = 6.97 (d, *J* = 8.0 Hz, 1H), 5.06 (ddd, *J* = 11.5, 7.4, 4.6 Hz, 1H), 4.69 (dd, *J* = 8.3, 4.6 Hz, 1H), 3.39 (dd, *J* = 17.8, 11.2 Hz, 1H), 3.24 (dd, *J* = 17.8, 7.4 Hz, 1H), 2.31 (t, *J* = 7.4 Hz, 2H), 2.23 – 2.17 (m, 3H), 1.75 (p, *J* = 7.1 Hz, 2H).
^{13}C NMR (126 MHz, CD_3CN) δ (ppm) = 173.61, 170.21, 150.69, 84.53, 82.62, 70.15, 55.08, 41.32, 34.95, 25.15, 18.12.
HRMS-ESI (m/z): $C_{11}H_{14}ClN_2O_4^+$ $[M+H]^+$, calc.: 273.0636, found: 273.0636.

4.1.4 (S)-2-((*Tert*-butoxycarbonyl)amino)-2-((S)-3-chloro-4,5-dihydroisoxazol-5-yl)acetic acid (4)

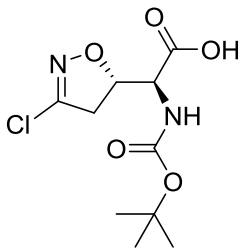

To a solution of 10.0 mg acivicin (0.056 mmol, 1.0 eq.) in 160 µL water a solution of 13.5 mg di-*tert*-butyl dicarbonate (0.061 mmol, 1.1 eq.) in 210 µL acetonitrile was added. 10 µL of triethylamine (0.072 mmol, 1.3 eq.) were added and the reaction was stirred for 14 h at RT. The solvent was removed under reduced pressure and gave 15 mg compound **4** as a yellow oil (97%). The product was used without further purification.

HPLC t_R = 13.5 min (5-60% MeCN, 0.1% TFA, 15 min)
^{1}H NMR (360 MHz, Acetonitrile-d_3) δ (ppm) = 5.75 (s, 1H), 5.14 – 5.04 (m, 1H), 4.03 (dd, *J* = 6.8, 2.8 Hz, 1H), 3.53 (dd, *J* = 17.1, 7.9 Hz, 1H), 3.23 (dd, *J* = 17.1, 11.4 Hz, 1H), 1.43 (s, 9H).
^{13}C NMR (91 MHz, CD_3CN) δ (ppm) = 171.51, 149.12, 146.79, 85.44, 78.47, 40.10, 30.47, 27.58.

4.1.5 *Tert*-butyl ((S)-1-((S)-3-chloro-4,5-dihydroisoxazol-5-yl)-2-oxo-2-(prop-2-yn-1-ylamino)ethyl)carbamate (5)

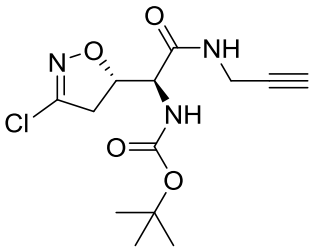

15.0 mg (0.056 mmol, 1.0 eq.) of **4** were dissolved in 50 µL acetonitrile. To this solution 24.0 mg COMU (0.056 mmol, 1.0 eq.) in 60 µL acetonitrile and 8.0 mg Oxyma Pure (0.056 mmol, 1.0 eq.) in 60 µL acetonitrile were added. Subsequently 10 µL *N*,*N*-diisopropylethylamine (0.056, 1.0 eq.) and the carboxylic acid was activated for 10 min at RT. After activation 8 µL propargylamine (0.061 mmol, 1.1 eq.) was added and the reaction mixture was stirred at RT for 1.5 h. Solvent was removed under reduced pressure and the compound was purified by HPLC (40-60% MeCN 0.1% TFA, 10 min) to give 12 mg of compound **5** (70%) as white solid.

HPLC t_R = 14.5 min (5-60% MeCN, 0.1% TFA, 15 min)
^{1}H NMR (360 MHz, Acetonitrile-d_3) δ (ppm) = 4.98 (dt, *J* = 10.8, 6.9 Hz, 1H), 4.00 – 3.92 (m, 2H), 3.34 (dd, *J* = 17.8, 10.9 Hz, 1H), 3.21 (dd, *J* = 17.8, 7.4 Hz, 1H), 2.47 (t, *J* = 2.5 Hz, 1H), 1.44 (s, 9H).
^{13}C NMR (91 MHz, CD_3CN) δ (ppm) = 169.52, 156.49, 150.61, 82.78, 80.75, 76.87, 71.96, 41.15, 29.23, 28.41.

4.1.6 (S)-2-amino-2-((S)-3-chloro-4,5-dihydroisoxazol-5-yl)-N-(prop-2-yn-1-yl)acetamide (6, ACV2)

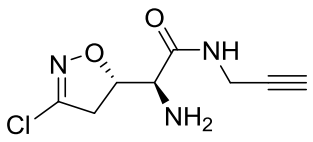

12.0 mg of **5** (0.038 mmol) were dissolved in 2.0 mL of a mixture of CH_2Cl_2:TFA (4:1) and stirred for 1 h. The solvent was evaporated under reduced pressure and the product was purified by HPLC (20-40% MeCN), 10 min to yield 7.0 mg of product **6** (87%) as white solid.

HPLC t_R = 6.7 min (2-50% MeCN, 10 min)

^{1}H NMR (500 MHz, Acetonitrile-d_3) δ (ppm) = 7.35 (s, 1H), 4.96 (ddd, *J* = 10.7, 8.7, 4.8 Hz, 1H), 3.94 (d, *J* = 5.8 Hz, 2H), 3.58 (d, *J* = 4.8 Hz, 1H), 3.29 – 3.14 (m, 2H), 2.43 (t, *J* = 2.5 Hz, 1H).

^{13}C NMR (126 MHz, CD_3CN) δ (ppm) = 171.95, 150.51, 84.84, 81.10, 71.64, 57.40, 39.68, 28.89.

HRMS-ESI (m/z): $C_8H_{11}ClN_3O_2^+$ $[M+H]^+$, calc.: 216.0534, found: 216.0536, δ = 0.93 ppm.

4.1.7 5-methoxy-4-(2-methyl-3-(3-methylbut-2-en-1-yl)oxiran-2-yl)-1-oxaspiro[2.5]octan-6-yl (2E,4E,6E,8E)-10-oxo-10-(prop-2-yn-1-ylamino) deca-2,4,6,8-tetraenoate (7, Fum)

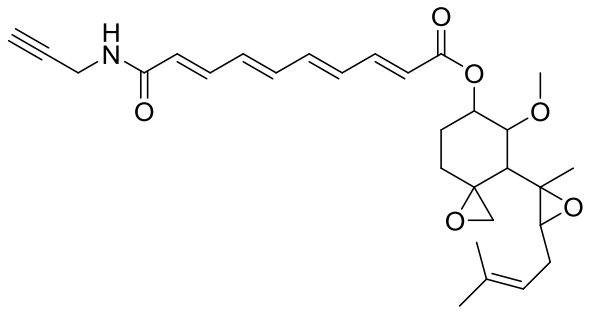

7.0 mg (0.016 mmol, 1.0 eq.) of fumagillin were dissolved in 50 µL CH_2Cl_2. To this solution 6.1 mg HATU (0.016 mmol, 1.0 eq.) in 50 µL CH_2Cl_2 and 2.2 mg HOAt (0.016 mmol, 1.0 eq.) in 50 µL CH_2Cl_2 were added. Subsequently 10 µL *N*,*N*-diisopropylethylamine (0.016, 1.0 eq.) and the carboxylic acid was activated for 10 min at RT. After activation 2 µL propargylamine (0.061 mmol, 1.1 eq.) was added and the reaction mixture was stirred at RT for 1.5 h in the dark. Solvent was removed under reduced pressure and the compound was purified by HPLC (60-80% MeCN, 13 min) to give 1.6 mg of compound **7** (20%) as white solid.

HPLC t_R = 38.2 min (5-80% MeCN, 40 min)

HRMS-ESI (m/z): $C_{29}H_{38}NO_6^+$ $[M+H]^+$, calc.: 496.2699, found: 496.2699.

4.2 Biochemistry

4.2.1 Materials

4.2.1.1 Bacterial strains

Escherichia coli SoluBL21, *Amsbio*
Escherichia coli BL21DE3, *Novagen*
Escherichia coli XL1-Blue, *Stratagene*
Escherichia coli TOP10, *Invitrogen*

4.2.1.2 Eukaryotic Cell Lines

A549, human carcinoma human alveolar basal epithelial cells, Universität Göttingen
HCT116, human colon cancer, Bayer HealthCare, Berlin
HeLa, human cervix carcinoma, Bayer HealthCare, Berlin
HEK293T, human embryonal kidney, Universität Würzburg
HepG2, human hepatocellular carcinoma, Helmholtz Zentrum München

4.2.1.3 Plasmids

CES1 pDONR, *Life Technologies*
pDONR 201, *Invitrogen*
pDEST 007, Carsten Pieck
pT-Rex™-DEST30, *Invitrogen*
ALDH1A1 pET 55, Dr. Tanja Wirth

4.2.1.4 Nucleotides

PCR CES1his primer

Forward primer: 5'-ggggacaagtttgtacaaaaaagcaggctttaaaaggctagctggctccgtgcctttatcc-3'
Reverse primer:
5'-ggggaccactttgtacaagaaafctgggtgtcaatgatgatgatgatgatgatgatgatgcagctctatgtgttctgtctg-3'

Mutagenesis primer

CES1S221A:
Forward primer: 5'-ctttctcctcccgctgcctctccaaagatggtc-3'
Reverse primer: 5'-gaccatctttggagaggcagcgggaggagaaag-3'

ALDH4A1C348A:
Forward primer: 5'-cgagcacgcggaagccttctggccaccg-3'
Reverse primer: 5'-cggtggccagaaggcttccgcgtgctcg-3'

4.2.1.5 Proteins and Antibodies

Proteins
CES1, recombimant Carboxylesterase, *Sigma Aldrich*

Antibodies
Anti-CES1 antibody, primary, polyconal rabbit, *Abcam*
Anti-CES1antibody, primary, polyconal rabbit, *Abnova*
Anti-ALDH4A1 antibody, primary, polyconal rabbit, *Abcam*
Anti-actin antibody, primary, polyconal goat, *Santa Cruz Biotechnology*
Anti-rabbit IgG HRP conjugate, secondary, donkey, *Pierce*
Anti-goat IgG HRP conjugate, secondary, donkey, *Pierce*

4.2.1.6 Media

LB	1% (w/v) Tryptone (Roth)
	0.5% (w/v) NaCl (Prolabo, VWR)
	0.5% (w/v) Yeast extract (Applichem, Roth)
	dissolved in ddH_2O
	pH 7.5
TB	1.2% (w/v) Tryptone (Roth)
	0.5% (v/v) Glycerol (Roth)
	2.4% (w/v) Yeast extract (Applichem, Roth)
	1.25% (w/v) K_2HPO_4
	0.23% (w/v) KH_2PO_4
	dissolved in ddH_2O
	pH 7.5

4.2.1.7 Buffers and Solutions

PBS	136.9 mM NaCl
	10.1 mM Na2HPO4
	1.8 mM KH2PO4
	2.7 mM KCl
	pH = 7.4
PBS-T	136.9 mM NaCl
	10.1 mM Na2HPO4
	1.8 mM KH2PO4
	2.7 mM KCl
	0.05% Tween 20®
	pH 7.4

Buffers for protein purification

Strep binding buffer	100 mM Tris-HCl 150 mM NaCl 1 mM EDTA pH 8.0
Strep elution buffer	100 mM Tris-HCl 150 mM NaCl 1 mM EDTA 2.5 mM desthiobiotin pH 8.0
His lysis buffer	136.9 mM NaCl 10.1 mM Na2HPO4 1.8 mM KH2PO4 2.7 mM KCl 10 mM Imidazole 0.1% SDS 1% DOC 1% NP-40 pH = 8.0
His wash buffer	50 mM Na2HPO4 300 mM NaCl 10 mM Imidazole pH = 8.0
His Buffer A	50 mM Na2HPO4 300 mM NaCl 40 mM Imidazole pH = 8.0

His Buffer B	50 mM Na2HPO4
	300 mM NaCl
	250 mM Imidazole
	pH = 8.0

Buffers for cloning and agarose-gel electrophoresis

50x TAE	2.0 M Tris
	1.0 M Acetic acid
	0.1 M EDTA
	dissolved in deion. water
	pH 7.0
TE	10 mM Tris
	1 mM EDTA
	dissolved in deion. water
	pH 8.0
6x DNA loading buffer	250 mg Bromophenol blue
	250 mg Xylencyanol
	33 mL 150 mM Tris-HCl
	60 mL Glycerol
	dissolved in 7 mL deion. water

Antibiotics

Kanamycin	25 mg/mL in H2O
Ampicillin	100 mg/mL in H2O
Chloramphenicol	34 mg/mL in ethanol

Induction solutions

Anhydrotetracycline (Atet) 10000x stock	2 g/L dissolved in DMF
IPTG 1000x stock	1 M dissolved in deion. water

Cell culture

Trypan blue stain	0.5% (w/v) Trypan blue 0.9% (w/v) NaCl dissolved in deion. water and filtered
1 x Trypsin/EDTA	10 x Trypsin/EDTA (PAA) diluted in PBS

SDS-PAGE

APS solution	10% (w/v) Ammoniumpersulfate in deion. water
10 x SDS buffer	0.25 M Tris 1.92 M Glycine 1% (w/v) SDS dissolved in deion. water pH 8.3
2x SDS loading buffer	63 mM Tris-HCl 10% (v/v) Glycerol 2% (w/v) SDS 0,0025% (w/v) Bromophenol blue 5% (v/v) 2-Mercaptoethanol dissolved in deion. water pH 8

Resolving gel buffer	3.0 M Tris dissolved in deion water pH 8.8
Stacking gel buffer	0.5 M Tris dissolved in deion. water pH 6.8
Coomassie destainer	10% (v/v) Acetic acid (conc.) 20% (v/v) Ethanol (abs.) issolved in deion. water
Coomassie stain	0.25% (w/v) Coomassie Brilliant Blue 9.2% (v/v) Acetic acid (conc.) 45.4% (v/v) Ethanol (abs.) dissolved in deion. water

Click Chemistry

100x Rhodamine azide	100 mM Rhodamine azide dissolved in DMSO
5 mM Rhodamine azide	100x Rhodamine azide 1:20 diluted in DMSO
100x Trifunctional linker (TFL)	100 mM Trifuncional linker dissolved in DMSO
10 mM TFL	100x TFL 1:10 diluted in DMSO
TCEP-Solution	53 mM Tris(2-carboxyethyl)phosphine
50x TBTA ligand	83 mM TBTA dissolved in DMSO
1x TBTA ligand	50x TBTA diluted 1:50 in DMSO / t-BuOH 1:4.4

$CuSO_4$ 50 mM $CuSO_4$

4.2.1.8 Agarose Gel Electrophoresis

For analysis and separation of DNA, 1% agarose-gels were used and the electrophoresis was performed in a Mini-Sub Cell GT from Bio-Rad with a Consort EV261 Electrophoresis Power Supply at 95 mA. Gels were prepared freshly with 300 mg agarose and 300 mL 1 x TAE buffer. 6 µL of the PCR-product were loaded on the gel. For staining the gels were incubated after the electrophoresis in an ethidium bromide bath (0.3−0.5 µg/mL) and the visualization was performed in a GenoView UV Transilluminator from VWR and documented with a video graphic printer UP-897MD from Sony.

4.2.1.9 SDS-PAGE

For SDS-PAGE, the gel electrophoresis system fro peQLab (Twin L) or the precast NuPAGE® Bis-Tris gels (invitrogen) with MOPS buffer (invitrogen) was used. The electrophoresis for the invitrogen system was performed with a Consort EV261 Electrophoresis Power Supply with 120 V and dynamic ampere. For the peQLab system, electrophoresis was performed with a Consort EV261 Electrophoresis Power Supply at 300 V or 55 mA and dynamic ampere or voltage. The gels had a size of 20 x 20 cm whereas the resolving gel had a volume of 36 mL and the stacking gel 14 mL. For analytical and preparative separation, a comb with 20 and 15 sample wells, respectively, was inserted. The polyacrylamide gels were prepared with 10−15% acrylamide for analytical and 10% for preparative gels. First the reagents for the resolving gel were combined under stirring and the polymerization started with the addition of the APS solution. To obtain a clean surface, the resolving gel was topped with a layer of isopropanol during polymerization in the gel device. Then the isopropanol layer was removed and replaced by the stacking gel. The respective comb was inserted before the polymerization was completed. The compositions of the resolving and stacking gels were the following:

Composition for the preparation of one polyacrylamide gel (20 x 20 cm):

Resolving gel (10%):

H2O	14.4 mL
Buffer	9 mL
10% (w/v) SDS	0.36 mL
Rotiphorese Gel 30	12 mL
TEMED	0.015 mL
APS	0.15 mL

Stacking gel (3.75%)

H2O	8.8 mL
Buffer	3.6 mL
10% (w/v) SDS	0.144 mL
Rotiphorese Gel 30	1.8 mL
TEMED	0.014 mL
APS	0.072 mL

4.2.2 Molecular Biology

4.2.2.1 Transformation

One aliquot of the cells were thawed on ice for 10 min. 4 µL of the cloning reaction (or 10 ng Plasmid) were added and the suspension was mixed by inversion of the tube and incubated for 30 min on ice. The transformation was initiated by a heatshock at 42 °C for 35 sec. 200 µL of prewarmed LB or SOC were added and placed sidewards in a shaker at 37 °C for 2 h. 100 µL and the rest of the suspension was plated each on an selective agar plate. After 14 h at 37 °C single colonies were picked and grown in a liquid LB-overnight culture containing the respective antibiotic. A cryostock was prepared from the cells (see 5.2.1.2.1). Cells were spinned down at 4000 g for 10 min and the plasmids were isolated using the Plasmid extraction Kit (, Germany). Concentrations were determined using a Tecan Image reader.

4.2.2.2 Cryostocks of Bacteria

5 mL of bacteria were grown over night in selective LB medium and harvested by centrifugation. The pellet was resuspended in 500 µL selective LB medium with 500 µL sterilized glycerol frozen in liquid nitrogen and stored at -80 °C.

4.2.2.3 PCR

For the creation of CES1his a 10x his tag was added to the C-terminus via PCR with a CFX96 Touch™ Real-Time PCR Detection System (*Bio-Rad*). The reaction was carried out using Phusion DNA Polymerase (*New England Biolabs*) with the following PCR mix and cycle protocol.

Mix:

10 µL	GC Buffer 5x
1 µL	10mM dNTP
2.5 µL	template (7.5 ng/µL)
2.5 µL	forward primer (10 pmol/µL)
2.5 µL	reverse primer (10 pmol/µL)
0.5 µL	Phusion DNA Polymerase
31 µL	nuclease free water
50 µL	reaction mixture

PCR cycle:

3 min	98°C	
10 s	98 °C	
15 s	68 °C	
45 s	72 °C	35x
10 min	72 °C	

PCR products were identified on agarose gels and amplified genes were extracted with an E.Z.N.A. Cycle pure™ Kit. Concentrations of DNA were determined by measuring the

absorption at 260 nm by a TECAN Infinite M200pro with a NanoQuant plate. The clean PCR product underwent BP reaction.

4.2.2.4 Gateway Cloning

ALDHs

For recombinant overexpression of target proteins in *E. coli* the *Invitrogen*™ Gateway® Technology was used. Genes ALDH2, ALDH1B1, ALDH4A1 were available in a pDONR™ vector system and were cloned into the pDEST 007 vector using the LR Clonase™ II enzyme mix.

1 µL	ALDH-pDONR clone (80-150 ng/µL)
1 µL	pDEST 007 (150 ng/µL)
8 µL	TE buffer
2 µL	LR clonase
10 µL	LR cloning reaction mix

24 h at rt.

The expression clone was transformed in chemically competent SoluBL21™ Competent *E. coli* cells (*Amsbio*) and selected on LB agar plates containing 100 µg mL^{-1} ampicillin. Cloning results were validated after plasmid amplification and preparation (*E.Z.N.A.*™ Plasmid Mini Kit) by sequencing.

CES1

CES1 was recombined into pT-Rex™-DEST30 Vector (*Invitrogen*) by LR Clonase™ II enzyme mix in TE buffer from PCR product.

1 µL	CES1-pDONR clone (80 ng/µL)
1 µL	pT-Rex™-DEST30 plasmid (150 ng/µL)
8 µL	TE buffer
2 µL	LR clonase
10 µL	LR cloning reaction mix

24 h at rt.

The expression clone was transformed in chemically competent One Shot® TOP10 *E. coli* (*Invitrogen*) and selected on LB agar plates containing 100 µg mL^{-1} ampicillin and grown in ampicillin TB. Cells were harvested and plasmids were isolated using a *QIAGEN* Plasmid Midi Kit. Validity of the clones was confirmed by plasmid sequence analysis.

CES1his

The PCR product was recombined into pDONR201 plasmid with the following BP reaction:

1 µL	PCR product (100 fmol/µL)
1 µL	DONR™201 plasmid (150 ng/µL)
8 µL	TE buffer
2 µL	BP clonase
10 µL	LR cloning reaction mix

24 h at rt.

After transformation of the BP cloning in chemically competentOne Shot® TOP10 E. coli (Invitrogen), cells were plated on LB agar plates containing 25 µg/mL kanamycin. Clones of transformed cells were selected and grown in kanamycin (25 µg/mL) LB medium. Cells were harvested and plasmids were isolated using an E.Z.N.A.™ Plasmid Mini Kit. The corresponding expression clone was generated by in vitro LR recombination reaction of the entry clone and the destination vector pT-Rex™-DEST30 Vector (*Invitrogen*) using LR Clonase™ II enzyme mix in TEbuffer. The LR reaction mixture was prepared as follows:

1 µL	CES1his-pDONR201 (100 ng/µL)
1 µL	DONR™201 plasmid (150 ng/µL)
8 µL	TE buffer
2 µL	LR clonase
10 µL	BP cloning reaction mix

24 h at rt.

The resulting clone was transformed in chemically competent One Shot® TOP10 *E. coli* (*Invitrogen*) and selected on LB agar plates containing 100 µg mL^{-1} ampicillin and grown in ampicillin TB. Cells were harvested and plasmids were isolated using a *QIAGEN* Plasmid Midi Kit. Validity of the clones was confirmed by plasmid sequence analysis.

4.2.2.5 Mutagenesis

For binding site identification mutagenesis was applied with primers generated using QuikChange Primer Design from Agilent Technologies. For the binding site of ACV2 in CES1 the active site serine was converted to alanine by mutagenesis using the S221A primers to create the mutant S221A with following PCR mix and PCR cycle:

Mix:

10 µL	HF Buffer 5x
1 µL	10mM dNTP
1 µL	template (5 ng/µL)
4 µL	forward primer (10 pmol/µL)
4 µL	reverse primer (10 pmol/µL)
1.5 µL	DMSO
0.5 µL	Phusion DNA Polymerase
28 µL	nuclease free water
50 µL	reaction mixture

PCR cycle:

2 min	98°C	
30 s	98 °C	
20 s	68 °C	
4 min	72 °C	22x
5 min	72 °C	

For ALDH4A1 the nucleophilic cysteine was exchanged by alanine to generate the mutant C348A with the same mix as shown above and the following PCR cycle:

2 min	98°C	
30 s	98 °C	
20 s	70 °C	
2:30 min	72 °C	22x
5 min	72 °C	

The point mutations were incorporated by PCR on the corresponding plasmid created before (CES1 on pT-Rex™-DEST30 vector and ALDH4A1 on pDEST 007 vector). After PCR a DpnI digest was performed and plasmids were transformed and amplified in chemically competent One Shot® TOP10 *E. coli* (*Invitrogen*) as described above.

4.2.2.6 Western Blotting

For ALDH4A1 and CES1 detection, the cell lysate samples were prepared in the identical way as for in-gel fluorescence scanning. The proteins separated by 10% SDS-PAGE were transferred to a PVDF membrane (*Biorad*) with a semi-dry blotter (*Biorad*) for 45 min at 12 V. The blots were saturated with 5% non-fat dried milk in PBS-T (PBS with 0.05% Tween 20®, pH 7.4) for 1 h at RT, washed three times with PBS-T for 15 min and incubated with primary rabbit polyclonal anti-CES1 antibody (*Abnova*, 1:5000 dilution in 5% milk in PBS-T) or rabbit polyclonal anti-ALDH4A1 antibody (*Abcam*, 1:5000 dilution in 5% milk in PBS-T) at 4 °C overnight, washed three times for 15 min with PBS-T and detected with goat anti-rabbit IgG HRP-conjugated secondary antibody (*Thermo Fisher Scientific*, 1:10000 dilution in 5% milk in PBS-T, 1 h at RT) and afterwards washed three times with PBS-T for 15 min. Signals were detected using *Amersham* ECL Plus Western Blotting Detection reagents (*GE Healthcare*) using a *Fujifilm* Las-4000 luminescent image analyser containing a VRF43LMD3 lens with no filter. For actin detection membrane was stripped by incubating in 62.5 mM TrisHCl, 100 mM ß-mercapto-Ethanol, 2% SDS, pH 6.8 for 40 min at 52 °C, followed by 10 washes with PBS-T for 15 min. The blots were blocked with 5% non-fat dried milk in PBS-T for 1 h at RT, washed three times with PBS-T for 15 min and incubated with primary goat polyclonal anti-actin antibody (*SCBT*, 1:5000 dilution in 5% milk in PBS-T) at 4 °C overnight. After incubation the blots were washed three times for 15 min with PBS-T and

incubated with donkey anti-goat IgG HRP-conjugated secondary antibody (*SCBT*, 1:10000 dilution in 5% milk in PBS-T, 1 h at RT), washed three times with PBS-T for 15 min and detected as described above.

4.2.3 Cell Culture

4.2.3.1 Cultivation of Eukaryotic Cell Lines

Cell culture media and supplements were purchased from PAA and Sigma Aldrich. HepG2, HEK293T and HeLa cells were cultivated in RPMI 1640 media supplemented with 10% fetal calf serum and 2 mM L-glutamine. A549 cells were cultivated in DMEM high glucose supplemented with 10% fetal calf serum and 2 mM L-glutamine. Cells were cultivated at 37 °C with 5% CO_2 in a Hera Cell 240i incubator (*Thermo Scientific*).

4.2.3.2 SILAC Cell Culture

HepG2 cells were cultivated in Silac-RPMI-1640 media (*PAA*) supplemented with 10% dialyzed fetal calf serum and 2 mM L-glutamine. The *heavy* medium was supplemented with 0.418 mM Lysine-8 (U-13C6; U15N2, *Cambridge Isotopes*) and 0.214 mM Arg-10 (U-13C6; U15N4, *Cambridge Isotopes*). The *medium* was supplemented with 0.418 mM Lysine-4 (4,4,5,5-D4, *Cambridge Isotopes*) and 0.214 mM Arg-6 (U-13C6, *Cambridge Isotopes*). HepG2 cells were cultivated until full incorporation of amino acid isotopes before carrying out experiments.

4.2.3.3 Cell Growth Assay

HepG2 cells from sub confluent cultures were used for the assay. Specifically, 6000 cells per well were seeded in 96 well flat-bottom plates (*Nunclon*) in 100 µL medium and cultured for 12 h with one plate for each time interval. Compounds were diluted 1:100 from 100x DMSO stocks in 100 µL of the appropriate culture medium and added to the cells after careful removal of the culture medium without compounds. After incubation (24 h, 48 h, 72 h, 96 h

and 120 h) 10 µL of 11% glutaraldehyde solution was added to each well and the plate was incubated at room temperature for 30 min. Media containing glutaraldehyde was removed and cells were washed 10 times with ddH_2O and dried overnight. After fixation cells were stained by adding 100 µL of 0.1% crystal violet solution in water to each well followed by a 30 min incubation step at room temperature. Crystal violet solution was removed and the wells were washed 10 times with ddH_2O and dried over night. Next 100 µL of 10% acetic acid was added to each well and incubated at room temperature to dissolve the crystal violet. The optical density at 590 nm was measured using a *TECAN* Infinite 200pro plate reader. All measurements were performed five times and in at least three independent experiments. Error bars were calculated from standard deviation from the mean. IC_{50} values were calculated from curve fittings by Origin Pro 8.5 (*OriginLab Corporation*).

4.2.3.4 siRNA Knockdown

Knockdown of CES1 and ALDH4A1 gene expression was performed with silencer select siRNA (*life technologies*, ALDH4A1 #4390624, CES1 #4392420). For determination of cell growth, HepG2 cells were reverse transfected with Lipofectamine® RNAiMax (*life technologies*) following the manufacturer's instructions in 96 well plates, with one plate for each time interval (24 h, 48 h, 72 h and 96 h). Cells only treated with transfection reagent served as negative control.

24 h, 48 h, 72 h and 96 h after the transfection, cells were fixed by addition of 12 µL 11% glutaraldehyde and incubation for 30 min. Media was removed and fixed cells were washed 10 times with ddH_2O and dried over night. The fixed cells were stained by adding 100 µL of 0.1% crystal violet solution in water to each well and incubated for 30 min at room temperature. Crystal violet solution was removed and the wells were washed 10 times with ddH_2O and dried over night. The dried stained cells were lysed by addition of 100 µL 10% acetic acid. The optical density at 590 nm was measured using a *TECAN* Infinite 200pro plate reader. All knockdowns and controls were done five times for each time interval and repeated in at least two independent trials. Error bars were calculated from standard deviation from the mean.

To evaluate knockdown efficiency 40 µg lysate were labeled with 10 µM FP for CES1 and 50 µM ACV1 for ALDH4A1 for 1 h and *Click reaction and analytical gel-based analysis* and Immunoblotting was carried out with actin as loading control

4.2.3.5 Expression Level Determination

HepG2 cells were cultivated in 6 wells until 70% confluent. Media was exchanged and 25 µM ACV1 and 10 µM ACV2 were added 1:1000 from DMSO stocks and one 1 mL media was supplemented with 1 µL DMSO as control. After incubation for DMSO control (24 h) and for probes (24 h, 48 h, 72 h, 96 h and 120 h) cells were harvested as described above and lysed using lysis buffer. Protein concentration was determined using BCA (Rotiquant universal, *Carl Roth Laborbedarf*) and 60 µg of proteome underwent *Western blotting*.

4.2.4 Protein Chemistry

4.2.4.1 Purification of ALDH4A1

Cells were grown in ampicillin M9 media at 37 °C until an OD600 of 0.7, then induced with anhydrotetracycline 1:20000 (200 ng/µL) and cultivated for 20 h at 20 °C. Bacteria were harvested by centrifugation (5000 g for 20 min), cell pellets were washed with PBS, resuspended in strep binding buffer (100 mM Tris-HCl pH 8.0, 150 mM NaCl, 1 mM EDTA) and lysed by French press. Cell debris was separated by centrifugation (20000 g 20 min) and the protein was purified with StrepTrap™ HP columns (*GE Healthcare*) and eluted with 100 mM Tris-HCl pH 8.0, 150 mM NaCl, 1 mM EDTA, 2.5 mM desthiobiotin. After exchanging the buffer to 50 mM Tris, 50 mM NaCl, 5% glycerol protein concentrations were determined by BCA assay (Rotiquant universal, *Carl Roth Laborbedarf*).

4.2.4.2 Purification of ALDH1A1

Cells were grown in ampicillin LB media at 37 °C until an OD600 of 0.6, then induced with IPTG 1:1000 and cultivated for 5 h at 37 °C. Bacteria were harvested by centrifugation (5000 g for 20 min), cell pellets were washed with PBS, resuspended in strep binding buffer (100 mM Tris-HCl pH 8.0, 150 mM NaCl, 1 mM EDTA) and lysed by French press. Cell debris was separated by centrifugation (20000 g 20 min) and the protein was purified with StrepTrap™ HP columns (*GE Healthcare*) and eluted with 100 mM Tris-HCl pH 8.0, 150 mM NaCl, 1 mM EDTA, 2.5 mM desthiobiotin. After exchanging the buffer to 50 mM

Tris, 10% glycerol pH = 7.5, protein concentrations were determined by BCA assay (Rotiquant universal, *Carl Roth Laborbedarf*).

4.2.4.3 Purification of CES1

CES1his clone was transfected into HEK cells using Lipofectamine® 2000 (*life technologies*) according to manufacturer's instructions in petri dishes (150 mm). 24 h after transfection media containing Lipofectamine® 2000 was exchanged and cells were grown for additionally 48 h. For metabolic labeling of CES1his the transfection media was exchanged 24 h after transfection with media containing 60 µM ACV2 and incubated for additional 48 h.
Cells were harvested by scraping and centrifugation (800g, 5 min) and lysed using 1 mL lysis buffer (PBS, 1% NP40, 1% DOC, pH 8.0, 10 mM imidazole) per dish. Cell debris was removed by centrifugation (21,000 g, 20 min) and the protein was purified using a His Trap HP column (*GE Healthcare*). The lysate was washed with his wash buffer (50 mM Sodium Phosphate, pH 8.0, 300 mM NaCl, 10 mM imidazole). The protein was eluted with a gradient of his buffer A (50 mM Sodium Phosphate, pH 8.0, 300 mM NaCl, 40 mM imidazole) to his buffer B (50 mM Sodium Phosphate, pH 8.0, 300 mM NaCl, 250 mM imidazole) form 0-100% his buffer B. Fractions containing CES1 were collected and buffer was exchanged with PBS, pH 7.4. Protein concentration was determined by BCA Assay (Rotiquant universal, *Carl Roth Laborbedarf*).

4.2.4.4 Protein Quantification via BCA assay

Protein concentrations were determined using Rotiquant universal, *Carl Roth Laborbedarf.* Standard curve was determined with BSA at concentrations 0, 25, 50, 100, 200, 400 µg/mL BSA. In a flat bottom 96-well-plate, 50 µL of BSA solution, protein solution or dilution was added. 100 µL of 15:1 solution of reagent 1 : reagent 2 was added to this solution and incubated at 60 °C for 15 min. The absorption at 503 nm or 492 nm was measured with a *TECAN* Infinite 200pro plate reader. All measurements were carried out as triplicates.

4.2.4.5 ALDH Activity Assay

For inhibition assays, 1 µl of probe stock with different concentrations was pre-incubated with 3.5 µg ALDH1A1 or ALDH4A1 in 49 µL 50 mM Tris-HCl (pH 8.5) for 30 min at RT. Afterwards, 50 µL substrate mixture containing 5 mM Tris-HCl, 100 mM KCl, 5 mM β-mercaptoethanol, 1 mM β-NAD^+ and 100 µM propionaldehyde were added to initiate the enzymatic reaction. The product formation of NADH was monitored by measuring the absorption increase at 340 nm at 37 °C in flat bottom 96-well-plates with a *TECAN* Infinite 200pro plate reader. Uninhibited ALDH1A1 served as control. All measurements were carried out as triplicates in at least three independent experiments. Error bars were calculated from standard deviation from the mean. EC_{50} values were calculated from curve fittings by Origin Pro 8.5 (*OriginLab Corporation*).

4.2.4.6 CES1 Activity Assay

In a 96 flat bottom well plate 2.5 µg CES1 (*Sigma Aldrich*) in 49 µL 100 mM sodium phosphate (pH 7.4) was pre-incubated with 1 µl probe stock, in different concentrations or DMSO as control, for different times (1 h, 2 h, 3 h, 4 h). After pre-incubation 50 µL 1 mM 4-nitrophenyl acetate in 100 mM sodium phosphate (pH 7.4) was added and the reaction was monitored at 410 nm, 37 °C for 20 min using a *TECAN* Infinite 200pro plate reader. All measurements were carried out in triplicates and in two independent trials. Error bars represent standard deviation from the mean.

4.2.4.7 Immunoprecipitation

Classic immunoprecipitation: HepG2 cells were grown in petri dishes (150 mm) until 70 % confluent. One dish was incubated with 30 µM ACV2 (1:10000 from DMSO stock) for 3 days and to one dish the corresponding amount of DMSO was added. After incubation cells were washed with PBS and harvested by scraping in PBS. Cells were pelleted by centrifugation at 800 g for 5 min and PBS was removed. Cells were lysed by resuspension in 2 mL IP-lysis buffer (PBS, 1% NP-40, 1% DOC, 1 mg/mL BSA) and incubation on ice for 10 min. To each sample 2. 5 µl antiCES1 antibody (Abnova) was added and incubated over night at 5 °C under gently rotation. 300 µL protein A/G resin (*Thermo Fisher Scientific*) was added to tube and

incubated for 2 h with gently rotation at 5 °C. Beads were pelleted by centrifugation at 500 g for 5 min and supernatant removed. The remaining beads were washed with 2 mL IP-lysis buffer followed 4 mL PBS. For washing the beads were pelleted by centrifugation at 500 g for 5 min and supernatant removed. The antigen was eluted 3 times with 100 µL 25 mM citric acid.

Direct IP: The direct immunoprecipitation was performed with columns, beads and solutions from a Pierce direct IP Kit (*Thermo Fisher Scientific*) according to manufacturers' instructions with 26 µg anti CES1 (Abcam) and 100 µL resin.

4.2.5 ABPP Experiments

4.2.5.1 *In situ* ABPP Labeling Experiments

Analytical labeling in PBS: Cells were grown in 6 well plates until a confluence of 70% was reached. The media was exchanged to PBS containing either probes at a concentration of 50 or 100 µM or the corresponding amount of DMSO as control. After incubation with probes for 2 h cells were washed with PBS and harvested by scraping in 1.5 mL PBS. Cells were pelleted by centrifugation at 800 g for 5 min and PBS was removed. Cells were lysed in 50 µL lysis buffer (PBS, 1% NP-40, 1% DOC) and incubated on ice for 10 min. Soluble and insoluble fractions were separated by centrifugation at 21000 g for 20 min at 5 °C. The insoluble fraction was resuspended in 50 µL lysis buffer by sonication under ice cooling. The samples then underwent *Click reaction and analytic gel-based analysis*.

Analytical labeling in medium: Cells were grown in 6 well plates until 70% confluent. The probes were added to the wells with a dilution of 1:1000 from DMSO stocks and the control well was supplemented with the corresponding amount of DMSO. After incubation for 3.5 h cells were washed with PBS and harvested by scraping in 1.5 mL PBS. Cells were pelleted by centrifugation at 800 g for 5 min and PBS was removed. Cells were lysed by resuspension in 50 µL lysis buffer (PBS, 1% NP-40, 1% DOC) and incubation on ice for 10 min. Soluble and insoluble fraction were isolated by centrifugation at 21000 g for 20 min at 5 °C and insoluble fraction was resuspended in 50 µL lysis buffer by sonication under ice cooling. The samples then underwent *Click reaction and analytic gel-based analysis*.

Preparative labeling in PBS: Cells were grown to 70% confluence in Petri dishes (150 mm). Then the medium was aspirated and cells were washed with 10 mL PBS and then harvested in

20 mL fresh PBS by scraping. Cells were washed (800 g, 5 min), resuspended in 1000 µL PBS containing probes at the appropriate concentration and incubated for 2 h at RT. Subsequently, cells were pelleted for 5 min at 800 g at RT to remove PBS with excess of the probe, washed twice with 500 µL PBS and resuspended in 500 µL lysis buffer. Soluble and insoluble fraction were separated by centrifugation at 21000 g for 60 min at 4 °C. Insoluble pellets were resuspended in 500 µL lysis buffer by sonication under ice cooling. Protein concentration was assayed (Rotiquant universal, *Carl Roth Laborbedarf*) and adjusted to 2 mg/mL in PBS.

Preparative labeling in medium: Cells were grown in petri dishes (150 mm) until 70% confluent. The probes were added to the wells with a dilution of 1:10000 from DMSO stocks and the control well was supplemented with the corresponding amount of DMSO. After incubation for 1 h cells were washed with PBS and harvested by scraping in PBS. Cells were pelleted by centrifugation at 800 g for 5 min and PBS was removed. Cells were lysed by resuspension in 2 mL lysis buffer (PBS, 1% NP-40, 1% DOC) and incubation on ice for 10 min. Soluble and insoluble fraction were isolated by centrifugation at 21000 g for 20 min at 5 °C and insoluble fraction was resuspended in 1 mL lysis buffer by sonication under ice cooling. Protein concentration was assayed (Rotiquant universal, *Carl Roth Laborbedarf*) and adjusted to 2 mg/mL in PBS.

4.2.5.2 Preparative *in situ* ABPP Labeling Experiments

Cells were grown to 70% confluence in Petri dishes (150 mm). The medium was aspirated and cells were washed with 10 mL PBS and then harvested in 20 mL fresh PBS by scraping. Cells were washed (800 g, 5 min), resuspended in 1000 µL PBS containing probes at the appropriate concentration and incubated for 2 hours at RT. Subsequently, cells were spun for 5 min at 800 g at RT to remove PBS with excess of probe, washed twice with 500 µL PBS and resuspended in 500 µL lysis buffer (PBS, 1% NP-40, 1% DOC). Soluble and insoluble fraction were separated by centrifugation at 14 800 rpm for 60 min at 4 °C. Insoluble pellets were resuspended in 500 µL lysis buffer by sonication under ice cooling. Protein concentration was assayed (Rotiquant universal, *Carl Roth Laborbedarf*) and adjusted to 2 mg/mL in PBS.

4.2.5.3 Click Reaction and Analytical Gel-Based Analysis

To 45 µL of proteome 1 µL RhN_3 (5 mM in DMSO) was added, followed by 1 µL TCEP solution (53 mM in ddH_2O) and 3 µL ligand TBTA (83 mM in DMSO/*tert*-butanol). Samples were gently vortexed and the cycloaddition was initiated by the addition of 1 µL $CuSO_4$ solution (50 mM in ddH_2O). The reaction was incubated for 1 h at RT. For analytical gel electrophoresis, 50 µL 2xSDS loading buffer were added and 50 µL were applied on the gel. Roti®-Mark STANDARD (*Carl Roth GmbH & Co. KG*, for Coomassie staining) and BenchMark™ Fluorescent Protein Standard (*Life Technologies*) were applied as markers to determine the protein mass. Fluorescence scans of SDS gels were performed with a *Fujifilm* Las-4000 luminescent image analyser containing a VRF43LMD3 lens and a 575DF20 filter.

4.2.5.4 Click Reaction and Preparative Gel-Based Analysis

To 947 µL proteome solution 3 µL trifunctional linker [309] (10 mM in DMSO) was added, followed by 10 µL TCEP solution (53 mM in ddH_2O) and 30 µL ligand TBTA (83 mM in DMSO/*tert*-butanol). The samples were gently vortexed and the cycloaddition was initiated by the addition of 10 µL $CuSO_4$ solution (50 mM in ddH_2O). The reaction was allowed to proceed for 1 h at RT. Reactions for enrichment were carried out together with a control lacking the probe to compare the results of the biotin-avidin enriched samples with the background of unspecific protein binding on avidin-agarose beads. The proteins were precipitated by addition of 4 volumes of cold acetone (4 mL, -20 °C) followed by an incubation for 18 h at -20 °C. Then the proteins were pelleted (30 min, 21,000 g, 4 °C) and the supernatant was discarded. The proteins were washed with prechilled methanol (2 x 200 µL, -20 °C) and resuspended by sonication (5-10 sec, 10% max. intensity; 15 min, 21,000 g, 4 °C). Subsequently, the pellet was dissolved at RT in 1 mL 0.2% SDS in PBS by sonication and incubated under gentle mixing with 50 µL of prewashed (3 x 1 mL 0.2 % SDS in PBS) avidin-agarose beads (avidin-agarose from egg white, 1.1 mg/mL in aqueous glycerol suspension, *Sigma-Aldrich*) for 2 h at RT. The beads were washed with 0.2% SDS in PBS (3 x 1 mL), 6 M urea (2 x 1 mL) and PBS (3 x 1 mL). 50 µL of 2xSDS loading buffer was added and the proteins were released for preparative SDS-PAGE by incubation for 6 min at 96 °C. The beads were pelletized (3 min, 21,000 g) and the supernatant was isolated and stored at -80 °C. The supernatant was applied on a preparative gel, and run for 4-5 h (300 V).

After gel electrophoresis, the bands were visualized using a *Fujifilm* Las-4000 luminescent image analyser containing a VRF43LMD3 lens and a 575DF20 filter. The observed bands were excised and diced into pieces of approximately 1 mm length, prior to further processing.

4.2.5.5 Long Term Labeling Experiments

Analytical: Cells were grown in 6 well plates until a confluence of 70% was reached. The probes were added 1:1000 from DMSO stocks and one 1 mL media was supplemented with 1 µL DMSO as control. The media was exchanged with 1 mL media containing probes at the appropriate concentrations. After incubation (24 h, 48 h, 72 h, 96 h and 120 h) cells were washed with PBS and harvested by scraping in 1.5 mL PBS. Cells were pelleted by centrifugation at 800 g for 5 min and PBS was aspirated. Cells were lysed by resuspension in 50 µL lysis buffer (PBS, 1% NP-40, 1% DOC) and incubation on ice for 10 min. Soluble and insoluble fraction were isolated by centrifugation at 21000 g for 20 min at 5 °C and insoluble fraction was resuspended in 50 µL lysis buffer by sonication under ice cooling. The samples then underwent *Click reaction and analytic gel-based analysis*.
Preparative: Cells were grown in Petri dishes (150 mm) until they reached 70% confluence. Then the media was exchanged with 10 mL media with appropriate probe concentration and media lacking the probe as control. After incubation (24 h, 48 h, 72 h, 96 h and 120 h) the cells were washed with 10 mL PBS and harvested by scraping in 20 mL PBS. Cells were pelleted by centrifugation at 800 g for 5 min. The cells were lysed by resuspending in 500 µL lysis buffer and incubation for 10 min on ice. Soluble and insoluble fraction were isolated by centrifugation at 21000 g for 20 min at 5 °C and insoluble fraction was resuspended in 50 µL lysis buffer by sonication under ice cooling. The samples then underwent subsequently *Click reaction and preparative gel-based analysis*.

4.2.5.6 Preparative SILAC Labeling

In situ: For preparative SILAC labeling cells were grown in media containing a combination of medium (L-[U-13C6,14N4]arginine and L-[2H4]lysine) or heavy (L-[U-13C6,15N4]arginine and L-[U-13C6,15N2]lysine) isotope-labeled forms of arginine and lysine until full incorporation of the amino acids. The further workflow followed the protocol described in the section *Preparative in situ ABPP labeling experiments.* The cell population

containing medium isotope-labeled arginine and lysine served as control cells while the cell population containing heavy isotope-labeled forms of the mentioned amino acids underwent treatment with probes. After cell lysis the protein concentration was determined and 2 mg of each SILAC labeled proteome mixed. The total volume was adjusted to 947 µL. The samples underwent *Click reaction and preparative gel-based analysis*.

Five day labeling: Cells grown in media substituted with medium-labeled isotopes of arginine and lysine served as controls and cells grown in media substituted with heavy-labeled isotopes of arginine and lysine were incubated with probe. Incubation and harvest was done according to *five day labeling (preparative)*. After lysis 2 mg of each cell population was mixed together and adjusted to a total volume of 947 µL. The samples underwent *Click reaction and preparative gel-based analysis*.

Competitive control labeling: For competitive labeling, applying the same labeling scheme as above, cells serving as controls were incubated for 15 min with 100 µM acivicin and afterwards 100 µM ACV1 was added and incubated for additional 2 h. The complementary cells were solely incubated with 100 µM ACV1 for 2 h. After incubation lysis was executed according to *Preparative in situ ABPP labeling experiments* and subsequently underwent *Click reaction and preparative gel-based analysis* and 50 µL of lysates underwent *Click reaction and analytic gel-based analysis*. The experiment was repeated once maintaining the same labeling scheme of SILAC cell labels and probe treatment. A third experiment was carried out with pre-treatment of heavy labeled cells with 100 µM acivicin for 15 min following incubation with 100 µM ACV1 for 2 h and treatment of medium labeled cells with 100 µM ACV1 for 2 h.

4.2.5.7 Mouse Liver Lysate

300 mg of mouse liver were cut into smaller pieces and added to a 2 mL tube containing ceramic beads (91-PCS-CKM, *peqlab*) and 1 mL cold PBS was added. The liver was homogenized by a Precellys 24 homogenizer (*peqlab*) with 5000 rpm for 10 sec in two cycles. Soluble and insoluble fraction were separated by spinning at 21000 g for 20 min at 5 °C. The insoluble pellet was resuspended in 1 mL PBS by sonication. Protein concentration was assayed (Rotiquant universal, *Carl Roth Laborbedarf*) and adjusted to 2 mg/mL in PBS.

4.2.5.8 Myoma and Myometrium Tissue Lysates

Myoma and Myometrium tissues were obtained from Alcedo Biotech or from the tissue collection of Bayer Schering Pharma (now Bayer HealthCare). Approximately 50 mg of myoma and myometrium tissue were cut into smaller pieces and added to a 2 mL tube containing ceramic beads (91-PCS-CKM or 91-PCS-CK28, *peqlab*) and 700 µL cold PBS, 0.1% sds was added. The tissues were homogenized with a Precellys 24 homogenizer (*peqlab*) with 5000 rpm for CKM beads or 6000 rpm for CK28 beads for 20 sec in three cycles. The lysate was transferred to a tube and the remaining beads were washed with 400 µL 5 M NaCl solution and this solution was added to the lysate. Soluble and insoluble fraction were separated by spinning at 21000 g for 20 min at 5 °C. The insoluble pellet was resuspended in 700 µL PBS, 0.1% sds by sonication. Protein concentration was assayed (Rotiquant universal, *Carl Roth Laborbedarf*) and adjusted to 2 mg/mL.

4.2.5.9 *In vitro* Labeling Experiments

Analytical: 1 µl probe stock was added to 44 µL proteome to adjust the desired concentration and incubated at RT for 1 h. After incubation *Click reaction and analytical gel-based analysis* was performed.
Preparative: 1 µL probe stock was added to 946 µL proteome solution to get the appropriate probe concentration (50 µM for ACVL probes and 100 µM ACV2 and 20 µM ACV1) with one sample lacking the probe as control. The solution was incubated for 1 h at RT. Subsequently *Click reaction and preparative gel-based analysis* was performed.

4.2.5.10 Labeling of Overexpressed Proteins

Expression clones ALDH1A1, ALDH1B1, ALDH2, ALDH4A1 and ACAA2 were grown in 10 mL ampicillin LB at 37 °C with two cultures for each gene until OD_{600} of 0.5 and subsequently one sample was induced with anhydrotetracycline and cultivated for additional 3 h the corresponding sample was cultivated the additional 3 h without induction. The bacterial cell pellets were washed with PBS and resuspended in 100 µL PBS containing 50 µM ACVL1 for ALDH1A1, ALDH1B1, ALDH2; 50 µM ACVL2a for ACAA2 and 50 µM ACV1 for ALDH4A1. The cells were incubated for 2 h at RT and lysed by sonication.

Soluble and insoluble fraction were separated by centrifugation (21000 g for 20 min at 5 °C). Insoluble pellets were resuspended in 100 µL PBS using sonication. The samples underwent *Click reaction and analytical gel-based analysis.*

4.2.5.11 Competitive Labeling Experiments

43 uL of proteome solution were incubated with 1 µL of acivicin stock to adjust the desired concentration (see gel below) and incubated for 15 min at RT. After pre-incubation 1 µL of probe stock was added to adjust the desired probe concentration and incubated for 1 h at RT. After that *Click reaction and analytical gel-based analysis* was performed.

4.2.5.12 Labeling of Recombinant CES1

1 µL of CES1 stock (5 µg/µL) was added to 43 µL PBS or 43 µL A549 lysate. One sample containing 44 µL PBS or 44 µL A549 lysate was incubated with 1 µL DMSO and served as control. The heat control consisted of 43 µL PBS or 43 µL A549 lysate with 1 µL CES1 stock (5 µg/µL) and was treated for 7 min at 96 °C. The samples were incubated with 1 µL probe stock to obtain a concentration of 10 µM FP-probe and 20 µM for ACV2 probe for 1 h at RT. After completion *Click reaction and analytical gel-based analysis* was performed.

4.2.5.13 Labeling of Recombinant CES1 for 24 h

Three samples were prepared by adding 1 µL of CES1 stock (5 µg/µL) to 43 µl PBS and two samples by adding 1 µL CES1 stock to 43 µL A549 lysate. One sample of each set served as control lacking probe and was incubated with 1 µL DMSO. Another sample from each set was incubated with ACV2 at a concentration of 20 µM and incubated for 24 h at RT. As a positive control one sample of CES1 in PBS was labeled with 10 µM FP probe for 1 h at RT. After completion of incubation *Click reaction and analytical gel-based analysis* was performed.

4.2.5.14 Labeling of CES1 and Mutant S221A

In a 6 well plate with HEK293T cells two wells were transfected with CES1(wt) and one well withS221A using Lipofectamine® 2000 as described above. 24 h after transfection one well transfected with CES1, one well transfected with S221A and one well containing only HEK293T cells were incubated with 25 µM ACV2. 3 days after transfection, cells were harvested and lysed as described above. One untreated CES1 transfection was incubated with 10 µM diisopropyl fluorophosphonate (DFP) for 15 min and subsequently incubated with 10 µM FP probe. Samples underwent *Click reaction analytical gel-based analysis and western blotting*.

4.2.5.15 Labeling of ALDH4A1 and Mutant C348A

pDEST 007 plasmid carrying ALDH4A1 (wt) and C348A were transformed into competent SoluBL21™ Competent *E. coli* cells (*Amsbio*) and overexpressed as described above (*Overexpression for target validation*). One sample for ALDH4A1 and C348A was not induced and served as a control and one sample overexpressing ALDH4A1 was incubated after lysis with 50 µM disulfiram 15 min prior to incubation with 50 µM ACV1. After incubation *Click reaction analytical gel-based analysis and Western blotting*.

4.2.6 Mass Spectrometry

4.2.6.1 In Gel Digestion

Protein bands were excised from the gel and subsequently washed with ddH_2O (100 µL, 15 min, 550 rpm, RT), 50 mM ammonium bicarbonate in MeCN (200 µL, 15 min, 550 rpm, RT) and dehydrated with 100% MeCN (100 µL, 10 min, 550 rpm, RT). The shrunken gel pieces were rehydrated in 50 mM ammonium bicarbonate (100 µL, 5 min, 550 rpm, RT), followed by a further dehydration step (100 µL MeCN, 15 min, 550 rpm, RT). The supernatant was removed and the gel pieces were again washed with MeCN (100 µL, 10 min, 550 rpm, RT) and then dried under vacuum in a centrifugal evaporator (15 min, 1 mbar, RT). The proteins were reduced by addition of DTT solution (10 mM in 50 mM ammonium

bicarbonate, 100 µL, 45 min, 550 rpm, 56 °C) to the gel pieces. Then the pieces were washed with MeCN (100 µL, 10 min, 550 rpm, RT), prior to alkylation with iodineacetamide solution (55 mM in 50 mM ammonium bicarbonate, 100 µL, 30 min in the dark, 550 rpm, RT). The gel pieces were afterwards washed with MeCN:50 mM ammonium bicarbonate (1:1) (100 µL, 15 min, 550 rpm, RT) and MeCN (100 µL, 10 min, 550 rpm, RT) and dried *in vacuo* in a centrifugal evaporator (15 min, 1 mbar, RT). 100 µL digest solution (0.5 µg trypsin in 100 µL 50 mM ammonium bicarbonate) was added and incubated for 10 min at 4 °C, followed by 37 °C, 300 rpm overnight. The next day the supernatant was transferred into a LoBind tube (*Eppendorf AG*) and 25 mM ammonium bicarbonate (100 µL, 15 min sonication, RT) was added to the gel pieces. Then MeCN (100 µL) was added and the sample sonicated for 15 min. The supernatant was transferred into the same LoBind tube. 5% FA (100 µL, 15 min sonication, RT) was added to the gel pieces, followed by additional MeCN (100 µL, 15 min sonication, RT). The supernatant was transferred into the same LoBind tube and replaced by MeCN (100 µL, 15 min sonication, RT). The supernatant was transferred into the LoBind tube and the solvent was removed *in vacuo* in a vacuum centrifuge (4 h, 1 mbar, RT). The remaining peptides were stored at -20 °C.[310]

4.2.6.2 Sample Preparation for Mass Spectrometry

Centrifugal filters (modified Nylon, 0.45 µm, low protein binding, *VWR International, LLC*) were pre-rinsed with ddH_2O (1 x 500 µL, 21000 g, 1 min, RT), 0.5 N NaOH (1 x 500 µL, 21000 g, 1 min, RT), ddH_2O (2 x 500 µL, 21000 g, 1 min, RT) and 1 % FA (1 x 500 µL, 21000 g, 1 min, RT). The peptides were dissolved in 1% FA (20 µL, 15 min sonication, RT) and added to the pre equilibrated filters and centrifuged (21000 g, 1 min, RT). The filtrate was transferred into a vial.

4.2.6.3 Mass Spectrometry and Bioinformatics

Measurements were performed using an Orbitrap XL coupled online to an Ultimate 3000 nano HPLC system (*Thermo Fisher Scientific*). Samples were loaded on a trap column and separated on a 15 cm C18 column (2 µm, 100 Å, *Thermo Fisher Scientific Inc.*). For protein identification either the five most intense ions of the full scan were fragmented using CID or a combination of CID of the three most intense ions and HCD of the two most intense ions was

performed. The mass spectrometry data were searched using the SEQUEST algorithm against the corresponding database (ipi.human.v3.68.fasta and ipi.mouse.v3.68.fasta) via the Proteome Discoverer Software 1.3 (*Thermo Fisher Scientific Inc.*). Peptides were considered with a minimal mass of 350 Da and a maximal mass of 10,000 Da. Protein *N*-terminal acetylation and oxidation on methionine were added as variable modifications. Carbamidomethylation on cysteine was added as fixed modification. Mass tolerances of the precursor and fragment ions were set to 10 ppm and 0.5 Da. Filters were set to further refine the search results. The Xcorr vs. charge state filter was set to Xcorr values of 1.5, 2.0, 2.25 and 2.5 for charge states +1, +2, +3 and +4, respectively. The number of different peptides had to be ≥ 2 and the peptide confidence filter was set to at least medium. These filter values are similar to others previously reported for SEQUEST analysis. Xcorr values (Score) of each run, the peptide spectrum matches (PSM) as well as the total number of obtained peptides, unique peptide, ratio from SILAC or precursor ion intensity ratio between labeled and control samples are reported below. Identified proteins from gel slices were defined as true probe targets when the peak area of labeled sample versus unlabeled (control) sample is significantly increased. Intensities of proteins from the same gel slice can be estimated by the score and the number of peptide spectral matches (PSMs). Proteins underlying the fluorescence bands in ABPP approaches posses in addition to an increased peak area a high score and number of PSMs compared to other proteins identified in the same slice.

4.2.6.4 Mass Spectrometry of Intact Proteins

Purified CES1 and CES1 labeled with metabolized ACV2 were diluted to a concentration of 0.1 mg/mL. Solutions were desalted on a Massprep on-line desalting cartridge (Waters) according to the manufacturer's procedure on a Dionex UltiMate 3000 HPLC system. Samples were measured on a Thermo LTQ FT Ultra mass spectrometer with electron spray ionization that was coupled to the Dionex UltiMate 3000 HPLC system. Thermo Scientific ProMass Deconvolution™ software was used for data analysis and deconvolution.

5 Zusammenfassung

Acivicin

Acivicin ist ein Naturstoff der aus *Streptomyces sviceus* isoliert wurde und antitumor Eigenschaften besitzt. In klinischen Studien konnte seine Antitumor Eigenschaften gezeigt werden, jedoch wurden keine Studien aufgrund der Nebenwirkungen weiterverfolgt. Unter den Naturstoffen nimmt Acivicin eine einzigartige Position aufgrund seines Elektrophils, des Chlordihydroisoxazols, ein. In vorhergehenden Untersuchungen wurden Sonden auf Basis dieses Elektrophils für Activity-based protein profiling synthetisiert, deren Reaktivität noch zusätzlich durch den Austausch von Chlor mit Brom erhöht wurde. ABPP beschreibt eine chemoproteomische technik mit der anhand von Sonden Proteine kovalent modifiziert (markiert) werden, die dann durch Clickchemie mit Fluoreszenzfarbstoffen zur Visualisierung oder Affinitätstags zur Anreicherung modifiziert werden können. Mit diesen Sonden konnte in Bakterien bereits eine Selektivität für Aldehyd-Dehydrogenasen festgestellt werden.

Für Acivicin waren aus bisherigen Studien keine Aldehyd-Dehydrogenasen als Zielproteine bekannt. Aus diesem Grund wurden die bereits Sonden mit zwei Sonden, die sich vom Naturstoff ableiten lassen erweitert und ABPP Experimente in Mausleberproteom und Leberkrebszellen (HepG2) durchgeführt. Es stellten sich wie erwartet, Aldehyd-Dehydrogenasen mit ihren Vertretern ALDH1A1, -1B1, -2 und ALDH4A1 als Zielproteine heraus. In Zellwachstumsstudien mit HepG2, konnte auch eine Inhibition des Zellwachstums der beiden neuen Acivicin abgeleiteten Sonden wie Acivicin gezeigt werden während die Bromdihydroisoxazolsonden keine Inhibition zeigten. Kompetitive ABPP Experimente mit Acivicin und Aktivitätsassays konnte gezeigt werden, dass es sich ALDH4A1 um ein neues Zielprotein von Acivicin handelt. In Langzeit ABPP Experimenten zeigte sich mit CES1 ein neues Zielprotein neben den Aldehyd-Dehydrogenasen. CES1 konnte weder direkt markiert noch in Aktivitäts assays mit den Acvicinsonden inhibiert werden. Nur eine längere Inkubation unter Einwirkung der ganzen Zelle konnte dies erreichen, sodass eine Metabolisierung nahe lag. Diese wurde auch durch transiente Überexpression von CES1 in HEK293T Zellen einhergehend Markierung nach längerer Inkubationszeit bewiesen. Für ALDH4A1 und CES1 wurden durch Mutagenesestudien die nucleophilen Aminosäuren Cystein and Serin als Reste für die kovalente Modifizierung identifiziert. Des weiteren wurde für beide Enzyme in siRNA Experimenten der Einfluss auf das Zellwachstum von HepG2 untersucht. Durch den Knockdown wurde bei beiden Enzymen eine Reduktion des

Zellwachstums festgestellt. Mit diesen Ergebnissen konnte mit ALDH4A1 ein neues Zielprotein von Acivicin, das einen Rolle bei der Zellwachstumsinhibierung spielt, wie auch eine mögliche Metabolisierung, wie sie seit längerem diskutiert wird, gezeigt werden.

Uterus myomatosus

Uterus myomatosus oder kurz Myome sind gutartige glattmuskuläre Uterustumore, die die häufigsten Tumore des Uterus darstellen. Beim Erreichen des fünfzigsten Lebensjahres haben 70-80% der Frauen bereits Myome entwickelt. Trotz ihrer Gutrarigkeit können Myome mit ihren Symptomen die Lebensqualität in negativer Hinsicht beeinflussen. Die Symptome umfassen gesteigerte und verlängerte Regelblutung, Anämie, Unterleibsschmerzen bis hin zu Unfruchtbarkeit und Frühgeburt. Trotz vieler Untersuchungen ist wenig über den Ursprung und die Pathogenese von Myomen bekannt. Ein hormoneller Hintergrund und deregulierte Mesenchymale Stammzellen werden zurzeit als Ursache für Myome vermutet. Die Behandlung von Myomen erfolgt durch Vergabe von Gonadotropin-Releasing Hormon Analoga (GnRHa), die einerseits einen Wachstumsstopp der Myome bewirken, jedoch einen menopausalen Zustand auf der anderen Seite und deswegen nur kurzzeitig eingesetzt werden. Neben medikamentösen Behandlungen werden hauptsächlich Operative Methoden bei der Myombehandlug eingesetzt. Zum einen besteht die Möglichkeit einer Myomektomie durch Laparoskopie oder die Entfernung des gesamten Uterus durch Hysterektomie.

In dieser Arbeit wurden Gewebeproben von Patientinnen auf Aktivität von Serin-Hydrolasen im Myomgewebe und dem entsprechendem gesunden Myometriumsgewebe untersucht. Serin-Hydrolasen spielen eine Rolle in verschiedene Prozessen, wie beispielsweise der Gestaltung der extrazellulären Matrix, und sind adressierbar durch Inhibitoren. Durch die Verwendung einer Fluorosphonatsonde in ABPP Experimenten konnte nach Etablierung einer Homogenisierungsmethode ein Aktivitätsprofil erstellt werden. Durch Untersuchung von neun Patientinnen konnten 32 verschiedene Serin-Hydrolasen identifiziert werden. Unter all diesen Serin-Hydrolasen zeigten TPSAB1, TPSB2, TPSD1, CMA1, CTSG, CES1, CTSA und RBBP9 ein unterschiedliches Aktivitätsprofil in Myom- und Myommetriumsgewebe. CES1 und CTSA zeigten sich aktiver im Myom von einigen Patientinnen aber nicht durchgehend. Für RBBP9 konnte eine höhere Aktivität im Myom von zwei Patientinnen festgestellt werden, jedoch wurden beide Proben während der Proliferativen Phase des Uteruszyklus entnommen. Die Serin-Hydrolasen TPSAB1, TPSB2, TPSD1, CMA1 und CTSG zeigten eine höhere Aktivität im Myometrium von fast allen Patientinnen bis auf jene beiden Patientinnen mit einer RBBP9 Aktivität im Myom. TPSAB1, TPSB2, TPSD1, CMA1 und CTSG spielen

wichtige Rollen im Entzündungsprozess und weiteren Prozessen. Ein wichtiger Prozess ist allerdings der Gewebemodellierung durch Aktivierung von TGF-β , einem Cytokin das in viele Prozesse involviert ist wie Zellwachstum, -differenzierung, -migration, Apoptose, und extrazellulärer Matrix Aufbau. RBBP9 spielt beim Thema TGF-β wiederrum auch eine Rolle, da es in den TGF-β Signalweg eingreift.

Mit dieser Arbeit konnten interessante Einblicke in das Aktivitätsmuster von Serin-Hydrolasen gewährt werden. Mit weiteren Patientinnen kann die Studie noch ausgeweitet werden, wobei weitere zusätzliche Proben besonders aus der proliferativen Phase untersucht werden sollten. Ein interessanter Aspekt ist die Rolle von TGF-β in der Pathogenese von Myomen der weiterführend Untersucht werden kann.

6 Summary

Acivicin

Acivicin is a natural product from *Streptomyces sviceus* with antitumor activity. Several clinical trials were carried out with acivicin on various tumors but all failed due to the severe side effects. The chlorodihydroisoxazole of the non canonical amino acid acivicin represents an unique electrophilic moiety among natural products. Previous work depicted this electrophilic moiety and enhanced the electrophilicity by exchanging chlorine by bromine to build probes for activity-based protein profiling. ABPP is chemoproteomic method that uses probes that are covalently linked to the target enzyme. Via click chemistry a reporter tag or a biotin tag can be attached for visualization or enrichment followed by mass spectrometry analysis. On the previous work aldehyde dehydrogenases were identified as preferred targets for this moiety in bacteria proteome.

However no aldehyde dehydrogenase was yet reported as a target of acivin. Based on these results two new probes were synthsized from the natural product. ABPP studies in mouse liver proteome and HepG2 cells revealed ALDH1A1, -1B1, -2 and ALDH4A1. Cell growth studies revealed growth inhibition of HepG2 cells by the two acivicin derived probes, while the bromodihydroisoxazole probes showed no effect. In competitive ABPP studies with acivicin and activity assays, ALDH4A1 turned out to be a target of acivicin and the other aldehyde dehydrogenases to be probe specific. This represents a new target among the enzymes already confirmed for acivicin. In long term labelings that mimic the conditions of the cell growth studies a new target with CES1 along with the ALDHs was identified. Labeling of CES1 occured after a certain amount of time and recombinant CES1 could not be labeled directly nor inhibited in an activity assay with acivicin probes. This implicated a metabolization of the probe before labeling. Overexpression of CES1 in HEK293T cells with extended labeling times showed labeling of the serine hydrolase CES1 and proofed the theory of metabolization. For the two enzymes ALDH4A1 and CES1 mutagenesis studies revealed the nucleophile cysteine and serine to be attacked by acivicin or probes. The same enzymes were investigated in terms of bioactivity with siRNA studies. Both enzymes were knocked down and their influence on tumor cell growth was investigated. Both enzymes showed growth reduction upon knockdown. These results conclude, that with ALDH4A1 a new target of acivicin was found that plays a role in the growth reduction mediated through acivicin.

Additionally a possible metabolization of the acivicin moiety, that was long discussed, was shown.

Uterine fibroids

Uterine fibroids or myoma are benign smooth muscle tumors of the uterus. By reaching the age of 50 years, 70-80% of women developed myomas. These tumors can affect life quality in a negative way with their symptoms that reach from heavy, irregular and prolonged menstrual bleeding, anemia, abdominal pain and even infertility to recurrent abortion and preterm labor. Despite many research on myomas their etiology and pathogenesis remains unknown. A hormonal background and deregulated mesenchymal stem cells are regarded as the origin of myomas. Treatment of myomas can be achieved by application of Gonadotropin-releasing hormone analoga (GnRHa) that stop myoma growth but also lead to a menopausal condition and are limited to short term treatment. Next to medical treatment, surgical methods are the treatment of choice with a laparoscopically excision (myomectomy) or the removal of the uterus (hysterectomy).

In this work patient samples were investigated for different activities of serine hydrolases in myoma tissue and the corresponding healthy myometrium tissue. Serine hydrolases are involved in processes like extracellular matrix remodeling and accessible with drugs. The activity profile was obtained with a fluorophosphonate probe by using ABPP. After establishment of tissue homogenization and labeling protocol, 9 patient samples were examined. A total of 32 different serine hydrolases were identified from these samples. Among those serine hydrolases, TPSAB1, TPSB2, TPSD1, CMA1, CTSG, CES1, CTSA and RBBP9 showed a different activity profile in myoma and myometrium. CES1 and CTSA showed higher activity in myoma in some patients but not in general. RBBP9 showed higher myoma activity in two patients but these samples were taken from the proliferative phase of the uterus. TPSAB1, TPSB2, TPSD1, CMA1 and CTSG showed higher activity in myometrium in general, but the activity was equal in both patients that showed RBBP9 activity. The three tryptases (TPSAB1, TPSB2 and TPSD1) together with CMA1 and CTSG are involved in a number of processes, e.g. inflammation, but especially tissue remodeling. Furthermore they are known to activate TGF-β. This cytokine plays many roles in terms of cell growth, differentiation, migration, apoptosis, and extracellular matrix production. In turn RBBP9 interferes in the TGF-β signaling pathway.

This work gave intersting insight in the activity profile of serine hydrolases of myoma and myometrium tissue. More patients samples would result in a deeper analysis, especially with

samples that were taken from the proliferative phase. Additionally the role of TGF-β in myoma formation myoma growth could deliver a better understanding of these tumors

7 Abbreviations

°C	degree Celsius
µL	microliter
µM	micromolar
ABPP	activity-based protein profiling
ACN	acetonitrile
ACV	acivicin
ALDH	aldehyde dehydrogenase
Asn	asparagine
Asp	aspartic acid
ATP	adenosine triphosphate
BOC	*t*-butyloxycarbonyl
BSA	bovine serum albumin
CaCl2	calcium cholride
CC	click chemistry
CID	collision-induced dissociation
cDNA	complementary DNA
cm	centimeter
CO_2	carbon dioxide
COMU	1-Cyano-2-ethoxy-2-oxoethylidenaminooxy)dimethylamino-morpholino-carbenium hexafluorophosphate
CTP	cytidine triphosphate
CuSO4	Copper(II) sulfate
cyc	cycle
Cys	cysteine
d	doublet
DCC	*N*,*N'*-Dicyclohexylcarbodiimide
DCM	dichloromethane
ddH_2O	deionized water
DFP	diisopropyl fluorophosphonate
DIPEA	*N*,*N*-Diisopropylethylamine
DMEM	Dulbecco's Modified Eagle's Medium

DMF	dimethylformamid
DMSO	dimethylsulfoxid
DNA	deoxyribonucleic acid
dNTP	deoxyribonucleotide triphosphate
dsDNA	double stranded DNA
DTT	dithiothreitol
EC_{50}	half maximal effective concentration
EDTA	ethylene diamine tetraacetat
e.g.	exempli gratia = for example
eq.	equivalents
ESI-MS	electrospray ionization mass-spectrometry
EtOAc	ethyl acetate
FBS	fetal bovine serum
FP	fluorophosphonate
g	gram
Glu	glutamine
h	hour
HATU	1-[Bis(dimethylamino)methylene]-1H-1,2,3-triazolo[4,5-b]pyridinium 3-oxid hexafluorophosphate
HCD	higher-energy collisional dissociation
HCl	hydrochloric acid
His	histidine
HIV	human immunodeficiency virus
HOAt	1-Hydroxy-7-azabenzotriazole
HOBt	1-Hydroxybenzotriazole
HPLC	High Performance Liquid Chromatography
HRP	horseradish peroxidase
Hz	Hertz
IC_{50}	half maximal inhibitory concentration
IPTG	Isopropyl β-D-1-thiogalactopyranoside
Kan	Kanamycin
kDA	kilo dalton
L2K	lipofectamine 2000
LB	Luria-broth

LC	liquid chromatography
LTQ-FT	Linear trap quadrupole - Fourier Transform
Lys	lysine
M	molar
m	multiplet
m/z	mass to charge ratio
MeCN	acetonitrile
mg	milligram
MHz	Megahertz
min	minute
mL	milliliter
mM	millimolar
MS	mass spectrometry
MW	molecular weight
NaCl	sodium chloride
NAD	nicotinamide adenine dinucleotide
nM	nanomolar
nm	nanometer
NMR	Nuclear magnetic resonance
OD	optical density
PAGE	polyacrylamide gel electrophoresis
PBS	Phosphate Buffered Saline
PCR	polymerase chain reaction
PEG	polyethylene glycol
ppm	parts per million
PTM	post-translational modification
PVDF	polyvinylidene difluoride
q	quartet
quint.	quintet
Rf	Retention factor
RhN3	Rhodium azide
RNA	ribonucleic acid
rpm	rotations per minute
RPMI	Roswell Park Memorial Institute medium

rt	room temperature
s	singlet
SDS	sodium dodecyl sulfate
sec	second
siRNA	small interfering RNA
SILAC	stable isotope labeling by amino acids in cell culture
t	triplet
TBTA	Tris-[(1-benzyl-1H-1,2,3-triazol-4-yl)methyl]amin)
TCEP	Tris-(2-carboxyethyl)-phosphine
TEMED	*N*,*N*,*N'*,*N'*-Tetramethylethylenediamine
TEV	Tobacco Etch Virus
TFA	Trifluoroacetic acid
TFL	Trifunctional linker
Tris	Tris-(hydroxymethyl)-aminomethan
wt	wild type

8 Literature

1. Lander, E.S., et al., *Initial sequencing and analysis of the human genome.* Nature, 2001. **409**(6822): p. 860-921.
2. Venter, J.C., et al., *The sequence of the human genome.* Science, 2001. **291**(5507): p. 1304-51.
3. Yates, J.R., 3rd, *Mass spectrometry and the age of the proteome.* Journal of mass spectrometry : JMS, 1998. **33**(1): p. 1-19.
4. Link, A.J., et al., *Direct analysis of protein complexes using mass spectrometry.* Nature biotechnology, 1999. **17**(7): p. 676-82.
5. Wolters, D.A., M.P. Washburn, and J.R. Yates, 3rd, *An automated multidimensional protein identification technology for shotgun proteomics.* Analytical chemistry, 2001. **73**(23): p. 5683-90.
6. Yates, J.R., 3rd, *Mass spectral analysis in proteomics.* Annual review of biophysics and biomolecular structure, 2004. **33**: p. 297-316.
7. Eng, J.K., A.L. McCormack, and J.R. Yates, *An approach to correlate tandem mass spectral data of peptides with amino acid sequences in a protein database.* Journal of the American Society for Mass Spectrometry, 1994. **5**(11): p. 976-89.
8. Yates, J.R., 3rd, et al., *Method to correlate tandem mass spectra of modified peptides to amino acid sequences in the protein database.* Analytical chemistry, 1995. **67**(8): p. 1426-36.
9. Perkins, D.N., et al., *Probability-based protein identification by searching sequence databases using mass spectrometry data.* Electrophoresis, 1999. **20**(18): p. 3551-67.
10. Cox, J., et al., *Andromeda: a peptide search engine integrated into the MaxQuant environment.* Journal of proteome research, 2011. **10**(4): p. 1794-805.
11. Steen, H. and M. Mann, *The ABC's (and XYZ's) of peptide sequencing.* Nature reviews. Molecular cell biology, 2004. **5**(9): p. 699-711.
12. *An integrated encyclopedia of DNA elements in the human genome.* Nature, 2012. **489**(7414): p. 57-74.
13. Kim, M.S., et al., *A draft map of the human proteome.* Nature, 2014. **509**(7502): p. 575-81.
14. Wilhelm, M., et al., *Mass-spectrometry-based draft of the human proteome.* Nature, 2014. **509**(7502): p. 582-7.
15. Ostrowski, K. and E.A. Barnard, *Application of isotopically-labelled specific inhibitors as a method in enzyme cytochemistry.* Experimental Cell Research, 1961. **25**(2): p. 465-468.
16. Ostrowski, K., et al., *Autoradiographic Methods in Enzyme Cytochemistry. I. Localisation of Acetylcholinesterase Activity Using a 3-H Labeled Irreversible Inhibitor.* Experimental Cell Research, 1963. **31**: p. 89-99.
17. Kam, C.M., et al., *Biotinylated isocoumarins, new inhibitors and reagents for detection, localization, and isolation of serine proteases.* Bioconjugate Chemistry, 1993. **4**(6): p. 560-7.
18. Abuelyaman, A.S., et al., *Fluorescent derivatives of diphenyl [1-(N-peptidylamino)alkyl]phosphonate esters: synthesis and use in the inhibition and cellular localization of serine proteases.* Bioconjugate Chemistry, 1994. **5**(5): p. 400-5.
19. Liu, Y., M.P. Patricelli, and B.F. Cravatt, *Activity-based protein profiling: the serine hydrolases.* Proceedings of the National Academy of Sciences of the United States of America, 1999. **96**(26): p. 14694-9.

20. Greenbaum, D., et al., *Epoxide electrophiles as activity-dependent cysteine protease profiling and discovery tools.* Chemistry & biology, 2000. **7**(8): p. 569-81.
21. Speers, A.E., G.C. Adam, and B.F. Cravatt, *Activity-based protein profiling in vivo using a copper(i)-catalyzed azide-alkyne [3 + 2] cycloaddition.* Journal of the American Chemical Society, 2003. **125**(16): p. 4686-7.
22. Verdoes, M., et al., *Azido-BODIPY acid reveals quantitative Staudinger-Bertozzi ligation in two-step activity-based proteasome profiling.* Chembiochem : a European journal of chemical biology, 2008. **9**(11): p. 1735-8.
23. Willems, L.I., et al., *Two-step labeling of endogenous enzymatic activities by Diels-Alder ligation.* Chembiochem : a European journal of chemical biology, 2010. **11**(12): p. 1769-81.
24. Willems, L.I., et al., *Triple bioorthogonal ligation strategy for simultaneous labeling of multiple enzymatic activities.* Angewandte Chemie, 2012. **51**(18): p. 4431-4.
25. Mackinnon, A.L. and J. Taunton, *Target Identification by Diazirine Photo-Cross-linking and Click Chemistry.* Current protocols in chemical biology, 2009. **1**: p. 55-73.
26. Saghatelian, A., et al., *Activity-based probes for the proteomic profiling of metalloproteases.* Proceedings of the National Academy of Sciences of the United States of America, 2004. **101**(27): p. 10000-5.
27. Fleet, G.W.J., R.R. Porter, and J.R. Knowles, *Affinity Labelling of Antibodies with Aryl Nitrene as Reactive Group.* Nature, 1969. **224**(5218): p. 511-512.
28. Galardy, R.E., L.C. Craig, and M.P. Printz, *Benzophenone triplet: a new photochemical probe of biological ligand-receptor interactions.* Nature: New biology, 1973. **242**(117): p. 127-8.
29. Smith, R.A. and J.R. Knowles, *Letter: Aryldiazirines. Potential reagents for photolabeling of biological receptor sites.* Journal of the American Chemical Society, 1973. **95**(15): p. 5072-3.
30. Gersch, M., J. Kreuzer, and S.A. Sieber, *Electrophilic natural products and their biological targets.* Natural product reports, 2012. **29**(6): p. 659-82.
31. Barglow, K.T. and B.F. Cravatt, *Activity-based protein profiling for the functional annotation of enzymes.* Nature methods, 2007. **4**(10): p. 822-7.
32. Sieber, S.A., et al., *Proteomic profiling of metalloprotease activities with cocktails of active-site probes.* Nature chemical biology, 2006. **2**(5): p. 274-81.
33. Cravatt, B.F., A.T. Wright, and J.W. Kozarich, *Activity-based protein profiling: from enzyme chemistry to proteomic chemistry.* Annual review of biochemistry, 2008. **77**: p. 383-414.
34. Serim, S., U. Haedke, and S.H. Verhelst, *Activity-based probes for the study of proteases: recent advances and developments.* ChemMedChem, 2012. **7**(7): p. 1146-59.
35. Willems, L.I., H.S. Overkleeft, and S.I. van Kasteren, *Current developments in activity-based protein profiling.* Bioconjugate Chemistry, 2014. **25**(7): p. 1181-91.
36. Fonovic, M. and M. Bogyo, *Activity-based probes as a tool for functional proteomic analysis of proteases.* Expert review of proteomics, 2008. **5**(5): p. 721-30.
37. Nodwell, M.B. and S.A. Sieber, *ABPP methodology: introduction and overview.* Topics in current chemistry, 2012. **324**: p. 1-41.
38. Shi, H., et al., *Cell-Based Proteome Profiling of Potential Dasatinib Targets by Use of Affinity-Based Probes.* Journal of the American Chemical Society, 2012. **134**(6): p. 3001-3014.
39. Bottcher, T. and S.A. Sieber, *Showdomycin as a versatile chemical tool for the detection of pathogenesis-associated enzymes in bacteria.* Journal of the American Chemical Society, 2010. **132**(20): p. 6964-72.

40. Bachovchin, D.A., et al., *Identification of selective inhibitors of uncharacterized enzymes by high-throughput screening with fluorescent activity-based probes.* Nature biotechnology, 2009. **27**(4): p. 387-94.
41. Hanka, L.J. and A. Dietz, *U-42, 126, a new antimetabolite antibiotic: production, biological activity, and taxonomy of the producing microorganism.* Antimicrob Agents Chemother, 1973. **3**(3): p. 425-31.
42. Hanka, L.J., D.G. Martin, and G.L. Neil, *A new antitumor antimetabolite, (alphaS,5S)-alpha-amino-3-chloro-4,5-dihydro-5-isoxazoleacetic acid (NSC-163501): antimicrobial reversal studies and preliminary evaluation against L1210 mouse leukemia in vivo.* Cancer Chemother Rep, 1973. **57**(2): p. 141-8.
43. Earhart, R.H. and G.L. Neil, *Acivicin in 1985.* Adv Enzyme Regul, 1985. **24**: p. 179-205.
44. Allen, L., R. Meck, and A. Yunis, *The inhibition of gamma-glutamyl transpeptidase from human pancreatic carcinoma cells by (alpha S,5S)-alpha-amino-3-chloro-4,5-dihydro-5-isoxazoleacetic acid (AT-125; NSC-163501).* Res Commun Chem Pathol Pharmacol, 1980. **27**(1): p. 175-82.
45. Jayaram, H.N., D. A. Cooney, J A. Ryan, G. Neil, R. L. Dion and V. H. Bono, *L-(αS,5S)-α-amino-3-chloro-4,5-dihydro-5-isoxazoleacetic acid (NSC-163501) A new amino acid antibiotic with the properties of an antagonist of L-glutamine* Cancer Chemother Rep, 1975(59): p. 481-491.
46. Neil, G.L., et al., *Biochemical and pharmacological effects of the fermentation-derived antitumor agent, (alphaS,5S)-alpha-amino-3-chloro-4,5-dihydro-5-isoxazoleacetic acid (AT-125).* Cancer Res, 1979. **39**(3): p. 852-6.
47. Tso, J.Y., S.G. Bower, and H. Zalkin, *Mechanism of inactivation of glutamine amidotransferases by the antitumor drug L-(alpha S, 5S)-alpha-amino-3-chloro-4,5-dihydro-5-isoxazoleacetic acid (AT-125).* J Biol Chem, 1980. **255**(14): p. 6734-8.
48. Lui, M.S., H. Kizaki, and G. Weber, *Biochemical pharmacology of acivicin in rat hepatoma cells.* Biochemical Pharmacology, 1982. **31**(21): p. 3469-73.
49. Miles, B.W., et al., *Inactivation of the amidotransferase activity of carbamoyl phosphate synthetase by the antibiotic acivicin.* J Biol Chem, 2002. **277**(6): p. 4368-73.
50. Sebolt, J.S., et al., *Inactivation by acivicin of carbamoyl-phosphate synthetase II of human colon carcinoma.* Biochemical Pharmacology, 1985. **34**(1): p. 97-100.
51. Elliott, W.L. and G. Weber, *In vivo inactivation of formylglycinamidine ribonucleotide synthetase in rat hepatoma.* Biochemical Pharmacology, 1985. **34**(2): p. 243-8.
52. Zhen, Y.S., M.S. Lui, and G. Weber, *Effects of acivicin and dipyridamole on hepatoma 3924A cells.* Cancer Research, 1983. **43**(4): p. 1616-9.
53. Weber, G., et al., *Regulation of purine and pyrimidine metabolism by insulin and by resistance to tiazofurin.* Advances in enzyme regulation, 1985. **23**: p. 81-99.
54. Fischer, P.H., et al., *Enhancement of the sensitivity of human colon cancer cells to growth inhibition by acivicin achieved through inhibition of nucleic acid precursor salvage by dipyridamole.* Cancer Research, 1984. **44**(8): p. 3355-9.
55. Kessel, D. and T.C. Hall, *Effects of persantin on deoxycytidine transport by murine leukemia cells.* Biochimica et biophysica acta, 1970. **211**(1): p. 88-94.
56. Williams, K., et al., *Crystal structure of acivicin-inhibited gamma-glutamyltranspeptidase reveals critical roles for its C-terminus in autoprocessing and catalysis.* Biochemistry, 2009. **48**(11): p. 2459-67.
57. Wada, K., et al., *Crystal structures of Escherichia coli gamma-glutamyltranspeptidase in complex with azaserine and acivicin: novel mechanistic implication for inhibition by glutamine antagonists.* J Mol Biol, 2008. **380**(2): p. 361-72.

58. Ida, T., et al., *Structure of Bacillus subtilis gamma-glutamyltranspeptidase in complex with acivicin: diversity of the binding mode of a classical and electrophilic active-site-directed glutamate analogue.* Acta crystallographica. Section D, Biological crystallography, 2014. **70**(Pt 2): p. 607-14.
59. Allen, L.M., M.V. Corrigan, and T. Meinking, *Interaction of AT-125, (alpha S,5S)-amino-3-chloro-4,5-dihydroisoxazoleacetic acid, with bovine kidney gamma-glutamyl transpeptidase.* Chemico-biological interactions, 1981. **33**(2-3): p. 361-5.
60. Wheeler, R.H., et al., *The cytokinetic and cytotoxic effects of ICRF-159 and ICRF-187 in vitro and ICRF-187 in human bone marrow in vivo.* Investigational new drugs, 1983. **1**(4): p. 283-95.
61. Aberkane, H., et al., *Acivicin induces apoptosis independently of gamma-glutamyltranspeptidase activity.* Biochem Biophys Res Commun, 2001. **285**(5): p. 1162-7.
62. Fleishman, G., et al., *Phase II trial of acivicin in advanced metastatic breast cancer.* Cancer treatment reports, 1983. **67**(9): p. 843-4.
63. Adolphson, C.C., et al., *Phase II trial of acivicin in patients with advanced colorectal carcinoma.* Am J Clin Oncol, 1986. **9**(3): p. 189-91.
64. Maroun, J.A., et al., *Phase I study of acivicin and cisplatin in non-small-cell lung cancer. A National Cancer Institute of Canada study.* Am J Clin Oncol, 1990. **13**(5): p. 401-4.
65. Olver, I.N., et al., *Phase II study of acivicin in patients with recurrent high grade astrocytoma.* J Clin Neurosci, 1998. **5**(1): p. 46-8.
66. Falkson, G., et al., *A randomized phase II study of acivicin and 4'deoxydoxorubicin in patients with hepatocellular carcinoma in an Eastern Cooperative Oncology Group study.* American journal of clinical oncology, 1990. **13**(6): p. 510-5.
67. O'Dwyer, P.J., M.T. Alonso, and B. Leyland-Jones, *Acivicin: a new glutamine antagonist in clinical trials.* Journal of clinical oncology : official journal of the American Society of Clinical Oncology, 1984. **2**(9): p. 1064-71.
68. Bonomi, P., D. Finkelstein, and A. Chang, *Phase II trial of acivicin versus etoposide-cisplatin in non-small cell lung cancer. An Eastern Cooperative Oncology Group study.* American journal of clinical oncology, 1994. **17**(3): p. 215-7.
69. Taylor, S.A., et al., *Objective antitumor activity of acivicin in patients with recurrent CNS malignancies: a Southwest Oncology Group trial.* Journal of clinical oncology : official journal of the American Society of Clinical Oncology, 1991. **9**(8): p. 1476-9.
70. Earhart, R.H., et al., *Phase I trial and pharmacokinetics of acivicin administered by 72-hour infusion.* Cancer treatment reports, 1983. **67**(7-8): p. 683-92.
71. Hofer, A., J.T. Ekanem, and L. Thelander, *Allosteric regulation of Trypanosoma brucei ribonucleotide reductase studied in vitro and in vivo.* The Journal of biological chemistry, 1998. **273**(51): p. 34098-104.
72. Hofer, A., et al., *Trypanosoma brucei CTP synthetase: a target for the treatment of African sleeping sickness.* Proc Natl Acad Sci U S A, 2001. **98**(11): p. 6412-6.
73. Conti, P., et al., *Synthesis and in vitro/in vivo evaluation of the antitrypanosomal activity of 3-bromoacivicin, a potent CTP synthetase inhibitor.* ChemMedChem, 2011. **6**(2): p. 329-33.
74. Orth, R., T. Bottcher, and S.A. Sieber, *The biological targets of acivicin inspired 3-chloro- and 3-bromodihydroisoxazole scaffolds.* Chemical Communications, 2010. **46**(44): p. 8475-7.
75. Vasiliou, V., A. Pappa, and D.R. Petersen, *Role of aldehyde dehydrogenases in endogenous and xenobiotic metabolism.* Chemico-biological interactions, 2000. **129**(1-2): p. 1-19.

76. Vasiliou, V., A. Pappa, and T. Estey, *Role of human aldehyde dehydrogenases in endobiotic and xenobiotic metabolism.* Drug metabolism reviews, 2004. **36**(2): p. 279-99.
77. Marchitti, S.A., R.A. Deitrich, and V. Vasiliou, *Neurotoxicity and metabolism of the catecholamine-derived 3,4-dihydroxyphenylacetaldehyde and 3,4-dihydroxyphenylglycolaldehyde: the role of aldehyde dehydrogenase.* Pharmacological reviews, 2007. **59**(2): p. 125-50.
78. Esterbauer, H., R.J. Schaur, and H. Zollner, *Chemistry and biochemistry of 4-hydroxynonenal, malonaldehyde and related aldehydes.* Free radical biology & medicine, 1991. **11**(1): p. 81-128.
79. O'Brien, P.J., A.G. Siraki, and N. Shangari, *Aldehyde sources, metabolism, molecular toxicity mechanisms, and possible effects on human health.* Critical reviews in toxicology, 2005. **35**(7): p. 609-62.
80. Sladek, N.E., *Human aldehyde dehydrogenases: potential pathological, pharmacological, and toxicological impact.* Journal of biochemical and molecular toxicology, 2003. **17**(1): p. 7-23.
81. Yokoyama, A., et al., *Alcohol and aldehyde dehydrogenase gene polymorphisms and oropharyngolaryngeal, esophageal and stomach cancers in Japanese alcoholics.* Carcinogenesis, 2001. **22**(3): p. 433-9.
82. Nadkarni, D.V. and L.M. Sayre, *Structural definition of early lysine and histidine adduction chemistry of 4-hydroxynonenal.* Chemical Research in Toxicology, 1995. **8**(2): p. 284-91.
83. Brooks, P.J. and J.A. Theruvathu, *DNA adducts from acetaldehyde: implications for alcohol-related carcinogenesis.* Alcohol, 2005. **35**(3): p. 187-93.
84. Pappa, A., et al., *Aldh3a1 protects human corneal epithelial cells from ultraviolet- and 4-hydroxy-2-nonenal-induced oxidative damage.* Free radical biology & medicine, 2003. **34**(9): p. 1178-89.
85. Lassen, N., et al., *Antioxidant function of corneal ALDH3A1 in cultured stromal fibroblasts.* Free radical biology & medicine, 2006. **41**(9): p. 1459-69.
86. Estey, T., et al., *Mechanisms involved in the protection of UV-induced protein inactivation by the corneal crystallin ALDH3A1.* The Journal of biological chemistry, 2007. **282**(7): p. 4382-92.
87. Lassen, N., et al., *Multiple and additive functions of ALDH3A1 and ALDH1A1: cataract phenotype and ocular oxidative damage in Aldh3a1(-/-)/Aldh1a1(-/-) knock-out mice.* The Journal of biological chemistry, 2007. **282**(35): p. 25668-76.
88. Uma, L., et al., *Corneal aldehyde dehydrogenase displays antioxidant properties.* Experimental eye research, 1996. **63**(1): p. 117-20.
89. Muzio, G., et al., *Aldehyde dehydrogenases and cell proliferation.* Free radical biology & medicine, 2012. **52**(4): p. 735-46.
90. Marchitti, S.A., et al., *Non-P450 aldehyde oxidizing enzymes: the aldehyde dehydrogenase superfamily.* Expert opinion on drug metabolism & toxicology, 2008. **4**(6): p. 697-720.
91. Liu, Z.J., et al., *The first structure of an aldehyde dehydrogenase reveals novel interactions between NAD and the Rossmann fold.* Nature structural biology, 1997. **4**(4): p. 317-26.
92. D'Ambrosio, K., et al., *The first crystal structure of a thioacylenzyme intermediate in the ALDH family: new coenzyme conformation and relevance to catalysis.* Biochemistry, 2006. **45**(9): p. 2978-86.
93. Hurley, T.D., C.G. Steinmetz, and H. Weiner, *Three-dimensional structure of mitochondrial aldehyde dehydrogenase. Mechanistic implications.* Advances in experimental medicine and biology, 1999. **463**: p. 15-25.

94. Koppaka, V., et al., *Aldehyde dehydrogenase inhibitors: a comprehensive review of the pharmacology, mechanism of action, substrate specificity, and clinical application.* Pharmacological reviews, 2012. **64**(3): p. 520-39.
95. Black, W.J., et al., *Human aldehyde dehydrogenase genes: alternatively spliced transcriptional variants and their suggested nomenclature.* Pharmacogenetics and genomics, 2009. **19**(11): p. 893-902.
96. Black, W. and V. Vasiliou, *The aldehyde dehydrogenase gene superfamily resource center.* Human genomics, 2009. **4**(2): p. 136-42.
97. Christ, O., et al., *Improved purification of hematopoietic stem cells based on their elevated aldehyde dehydrogenase activity.* Haematologica, 2007. **92**(9): p. 1165-72.
98. Marcato, P., et al., *Aldehyde dehydrogenase: its role as a cancer stem cell marker comes down to the specific isoform.* Cell cycle, 2011. **10**(9): p. 1378-84.
99. Jones, R.J., et al., *Assessment of aldehyde dehydrogenase in viable cells.* Blood, 1995. **85**(10): p. 2742-6.
100. Ma, I. and A.L. Allan, *The role of human aldehyde dehydrogenase in normal and cancer stem cells.* Stem cell reviews, 2011. **7**(2): p. 292-306.
101. Kreuzer, J., et al., *Target discovery of acivicin in cancer cells elucidates its mechanism of growth inhibition.* Chemical science, 2015. **6**(1): p. 237-245.
102. Rosenfeld, H. and J. Roberts, *Enhancement of antitumor activity of glutamine antagonists 6-diazo-5-oxo-L-norleucine and acivicin in cell culture by glutaminase-asparaginase.* Cancer Research, 1981. **41**(4): p. 1324-8.
103. Geier, E.G., et al., *Structure-based ligand discovery for the Large-neutral Amino Acid Transporter 1, LAT-1.* Proceedings of the National Academy of Sciences of the United States of America, 2013. **110**(14): p. 5480-5.
104. Bottcher, T. and S.A. Sieber, *Beta-lactones as privileged structures for the active-site labeling of versatile bacterial enzyme classes.* Angewandte Chemie, 2008. **47**(24): p. 4600-3.
105. Rosenfeld, J., et al., *In-gel digestion of proteins for internal sequence analysis after one- or two-dimensional gel electrophoresis.* Analytical biochemistry, 1992. **203**(1): p. 173-9.
106. Eng, J.K., et al., *A fast SEQUEST cross correlation algorithm.* Journal of proteome research, 2008. **7**(10): p. 4598-602.
107. McHugh, L. and J.W. Arthur, *Computational methods for protein identification from mass spectrometry data.* PLoS computational biology, 2008. **4**(2): p. e12.
108. Kall, L., et al., *Assigning significance to peptides identified by tandem mass spectrometry using decoy databases.* Journal of proteome research, 2008. **7**(1): p. 29-34.
109. Nees, D.W., et al., *Structurally normal corneas in aldehyde dehydrogenase 3a1-deficient mice.* Molecular and cellular biology, 2002. **22**(3): p. 849-55.
110. Kwon, H.J., et al., *Aldehyde dehydrogenase 2 deficiency ameliorates alcoholic fatty liver but worsens liver inflammation and fibrosis in mice.* Hepatology, 2014. **60**(1): p. 146-57.
111. Gasparetto, M., et al., *Varying levels of aldehyde dehydrogenase activity in adult murine marrow hematopoietic stem cells are associated with engraftment and cell cycle status.* Experimental hematology, 2012. **40**(10): p. 857-66 e5.
112. Makia, N.L., et al., *Murine hepatic aldehyde dehydrogenase 1a1 is a major contributor to oxidation of aldehydes formed by lipid peroxidation.* Chemico-biological interactions, 2011. **191**(1-3): p. 278-87.
113. Pagliarini, D.J., et al., *A mitochondrial protein compendium elucidates complex I disease biology.* Cell, 2008. **134**(1): p. 112-23.

114. Wilcox, F.H. and B.A. Taylor, *Genetics of the Akp-2 locus for alkaline phosphatase of liver, kidney, bone, and placenta in the mouse. Linkage with the Ahd-1 locus on chromosome 4.* The Journal of heredity, 1981. **72**(6): p. 387-90.
115. Pemberton, T.A. and J.J. Tanner, *Structural basis of substrate selectivity of Delta(1)-pyrroline-5-carboxylate dehydrogenase (ALDH4A1): semialdehyde chain length.* Archives of biochemistry and biophysics, 2013. **538**(1): p. 34-40.
116. Mootha, V.K., et al., *Integrated analysis of protein composition, tissue diversity, and gene regulation in mouse mitochondria.* Cell, 2003. **115**(5): p. 629-40.
117. Kim, S.C., et al., *Substrate and functional diversity of lysine acetylation revealed by a proteomics survey.* Molecular cell, 2006. **23**(4): p. 607-18.
118. Da Cruz, S., et al., *Proteomic analysis of the mouse liver mitochondrial inner membrane.* The Journal of biological chemistry, 2003. **278**(42): p. 41566-71.
119. Ong, S.E., et al., *Stable isotope labeling by amino acids in cell culture, SILAC, as a simple and accurate approach to expression proteomics.* Molecular & cellular proteomics : MCP, 2002. **1**(5): p. 376-86.
120. Ross, S.A., et al., *Retinoids in embryonal development.* Physiological reviews, 2000. **80**(3): p. 1021-54.
121. Haselbeck, R.J., I. Hoffmann, and G. Duester, *Distinct functions for Aldh1 and Raldh2 in the control of ligand production for embryonic retinoid signaling pathways.* Developmental genetics, 1999. **25**(4): p. 353-64.
122. Niederreither, K., et al., *Differential expression of retinoic acid-synthesizing (RALDH) enzymes during fetal development and organ differentiation in the mouse.* Mechanisms of development, 2002. **110**(1-2): p. 165-71.
123. Yoshida, A., L.C. Hsu, and V. Dave, *Retinal oxidation activity and biological role of human cytosolic aldehyde dehydrogenase.* Enzyme, 1992. **46**(4-5): p. 239-44.
124. Dickman, E.D., C. Thaller, and S.M. Smith, *Temporally-regulated retinoic acid depletion produces specific neural crest, ocular and nervous system defects.* Development, 1997. **124**(16): p. 3111-21.
125. Duester, G., *Families of retinoid dehydrogenases regulating vitamin A function: production of visual pigment and retinoic acid.* European journal of biochemistry / FEBS, 2000. **267**(14): p. 4315-24.
126. Mandel, S., et al., *Gene expression profiling of sporadic Parkinson's disease substantia nigra pars compacta reveals impairment of ubiquitin-proteasome subunits, SKP1A, aldehyde dehydrogenase, and chaperone HSC-70.* Annals of the New York Academy of Sciences, 2005. **1053**: p. 356-75.
127. Galter, D., et al., *ALDH1 mRNA: presence in human dopamine neurons and decreases in substantia nigra in Parkinson's disease and in the ventral tegmental area in schizophrenia.* Neurobiology of disease, 2003. **14**(3): p. 637-47.
128. King, G. and R. Holmes, *Human corneal and lens aldehyde dehydrogenases. Purification and properties of human lens ALDH1 and differential expression as major soluble proteins in human lens (ALDH1) and cornea (ALDH3).* Advances in experimental medicine and biology, 1997. **414**: p. 19-27.
129. Ueshima, Y., et al., *Role of the aldehyde dehydrogenase-1 isozyme in the metabolism of acetaldehyde.* Alcohol and alcoholism, 1993. **1B**: p. 15-9.
130. Ward, R.J., et al., *Identification and characterisation of alcohol-induced flushing in Caucasian subjects.* Alcohol and alcoholism, 1994. **29**(4): p. 433-8.
131. Yoshida, A., et al., *Cytosolic aldehyde dehydrogenase (ALDH1) variants found in alcohol flushers.* Annals of human genetics, 1989. **53**(Pt 1): p. 1-7.
132. Stewart, M.J., et al., *The novel aldehyde dehydrogenase gene, ALDH5, encodes an active aldehyde dehydrogenase enzyme.* Biochemical and biophysical research communications, 1995. **211**(1): p. 144-51.

133. Sladek, N.E., *Aldehyde dehydrogenase-mediated cellular relative insensitivity to the oxazaphosphorines.* Current pharmaceutical design, 1999. **5**(8): p. 607-25.
134. Moreb, J.S., et al., *RNAi-mediated knockdown of aldehyde dehydrogenase class-1A1 and class-3A1 is specific and reveals that each contributes equally to the resistance against 4-hydroperoxycyclophosphamide.* Cancer chemotherapy and pharmacology, 2007. **59**(1): p. 127-36.
135. Klyosov, A.A., *Kinetics and specificity of human liver aldehyde dehydrogenases toward aliphatic, aromatic, and fused polycyclic aldehydes.* Biochemistry, 1996. **35**(14): p. 4457-67.
136. Goedde, H.W., et al., *Distribution of ADH2 and ALDH2 genotypes in different populations.* Human genetics, 1992. **88**(3): p. 344-6.
137. Peng, G.S., et al., *Pharmacokinetic and pharmacodynamic basis for partial protection against alcoholism in Asians, heterozygous for the variant ALDH2*2 gene allele.* Pharmacogenetics and genomics, 2007. **17**(10): p. 845-55.
138. Li, Y., et al., *Mitochondrial aldehyde dehydrogenase-2 (ALDH2) Glu504Lys polymorphism contributes to the variation in efficacy of sublingual nitroglycerin.* The Journal of clinical investigation, 2006. **116**(2): p. 506-11.
139. Hu, C.A., W.W. Lin, and D. Valle, *Cloning, characterization, and expression of cDNAs encoding human delta 1-pyrroline-5-carboxylate dehydrogenase.* The Journal of biological chemistry, 1996. **271**(16): p. 9795-800.
140. Forte-McRobbie, C.M. and R. Pietruszko, *Purification and characterization of human liver "high Km" aldehyde dehydrogenase and its identification as glutamic gamma-semialdehyde dehydrogenase.* The Journal of biological chemistry, 1986. **261**(5): p. 2154-63.
141. Haslett, M.R., et al., *Assay and subcellular localization of pyrroline-5-carboxylate dehydrogenase in rat liver.* Biochimica et biophysica acta, 2004. **1675**(1-3): p. 81-6.
142. Geraghty, M.T., et al., *Mutations in the Delta1-pyrroline 5-carboxylate dehydrogenase gene cause type II hyperprolinemia.* Human molecular genetics, 1998. **7**(9): p. 1411-5.
143. Onenli-Mungan, N., et al., *Type II hyperprolinemia: a case report.* The Turkish journal of pediatrics, 2004. **46**(2): p. 167-9.
144. Farrant, R.D., et al., *Pyridoxal phosphate de-activation by pyrroline-5-carboxylic acid. Increased risk of vitamin B6 deficiency and seizures in hyperprolinemia type II.* The Journal of biological chemistry, 2001. **276**(18): p. 15107-16.
145. Lheureux, P., A. Penaloza, and M. Gris, *Pyridoxine in clinical toxicology: a review.* European journal of emergency medicine : official journal of the European Society for Emergency Medicine, 2005. **12**(2): p. 78-85.
146. Farres, J., P. Julia, and X. Pares, *Aldehyde oxidation in human placenta. Purification and properties of 1-pyrroline-5-carboxylate dehydrogenase.* The Biochemical journal, 1988. **256**(2): p. 461-7.
147. Yoon, K.A., Y. Nakamura, and H. Arakawa, *Identification of ALDH4 as a p53-inducible gene and its protective role in cellular stresses.* Journal of human genetics, 2004. **49**(3): p. 134-40.
148. Danielsen, J.M., et al., *Mass spectrometric analysis of lysine ubiquitylation reveals promiscuity at site level.* Molecular & cellular proteomics : MCP, 2011. **10**(3): p. M110 003590.
149. Abe, H., et al., *Cloning and sequence analysis of a full length cDNA encoding human mitochondrial 3-oxoacyl-CoA thiolase.* Biochimica et biophysica acta, 1993. **1216**(2): p. 304-6.

150. Cao, W., et al., *Acetyl-Coenzyme A acyltransferase 2 attenuates the apoptotic effects of BNIP3 in two human cell lines.* Biochimica et biophysica acta, 2008. **1780**(6): p. 873-80.
151. Seedorf, U., P. Ellinghaus, and J. Roch Nofer, *Sterol carrier protein-2.* Biochimica et biophysica acta, 2000. **1486**(1): p. 45-54.
152. Shibata, F., et al., *Molecular cloning and characterization of a human carboxylesterase gene.* Genomics, 1993. **17**(1): p. 76-82.
153. Becker, A., et al., *Purification, cloning, and expression of a human enzyme with acyl coenzyme A: cholesterol acyltransferase activity, which is identical to liver carboxylesterase.* Arteriosclerosis and thrombosis : a journal of vascular biology / American Heart Association, 1994. **14**(8): p. 1346-55.
154. Xu, J., et al., *Hepatic carboxylesterase 1 is essential for both normal and farnesoid X receptor-controlled lipid homeostasis.* Hepatology, 2014. **59**(5): p. 1761-71.
155. Bencharit, S., et al., *Structural basis of heroin and cocaine metabolism by a promiscuous human drug-processing enzyme.* Nature structural biology, 2003. **10**(5): p. 349-56.
156. Markey, G.M., et al., *Monocyte esterase? A factor involved in the pathogenesis of lymphoproliferative neoplasia.* Leukemia, 1987. **1**(3): p. 236-9.
157. Markey, G.M., et al., *Hereditary monocyte esterase deficiency.* British journal of haematology, 1986. **63**(2): p. 359-62.
158. Bell, A.L., et al., *Myeloperoxidase deficiency in a patient with rheumatoid arthritis: oxygenation and radical activity by phagocytic cells.* British journal of rheumatology, 1993. **32**(2): p. 162-5.
159. Bie, J., et al., *Liver-specific cholesteryl ester hydrolase deficiency attenuates sterol elimination in the feces and increases atherosclerosis in ldlr-/- mice.* Arteriosclerosis, thrombosis, and vascular biology, 2013. **33**(8): p. 1795-802.
160. Blais, D.R., et al., *Activity-based protein profiling identifies a host enzyme, carboxylesterase 1, which is differentially active during hepatitis C virus replication.* The Journal of biological chemistry, 2010. **285**(33): p. 25602-12.
161. Blais, D.R., et al., *Activity-based proteome profiling of hepatoma cells during hepatitis C virus replication using protease substrate probes.* Journal of proteome research, 2010. **9**(2): p. 912-23.
162. Morris, P.J., et al., *Organophosphorus flame retardants inhibit specific liver carboxylesterases and cause serum hypertriglyceridemia.* ACS Chemical Biology, 2014. **9**(5): p. 1097-103.
163. Walhout, A.J., et al., *GATEWAY recombinational cloning: application to the cloning of large numbers of open reading frames or ORFeomes.* Methods in enzymology, 2000. **328**: p. 575-92.
164. Georgiou, G. and P. Valax, *Isolating inclusion bodies from bacteria.* Methods in enzymology, 1999. **309**: p. 48-58.
165. Yasukawa, T., et al., *Increase of solubility of foreign proteins in Escherichia coli by coproduction of the bacterial thioredoxin.* The Journal of biological chemistry, 1995. **270**(43): p. 25328-31.
166. Dykxhoorn, D.M., C.D. Novina, and P.A. Sharp, *Killing the messenger: short RNAs that silence gene expression.* Nature reviews. Molecular cell biology, 2003. **4**(6): p. 457-67.
167. Cramer, S.F. and A. Patel, *The frequency of uterine leiomyomas.* American journal of clinical pathology, 1990. **94**(4): p. 435-8.
168. Stewart, E.A., *Uterine fibroids.* Lancet, 2001. **357**(9252): p. 293-8.
169. Wallach, E.E. and N.F. Vlahos, *Uterine myomas: an overview of development, clinical features, and management.* Obstetrics and gynecology, 2004. **104**(2): p. 393-406.

170. Ryan, G.L., C.H. Syrop, and B.J. Van Voorhis, *Role, epidemiology, and natural history of benign uterine mass lesions.* Clinical obstetrics and gynecology, 2005. **48**(2): p. 312-24.
171. Sankaran, S. and I.T. Manyonda, *Medical management of fibroids.* Best practice & research. Clinical obstetrics & gynaecology, 2008. **22**(4): p. 655-76.
172. Sunkara, S.K., et al., *The effect of intramural fibroids without uterine cavity involvement on the outcome of IVF treatment: a systematic review and meta-analysis.* Human reproduction, 2010. **25**(2): p. 418-29.
173. Rein, M.S., R.L. Barbieri, and A.J. Friedman, *Progesterone: a critical role in the pathogenesis of uterine myomas.* American journal of obstetrics and gynecology, 1995. **172**(1 Pt 1): p. 14-8.
174. Rein, M.S., *Advances in uterine leiomyoma research: the progesterone hypothesis.* Environmental health perspectives, 2000. **108 Suppl 5**: p. 791-3.
175. Andersen, J., *Growth factors and cytokines in uterine leiomyomas.* Seminars in reproductive endocrinology, 1996. **14**(3): p. 269-82.
176. Fields, K.R. and L.S. Neinstein, *Uterine myomas in adolescents: case reports and a review of the literature.* Journal of pediatric and adolescent gynecology, 1996. **9**(4): p. 195-8.
177. Romagnolo, B., et al., *Estradiol-dependent uterine leiomyomas in transgenic mice.* The Journal of clinical investigation, 1996. **98**(3): p. 777-84.
178. Ross, R.K., et al., *Risk factors for uterine fibroids: reduced risk associated with oral contraceptives.* British medical journal, 1986. **293**(6543): p. 359-62.
179. Asada, H., et al., *Potential link between estrogen receptor-alpha gene hypomethylation and uterine fibroid formation.* Molecular human reproduction, 2008. **14**(9): p. 539-45.
180. Yamagata, Y., et al., *Aberrant DNA methylation status in human uterine leiomyoma.* Molecular human reproduction, 2009. **15**(4): p. 259-67.
181. Vikhlyaeva, E.M., Z.S. Khodzhaeva, and N.D. Fantschenko, *Familial predisposition to uterine leiomyomas.* International journal of gynaecology and obstetrics: the official organ of the International Federation of Gynaecology and Obstetrics, 1995. **51**(2): p. 127-31.
182. Bullerdiek, J., *Leiomyoma--do viruses play the main role?* Genes, chromosomes & cancer, 1999. **26**(2): p. 181.
183. Luo, X., et al., *Genomic and proteomic profiling II: comparative assessment of gene expression profiles in leiomyomas, keloids, and surgically-induced scars.* Reproductive biology and endocrinology : RB&E, 2007. **5**: p. 35.
184. Marsh, E.E., et al., *Differential expression of microRNA species in human uterine leiomyoma versus normal myometrium.* Fertility and sterility, 2008. **89**(6): p. 1771-6.
185. Wei, J.J. and P. Soteropoulos, *MicroRNA: a new tool for biomedical risk assessment and target identification in human uterine leiomyomas.* Seminars in reproductive medicine, 2008. **26**(6): p. 515-21.
186. Parker, W.H., *Etiology, symptomatology, and diagnosis of uterine myomas.* Fertility and sterility, 2007. **87**(4): p. 725-36.
187. Sabry, M. and A. Al-Hendy, *Medical treatment of uterine leiomyoma.* Reproductive sciences, 2012. **19**(4): p. 339-53.
188. Charles Ascher-Walsh, Fibroid Center New York. http://www.fibroidcenterofnewyork.com (accessed April 20, 2014).
189. StudyBlue inc. http://www.studyblue.com (accessed April 20, 2014).
190. Ligon, A.H. and C.C. Morton, *Genetics of uterine leiomyomata.* Genes, chromosomes & cancer, 2000. **28**(3): p. 235-45.

191. Gartler, S.M. and D. Linder, *Selection in Mammalian Mosaic Cell Populations.* Cold Spring Harbor symposia on quantitative biology, 1964. **29**: p. 253-60.
192. Townsend, D.E., et al., *Unicellular histogenesis of uterine leiomyomas as determined by electrophoresis by glucose-6-phosphate dehydrogenase.* American journal of obstetrics and gynecology, 1970. **107**(8): p. 1168-73.
193. Mashal, R.D., S.C. Lester, and J. Sklar, *Clonal analysis by study of X chromosome inactivation in formalin-fixed paraffin-embedded tissue.* Cancer Research, 1994. **54**(7): p. 1873.
194. Hashimoto, K., et al., *Clonal determination of uterine leiomyomas by analyzing differential inactivation of the X-chromosome-linked phosphoglycerokinase gene.* Gynecologic and obstetric investigation, 1995. **40**(3): p. 204-8.
195. Dixon, D., et al., *Cell proliferation and apoptosis in human uterine leiomyomas and myometria.* Virchows Archiv : an international journal of pathology, 2002. **441**(1): p. 53-62.
196. DeWaay, D.J., et al., *Natural history of uterine polyps and leiomyomata.* Obstetrics and gynecology, 2002. **100**(1): p. 3-7.
197. Peddada, S.D., et al., *Growth of uterine leiomyomata among premenopausal black and white women.* Proceedings of the National Academy of Sciences of the United States of America, 2008. **105**(50): p. 19887-92.
198. Mooi, W.J. and D.S. Peeper, *Oncogene-induced cell senescence--halting on the road to cancer.* The New England journal of medicine, 2006. **355**(10): p. 1037-46.
199. Michaloglou, C., et al., *BRAFE600-associated senescence-like cell cycle arrest of human naevi.* Nature, 2005. **436**(7051): p. 720-4.
200. Braig, M., et al., *Oncogene-induced senescence as an initial barrier in lymphoma development.* Nature, 2005. **436**(7051): p. 660-5.
201. Chen, Z., et al., *Crucial role of p53-dependent cellular senescence in suppression of Pten-deficient tumorigenesis.* Nature, 2005. **436**(7051): p. 725-30.
202. Collado, M., et al., *Tumour biology: senescence in premalignant tumours.* Nature, 2005. **436**(7051): p. 642.
203. Matsumura, T., Z. Zerrudo, and L. Hayflick, *Senescent human diploid cells in culture: survival, DNA synthesis and morphology.* Journal of gerontology, 1979. **34**(3): p. 328-34.
204. Laser, J., P. Lee, and J.J. Wei, *Cellular senescence in usual type uterine leiomyoma.* Fertility and sterility, 2010. **93**(6): p. 2020-6.
205. Bulun, S.E., *Uterine fibroids.* The New England journal of medicine, 2013. **369**(14): p. 1344-55.
206. Ono, M., et al., *Side population in human uterine myometrium displays phenotypic and functional characteristics of myometrial stem cells.* Proceedings of the National Academy of Sciences of the United States of America, 2007. **104**(47): p. 18700-5.
207. Ono, M., et al., *Role of stem cells in human uterine leiomyoma growth.* PloS one, 2012. **7**(5): p. e36935.
208. Zhou, S., et al., *Hypoxia: the driving force of uterine myometrial stem cells differentiation into leiomyoma cells.* Medical hypotheses, 2011. **77**(6): p. 985-6.
209. Makinen, N., et al., *Exomic landscape of MED12 mutation-negative and -positive uterine leiomyomas.* International journal of cancer. Journal international du cancer, 2014. **134**(4): p. 1008-12.
210. Markowski, D.N., et al., *MED12 mutations in uterine fibroids--their relationship to cytogenetic subgroups.* International journal of cancer. Journal international du cancer, 2012. **131**(7): p. 1528-36.
211. Markowski, D.N., et al., *HMGA2 and p14Arf: major roles in cellular senescence of fibroids and therapeutic implications.* Anticancer research, 2011. **31**(3): p. 753-61.

212. Tanwar, P.S., et al., *Constitutive activation of Beta-catenin in uterine stroma and smooth muscle leads to the development of mesenchymal tumors in mice.* Biology of reproduction, 2009. **81**(3): p. 545-52.
213. Arici, A. and I. Sozen, *Transforming growth factor-beta3 is expressed at high levels in leiomyoma where it stimulates fibronectin expression and cell proliferation.* Fertility and sterility, 2000. **73**(5): p. 1006-11.
214. Lee, B.S. and R.A. Nowak, *Human leiomyoma smooth muscle cells show increased expression of transforming growth factor-beta 3 (TGF beta 3) and altered responses to the antiproliferative effects of TGF beta.* The Journal of clinical endocrinology and metabolism, 2001. **86**(2): p. 913-20.
215. Catherino, W.H., et al., *Reduced dermatopontin expression is a molecular link between uterine leiomyomas and keloids.* Genes, chromosomes & cancer, 2004. **40**(3): p. 204-17.
216. Ravina, J.H., et al., *Arterial embolisation to treat uterine myomata.* Lancet, 1995. **346**(8976): p. 671-2.
217. Goodwin, S.C. and J.B. Spies, *Uterine fibroid embolization.* The New England journal of medicine, 2009. **361**(7): p. 690-7.
218. Khan, K.N., et al., *Changes in tissue inflammation, angiogenesis and apoptosis in endometriosis, adenomyosis and uterine myoma after GnRH agonist therapy.* Human reproduction, 2010. **25**(3): p. 642-53.
219. Chen, W., et al., *Gonadotropin-releasing hormone antagonist cetrorelix down-regulates proliferating cell nuclear antigen and epidermal growth factor expression and up-regulates apoptosis in association with enhanced poly(adenosine 5'-diphosphate-ribose) polymerase expression in cultured human leiomyoma cells.* The Journal of clinical endocrinology and metabolism, 2005. **90**(2): p. 884-92.
220. Wiznitzer, A., et al., *Gonadotropin-releasing hormone specific binding sites in uterine leiomyomata.* Biochemical and biophysical research communications, 1988. **152**(3): p. 1326-31.
221. Rawlings, N.D., A.J. Barrett, and A. Bateman, *MEROPS: the peptidase database.* Nucleic acids research, 2010. **38**(Database issue): p. D227-33.
222. Davie, E.W. and O.D. Ratnoff, *Waterfall Sequence for Intrinsic Blood Clotting.* Science, 1964. **145**(3638): p. 1310-2.
223. Whitcomb, D.C. and M.E. Lowe, *Human pancreatic digestive enzymes.* Digestive diseases and sciences, 2007. **52**(1): p. 1-17.
224. Lane, R.M., S.G. Potkin, and A. Enz, *Targeting acetylcholinesterase and butyrylcholinesterase in dementia.* The international journal of neuropsychopharmacology / official scientific journal of the Collegium Internationale Neuropsychopharmacologicum, 2006. **9**(1): p. 101-24.
225. Bonventre, J.V., *Roles of phospholipases A2 in brain cell and tissue injury associated with ischemia and excitotoxicity.* Journal of lipid mediators and cell signalling, 1997. **17**(1): p. 71-9.
226. Bonventre, J.V., et al., *Reduced fertility and postischaemic brain injury in mice deficient in cytosolic phospholipase A2.* Nature, 1997. **390**(6660): p. 622-5.
227. Menendez, J.A. and R. Lupu, *Fatty acid synthase and the lipogenic phenotype in cancer pathogenesis.* Nature reviews. Cancer, 2007. **7**(10): p. 763-77.
228. Nomura, D.K., et al., *Monoacylglycerol lipase regulates a fatty acid network that promotes cancer pathogenesis.* Cell, 2010. **140**(1): p. 49-61.
229. Steuber, H. and R. Hilgenfeld, *Recent advances in targeting viral proteases for the discovery of novel antivirals.* Current topics in medicinal chemistry, 2010. **10**(3): p. 323-45.

230. Shahiduzzaman, M., et al., *Proteasomal serine hydrolases are up-regulated by and required for influenza virus infection.* Journal of proteome research, 2014. **13**(5): p. 2223-38.
231. Singaravelu, R., et al., *Activity-based protein profiling of the hepatitis C virus replication in Huh-7 hepatoma cells using a non-directed active site probe.* Proteome science, 2010. **8**: p. 5.
232. Esler, W.P. and M.S. Wolfe, *A portrait of Alzheimer secretases--new features and familiar faces.* Science, 2001. **293**(5534): p. 1449-54.
233. Bot, I., G.P. Shi, and P.T. Kovanen, *Mast Cells as Effectors in Atherosclerosis.* Arteriosclerosis, thrombosis, and vascular biology, 2014.
234. Takai, S., et al., *Chymase as a novel target for the prevention of vascular diseases.* Trends in pharmacological sciences, 2004. **25**(10): p. 518-22.
235. Bachovchin, D.A. and B.F. Cravatt, *The pharmacological landscape and therapeutic potential of serine hydrolases.* Nature reviews. Drug discovery, 2012. **11**(1): p. 52-68.
236. Perona, J.J. and C.S. Craik, *Structural basis of substrate specificity in the serine proteases.* Protein science : a publication of the Protein Society, 1995. **4**(3): p. 337-60.
237. Yousef, G.M., et al., *Sequence and evolutionary analysis of the human trypsin subfamily of serine peptidases.* Biochimica et biophysica acta, 2004. **1698**(1): p. 77-86.
238. Yousef, G.M., et al., *Genomic overview of serine proteases.* Biochemical and biophysical research communications, 2003. **305**(1): p. 28-36.
239. Simon, G.M. and B.F. Cravatt, *Activity-based proteomics of enzyme superfamilies: serine hydrolases as a case study.* The Journal of biological chemistry, 2010. **285**(15): p. 11051-5.
240. Long, J.Z. and B.F. Cravatt, *The metabolic serine hydrolases and their functions in mammalian physiology and disease.* Chemical reviews, 2011. **111**(10): p. 6022-63.
241. Di Nisio, M., S. Middeldorp, and H.R. Buller, *Direct thrombin inhibitors.* The New England journal of medicine, 2005. **353**(10): p. 1028-40.
242. Eisert, W.G., et al., *Dabigatran: an oral novel potent reversible nonpeptide inhibitor of thrombin.* Arteriosclerosis, thrombosis, and vascular biology, 2010. **30**(10): p. 1885-9.
243. Perzborn, E., et al., *The discovery and development of rivaroxaban, an oral, direct factor Xa inhibitor.* Nature reviews. Drug discovery, 2011. **10**(1): p. 61-75.
244. Bar-On, P., et al., *Kinetic and structural studies on the interaction of cholinesterases with the anti-Alzheimer drug rivastigmine.* Biochemistry, 2002. **41**(11): p. 3555-64.
245. Harvey, A.L., *The pharmacology of galanthamine and its analogues.* Pharmacology & therapeutics, 1995. **68**(1): p. 113-28.
246. Weibel, E.K., et al., *Lipstatin, an inhibitor of pancreatic lipase, produced by Streptomyces toxytricini. I. Producing organism, fermentation, isolation and biological activity.* The Journal of antibiotics, 1987. **40**(8): p. 1081-5.
247. Augeri, D.J., et al., *Discovery and preclinical profile of Saxagliptin (BMS-477118): a highly potent, long-acting, orally active dipeptidyl peptidase IV inhibitor for the treatment of type 2 diabetes.* Journal of Medicinal Chemistry, 2005. **48**(15): p. 5025-37.
248. Eckhardt, M., et al., *8-(3-(R)-aminopiperidin-1-yl)-7-but-2-ynyl-3-methyl-1-(4-methyl-quinazolin-2-ylme thyl)-3,7-dihydropurine-2,6-dione (BI 1356), a highly potent, selective, long-acting, and orally bioavailable DPP-4 inhibitor for the treatment of type 2 diabetes.* Journal of Medicinal Chemistry, 2007. **50**(26): p. 6450-3.
249. Brik, A. and C.H. Wong, *HIV-1 protease: mechanism and drug discovery.* Organic & Biomolecular Chemistry, 2003. **1**(1): p. 5-14.

250. Coussens, L.M., B. Fingleton, and L.M. Matrisian, *Matrix metalloproteinase inhibitors and cancer: trials and tribulations.* Science, 2002. **295**(5564): p. 2387-92.
251. Overall, C.M. and O. Kleifeld, *Tumour microenvironment - opinion: validating matrix metalloproteinases as drug targets and anti-targets for cancer therapy.* Nature reviews. Cancer, 2006. **6**(3): p. 227-39.
252. Zucker, S., et al., *Membrane type-matrix metalloproteinases (MT-MMP).* Current topics in developmental biology, 2003. **54**: p. 1-74.
253. Arfin, S.M., et al., *Eukaryotic methionyl aminopeptidases: two classes of cobalt-dependent enzymes.* Proceedings of the National Academy of Sciences of the United States of America, 1995. **92**(17): p. 7714-8.
254. Wang, J., et al., *Physiologically relevant metal cofactor for methionine aminopeptidase-2 is manganese.* Biochemistry, 2003. **42**(17): p. 5035-42.
255. Sin, N., et al., *The anti-angiogenic agent fumagillin covalently binds and inhibits the methionine aminopeptidase, MetAP-2.* Proc Natl Acad Sci U S A, 1997. **94**(12): p. 6099-103.
256. Wang, J., P. Lou, and J. Henkin, *Selective inhibition of endothelial cell proliferation by fumagillin is not due to differential expression of methionine aminopeptidases.* Journal of cellular biochemistry, 2000. **77**(3): p. 465-73.
257. Kanno, T., et al., *High expression of methionine aminopeptidase type 2 in germinal center B cells and their neoplastic counterparts.* Laboratory investigation; a journal of technical methods and pathology, 2002. **82**(7): p. 893-901.
258. Joharapurkar, A.A., N.A. Dhanesha, and M.R. Jain, *Inhibition of the methionine aminopeptidase 2 enzyme for the treatment of obesity.* Diabetes, metabolic syndrome and obesity : targets and therapy, 2014. **7**: p. 73-84.
259. Min, H.K., N. Kambe, and L.B. Schwartz, *Human mouse mast cell protease 7-like tryptase genes are pseudogenes.* The Journal of allergy and clinical immunology, 2001. **107**(2): p. 315-21.
260. Wang, H.W., et al., *Delta tryptase is expressed in multiple human tissues, and a recombinant form has proteolytic activity.* Journal of Immunology, 2002. **169**(9): p. 5145-52.
261. Wong, G.W., et al., *Ancient origin of mast cells.* Biochemical and biophysical research communications, 2014. **451**(2): p. 314-8.
262. Douaiher, J., et al., *Development of mast cells and importance of their tryptase and chymase serine proteases in inflammation and wound healing.* Advances in immunology, 2014. **122**: p. 211-52.
263. Hodges, K., et al., *Mast cells, disease and gastrointestinal cancer: A comprehensive review of recent findings.* Translational gastrointestinal cancer, 2012. **1**(2): p. 138-150.
264. Lee, D.M., et al., *Mast cells: a cellular link between autoantibodies and inflammatory arthritis.* Science, 2002. **297**(5587): p. 1689-92.
265. Taipale, J., et al., *Human mast cell chymase and leukocyte elastase release latent transforming growth factor-beta 1 from the extracellular matrix of cultured human epithelial and endothelial cells.* The Journal of biological chemistry, 1995. **270**(9): p. 4689-96.
266. Tatler, A.L., et al., *Tryptase activates TGFbeta in human airway smooth muscle cells via direct proteolysis.* Biochemical and biophysical research communications, 2008. **370**(2): p. 239-42.
267. Kinoshita, M., et al., *Mast cell tryptase in mast cell granules enhances MCP-1 and interleukin-8 production in human endothelial cells.* Arteriosclerosis, thrombosis, and vascular biology, 2005. **25**(9): p. 1858-63.

268. Usami, Y., et al., *Detection of chymase-digested C-terminally truncated apolipoprotein A-I in normal human serum.* Journal of immunological methods, 2011. **369**(1-2): p. 51-8.
269. Leskinen, M.J., et al., *Mast cell chymase induces smooth muscle cell apoptosis by disrupting NF-kappaB-mediated survival signaling.* Experimental Cell Research, 2006. **312**(8): p. 1289-98.
270. Heikkila, H.M., et al., *Activated mast cells induce endothelial cell apoptosis by a combined action of chymase and tumor necrosis factor-alpha.* Arteriosclerosis, thrombosis, and vascular biology, 2008. **28**(2): p. 309-14.
271. Ihara, M., et al., *Increased chymase-dependent angiotensin II formation in human atherosclerotic aorta.* Hypertension, 1999. **33**(6): p. 1399-405.
272. Wang, Y., et al., *Mast cell chymase inhibits smooth muscle cell growth and collagen expression in vitro: transforming growth factor-beta1-dependent and -independent effects.* Arteriosclerosis, thrombosis, and vascular biology, 2001. **21**(12): p. 1928-33.
273. Weller, K., et al., *Mast cells are required for normal healing of skin wounds in mice.* FASEB journal : official publication of the Federation of American Societies for Experimental Biology, 2006. **20**(13): p. 2366-8.
274. Theoharides, T.C. and P. Conti, *Mast cells: the Jekyll and Hyde of tumor growth.* Trends in immunology, 2004. **25**(5): p. 235-41.
275. Korkmaz, B., T. Moreau, and F. Gauthier, *Neutrophil elastase, proteinase 3 and cathepsin G: physicochemical properties, activity and physiopathological functions.* Biochimie, 2008. **90**(2): p. 227-42.
276. Pham, C.T., *Neutrophil serine proteases fine-tune the inflammatory response.* The international journal of biochemistry & cell biology, 2008. **40**(6-7): p. 1317-33.
277. Bank, U. and S. Ansorge, *More than destructive: neutrophil-derived serine proteases in cytokine bioactivity control.* Journal of leukocyte biology, 2001. **69**(2): p. 197-206.
278. Sambrano, G.R., et al., *Cathepsin G activates protease-activated receptor-4 in human platelets.* The Journal of biological chemistry, 2000. **275**(10): p. 6819-23.
279. Pham, C.T., *Neutrophil serine proteases: specific regulators of inflammation.* Nature reviews. Immunology, 2006. **6**(7): p. 541-50.
280. Korkmaz, B., et al., *Neutrophil elastase, proteinase 3, and cathepsin G as therapeutic targets in human diseases.* Pharmacological reviews, 2010. **62**(4): p. 726-59.
281. Grzywa, R., et al., *Determination of cathepsin G in endometrial tissue using a surface plasmon resonance imaging biosensor with tailored phosphonic inhibitor.* European journal of obstetrics, gynecology, and reproductive biology, 2014. **182C**: p. 38-42.
282. Swedenborg, J., M.I. Mayranpaa, and P.T. Kovanen, *Mast cells: important players in the orchestrated pathogenesis of abdominal aortic aneurysms.* Arteriosclerosis, thrombosis, and vascular biology, 2011. **31**(4): p. 734-40.
283. Isobe, A., et al., *Dual repressive effect of angiotensin II-type 1 receptor blocker telmisartan on angiotensin II-induced and estradiol-induced uterine leiomyoma cell proliferation.* Human reproduction, 2008. **23**(2): p. 440-6.
284. Kolf, C.M., E. Cho, and R.S. Tuan, *Mesenchymal stromal cells. Biology of adult mesenchymal stem cells: regulation of niche, self-renewal and differentiation.* Arthritis research & therapy, 2007. **9**(1): p. 204.
285. Hutchison, N., C. Fligny, and J.S. Duffield, *Resident mesenchymal cells and fibrosis.* Biochimica et biophysica acta, 2013. **1832**(7): p. 962-71.
286. Rosenbloom, J., F.A. Mendoza, and S.A. Jimenez, *Strategies for anti-fibrotic therapies.* Biochimica et biophysica acta, 2013. **1832**(7): p. 1088-103.
287. Hiraiwa, M., *Cathepsin A/protective protein: an unusual lysosomal multifunctional protein.* Cellular and molecular life sciences : CMLS, 1999. **56**(11-12): p. 894-907.

288. Potier, M., et al., *Structure of the lysosomal neuraminidase-beta-galactosidase-carboxypeptidase multienzymic complex.* The Biochemical journal, 1990. **267**(1): p. 197-202.
289. D'Azzo, A., et al., *Molecular defect in combined beta-galactosidase and neuraminidase deficiency in man.* Proceedings of the National Academy of Sciences of the United States of America, 1982. **79**(15): p. 4535-9.
290. Seyrantepe, V., et al., *Enzymatic activity of lysosomal carboxypeptidase (cathepsin) A is required for proper elastic fiber formation and inactivation of endothelin-1.* Circulation, 2008. **117**(15): p. 1973-81.
291. Jackman, H.L., et al., *Inactivation of endothelin I by deamidase (lysosomal protective protein).* The Journal of biological chemistry, 1992. **267**(5): p. 2872-5.
292. Jackman, H.L., et al., *Angiotensin 1-9 and 1-7 release in human heart: role of cathepsin A.* Hypertension, 2002. **39**(5): p. 976-81.
293. Hanna, W.L., et al., *Dominant chymotrypsin-like esterase activity in human lymphocyte granules is mediated by the serine carboxypeptidase called cathepsin A-like protective protein.* Journal of Immunology, 1994. **153**(10): p. 4663-72.
294. Cuervo, A.M., et al., *Cathepsin A regulates chaperone-mediated autophagy through cleavage of the lysosomal receptor.* The EMBO journal, 2003. **22**(1): p. 47-59.
295. Amith, S.R., et al., *Dependence of pathogen molecule-induced toll-like receptor activation and cell function on Neu1 sialidase.* Glycoconjugate journal, 2009. **26**(9): p. 1197-212.
296. Amith, S.R., et al., *Neu1 desialylation of sialyl alpha-2,3-linked beta-galactosyl residues of TOLL-like receptor 4 is essential for receptor activation and cellular signaling.* Cellular signalling, 2010. **22**(2): p. 314-24.
297. Seyrantepe, V., et al., *Regulation of phagocytosis in macrophages by neuraminidase 1.* The Journal of biological chemistry, 2010. **285**(1): p. 206-15.
298. Miura, S., et al., *Differential infiltration of macrophages and prostaglandin production by different uterine leiomyomas.* Human reproduction, 2006. **21**(10): p. 2545-54.
299. Vorobiev, S.M., et al., *Crystal structure of human retinoblastoma binding protein 9.* Proteins, 2009. **74**(2): p. 526-9.
300. Woitach, J.T., et al., *A retinoblastoma-binding protein that affects cell-cycle control and confers transforming ability.* Nature genetics, 1998. **19**(4): p. 371-4.
301. Shields, D.J., et al., *RBBP9: a tumor-associated serine hydrolase activity required for pancreatic neoplasia.* Proceedings of the National Academy of Sciences of the United States of America, 2010. **107**(5): p. 2189-94.
302. Vorobiev, S.M., et al., *Human retinoblastoma binding protein 9, a serine hydrolase implicated in pancreatic cancers.* Protein and peptide letters, 2012. **19**(2): p. 194-7.
303. Nachmany, H., et al., *Two potential biomarkers identified in mesenchymal stem cells and leukocytes of patients with sporadic amyotrophic lateral sclerosis.* Disease markers, 2012. **32**(4): p. 211-20.
304. O'Connor, M.D., et al., *Retinoblastoma-binding proteins 4 and 9 are important for human pluripotent stem cell maintenance.* Experimental hematology, 2011. **39**(8): p. 866-79 e1.
305. Griffith, E.C., et al., *Methionine aminopeptidase (type 2) is the common target for angiogenesis inhibitors AGM-1470 and ovalicin.* Chemistry & biology, 1997. **4**(6): p. 461-71.
306. Chen, X., et al., *Fumagillin and fumarranol interact with P. falciparum methionine aminopeptidase 2 and inhibit malaria parasite growth in vitro and in vivo.* Chemistry & biology, 2009. **16**(2): p. 193-202.

307. Rudolf, G.C. and S.A. Sieber, *Copper-assisted click reactions for activity-based proteomics: fine-tuned ligands and refined conditions extend the scope of application.* Chembiochem : a European journal of chemical biology, 2013. **14**(18): p. 2447-55.
308. Eirich, J., R. Orth, and S.A. Sieber, *Unraveling the protein targets of vancomycin in living S. aureus and E. faecalis cells.* Journal of the American Chemical Society, 2011. **133**(31): p. 12144-53.
309. Eirich, J., et al., *Pretubulysin derived probes as novel tools for monitoring the microtubule network via activity-based protein profiling and fluorescence microscopy.* Mol Biosyst, 2012. **8**(8): p. 2067-75.
310. Sieber, S.A., et al., *Proteomic profiling of metalloprotease activities with cocktails of active-site probes.* Nat Chem Biol, 2006. **2**(5): p. 274-81.

9 Appendix

9.1 Chemical Structures

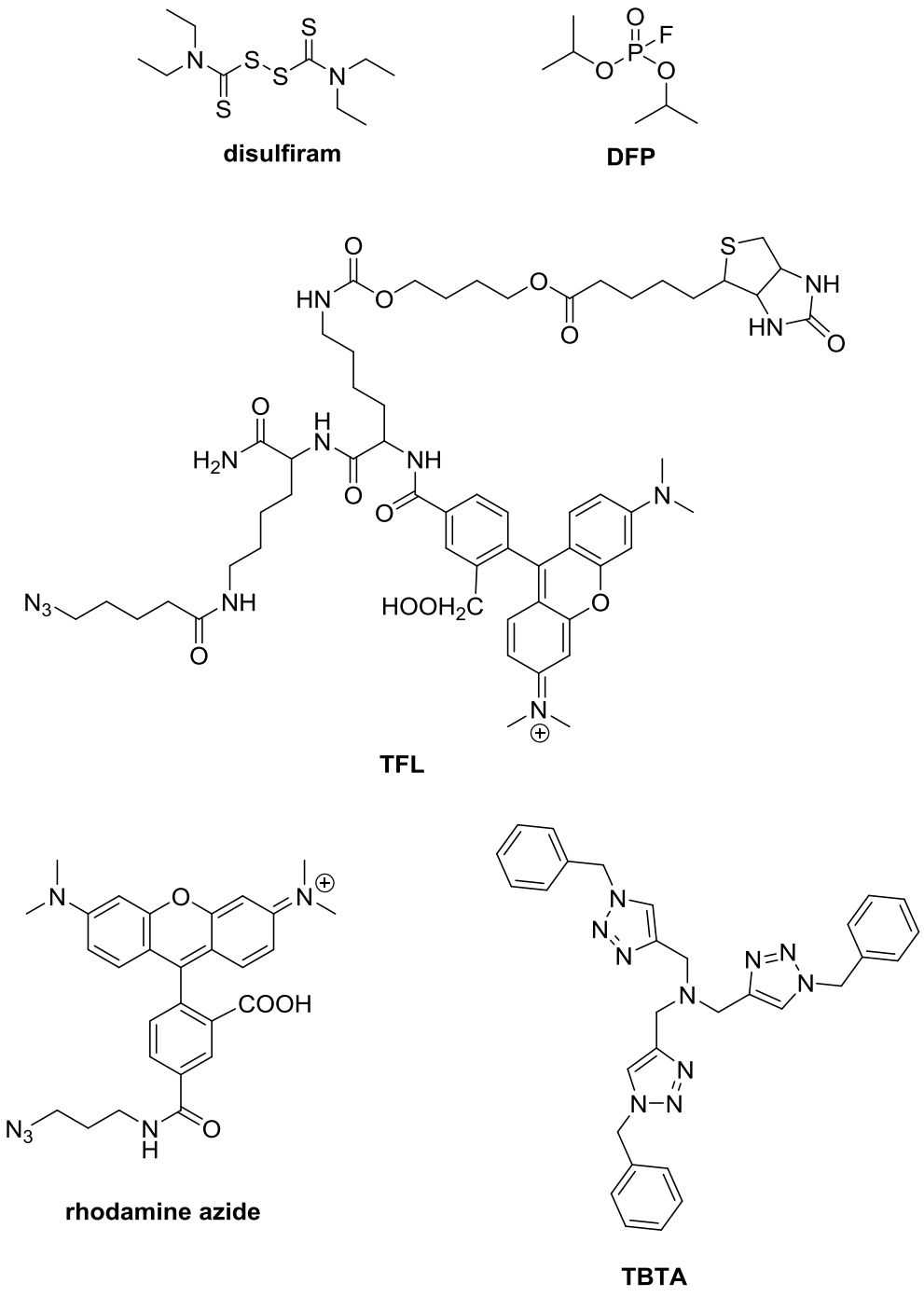

Figure 56. Chemical structures of compound used in this work

9.2 Patient 927

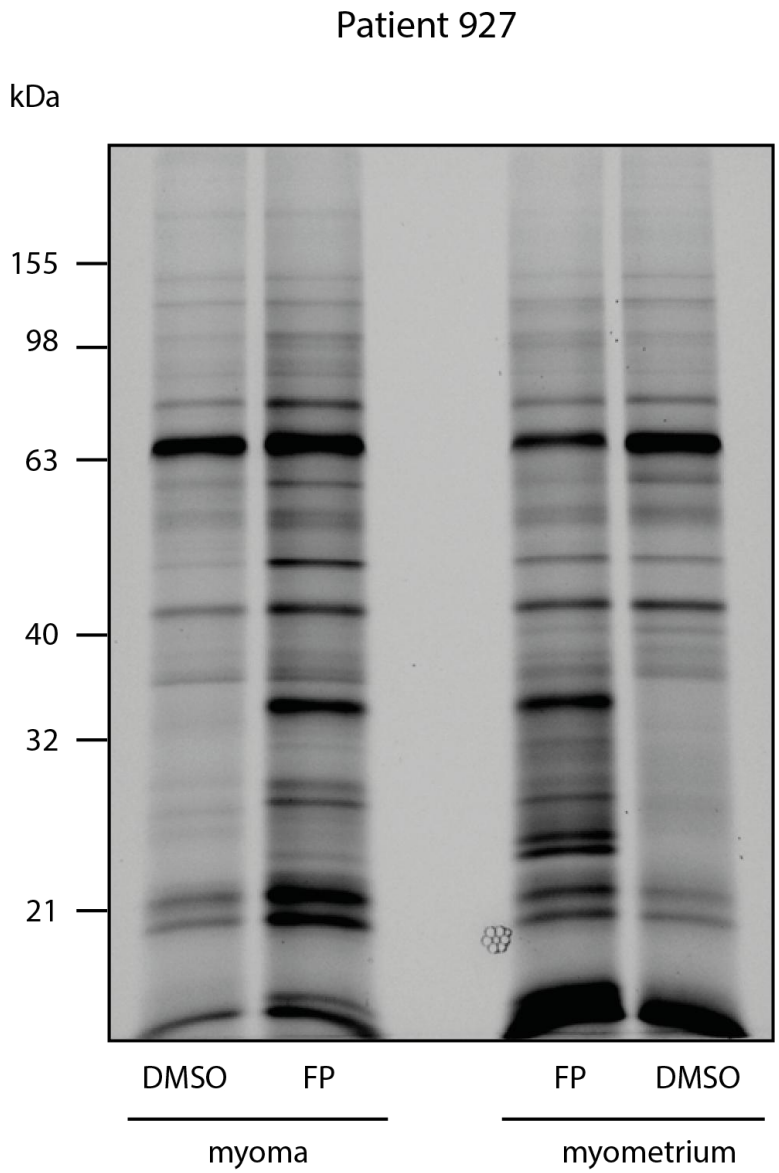

Figure 57. Fluorescence scan of paired myoma and myometrium samples of patient 927 incubated with FP.

Myoma

Target	Accession	Description	Area		FP			DMSO			General information			(Area FP)/(Area DMSO)	(Area Myoma)/(Area Myometrium)
			FP	DMSO	Score	# Peptides	# PSM	Score	# Peptides	# PSM	# AAs	MW [kDa]	Sequence coverage		
DPP4	IPI00018953.1	Dipeptidyl peptidase 4	1,68E+07	0,00E+00	5,59	2	2	0,00	0	0	766	88,2	3,00	100	0,68
FAP	IPI00295461.4	Isoform 1 of Seprase	2,89E+07	0,00E+00	22,95	4	7	0,00	0	0	760	87,7	6,32	100	2,07
APEH	IPI00337741.4	Acylamino-acid-releasing enzyme	3,76E+07	0,00E+00	13,06	2	5	0,00	0	0	732	81,2	3,55	100	0,22
PREP	IPI00008164.2	Prolyl endopeptidase	5,63E+07	0,00E+00	17,96	4	6	0,00	0	0	710	80,6	7,61	100	1,8
CES1	IPI00010180.4	Isoform 1 of Liver carboxylesterase 1	2,41E+08	0,00E+00	47,10	7	16	0,00	0	0	567	62,5	15,17	100	100
CTSA	IPI00021794.8	Lysosomal protective protein	2,75E+07	0,00E+00	11,03	2	3	0,00	0	0	480	54,4	4,17	100	100
ACOT1	IPI00333838.1	Acyl-coenzyme A thioesterase 1	1,25E+08	0,00E+00	89,16	12	28	0,00	0	0	421	46,2	39,43	100	100
ACOT2	IPI00220906.6	Acyl-coenzyme A thioesterase 2, mitochondrial	1,21E+08	0,00E+00	79,64	11	25	0,00	0	0	483	53,2	31,68	100	7,56
ESD	IPI00411706.1	S-formylglutathione hydrolase	5,36E+08	3,48E+07	115,62	9	38	43,63	6	13	282	31,4	51,06	15,39	3,01

Myometrium

Target	Accession	Description	Area		FP			DMSO			General information			(Area FP)/(Area DMSO)	(Area Myoma)/(Area Myometrium)
			FP	DMSO	Score	# Peptides	# PSM	Score	# Peptides	# PSM	# AAs	MW [kDa]	Sequence coverage		
DPP4	IPI00018953.1	Dipeptidyl peptidase 4	2,47E+07	0,00E+00	13,49	4	5	0,00	0	0	766	88,2	6,66	100	0,68
FAP	IPI00295461.4	Isoform 1 of Seprase	1,40E+07	0,00E+00	11,12	2	3	0,00	0	0	760	87,7	3,42	100	2,07
APEH	IPI00337741.4	Acylamino-acid-releasing enzyme	1,66E+08	1,56E+07	38,87	8	14	14,77	4	5	732	81,2	16,26	10,61	0,22
PREP	IPI00008164.2	Prolyl endopeptidase	3,11E+07	0,00E+00	15,24	4	4	0,00	0	0	710	80,6	8,87	100	1,8
F2	IPI00019568.1	Prothrombin (Fragment)	2,93E+07	0,00E+00	5,29	2	2	0,00	0	0	622	70,0	4,02	100	0
F12	IPI00019581.2	Coagulation factor XII	2,48E+07	0,00E+00	5,93	2	2	0,00	0	0	615	67,7	4,39	100	0
CFI	IPI00291867.4	Complement factor I	1,63E+07	0,00E+00	6,76	2	2	0,00	0	0	583	65,7	4,46	100	0
ACOT2	IPI00220906.6	Acyl-coenzyme A thioesterase 2, mitochondrial	1,63E+07	8,65E+06	21,47	2	8	0,00	0	0	483	53,2	2,69	100	7,56
ESD	IPI00411706.1	S-formylglutathione hydrolase	1,78E+08	4,90E+07	83,12	7	24	42,53	6	12	282	31,4	50,00	3,63	3,01
TPSAB1	IPI00472739.1	Isoform 2 of Tryptase alpha/beta-1	3,63E+08	2,65E+07	84,70	7	28	43,19	3	12	266	29,5	21,8	13,72	0
TPSB2	IPI00419942.2	Tryptase beta-2	3,34E+08	2,24E+07	83,90	6	26	40,11	2	11	275	30,5	21,09	14,94	0

TPSD1	IPI00376200.3	Isoform 2 of Tryptase delta	2,86E+08	4,04E+07	58,59	3	17	0,00	0	0	233	25,6	10,73	100	0
CTSG	IPI00028064.1	Cathepsin G	1,95E+08	0,00E+00	43,07	4	16	0,00	0	0	255	28,8	16,47	100	0
ELA2	IPI00027769.1	Neutrophil elastase	3,20E+07	0,00E+00	20,86	2	6	0,00	0	0	267	28,5	6,74	100	0
PRTN3	IPI00027409.1	Myeloblastin	5,81E+07	0,00E+00	28,28	2	9	0,00	0	0	256	27,8	14,06	100	0

Table 10. Protein hits for patient 927.

9.3 Patient 141

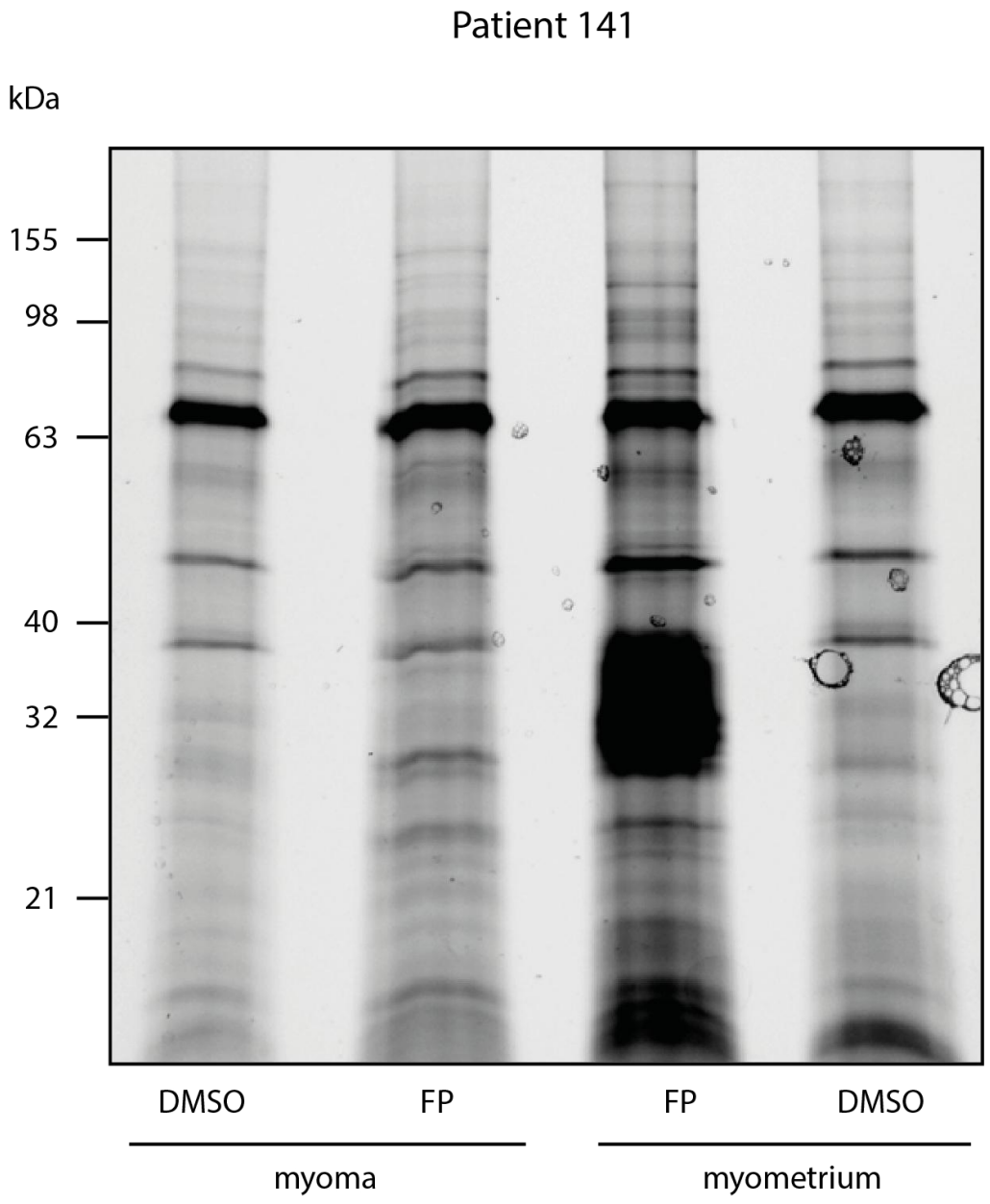

Figure 58. Fluorescence scan of paired myoma and myometrium samples of patient 141 incubated with FP.

Myoma

Target	Accession	Description	Area		FP			DMSO			General information			(Area FP)/(Area DMSO)	(Area Myoma)/(Area Myometrium)
			FP	DMSO	Score	# Peptides	# PSM	Score	# Peptides	# PSM	# AAs	MW [kDa]	Sequence coverage		
CFI	IPI00921523.1	Isoform 1 of Complement factor B (Fragment)	1,07E+08	4,98E+07	10,93	4	4	0,00	0	0	583	65,7	6,15	100	0,58
CES1	IPI00942507.4	Liver carboxylesterase 1	6,90E+07	0,00E+00	7,86	2	2	0,00	0	0	567	62,5	5,64	100	100
ACOT1	IPI00333838.1	Acyl-coenzyme A thioesterase 1	4,70E+07	0,00E+00	7,10	2	2	0,00	0	0	421	46,2	7,13	100	1,04
ACOT2	IPI00220906.6	Acyl-coenzyme A thioesterase 2, mitochondrial	4,70E+07	0,00E+00	7,10	3	3	0,00	0	0	483	53,2	6,21	100	1,2
ESD	IPI00411706.1	S-formylglutathione hydrolase	2,74E+07	3,12E+07	11,02	2	3	0,00	0	0	282	31,4	10,64	100	0,34

Myometrium

Target	Accession	Description	Area		FP			DMSO			General information			(Area FP)/(Area DMSO)	(Area Myoma)/(Area Myometrium)
			FP	DMSO	Score	# Peptides	# PSM	Score	# Peptides	# PSM	# AAs	MW [kDa]	Sequence coverage		
PREP	IPI00008164.2	Prolyl endopeptidase	5,10E+07	0,00E+00	16,25	2	4	0,00	0	0	710	80,6	5,49	100	0
F2	IPI00019568.1	Prothrombin (Fragment)	6,25E+07	0,00E+00	9,34	2	3	0,00	0	0	622	70,0	4,50	100	0
CFI	IPI00921523.1	Isoform 1 of Complement factor B (Fragment)	1,84E+08	0,00E+00	12,83	4	4	0,00	0	0	764	85,5	7,72	100	0,58
ACOT1	IPI00333838.1	Acyl-coenzyme A thioesterase 1	6,58E+07	0,00E+00	27,63	5	8	0,00	0	0	421	46,2	18,76	100	1,04
ACOT2	IPI00220906.6	Acyl-coenzyme A thioesterase 2, mitochondrial	6,58E+07	0,00E+00	27,63	6	10	0,00	0	0	483	53,2	20,36	100	1,2
ABHD10	IPI00020075.4	Abhydrolase domain-containing protein 10, mitochondrial	2,81E+07	0,00E+00	13,78	2	4	0,00	0	0	306	33,9	8,50	100	0
ESD	IPI00411706.1	S-formylglutathione hydrolase	9,09E+07	2,20E+07	14,60	3	5	7,05	2	2	282	31,4	12,64	4,13	0,34
TPSAB1	IPI00472739.1	Isoform 2 of Tryptase alpha/beta-1	2,43E+09	1,76E+08	670,37	9	207	96,88	6	27	266	29,5	31,58	13,78	0
TPSB2	IPI00419942.2	Tryptase beta-2	2,56E+09	1,24E+08	675,72	10	208	96,88	6	27	275	30,5	42,80	20,59	0
TPSD1	IPI00376200.3	Isoform 2 of Tryptase delta	1,65E+09	1,66E+08	320,76	3	87	44,57	2	11	233	25,6	10,73	9,94	0
PAFAH1B2	IPI00026546.1	Platelet-activating factor acetylhydrolase IB subunit beta	8,22E+07	0,00E+00	14,96	2	5	0,00	0	0	229	25,6	12,23	100	0

Table 11. Protein hits for patient 141.

9.4 Patient 142

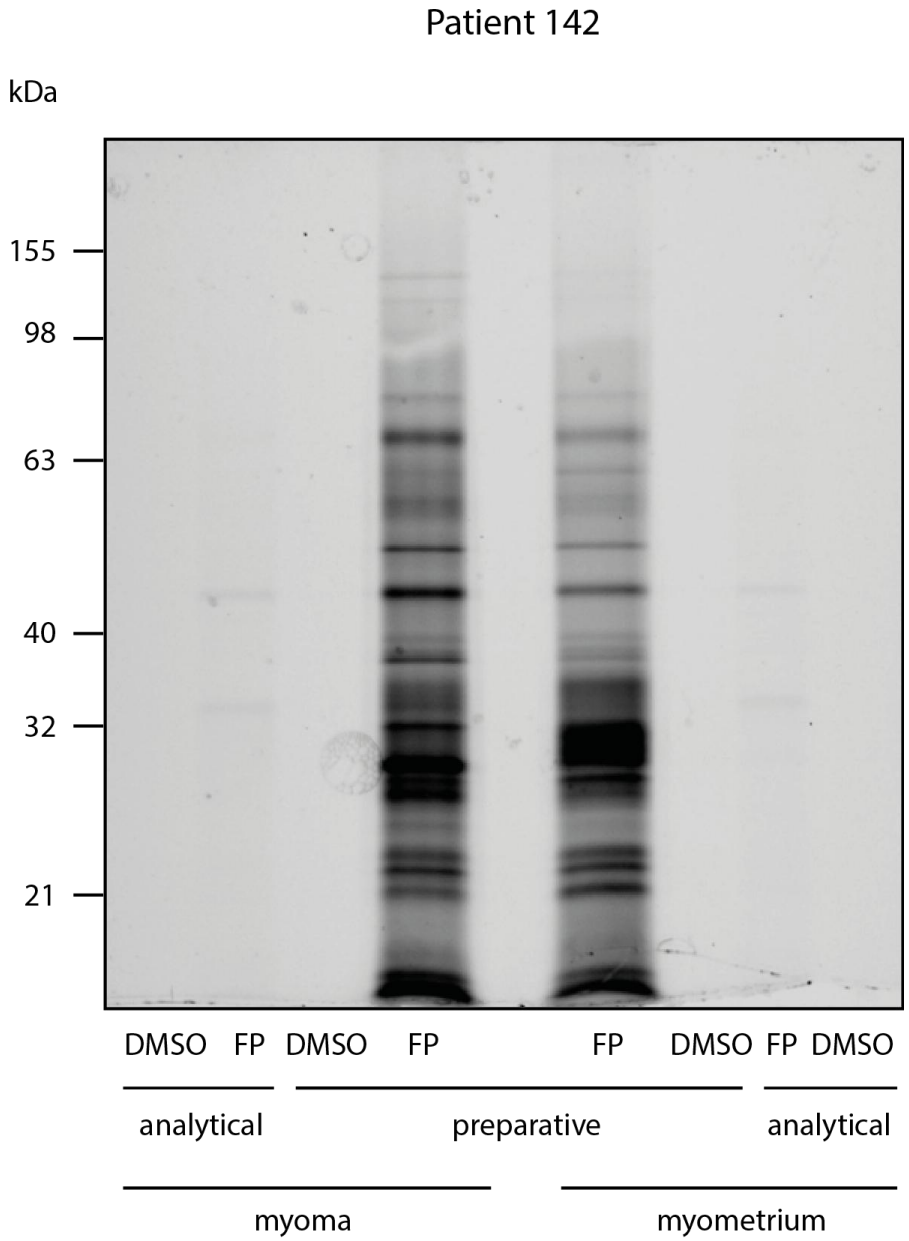

Figure 59. Fluorescence scan of paired myoma and myometrium samples of patient 142 incubated with FP, with analytical samples flanking the preparative samples from avidin enrichment.

Myoma

Target	Accession	Description	Area		FP			DMSO			General information			(Area FP)/(Area DMSO)	(Area Myoma)/(Area Myometrium)
			FP	DMSO	Score	# Peptides	# PSM	Score	# Peptides	# PSM	# AAs	MW [kDa]	Sequence coverage		
LYPLA1	IPI00514320.4	Acyl-protein thioesterase 1	1,68E+08	0,00E+00	48,60	10	16	0,00	0,00	0,00	565	62,8	22,48	100	100
CTSA	IPI00021794.8	Lysosomal protective protein	1,29E+08	0,00E+00	37,51	4	11	0,00	0,00	0,00	480	54,4	9,17	100	100
CPVL	IPI00301395.4	Probable serine carboxypeptidase CPVL	3,06E+08	0,00E+00	15,54	4	5	0,00	0,00	0,00	476	54,1	9,03	100	5,33
ACOT1	IPI00333838.1	Acyl-coenzyme A thioesterase 1	2,89E+08	0,00E+00	64,82	12	18	0,00	0,00	0,00	421	46,2	41,81	100	1,76
ACOT2	IPI00220906.6	Acyl-coenzyme A thioesterase 2, mitochondrial	2,89E+08	0,00E+00	61,38	11	17	0,00	0,00	0,00	483	53,2	33,75	100	1,65
PPME1	IPI00007694.5	Protein phosphatase methylesterase 1	2,04E+07	0,00E+00	9,20	3	3	0,00	0,00	0,00	386	42,3	11,66	100	100
ABHD10	IPI00020075.4	Abhydrolase domain-containing protein 10, mitochondrial	2,57E+08	0,00E+00	77,49	7	26	0,00	0,00	0,00	306	33,9	28,10	100	4,97
ESD	IPI00411706.1	S-formylglutathione hydrolase	7,99E+07	0,00E+00	73,02	5	24	0,00	0,00	0,00	282	31,4	22,34	100	1,77
TPSAB1	IPI00472739.1	Tryptase alpha/beta-1	8,45E+08	0,00E+00	226,01	9	78	0,00	0,00	0,00	266	29,5	26,32	100	0,42
TPSB2	IPI00419942.2	Tryptase beta-2	8,45E+08	0,00E+00	224,01	8	74	0,00	0,00	0,00	275	30,5	25,45	100	0,32
TPSD1	IPI00419573.3	Isoform 1 of Tryptase delta	5,94E+08	0,00E+00	127,44	3	38	0,00	0,00	0,00	242	26,6	10,33	100	0,36
CTSG	IPI00028064.1	Cathepsin G	2,47E+08	0,00E+00	42,30	6	14	0,00	0,00	0,00	255	28,8	26,67	100	1,19
CMA1	IPI00013937.1	Chymase	2,47E+07	0,00E+00	12,16	3	4	0,00	0,00	0,00	247	27,3	21,05	100	0,33
PAFAH1B2	IPI00026546.1	Platelet-activating factor acetylhydrolase IB subunit beta	2,01E+08	0,00E+00	28,18	2	10	0,00	0,00	0,00	229	25,6	12,23	100	100
PAFAH1B3	IPI00014808.1	Platelet-activating factor acetylhydrolase IB subunit gamma	3,39E+07	0,00E+00	10,86	3	4	0,00	0,00	0,00	231	25,7	17,32	100	100

Myometrium

Target	Accession	Description	Area		FP			DMSO			General information			(Area FP)/(Area DMSO)	(Area Myoma)/(Area Myometrium)
			FP	DMSO	Score	# Peptides	# PSM	Score	# Peptides	# PSM	# AAs	MW [kDa]	Sequence coverage		
CPVL	IPI00301395.4	Probable serine carboxypeptidase CPVL	5,75E+07	0,00E+00	9,43	2	3	0,00	0,00	0,00	476	54,1	4,41	100	5,33
ACOT1	IPI00333838.1	Acyl-coenzyme A thioesterase 1	1,65E+08	0,00E+00	30,48	5	9	0,00	0,00	0,00	421	46,2	16,86	100	1,76
ACOT2	IPI00220906.6	Acyl-coenzyme A thioesterase 2, mitochondrial	1,65E+08	0,00E+00	30,48	5	9	0,00	0,00	0,00	483	53,2	14,7	100	1,65

ABHD10	IPI00020075.4	Abhydrolase domain-containing protein 10, mitochondrial	5,17E+07	0,00E+00	20,82	4	7	0,00	0,00	0,00	306	33,9	18,63	100	4,97
ABDHD14B	IPI00063827.1	Isoform 1 of Abhydrolase domain-containing protein 14B	2,44E+07	0,00E+00	11,59	3	3	0,00	0,00	0,00	210	22,3	21,43	100	0
ESD	IPI00411706.1	S-formylglutathione hydrolase	4,07E+07	0,00E+00	33,18	5	12	0,00	0,00	0,00	282	31,4	22,34	100	1,77
TPSAB1	IPI00472739.1	Tryptase alpha/beta-1	1,90E+09	0,00E+00	489,19	10	165	0,00	0,00	0,00	266	29,5	31,58	100	0,42
TPSB2	IPI00419942.2	Tryptase beta-2	1,68E+09	0,00E+00	463,11	9	150	0,00	0,00	0,00	275	30,5	30,55	100	0,32
TPSD1	IPI00419573.3	Isoform 1 of Tryptase delta	8,03E+08	0,00E+00	239,20	3	68	0,00	0,00	0,00	233	26,6	10,73	100	0,36
CTSG	IPI00028064.1	Cathepsin G	1,63E+08	0,00E+00	26,17	3	9	0,00	0,00	0,00	255	28,8	14,9	100	1,19
CMA1	IPI00013937.1	Chymase	7,80E+07	0,00E+00	36,29	3	12	0,00	0,00	0,00	247	27,3	26,19	100	0,33

Table 12. Protein hits for patient 142.

9.5 Patient 144

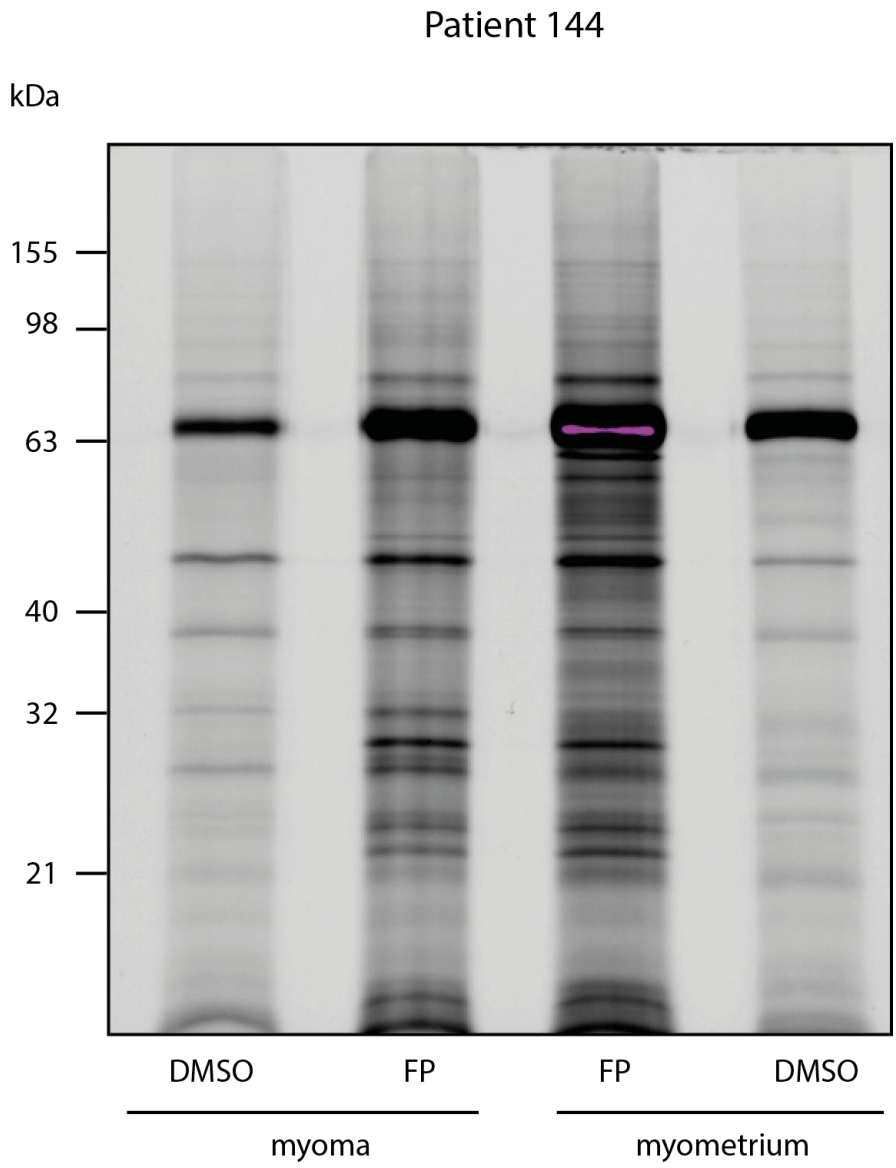

Figure 60. Fluorescence scan of paired myoma and myometrium samples of patient 144 incubated with FP.

Myoma

Target	Accession	Description	Area		FP			DMSO			General information			(Area FP)/(Area DMSO)	(Area Myoma)/(Area Myometrium)
			FP	DMSO	Score	# Peptides	# PSM	Score	# Peptides	# PSM	# AAs	MW [kDa]	Sequence coverage		
APEH	IPI00337741.4	Acylamino-acid-releasing enzyme	8,35E+07	0,00E+00	27,54	9	9	0,00	0	0	732	81,2	14,34	100	0,88
PREP	IPI00008164.2	Prolyl endopeptidase	5,18E+07	0,00E+00	26,99	7	7	0,00	0	0	710	80,6	14,79	100	1,27
CFI	IPI00291867.4	Complement factor I	2,89E+07	0,00E+00	5,64	2	2	0,00	0	0	583	65,7	3,6	100	0,84
CTSA	IPI00641157.2	lysosomal protective protein isoform c precursor	1,32E+08	0,00E+00	21,02	4	5	0,00	0	0	480	54,4	8,36	100	2,25
DPP2	IPI00296141.4	Dipeptidyl peptidase 2	1,69E+07	0,00E+00	6,65	2	2	0,00	0	0	492	54,3	6,1	100	0,57
ACOT1	IPI00333838.1	Acyl-coenzyme A thioesterase 1	4,15E+07	0,00E+00	11,93	4	4	0,00	0	0	421	46,2	12,59	100	0,17
ACOT2	IPI00220906.6	Isoform 1 of Acyl-coenzyme A thioesterase 2, mitochondrial	4,12E+07	0,00E+00	9,33	3	3	0,00	0	0	483	53,2	8,28	100	0,16
PPME1	IPI00007694.5	Isoform 1 of Protein phosphatase methylesterase 1	6,69E+07	0,00E+00	9,37	3	3	0,00	0	0	386	42,3	10,36	100	100
ABHD10	IPI00020075.4	Abhydrolase domain-containing protein 10, mitochondrial	1,99E+08	0,00E+00	89,28	11	27	0,00	0	0	306	33,9	51,31	100	3,07
ESD	IPI00411706.1	S-formylglutathione hydrolase	8,70E+07	2,40E+07	35,11	5	13	11,47	3	4	282	31,4	20,92	3,62	0,75
TPSAB1	IPI00472739.1	Isoform 2 of Tryptase alpha/beta-1	1,30E+08	0,00E+00	59,84	5	22	0,00	0	0	266	29,5	22,55	100	0,86
TPSB2	IPI00419942.2	Tryptase beta-2	1,18E+08	0,00E+00	59,84	4	19	0,00	0	0	275	30,5	18,91	100	0,85
CTSG	IPI00028064.1	Cathepsin G	7,62E+07	0,00E+00	29,94	5	7	0,00	0	0	255	28,8	21,57	100	100
PAFAH1B2	IPI00026546.1	Platelet-activating factor acetylhydrolase IB subunit beta	2,34E+08	0,00E+00	19,75	3	6	0,00	0	0	229	25,6	17,47	100	1,64
PAFAH1B3	IPI00014808.1	Platelet-activating factor acetylhydrolase IB subunit gamma	2,12E+07	0,00E+00	4,75	2	2	0,00	0	0	231	25,7	7,36	100	100
LYPLAL1	IPI00059762.5	Isoform 1 of Lysophospholipase-like protein 1	3,39E+07	0,00E+00	14,74	3	6	0,00	0	0	237	26,3	11,39	100	100
RBBP9	IPI00034181.1	Isoform 1 of Putative hydrolase RBBP9	5,49E+07	0,00E+00	10,33	3	3	0,00	0	0	186	21,0	27,96	100	100
IAH1	IPI00419194.2	Isoamyl acetate-hydrolyzing esterase 1 homolog	5,79E+07	0,00E+00	7,78	2	2	0,00	0	0	248	27,6	12,1	100	100

Myometrium

Target	Accession	Description	Area		FP			DMSO			General information			(Area FP)/(Area DMSO)	(Area Myoma)/(Area Myometrium)
			FP	DMSO	Score	# Peptides	# PSM	Score	# Peptides	# PSM	# AAs	MW [kDa]	Sequence coverage		
APEH	IPI00337741.4	Acylamino-acid-releasing enzyme	9,51E+07	0,00E+00	15,65	5	5	0,00	0	0	732	81,2	8,2	100	0,88

PREP	IPI00008164.2	Prolyl endopeptidase	4,06E+07	0,00E+00	11,93	3	3	0,00	0	0	710	80,6	5,77	100	1,27
CFI	IPI00291867.4	Complement factor I	3,44E+07	0,00E+00	5,39	2	2	0,00	0	0	583	65,7	3,06	100	0,84
CES1	IPI00010180.4	Isoform 1 of Liver carboxylesterase 1	8,85E+08	0,00E+00	95,17	15	27	0,00	0	0	567	62,5	31,57	100	0
CTSA	IPI00641157.2	lysosomal protective protein isoform c precursor	5,88E+07	0,00E+00	8,20	2	2	0,00	0	0	480	54,4	4,99	100	2,25
CPVL	IPI00301395.4	Probable serine carboxypeptidase CPVL	1,47E+08	0,00E+00	18,04	4	6	0,00	0	0	476	54,1	9,03	100	0
DPP2	IPI00296141.4	Dipeptidyl peptidase 2	2,96E+07	0,00E+00	20,88	4	6	0,00	0	0	492	54,3	11,18	100	0,57
ACOT1	IPI00333838.1	Acyl-coenzyme A thioesterase 1	2,56E+08	0,00E+00	42,48	8	13	0,00	0	0	421	46,2	26,13	100	0,17
ACOT2	IPI00220906.6	Isoform 1 of Acyl-coenzyme A thioesterase 2, mitochondrial	2,53E+08	0,00E+00	36,47	7	11	0,00	0	0	483	53,2	20,08	100	0,16
ABHD10	IPI00020075.4	Abhydrolase domain-containing protein 10, mitochondrial	6,47E+07	0,00E+00	29,30	7	9	0,00	0	0	306	33,9	28,76	100	3,07
ESD	IPI00411706.1	S-formylglutathione hydrolase	1,17E+08	3,98E+07	66,07	7	22	34,52	6	12	282	31,4	29,08	2,95	0,74
TPSAB1	IPI00472739.1	Isoform 2 of Tryptase alpha/beta-1	1,54E+08	0,00E+00	71,39	5	22	0,00	0	0	266	29,5	23,31	100	0,86
TPSB2	IPI00419942.2	Tryptase beta-2	1,86E+08	0,00E+00	78,99	6	28	0,00	0	0	275	30,5	22,55	100	0,85
TPSD1	IPI00376200.3	Isoform 2 of Tryptase delta	1,58E+08	0,00E+00	28,37	2	7	0,00	0	0	233	25,6	10,73	100	0
PAFAH1B2	IPI00026546.1	Platelet-activating factor acetylhydrolase IB subunit beta	1,43E+08	0,00E+00	11,41	2	3	0,00	0	0	229	25,6	9,17	100	1,64

Table 13. Protein hits for patient 144.

9.6 Patient 150

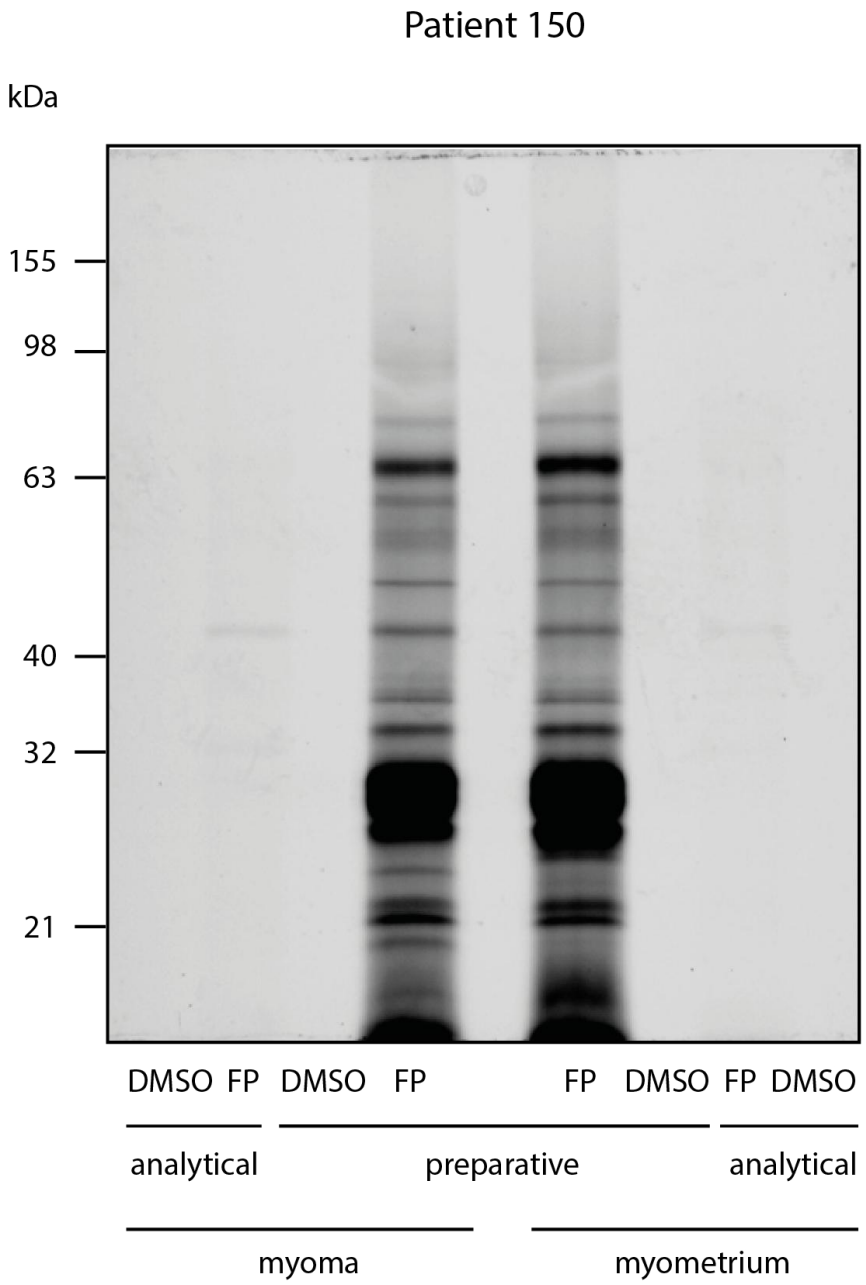

Figure 61. Fluorescence scan of paired myoma and myometrium samples of patient 150 incubated with FP, with analytical samples flanking the preparative samples from avidin enrichment.

Myoma

Target	Accession	Description	Area		FP			DMSO			General information			(Area FP)/(Area DMSO)	(Area Myoma)/(Area Myometrium)
			FP	DMSO	Score	# Peptides	# PSM	Score	# Peptides	# PSM	# AAs	MW [kDa]	Sequence coverage		
CFI	IPI00291867.4	Complement factor I	4,00E+07	0,00E+00	5,97	2	2	0,00	0	0	583	65,7	3,95	100	0,48
CTSA	IPI00021794.8	Lysosomal protective protein	5,28E+07	0,00E+00	9,68	3	3	0,00	0	0	480	54,4	7,75	100	0,46
CPVL	IPI00301395.4	Probable serine carboxypeptidase CPVL	7,90E+07	0,00E+00	12,50	2	4	0,00	0	0	476	54,1	4,83	100	100
ACOT1	IPI00333838.1	Acyl-coenzyme A thioesterase 1	8,18E+07	0,00E+00	37,94	7	12	0,00	0	0	421	46,2	24,7	100	1,13
ACOT2	IPI00220906.6	Isoform 1 of Acyl-coenzyme A thioesterase 2, mitochondrial	8,18E+07	0,00E+00	34,51	6	11	0,00	0	0	483	53,2	18,84	100	100
ABHD10	IPI00020075.4	Abhydrolase domain-containing protein 10, mitochondrial	3,55E+08	0,00E+00	66,29	8	21	0,00	0	0	306	33,9	33,01	100	0,83
ABHD14B	IPI00063827.1	Isoform 1 of Abhydrolase domain-containing protein 14B	6,63E+07	0,00E+00	16,77	4	5	0,00	0	0	210	22,3	30,00	100	1,03
ESD	IPI00411706.1	S-formylglutathione hydrolase	2,65E+08	0,00E+00	88,12	7	28	0,00	0	0	282	31,4	34,04	100	1,55
TPSAB1	IPI00472739.1	Isoform 2 of Tryptase alpha/beta-1	1,05E+10	1,23E+07	1240,80	9	388	13,03	2	4	266	29,5	31,58	851,67	0,93
TPSB2	IPI00419942.2	Tryptase beta-2	1,07E+10	1,32E+07	1140,40	9	378	13,13	2	4	275	30,5	30,55	810,34	0,92
TPSD1	IPI00419573.3	Isoform 1 of Tryptase delta	5,70E+09	1,34E+07	775,64	3	223	0,00	0	0	242	26,6	10,33	100	0,91
PAFAH1B2	IPI00026546.1	Platelet-activating factor acetylhydrolase IB subunit beta	8,01E+07	0,00E+00	10,45	2	4	0,00	0	0	229	25,6	8,30	100	0,4
RBBP9	IPI00034181.1	Isoform 1 of Putative hydrolase RBBP9	7,62E+07	0,00E+00	4,49	2	2	0,00	0	0	186	21,0	11,29	100	100

Myometrium

Target	Accession	Description	Area		FP			DMSO			General information			(Area FP)/(Area DMSO)	(Area Myoma)/(Area Myometrium)
			FP	DMSO	Score	# Peptides	# PSM	Score	# Peptides	# PSM	# AAs	MW [kDa]	Sequence coverage		
CFI	IPI00291867.4	Complement factor I	8,31E+07	0,00E+00	5,34	2	2	0,00	0	0	583	65,7	4,12	100	0,48
CTSA	IPI00021794.8	Lysosomal protective protein	1,14E+08	0,00E+00	12,22	2	3	0,00	0	0	480	54,4	5,42	100	0,46
ACOT1	IPI00333838.1	Acyl-coenzyme A thioesterase 1	7,23E+07	0,00E+00	10,10	2	3	0,00	0	0	421	46,2	7,84	100	1,13
ABHD10	IPI00020075.4	Abhydrolase domain-containing protein 10, mitochondrial	4,26E+08	0,00E+00	64,23	8	20	0,00	0	0	306	33,9	33,01	100	0,83
ABHD14B	IPI00063827.1	Isoform 1 of Abhydrolase domain-containing protein 14B	6,42E+07	0,00E+00	20,68	3	6	0,00	0	0	210	22,3	23,33	100	1,03
ESD	IPI00411706.1	S-formylglutathione hydrolase	1,70E+08	0,00E+00	59,00	5	18	0,00	0	0	282	31,4	24,47	100	1,55

TPSAB1	IPI00472739.1	Isoform 2 of Tryptase alpha/beta-1	1,14E+10	6,30E+06	1368,66	9	430	5,27	2	2	266	29,5	31,58	1808,17	0,93
TPSB2	IPI00419942.2	Tryptase beta-2	1,16E+10	6,21E+06	1381,05	10	433	5,25	2	2	275	30,5	32,00	1866,57	0,92
TPSD1	IPI00419573.3	Isoform 1 of Tryptase delta	6,29E+09	0,00E+00	864,29	4	246	0,00	0	0	242	26,6	11,98	100	0,91
CTSG	IPI00028064.1	Cathepsin G	3,28E+08	0,00E+00	55,67	5	19	0,00	0	0	255	28,8	22,75	100	0
CMA1	IPI00013937.1	Chymase	1,69E+08	0,00E+00	52,20	5	17	0,00	0	0	247	27,3	29,15	100	0
PAFAH1B2	IPI00026546.1	Platelet-activating factor acetylhydrolase IB subunit beta	1,99E+08	0,00E+00	14,09	3	5	0,00	0	0	229	25,6	9,17	100	0,4

Table 14. Protein hits for patient 150.

9.7 Patient 151

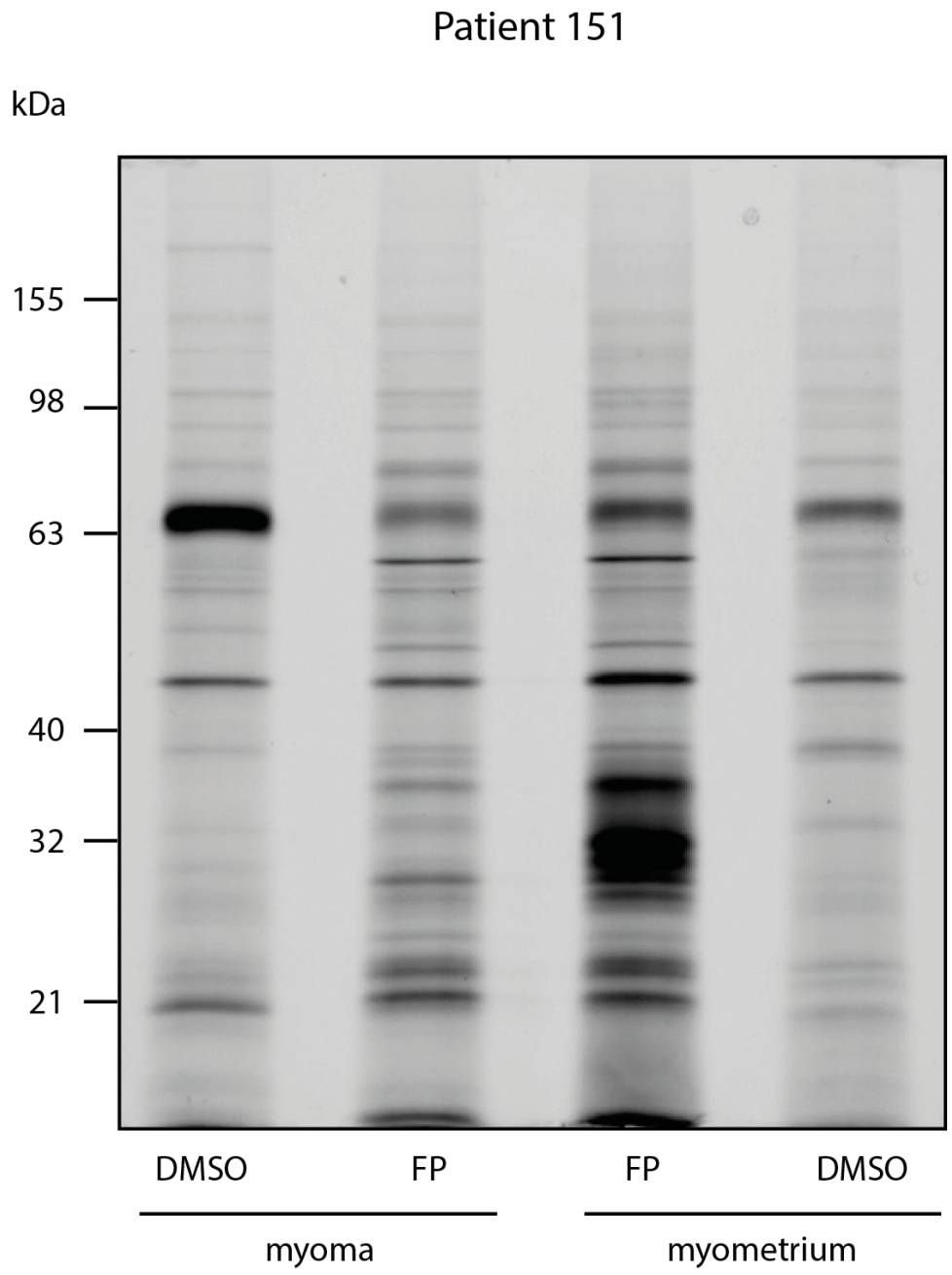

Figure 62. Fluorescence scan of paired myoma and myometrium samples of patient 151 incubated with FP.

Myoma

Target	Accession	Description	Area		FP			DMSO			General information			(Area FP)/(Area DMSO)	(Area Myoma)/(Area Myometrium)
			FP	DMSO	Score	# Peptides	# PSM	Score	# Peptides	# PSM	# AAs	MW [kDa]	Sequence coverage		
APEH	IPI00337741.4	Acylamino-acid-releasing enzyme	8,70E+07	2,32E+07	25,89	6	9	22,72	6	8	732	81,2	10,52	3,75	0,87
PREP	IPI00008164.2	Prolyl endopeptidase	3,47E+08	0,00E+00	70,39	15	20	0,00	0	0	710	80,6	32,68	100	1,47
F12	IPI00019581.2	Coagulation factor XII	1,46E+08	1,77E+07	16,17	3	5	5,48	2	2	615	67,7	8,94	8,26	0,86
CES1	IPI00010180.4	Isoform 1 of Liver carboxylesterase 1	5,39E+08	0,00E+00	42,28	9	13	0,00	0	0	567	62,5	19,05	100	0,59
ACOT1	IPI00333838.1	Acyl-coenzyme A thioesterase 1	3,24E+08	1,24E+07	51,39	12	16	5,90	2	2	421	46,2	41,81	26,26	0,9
ACOT2	IPI00220906.6	Isoform 1 of Acyl-coenzyme A thioesterase 2, mitochondrial	3,13E+08	1,04E+07	49,68	11	16	5,88	2	2	483	53,2	36,44	30,27	0,93
ESD	IPI00411706.1	S-formylglutathione hydrolase	4,87E+08	1,03E+08	93,16	11	31	45,29	9	21	282	31,4	57,85	4,75	0,83
TPSAB1	IPI00472739.1	Isoform 2 of Tryptase alpha/beta-1	1,31E+07	0,00E+00	5,37	2	2	0,00	0	0	266	29,5	9,4	100	0,01
TPSB2	IPI00419942.2	Tryptase beta-2	1,31E+07	0,00E+00	5,37	2	2	0,00	0	0	275	30,5	9,09	100	0,01
PAFAH1B1	IPI00218728.4	Isoform 1 of Platelet-activating factor acetylhydrolase IB subunit alpha	3,91E+07	1,47E+07	19,51	5	6	6,82	2	2	410	46,6	16,1	2,66	0,73
PAFAH1B2	IPI00026546.1	Platelet-activating factor acetylhydrolase IB subunit beta	1,64E+08	0,00E+00	14,30	3	4	0,00	0	0	229	25,6	17,47	100	1,23
PAFAH1B3	IPI00014808.1	Platelet-activating factor acetylhydrolase IB subunit gamma	1,24E+08	0,00E+00	10,01	4	4	0,00	0	0	231	25,7	16,45	100	100

Myometrium

Target	Accession	Description	Area		FP			DMSO			General information			(Area FP)/(Area DMSO)	(Area Myoma)/(Area Myometrium)
			FP	DMSO	Score	# Peptides	# PSM	Score	# Peptides	# PSM	# AAs	MW [kDa]	Sequence coverage		
APEH	IPI00337741.4	Acylamino-acid-releasing enzyme	1,00E+08	0,00E+00	24,47	6	8	0,00	0	0	732	81,2	9,84	100	0,87
PREP	IPI00008164.2	Prolyl endopeptidase	2,35E+08	0,00E+00	93,97	16	26	0,00	0	0	710	80,6	30,56	100	1,47
F12	IPI00019581.2	Coagulation factor XII	1,69E+08	1,85E+07	27,86	4	8	5,30	2	2	615	67,7	13,01	9,13	0,86
CFI	IPI00291867.4	Complement factor I	4,84E+07	0,00E+00	7,80	2	3	0,00	0	0	583	65,7	3,6	100	0
CES1	IPI00010180.4	Isoform 1 of Liver carboxylesterase 1	9,07E+08	1,28E+07	121,26	21	38	17,91	6	6	567	62,5	43,74	71,00	0,59
ACOT1	IPI00333838.1	Acyl-coenzyme A thioesterase 1	3,50E+08	0,00E+00	50,29	10	18	0,00	0	0	421	46,2	30,4	100	0,9
ACOT2	IPI00220906.6	Isoform 1 of Acyl-coenzyme A thioesterase 2, mitochondrial	3,40E+08	0,00E+00	47,72	9	17	0,00	0	0	483	53,2	26,09	100	0,93
ABHD10	IPI00020075.4	Abhydrolase domain-containing protein 10, mitochondrial	8,39E+07	0,00E+00	17,98	5	6	0,00	0	0	306	33,9	21,57	100	0

ESD	IPI00411706.1	S-formylglutathione hydrolase	5,41E+08	6,06E+07	134,75	11	41	46,38	7	14	282	31,4	57,45	8,94	0,83
TPSAB1	IPI00472739.1	Isoform 2 of Tryptase alpha/beta-1	1,71E+09	0,00E+00	347,61	8	119	0,00	0	0	266	29,5	26,32	100	0,01
TPSB2	IPI00419942.2	Tryptase beta-2	2,82E+09	0,00E+00	347,61	8	119	0,00	0	0	275	30,5	25,45	100	0,01
TPSD1	IPI00419573.3	Isoform 1 of Tryptase delta	8,30E+08	0,00E+00	136,00	3	41	0,00	0	0	242	26,6	10,33	100	0
CTSG	IPI00028064.1	Cathepsin G	2,83E+07	0,00E+00	5,62	2	2	0,00	0	0	255	28,8	8,63	100	0
CMA1	IPI00013937.1	Chymase	7,09E+07	0,00E+00	14,08	2	5	0,00	0	0	247	27,3	10,53	100	0
PAFAH1B1	IPI00218728.4	Isoform 1 of Platelet-activating factor acetylhydrolase IB subunit alpha	5,32E+07	1,93E+07	19,23	5	6	12,40	3	4	410	46,6	16,1	2,76	0,73
PAFAH1B2	IPI00980480.1	platelet-activating factor acetylhydrolase IB subunit beta isoform b	6,67E+07	0,00E+00	8,03	2	2	0,00	0	0	202	22,7	15,35	100	1,23

Table 15. Protein hits for patient 151.

9.8 Patient 157

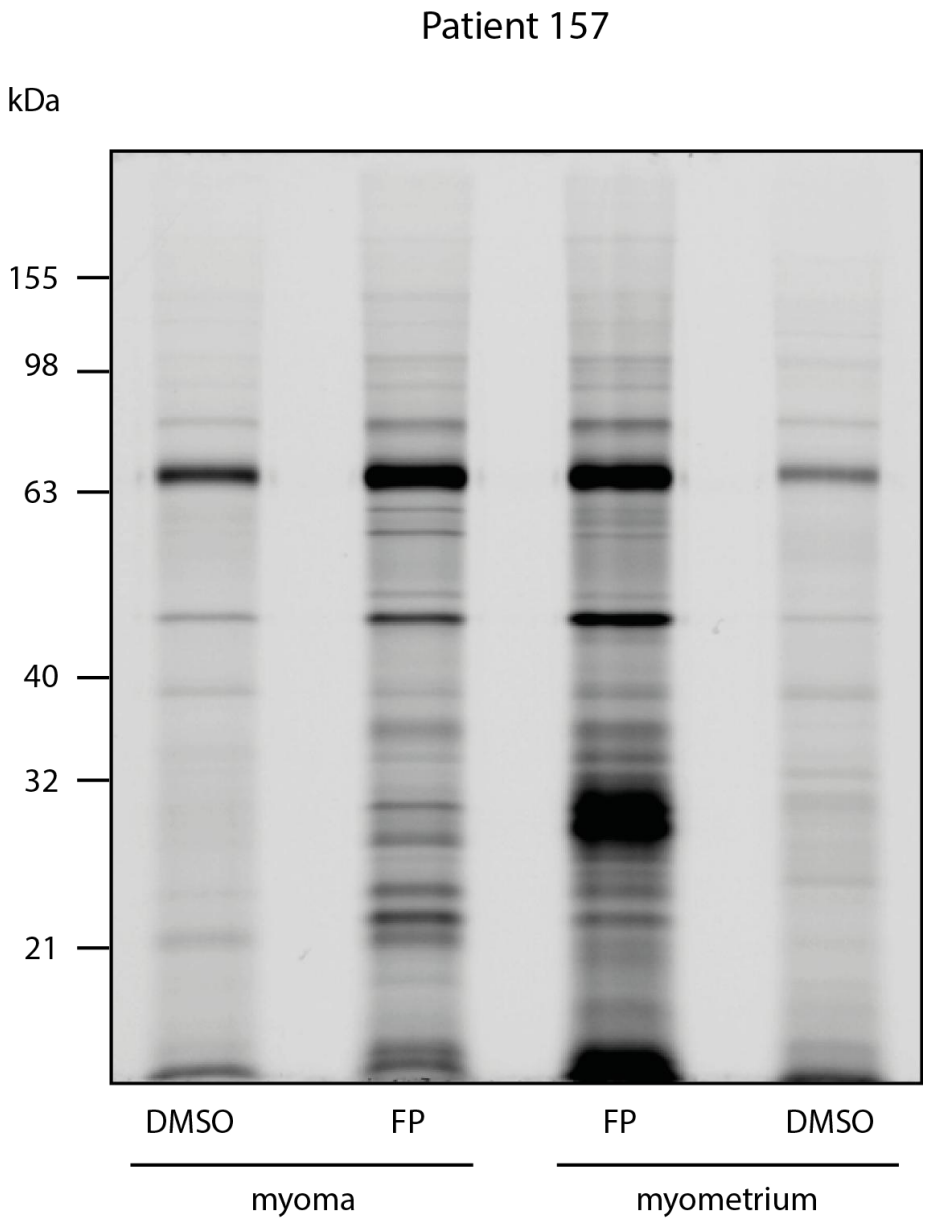

Figure 63. Fluorescence scan of paired myoma and myometrium samples of patient 157 incubated with FP.

Myoma

Target	Accession	Description	Area		FP			DMSO			General information			(Area FP)/(Area DMSO)	(Area Myoma)/(Area Myometrium)
			FP	DMSO	Score	# Peptides	# PSM	Score	# Peptides	# PSM	# AAs	MW [kDa]	Sequence coverage		
APEH	IPI00337741.4	Acylamino-acid-releasing enzyme	9,77E+07	0,00E+00	14,27	4	5	0,00	0	0	732	81,2	6,15	100	1,38
PREP	IPI00008164.2	Prolyl endopeptidase	1,12E+08	0,00E+00	36,12	8	11	0,00	0	0	710	80,6	16,2	100	2,51
F2	IPI00019568.1	Prothrombin (Fragment)	4,49E+07	0,00E+00	7,47	2	3	0,00	0	0	622	70,0	3,38	100	0,31
F12	IPI00019581.2	Coagulation factor XII	7,36E+07	0,00E+00	6,61	2	2	0,00	0	0	615	67,7	4,72	100	1,01
ACOT1	IPI00333838.1	Acyl-coenzyme A thioesterase 1	2,56E+08	0,00E+00	58,73	11	17	0,00	0	0	421	46,2	39,9	100	1,73
ACOT2	IPI00220906.6	Isoform 1 of Acyl-coenzyme A thioesterase 2, mitochondrial	2,55E+08	0,00E+00	53,04	11	15	0,00	0	0	483	53,2	37,06	100	1,75
ESD	IPI00411706.1	S-formylglutathione hydrolase	7,25E+08	7,83E+07	189,12	12	57	46,56	7	15	282	31,4	57,45	9,25	1,09
PAFAH1B1	IPI00218728.4	Isoform 1 of Platelet-activating factor acetylhydrolase IB subunit alpha	6,92E+07	1,37E+07	15,54	4	5	7,38	2	2	410	46,6	13,17	5,06	1,22
PAFAH1B2	IPI00026546.1	Platelet-activating factor acetylhydrolase IB subunit beta	1,22E+08	0,00E+00	5,94	2	2	0,00	0	0	229	25,6	12,23	100	0,42

Myometrium

Target	Accession	Description	Area		FP			DMSO			General information			(Area FP)/(Area DMSO)	(Area Myoma)/(Area Myometrium)
			FP	DMSO	Score	# Peptides	# PSM	Score	# Peptides	# PSM	# AAs	MW [kDa]	Sequence coverage		
APEH	IPI00337741.4	Acylamino-acid-releasing enzyme	7,09E+07	0,00E+00	23,45	5	8	0,00	0	0	732	81,2	8,33	100	1,38
PREP	IPI00008164.2	Prolyl endopeptidase	4,49E+07	0,00E+00	16,53	3	5	0,00	0	0	710	80,6	7,32	100	2,51
F2	IPI00019568.1	Prothrombin (Fragment)	1,43E+08	0,00E+00	29,56	5	11	0,00	0	0	622	70,0	11,25	100	0,31
F12	IPI00019581.2	Coagulation factor XII	7,31E+07	0,00E+00	9,43	2	3	0,00	0	0	615	67,7	4,39	100	1,01
ACOT1	IPI00333838.1	Acyl-coenzyme A thioesterase 1	1,48E+08	0,00E+00	36,02	8	11	0,00	0	0	421	46,2	26,6	100	1,73
ACOT2	IPI00220906.6	Isoform 1 of Acyl-coenzyme A thioesterase 2, mitochondrial	1,45E+08	0,00E+00	30,16	7	9	0,00	0	0	483	53,2	20,5	100	1,75
ABHD10	IPI00020075.4	Abhydrolase domain-containing protein 10, mitochondrial	6,53E+07	0,00E+00	20,07	4	7	0,00	0	0	306	33,9	15,03	100	0
ESD	IPI00411706.1	S-formylglutathione hydrolase	6,65E+08	7,30E+07	201,29	11	59	51,29	7	17	282	31,4	57,45	9,12	1,09
TPSAB1	IPI00472739.1	Isoform 2 of Tryptase alpha/beta-1	5,25E+08	0,00E+00	121,13	8	40	0,00	0	0	266	29,5	26,32	100	0
TPSB2	IPI00419942.2	Tryptase beta-2	5,25E+08	0,00E+00	121,13	8	40	0,00	0	0	275	30,5	25,45	100	0
TPSD1	IPI00376200.3	Isoform 2 of Tryptase delta	2,45E+08	0,00E+00	55,81	3	16	0,00	0	0	233	25,6	10,73	100	0
CTSG	IPI00028064.1	Cathepsin G	6,91E+08	0,00E+00	59,87	6	22	0,00	0	0	255	28,8	25,1	100	0

CMA1	IPI00013937.1	Chymase	4,91E+09	0,00E+00	573,67	9	188	0,00	0	0	247	27,3	44,53	100	0
PAFAH1B1	IPI00218728.4	Isoform 1 of Platelet-activating factor acetylhydrolase IB subunit alpha	5,67E+07	1,45E+07	9,89	3	3	7,78	2	2	410	46,6	10,49	3,91	1,22
PAFAH1B2	IPI00026546.1	Platelet-activating factor acetylhydrolase IB subunit beta	2,79E+08	0,00E+00	29,41	3	8	0,00	0	0	229	25,6	17,47	100	0,42

Table 16. Protein hits for patient 157.

9.9 Patient 172

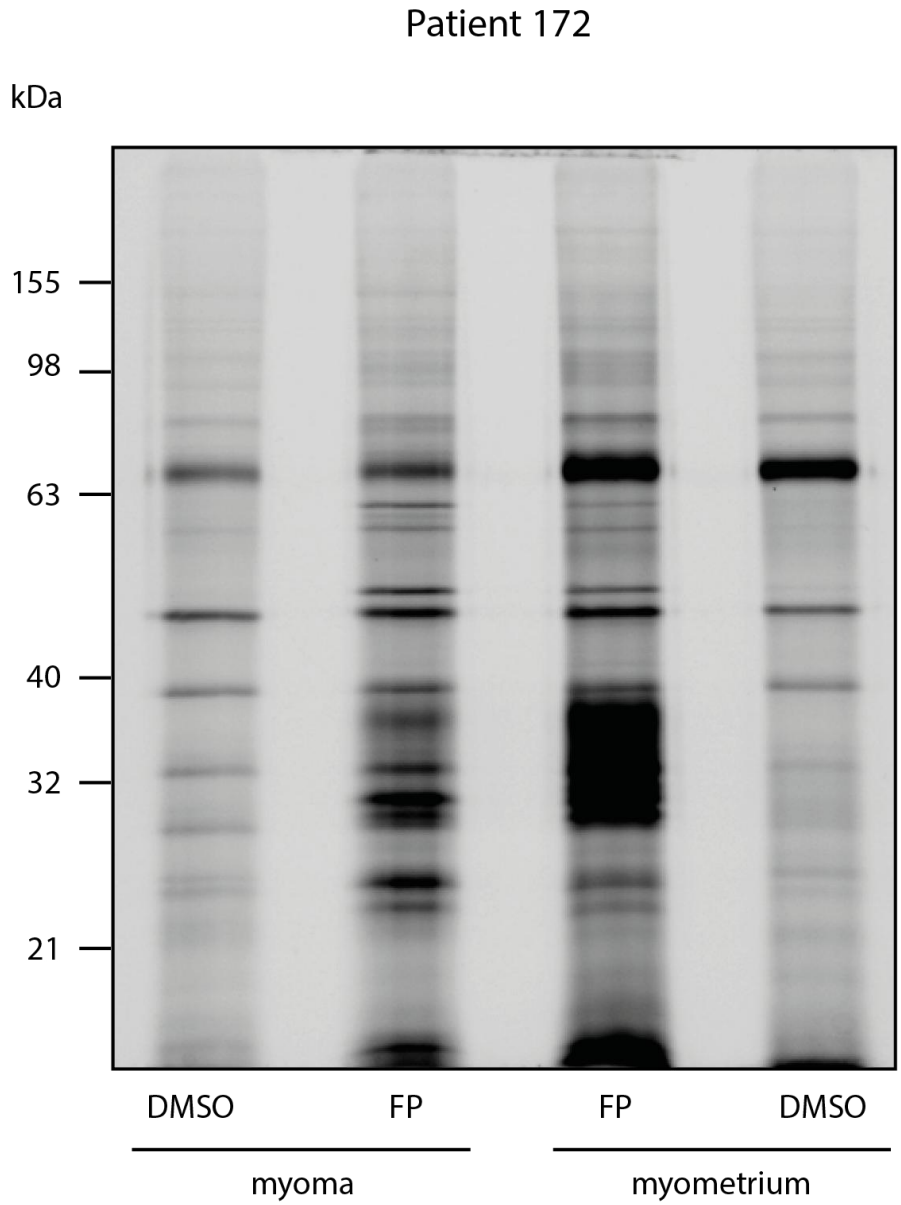

Figure 64. Fluorescence scan of paired myoma and myometrium samples of patient 172 incubated with FP.

Myoma

Target	Accession	Description	Area		FP			DMSO			General information			(Area FP)/(Area DMSO)	(Area Myoma)/(Area Myometrium)
			FP	DMSO	Score	# Peptides	# PSM	Score	# Peptides	# PSM	# AAs	MW [kDa]	Sequence coverage		
APEH	IPI00337741.4	Acylamino-acid-releasing enzyme	4,78E+07	0,00E+00	14,38	5	5	0,00	0	0	732	81,2	7,79	100	1,25
PREP	IPI00008164.2	Prolyl endopeptidase	7,72E+07	0,00E+00	37,02	9	10	0,00	0	0	710	80,6	19,15	100	1,37
CTSA	IPI00021794.8	Lysosomal protective protein	7,55E+07	0,00E+00	13,68	3	4	0,00	0	0	480	54,4	7,29	100	100
ACOT1	IPI00333838.1	Acyl-coenzyme A thioesterase 1	5,90E+08	0,00E+00	90,74	14	26	0,00	0	0	421	46,2	39,9	100	1,58
ACOT2	IPI00220906.6	Isoform 1 of Acyl-coenzyme A thioesterase 2, mitochondrial	5,90E+08	0,00E+00	79,13	12	23	0,00	0	0	483	53,2	30,23	100	1,62
ABHD10	IPI00020075.4	Abhydrolase domain-containing protein 10, mitochondrial	1,16E+08	0,00E+00	71,48	9	23	0,00	0	0	306	33,9	38,89	100	2,44
ESD	IPI00411706.1	S-formylglutathione hydrolase	1,84E+08	3,48E+07	98,28	8	34	43,63	6	13	282	31,4	49,29	5,27	1,03
TPSAB1	IPI00472739.1	Isoform 2 of Tryptase alpha/beta-1	4,97E+08	0,00E+00	227,82	8	73	0,00	0	0	266	29,5	26,32	100	0,41
TPSB2	IPI00419942.2	Tryptase beta-2	4,79E+08	0,00E+00	212,16	7	71	0,00	0	0	275	30,5	25,45	100	0,43
TPSD1	IPI00419573.3	Isoform 1 of Tryptase delta	2,36E+08	0,00E+00	122,76	3	34	0,00	0	0	242	26,6	10,33	100	0,31
CTSG	IPI00028064.1	Cathepsin G	9,17E+07	0,00E+00	25,38	4	9	0,00	0	0	255	28,8	18,43	100	0,41
PAFAH1B2	IPI00026546.1	Platelet-activating factor acetylhydrolase IB subunit beta	1,04E+08	0,00E+00	19,36	3	6	0,00	0	0	229	25,6	17,47	100	1,04
LYPLAL1	IPI00059762.5	Isoform 1 of Lysophospholipase-like protein 1	3,80E+07	0,00E+00	6,36	2	2	0,00	0	0	237	26,3	12,24	100	100

Myometrium

Target	Accession	Description	Area		FP			DMSO			General information			(Area FP)/(Area DMSO)	(Area Myoma)/(Area Myometrium)
			FP	DMSO	Score	# Peptides	# PSM	Score	# Peptides	# PSM	# AAs	MW [kDa]	Sequence coverage		
APEH	IPI00337741.4	Acylamino-acid-releasing enzyme	5,83E+07	1,56E+07	14,77	4	5	9,15	3	3	732	81,2	7,79	3,73	1,25
PREP	IPI00008164.2	Prolyl endopeptidase	5,64E+07	0,00E+00	11,35	3	3	0,00	0	0	710	80,6	6,20	100	1,37
F12	IPI00019581.2	Coagulation factor XII	7,41E+07	0,00E+00	8,99	3	3	0,00	0	0	615	67,7	7,64	100	0
ACOT1	IPI00333838.1	Acyl-coenzyme A thioesterase 1	3,72E+08	0,00E+00	83,21	14	23	0,00	0	0	421	46,2	48,93	100	1,58
ACOT2	IPI00220906.6	Isoform 1 of Acyl-coenzyme A thioesterase 2, mitochondrial	3,62E+08	0,00E+00	83,43	13	22	0,00	0	0	483	53,2	44,93	100	1,62
ABHD10	IPI00020075.4	Abhydrolase domain-containing protein 10, mitochondrial	4,77E+07	0,00E+00	19,89	6	7	0,00	0	0	306	33,9	21,90	100	2,44
ESD	IPI00411706.1	S-formylglutathione hydrolase	1,78E+08	3,90E+07	125,98	9	43	48,53	7	15	282	31,4	48,98	4,56	1,03
TPSAB1	IPI00472739.1	Isoform 2 of Tryptase alpha/beta-1	1,22E+09	2,65E+07	410,13	9	138	43,19	3	12	266	29,5	31,58	46,02	0,41

TPSB2	IPI00419942.2	Tryptase beta-2	1,12E+09	2,45E+07	410,13	8	134	43,19	3	12	275	30,5	30,55	45,54	0,43
TPSD1	IPI00419573.3	Isoform 1 of Tryptase delta	7,62E+08	4,04E+07	181,40	3	53	0,00	0	0	242	26,6	10,33	100	0,31
CTSG	IPI00028064.1	Cathepsin G	2,24E+08	0,00E+00	46,02	5	15	0,00	0	0	255	28,8	21,57	100	0,41
CMA1	IPI00013937.1	Chymase	1,31E+08	0,00E+00	65,30	7	21	0,00	0	0	247	27,3	34,01	100	0
PAFAH1B2	IPI00026546.1	Platelet-activating factor acetylhydrolase IB subunit beta	2,01E+08	0,00E+00	28,18	2	10	0,00	0	0	229	25,6	12,23	100	1,04

Table 17. Protein hits for patient 172.

9.10 Fum MDA-MB231

Target	Accession	Description	Area				Fum (1)			Fum (2)			DMSO (1)			DMSO (2)			General information			(Area Fum)/(Area DMSO)	
			Fum (1)	Fum (2)	Control (1)	Control (2)	Score	# Peptides	# PSM	Score	# Peptides	# PSM	Score	# Peptides	# PSM	Score	# Peptides	# PSM	# AAs	MW [kDa]	Sequence coverage	(1)	(2)
MetAP2	IPI00033036.1	Methionine aminopeptidase 2	1,423E8	6,669E7	0,000E0	0,000E0	87,6	12	24	80,4	12	22							478	52,9	34,9	100,00	100,00

Table 18. Protein hit identified from MDA-MB231 upon Fum pulldown.

10 Publications

Publications in international peer reviewed journals

J. Kreuzer, N.C Bach., D. Forler, S.A. Sieber, "Target discovery of acivicin in cancer cells elucidates its mechanism of growth inhibition", *Chem. Sci.* **2015**, 6 (1), 237-245.

J.M. Krysiak, **J. Kreuzer**, P. Macheroux, A. Hermetter, S.A. Sieber and R. Breinbauer; "Novel activity-based probes for studying the activity of flavin-dependent oxidases and for the protein target profiling of MAO-inhibitors", *Angew. Chem.* **2012**, *51* (28), 7035-7040.

M. Gersch, **J. Kreuzer** and S.A. Sieber; "Electrophilic natural products and their biological targets"; *Nat. Prod. Rep.* **2012**, *29*, 659-682.

Poster presentations and talks

Johannes Kreuzer, Ronald Frohnapfel, Daniel Forler and Stephan A. Sieber, "Acivicin derived scaffolds for target identification", CIPSM-Bayer HealthCare-Symposium 2013, Munich

Johannes Kreuzer, Joanna M. Krysiak, Ronald Frohnapfel, Daniel Forler and Stephan A. Sieber, "ABPP as a tool for pharmaceutical industry", BHC-Young-Scientist-Postersession 2012, Berlin

Johannes Kreuzer, Ronald Frohnapfel Stephan A. Sieber, "New targets of the natural product acivicin" Young Scientist Forum 2012, Harvard University, Boston

Johannes Kreuzer, "Acivicin as a probe for ABPP", Young Scientist Forum 2011, Ludwig Maximilians University, Munich

Johannes Kreuzer, "Acivicin as a probe for ABPP", 4th West-European Activity-based Proteomics Meeting 2011, Essen